2007-01-01

Integrated Geophysical Data Processing and Interpretation of Crustal Structure in Ethiopia with Emphasis on the Ogaden Basin and Adjacent Areas

Ketsela Tadesse
University of Texas at El Paso, ktadesse@hotmail.com

INTEGRATED GEOPHYSICAL DATA PROCESSING AND INTERPRETATION OF CRUSTAL STRUCTURE IN ETHIOPIA WITH EMPHASIS ON THE OGADEN BASIN AND ADJACENT AREAS

KETSELA TADESSE

Department of Department of Geological Sciences

APPROVED:

G. Randy Keller, Ph.D., Chair

Diane Doser , Ph.D.

Kate C. Miller, Ph.D.

Richard Langford, Ph.D.

Jose Hurtado Jr., Ph.D.

Vladik Kreinovich, Ph.D.

Pablo Arenaz, Ph.D.
Dean of the Graduate School

Dedication

Dedicated to

The Late W/ro Workie Abayneh

INTEGRATED GEOPHYSICAL DATA PROCESSING AND INTERPRETATION OF CRUSTAL STRUCTURE IN ETHIOPIA WITH EMPHASIS ON THE OGADEN BASIN AND ADJACENT AREAS

by

KETSELA TADESSE, BSc., MPhil.

DISSERTATION

Presented to the Faculty of the Graduate School of

The University of Texas at El Paso

in Partial Fulfillment

of the Requirements

for the Degree of

DOCTOR OF PHILOSOPHY

Department of Geological Sciences

THE UNIVERSITY OF TEXAS AT EL PASO

July 2007

Acknowledgements

I would like to express my deepest gratitude to my advisor Dr. G. Randy Keller for his excellent guidance, continuous support and encouragement through out this study. I would also like to extend special gratitude to Joyce Keller for her encouragement and support at various times. Thanks are also extended to my committee members Dr. Diane Doser, Dr. Kate C. Miller, Dr. Richard R. Langford and Dr. Jose Hurtado for their willingness to serve as committee members and their valuable comments in the dissertation work, in addition to the thought courses they offered me, from which I benefited a lot. I would also like to thank Dr. Vladik Kreinovich for his comments.

I would also like to thank Mr. Carlos Montana for his full support in UNIX platform projects and UNIX application software throughout this study. Dr. Steven Harder and Dr. Raed Aldouri are also thanked for their support at various times. The non-seismic group is thanked for our wonderful time in the weekly meetings and sharing knowledge and experiences.

Many people have contributed for my success. Mr. Kenny and Mrs. Sarahi Gross, Amsale and Belete, Almaz and HaileMariam including their family, Seble, Mulatua and Lakew. I appreciate Dr. Kevin Mickus for his willingness to work together both in the field and in the school and to share his experience as well as information with me. Benjamin Drenth is thanked for allowing me to use the Euler Deconvolution software and his computer. My gratitude also goes to the Department Geological Sciences staff and students.

I would particularly like to thank Ato Abiy Hunegnaw, Head, Petroleum Operations Department and the Ministry of Mines and Energy of Ethiopia for their kind support and permission to use the Ogaden and Blue Nile data in this dissertation. My deepest gratitude goes to all POD personnel and my friends who contributed for the success of this study including Mamushet Zewge and Dr. Girma Woldetinsae from the Geological Survey of Ethiopia.

Special thanks are due to my wife Alemnesh Abate, my children Nahom and Mahlet, Ato Abate and family, Lakew Gebreyes and his family, Woldearegay and Lishan and also my parents and sisters for their moral support, patience to stay together until I finish my study.

This study was supported in large part by a grant from the Continental Dynamics program of the National Science Foundation for the EAGLE (Ethiopia-Afar Geoscientific Lithospheric Experiment) project. I thank the EAGLE team for their support and encouragement.

Abstract

The combined effects of magmatism and stretching due to asthenosphere upwelling modifies the crustal structure of the Earth as seen in the Ethiopian rift and adjacent areas. The Ethiopian rift provides unique opportunities to understand the nature of rifted crust and the intensity of its modification by magmatic processes. I used geological and geophysical data to conduct an integrated study in and around the Ethiopian rift including the northern Kenyan rift and the northern part of the Kenyan dome. New gravity, controlled source seismic, and teleseismic data from the EAGLE (Ethiopia-Afar Geoscientific Lithospheric Experiment) were used as additional constraints in my analysis of the crustal structure of Ethiopian rift and adjacent plateaus.

Application of a residual gravity anomaly filtering technique using upward continuation revealed various crustal features within the Ethiopian rift and the flanking plateau regions. Short wavelength high amplitude positive anomalies coincide with the local volcanic complexes and calderas. In addition low gravity anomalies are associated with areas of thicker sediments within the rift valley.

Axial and cross rift gravity profiles were modeled in 2.5 dimensions constrained with seismic refraction and geologic data. The axial model connects the Kenyan dome through Turkana rift and Main Ethiopian rift (MER) up to the Afar triple junction and provides a new integrated picture of lithospheric structure along the rift for over 1000 km. This model indicates a thin crust (26 km) underlying the Afar region. The crust gradually thickens towards the MER where it is about 35-40 km thick. Towards the south the crust thins and is only 22 km thick when it reaches the Turkana area. The southern section of the axial model indicates that the crust is about 35 km thick beneath the central Kenyan rift. All these thickness values are in agreement with the EAGLE and Kenya Rift International Seismic Project (KRISP) and earlier refraction

results and ties these results together to form a complete picture of the axial structure of the rift. The cross profiles, which are interlocked with the axial rift profile, indicate that thick (~45km) crust is present beneath a broad region of the western plateau. The EAGLE seismic results indicate that the part of the western plateau adjacent to the rift is thickened via underplating. The Bale Mountain region on the eastern rift flank has relatively thick (~40 km) crust, which is in agreement with receiver function results. In general, asthenospheric upwelling affects a wide zone near Afar and the southern Ethiopian rift, whereas the area of upwelling is narrower around the MER.

The Abbay or Blue Nile basin was another target of my study. Integrated geophysical (seismic, remote sensing, and gravity) and geological data suggest that the sedimentary section of Abbay basin extends well to the east of the known extent of its sedimentary fill. Gravity modeling results suggest approximately 3 km of sub-volcanic sedimentary strata exist over a wide area.

I also undertook an integrated analysis of the Ogaden basin that lies east of the rift valley and is associated with the break-up of Gondwanaland by Karroo rifting. Seismic reflection data were processed and interpreted and combined with gravity and magnetic data to study the evolution of the basin and its geometry. The existence of a tri-radial rift that connects to the Abbay basin is suggested by the isostatic residual gravity anomaly map produced in this study. This result provides new evidence for the relationship of the Ogaden and Abbay basins via a northwest-southeast trending Permo-Triassic rift system.

The northeastern part of the Ogaden basin shows distinct gravity anomalies trending in a northeast-southwest direction that appear to be due to a series of grabens and horsts. 3D Euler deconvolution of gravity data and modeling results suggest a sedimentary thickness of about 5 km sedimentary strata in some of the grabens.

Integrated gravity models in the southwest part of the Ogaden basin indicate a sediment thickness of 8 km. Interpretation of seismic reflection data indicates potential stratigraphic and structural traps for hydrocarbons in the Ogaden basin. Older strata such as the Karroo strata appear to pinch out towards the uplifted basement to the northwest. Fault structures are associated with the basement. Channels that appear as distinct features on 2D reflection seismic data may be developed in various places with hanging wall incision. Attribute analysis and interpretation suggest possible hydrocarbon bearing zones or at least porous formations and continuity of reflection horizons.

In summary, this dissertation presents a new integrated analysis of Permian and younger rifting in Ethiopia and northern Kenya. The basins related to Permo-Triassic were analyzed and connections across Ethiopia from the Ogaden basin to the western plateau are suggested. The seismic results of the EAGLE and KRISP project were tied together and extended beyond the rift valley regions and revealed large variations in structure along the rift system.

Table of Contents

List of Tables

List of Figures

Chapter 1: Introduction

1.1 Rifting Mechanisms

Continental rifting is the process by which the lithosphere stretches and thereby thins. The thinning process could be uniform (pure shear) or take place via simple shear. Rifting plays an important role in reshaping the earth's surface. The gradual stretching of the lithosphere may eventually cause separation, resulting in the formation of basins, horsts and grabens bounded by faults. Further extension may lead to the birth of new oceans. The thinning of the lithosphere caused by rifting reduces the lithostatic pressure on the asthenosphere. As the asthenosphere is very hot, the reduction in pressure causes partial melting of the rocks to create magma. The magma created is less dense than the overlying lithosphere and rises due to buoyancy. This magma finds its way to the surface through zones of weakness in the lithosphere causing volcanism. The volcanic products include calderas, volcanic complexes, sills, dikes, magmatic underplating, and flood basalts. Studies of these volcanic products provide information on the pre-rift lithospheric structure and the magmatic processes at work during rifting.

In addition to contributing to our understanding of the nature of the rifting process, the structures and magmatism caused by rifting lead to potential geothermal energy resources, mineral resources, and sediment filled basins in which hydrocarbons resources may form. Although the Ethiopian rift and Afar triple junction seem the best places to study rifting mechanisms, at present there are still limitations in the types and amount of geological and geophysical data available. In addition, there is a lack of agreement about the various forms of rift development. This study has attempted to address some of the questions about the structure and evolution of rift systems in Ethiopia and has used available geophysical data to generate crustal models and a number of regional maps. Also, a significant amount of modern high-

quality gravity data have been added to fill in important areas lacking data for detailed analyses and to help tie existing data together better.

The tectonically active regions of the Afar triple junction and the Ethiopian rift have been the focus of scientific research and teaching in the Earth sciences by universities and other institutions for decades. Rift related volcanics cover much of the country and there are a few outcrops of the Precambrian basement. Sedimentary rocks are estimated to cover two thirds of the country, and basins occur in many different parts of the country. The development of most of the basins is related to extensional tectonics that has taken place at times since the Late Paleozoic and continues today.

Exploration activities in a few of the basins, available geophysical, geochemical and geological data indicate that the petroleum potential in some of the sedimentary basins is significant. Reported and analyzed oil seeps, discoveries of gas and gas condensate as well as oil shows in some of the exploratory wells, mainly in the Ogaden basin, have proved that there are several prospective areas in Ethiopia. In addition to the regional investigation made in this study, specific and detailed data processing and interpretation of some sedimentary basins has been carried out.

Previous geophysical and geological studies of the Ethiopian rift have focused on small areas such as the main Ethiopian rift or specific geothermal areas. This study embraces the whole of the Ethiopian rift and the Northern Kenyan rift, which is well studied by various geophysical techniques (e.g., Mechie et al., 1994; Simiyu and Keller, 1997, Mariita and Keller, 2007). The Eastern and Western Plateaus of Ethiopia, which were formed by large flood volcanic edifices, were also targeted in this study. Study of these large areas helped to generate lithospheric scale models that revealed the nature of the crust beneath the Ethiopian rift and its adjacent plateaus.

1.2 Organization of this Dissertation

In this dissertation, my studies include almost the whole of Ethiopia (Fig. 1.1) and focused on investigating the crustal structure of the Ethiopian rift and adjacent areas at both regional and local scales. My study area includes part of the Kenya rift, especially the Turkana region, and I have applied my findings to study regional tectonics and to various energy resource exploration efforts. I have added a significant amount of gravity data from the Ethiopian rift and adjacent areas to the East Africa database at the University of Texas at El Paso and analyzed these data at both regional and local scales along with seismic data from the EAGLE project and industry exploration efforts. I analyzed the geometry of sub-volcanic sediments in the Blue Nile or Abbay basin via an integrated geophysical analysis. I also used industry seismic reflection data to study the Ogaden basin. I then explored the relationships between the Ogaden basin and the Abbay basin by exploring the hypothesis the existence of a northwest-southeast trending, late Paleozoic rift system has been widely discussed by Ethiopian geologists.

This dissertation integrates gravity, reflection and refraction seismic data, remote sensing, Digital Elevation Maps (DEM) and also satellite gravity data to answer the following questions:

1. What are variations and geometry of the axial crustal structure of the East African rift from the northern Kenyan rift up to the Afar triple junction?
2. What is the geometry of the subvolcanic sediments in the Abbay or Blue Nile basin?
3. What is the general geometry of the Ogaden basin and depth to the basement?
4. Is there a structural relationship between the Ogaden basin and the Abbay basin that can be defined geophysically?
5. What are the possible hydrocarbon trapping mechanisms in the Ogaden basin?
6. Can reprocessing of existing seismic reflection data in the Ogaden basin reveal further information?

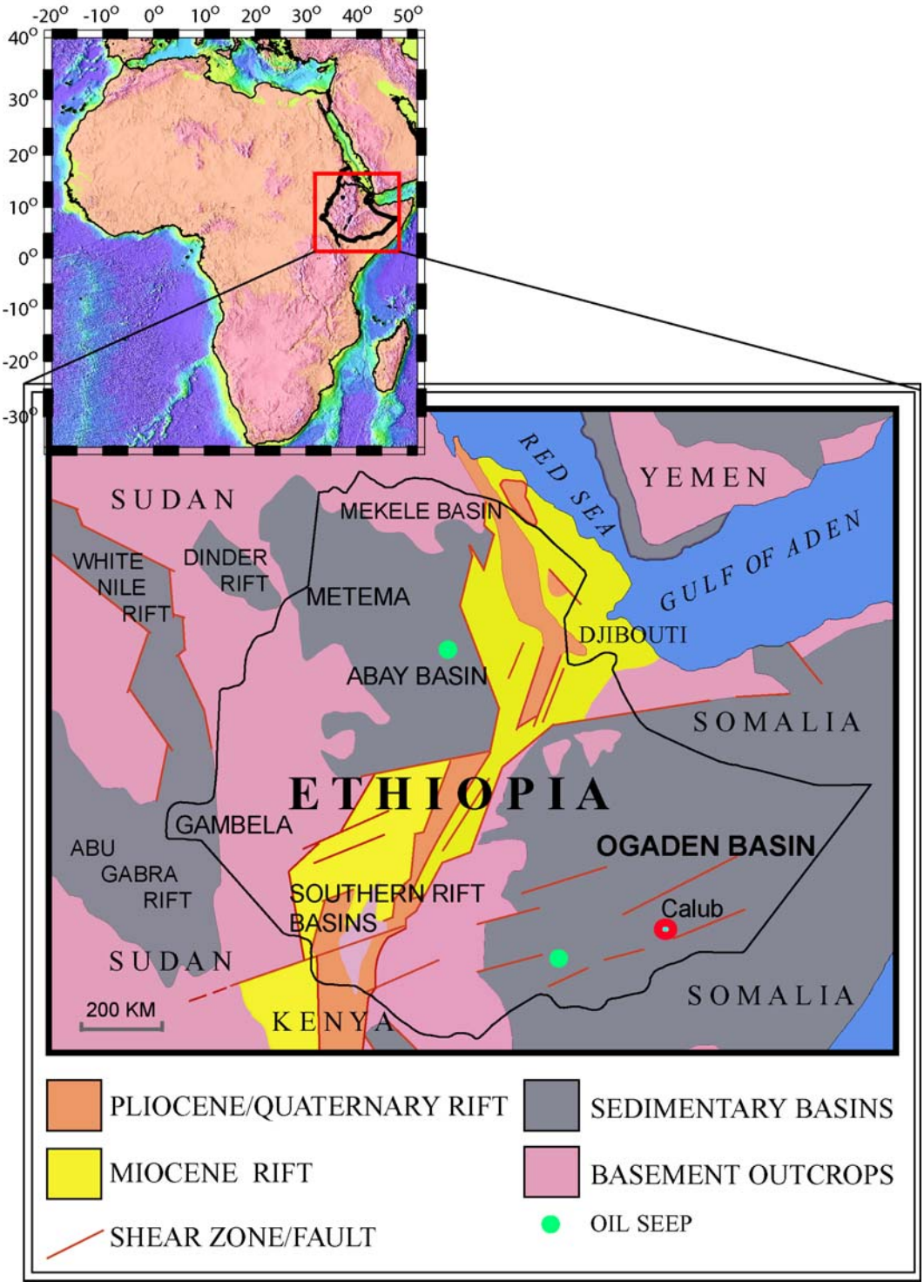

Figure 1.1: Index map of the study area and the regional tectonic setting that also shows the locations of important potential energy resources. Red circle is the Calub gas discovery in the Ogaden Basin. Inset is map of Africa showing the location of Ethiopia in the red box.

Providing answers to these questions based on geophysical models and maps of the areas will allow me to better and systematically provide detailed structural interpretations for important scientific and energy resource exploration efforts for the country. In this way, I am in a better position to recommend further exploration targets in the Ethiopian rift and outside the rift in some hydrocarbon prospect areas.

This dissertation consists of six chapters that are intended to form four independent scientific papers. In this first chapter, I have introduced the overall research project and goals. I have highlighted the type of research that has been undertaken in the Ethiopian rift and explained the need for more research and exploration efforts in the sedimentary basins of Ethiopia. Chapter 2 focuses on the regional crustal structure of the Ethiopian rift and adjacent areas including the Northern Kenya rift, especially the Lake Turkana region. The review of the literature presented in this chapter gives the reader an overview of the type of research that has been undertaken in the Ethiopian rift and reveals the need for more research and exploration efforts in the sedimentary basins of Ethiopia. Chapter 3 deals with the Abbay basin and the integration of a variety of geophysical techniques to delineate the geometry of this sedimentary basin and sub-volcanic sediment thickness. Chapter 4 deals broadly with the Ogaden basin, and employs integrated geophysical data processing and analysis of gravity and magnetic data along with seismic reflection data to determine depth to the basement and geometry of the basin. The evolution of this basin on a regional scale was also investigated. Chapter 5 deals with the relationship of the Ogaden and Abbay basins. Finally, my overall conclusions are contained in Chapter 6.

Chapter 2: Crustal Structure of the Ethiopian rift and adjacent plateaus

2.1 Introduction

The East African Rift System (EARS) is recognized as the continental extension of oceanic spreading that forms a tri-radial rifting pattern that includes the Red Sea and the Gulf of Aden rift systems (Fig. 2.1). Early geological and geophysical investigations (e.g., Williams, 1970; Baker and Wohlenberg, 1971; Mohr et al., 1972; Girdler, 1991) indicated that the EARS is an extensional feature that possibly represents an initial stage of continental breakup. The EARS is divided into three parts: the Ethiopian rift, the Eastern rift and the Western rift (Fig. 2.1). Because of its close proximity to the oceanic spreading centers in the Red Sea and Gulf of Aden, the Ethiopian part of the EARS (Fig. 2) has special significance because it contains the transition from a continental rift to incipient oceanic spreading center (e.g. Ebinger and Casey, 2001; Kendall et al., 2005).

The part of the Ethiopian rift that has been most studied is the Afar triple junction (Fig. 2.2). It is generally accepted that the Afar triple junction lies above or near a mantle plume (e.g., Courtillot et al., 1984; Hayward and Ebinger, 1996; Montelli et al., 2004). The composition and thickness of the crust of the Afar triple junction has been debated by a number of researchers. Early studies (Berkhemer et al., 1975; Makris and Ginzburg, 1987) indicated that the crustal thickness is 14 to 26 km and suggested that the crust is more of a continental nature than oceanic. Others have suggested the crust beneath the Afar is oceanic (e.g., Barberi and Varet, 1977). Recent gravity studies carried out by Mamo (2004) and Tiberi et al. (2005) suggested a 26 km thick crust beneath Afar. Other crustal thickness estimates suggest a range of 8 to 10 km (Ruegg, 1975; Sandvol et al., 1998). The later estimate led some researchers to conclude that the crust beneath the Afar is indeed oceanic. Others have argued that the crust is new igneous material

(Mohr, 1989; Dugda, et al., 2005). These large crustal thickness estimate variations indicate the need for further investigations and integrated interpretations.

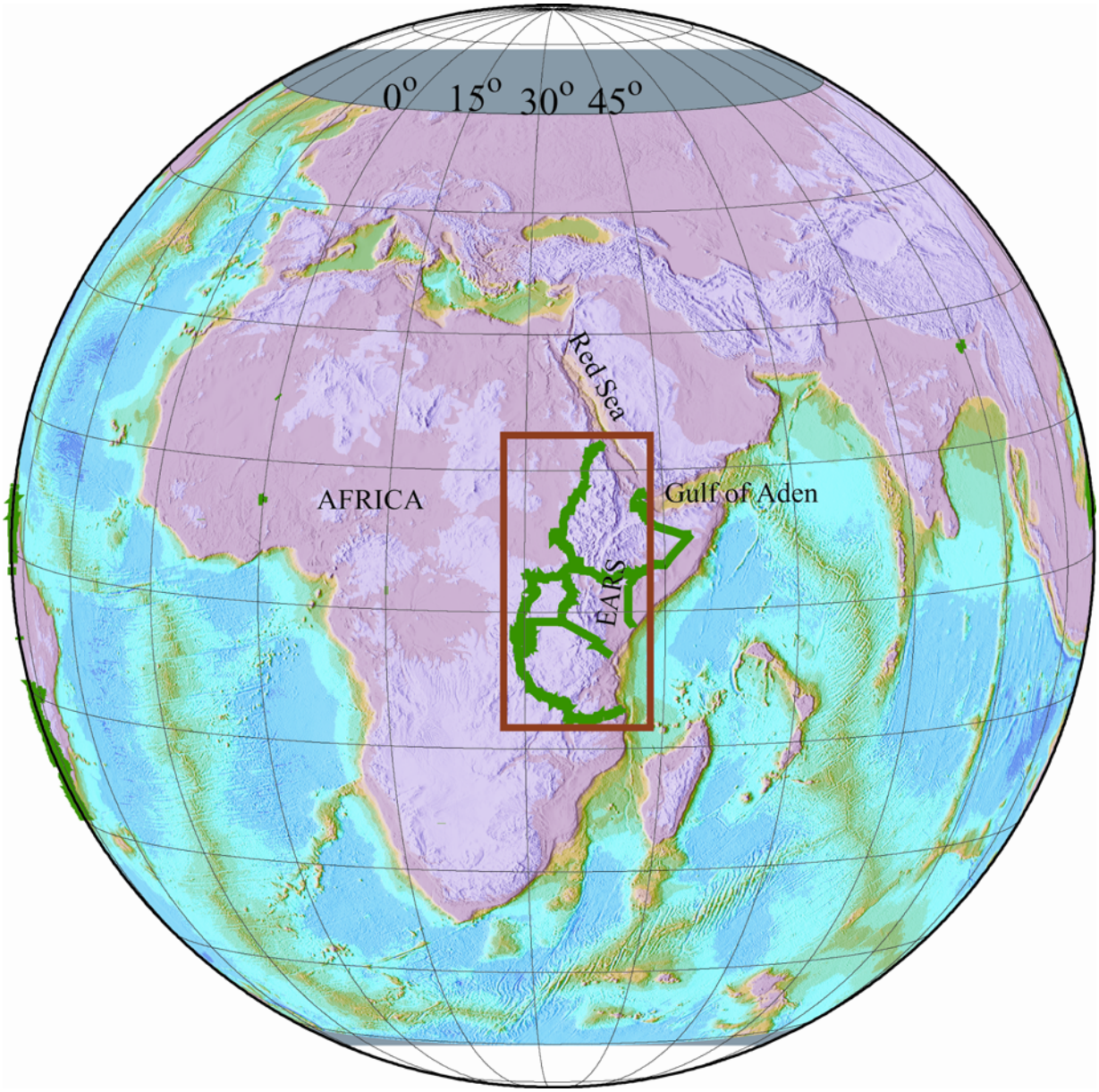

Figure 2.1: Index map of the East African rift, relative to the world and the adjacent areas of the Red Sea and Gulf of Aden rifts. For regional tectonic analysis the area in the red box is included and topographic and gravity maps generated for this region. The expanded version of this area is shown in Figures 2.2 and 2. 3.

The main Ethiopian rift (MER) occupies the central part of the EARS in Ethiopia and is a symmetrical graben bounded by steep faults (WoldeGabriel et al., 1990). The MER divides the 1000 km wide uplifted region of the Ethiopian plateau into two plateaus: the western plateau to the northwest and the eastern plateau to the southeast (Fig. 2.2). Compared to the Afar triple junction, the MER is one of the least studied regions in the EARS. The thickness of the crust, the extension direction in the rift and, the depth and geometry of the rift basins, as well as the nature of the volcanism are among the issues debated in regard to the MER. Until the recent Ethiopian Afar Geoscientifc Lithospheric Experiment (EAGLE) no controlled source seismic experiment had been conducted in this region other than the early work of Berkhemer et al. (1975) that focused on Afar.

In this study we performed an investigation of the crustal structure including basin structures by constructing a series of gravity maps and a series of 2.5D integrated gravity models that extended across and along the rift. Our models are constrained by the EAGLE controlled source experiment in the MER (e.g., Maguire et al., 2006) and the Kenyan Rift International Seismic Project (KRISP) results (Keller et al., 1994; Mechie et al., 1994).

2.2 The Study Area

Our study area includes the EARS, which is part of the Afro-Arabian rift system that extends from the Dead Sea to Mozambique (e.g., Mechie and Prodehl, 1988) (Fig.2.3). This study focuses mainly on the Ethiopian plateaus (eastern and western), the Afar triple junction, the MER, the Southern Ethiopian rift (SER) and the Turkana region of the Kenya rift.

2.3 Regional Setting

The unique topography, structures, and volcanic features in East Africa have interested the geoscientific community for many years. Central to this attraction is the EARS, which is a natural laboratory for studying crustal as well as lithospheric extensional features. The faults

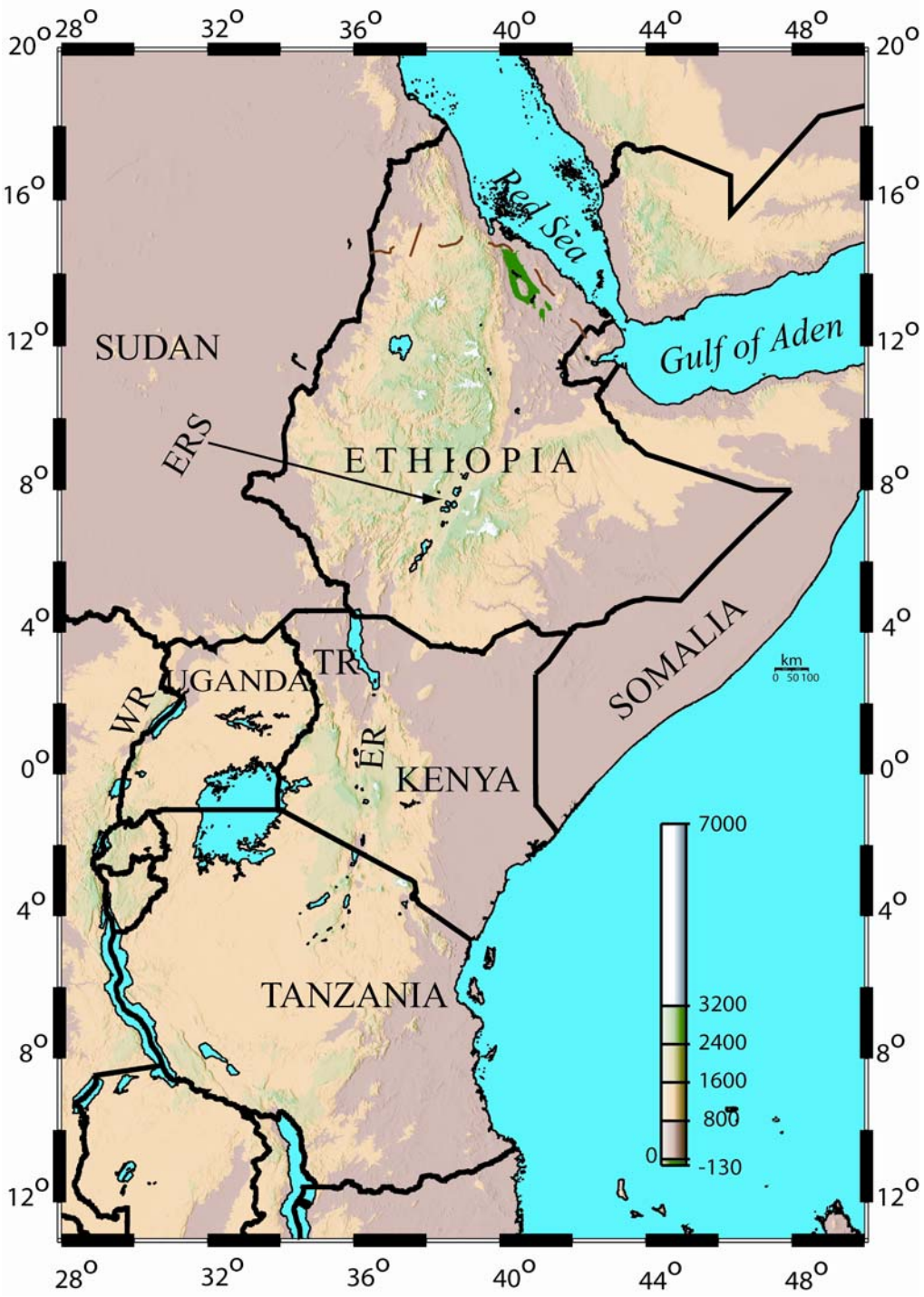

Figure 2.2: The East African Rift system (EARS) starting from the junction of the tri-rift system (Red Sea, Gulf of Aden and EARS) at Afar in the north to Mozambique in the south is about 3000 km long. This topographic map of the region shows different parts of the EARS, the Ethiopian rift (ERS), Eastern rift (ER) and the Western rift (WR). Also included in this map are the Western and Eastern plateaus of Ethiopia (the Ethiopian dome) and the Kenyan dome.

within the EARS (Fig. 2.2) often display several kilometers of vertical displacement which results in deep grabens that form basins and volcanic complexes in various parts of the rift system. In the context of the Ethiopian rift, both the eastern and western rift margins are characterized by normal faults with at least one to two kilometers of offset between the rift floor and the top part of the uplifted flanks of the rift margins (Figs. 2.4 and 2.5).These include the Butajira border fault (BU) on the western rift flank of the main Ethiopian rift (MER) (Fig. 2.5). The Degaga fault zone is located along the eastern side of the MER and is also marked by offsets of step faults, (Fig. 2.5). To the north of this fault zone, the Asela-Sire border fault (AS) differentiates the funnel shaped Afar triple junction from the Eastern plateau. On the western side of the rift north of the Butajira region, the Addis Ababa - Debrezeit embayment (AE) is characterized by subdued topography and wide spread cinder cones and crater lakes. Normal faults of various lengths can be observed northwest and west of Nazreth (N). More border fault zones that clearly mark the boundary between the rift flank and the rift floor are found further north along the western Ethiopian rift margin and the Afar triple junction. In general, the MER is a symmetric feature between the border faults (e.g. Di Pola, 1976; Ebinger et al., 1989; WoldeGabriel, 1990; Ebinger et al., 2000).

South of Degaga (DE), there exists an oblique displacement of fault zones, which is thought to be associated with the extension direction of the MER around Shashemene (SH) (e.g., Boccaletii et al., 1998; 1992). South of Shashemene (SH), the rift is clearly marked by high angle normal faults for few tens of kilometers further to the south. Around the Lake Abaya region, the Chencha plateau (CH) is separated by the fault zone on the west that is parallel to Lake Abaya (LA). The southern Ethiopian rift system consists of several rift basins such as Omo (O) and Chew Bahir (CB) that are bordered by numerous fault splays. This region, together with Turkana and the northern Kenya rift, exhibits evidence for multiple episodes of rifting (Morley et al., 1992; Ebinger and Ibrahim, 1994; Hendrie et al., 1994).

The detailed geology of the Ethiopian rift and surrounding areas has been described in many studies (e.g., Dainielli, 1943; Mohr, 1962b 1971; Di Pola, 1972; WoldeGabriel, 1990). The

Cenozoic history of the crust in Ethiopia was affected by a major change in plate motion that led to the onset of rifting between the Nubian and Arabian plates at 25 Ma (Ukstins et al., 2002). Rifting in the southern Red Sea had commenced by 29 Ma (Wolfenden et al., 2005); whereas, initial rifting in the northernmost MER initiated around 11 Ma (Chernet et al., 1998). Crustal extension within the central and southern MER commenced between 18 and 15 Ma (Ebinger et al. 1989; WoldeGabriel et al., 1990). Others set the onset of MER faulting extension from 9.7 to 8.3 Ma and more recently at 6 - 5 Ma (e.g., WoldeGabriel, et al., 1990 and Bonini et al., 2005).

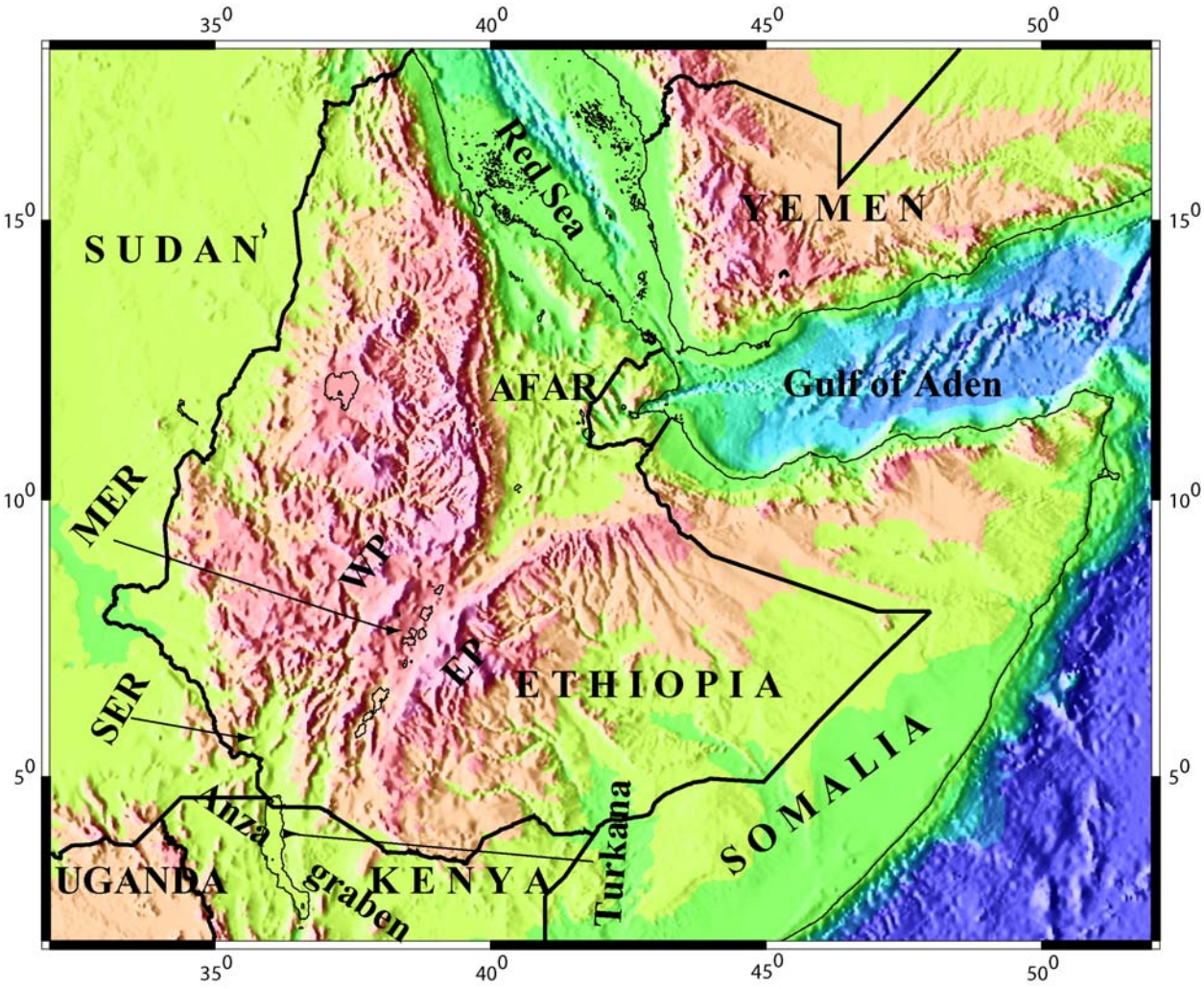

Figure 2.3: Location of the main study area shown as topographic map based on STRM90 meter data. The rift valley sections are clearly segregated from the plateaus characterized by low elevation bounded by sharp elevation gradients on both sides of the rift system.

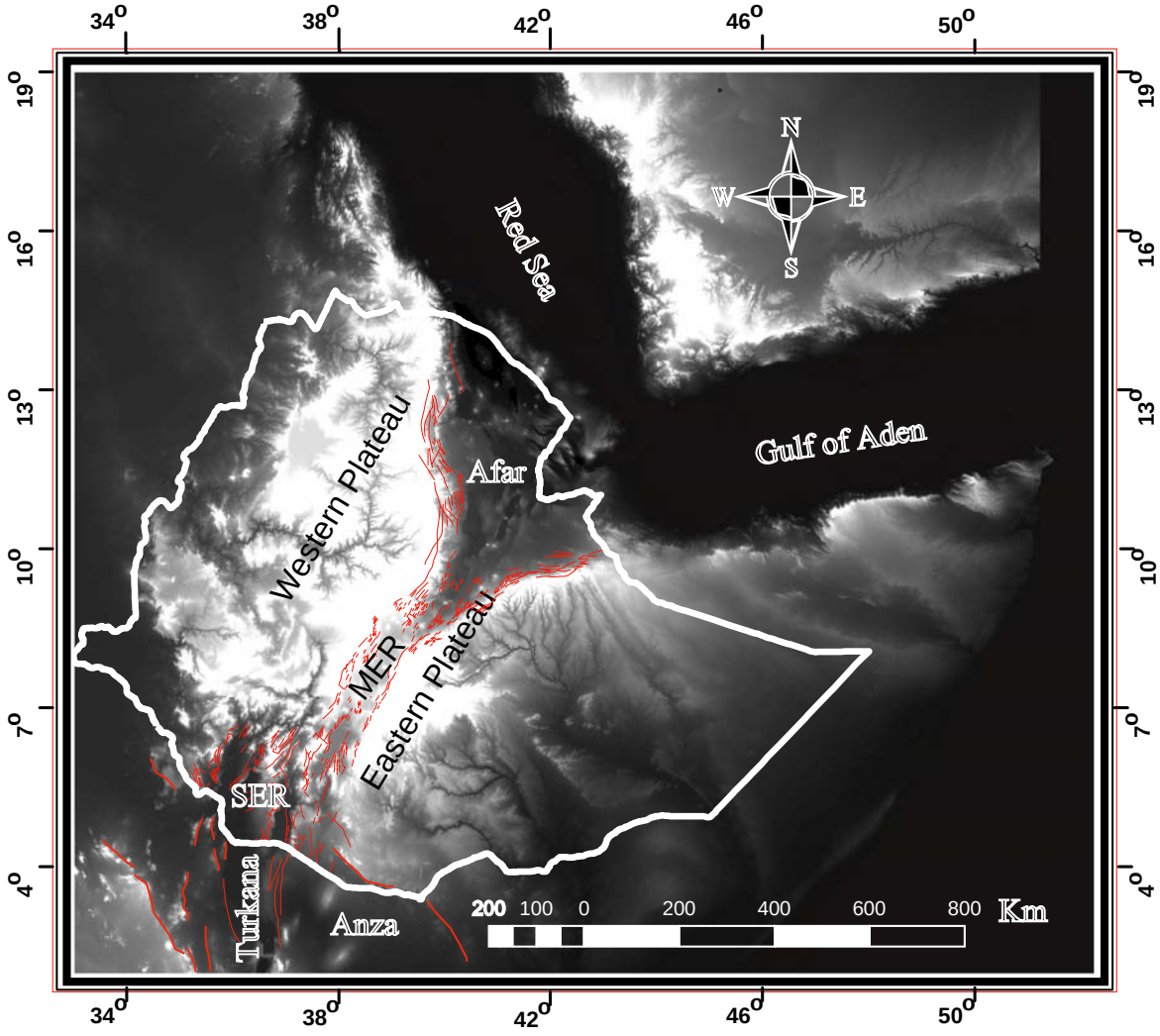

Figure 2.4: Digital Elevation Map of Ethiopia and surrounding regions showing the rift from northeast to southwest. Border faults and en echelon fault systems within the rift floor are shown in red on the DEM map.

Geological, geophysical and geochemical studies suggest that the Ethiopian flood basalts and rhyolites that are up to 2 km thick in places were erupted during the Oligocene around 31 Ma mostly in the southern Red Sea region (Hoffman et al. 1997; Pik et al., 2003). Volcanism in the southwestern part of Ethiopia is believed to have been less widespread but it probably related to the activity in the north during the Eocene (45-39 Ma) (Ebinger et al., 2000). This activity was then followed by the eruption of the Ethiopian –Yemen flood basalts or Trap series between 31 and 29 Ma (Baker et al., 1996; Hoffman et al., 1999; Utkins et al., 2002; Wolfenden et al., 2004).

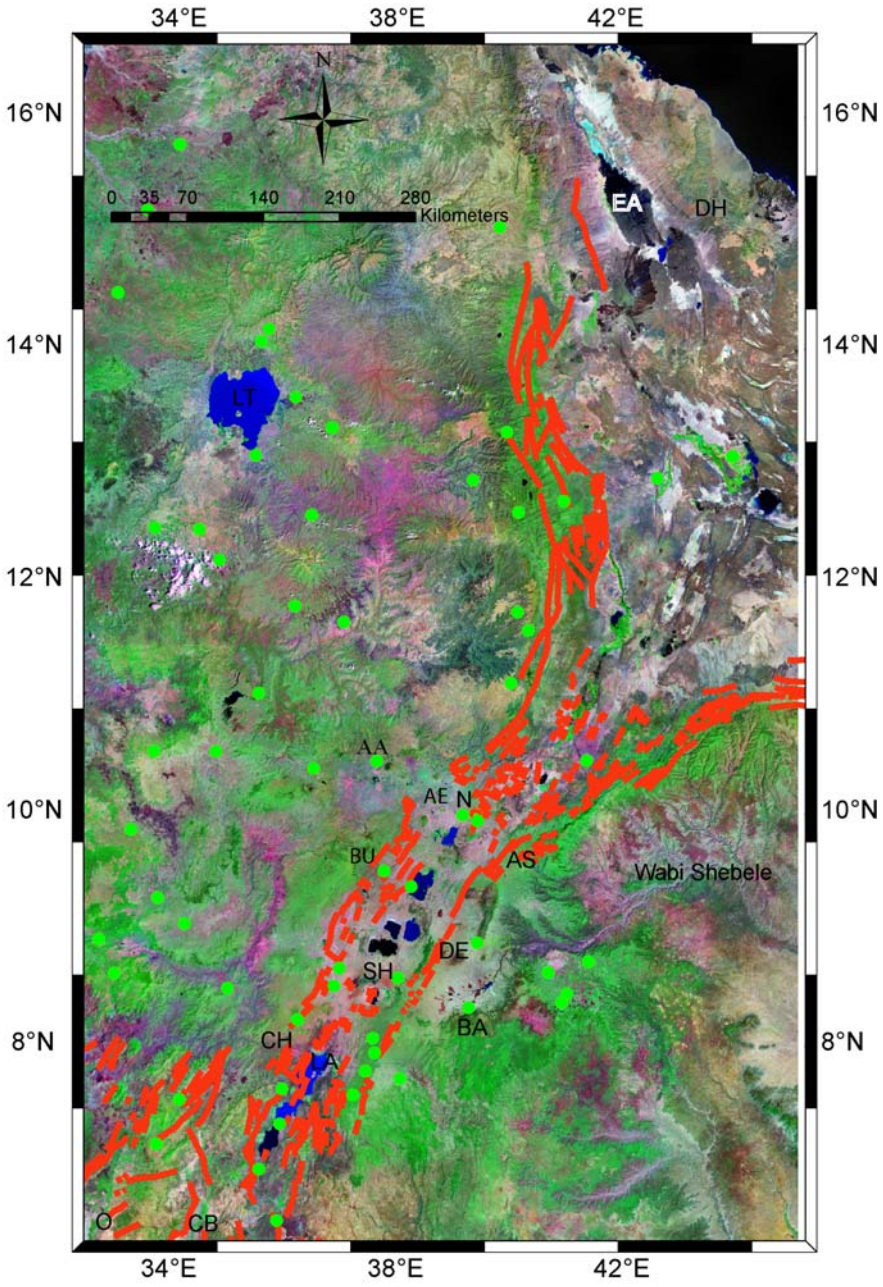

Figure 2.5: Landsat image constructed using Bands 7, 4 and 2 displayed, showing the different fault patterns and displacement form and accommodation or transfer zones characterized by offset and arcuate shape and small displacement. Different localities are: LT =Lake Tana, AA=Addis Ababa, AE = Addis Ababa –Debrezeit Embayment, BU= Butajira boarder fault, CH= Chencha, DE= Degaga Fault zone, AS= Asela-Sire Fault zone, N=Nazreth , LA= Lake Abaya, BA= Bale mountains, EA= Erte Ale, DH= Danakil horst, O= Omo, CB= Chew Bahir, CO= Corrbetti, GE=Gedemsa, T= Tulu Moye, D= Dofen, F=Fantale.

Estimates of the volume of basaltic material erupted ranges from 250,000 km^3 to 10^6 km^3. These rocks covered present-day central Ethiopia, the Southern Arabian peninsula, Djibouti and part of Somalia (e.g. Mohr, 1983; Courtillot et al., 1999; Pik et al., 2003; Rogers, 2006). Rogers (2006) argues that magma migration from southern Ethiopia to northern Tanzania is a consequence of plate motion over the East African plume, while magmatism in northern Ethiopia resulted initially from the impact of the Afar plume. In Ethiopia, these flood basalts rest on basement rock formations and Paleozoic and Mesozoic sediments such as the Abbay basin on the Western plateau and the northwestern Ogaden on the Eastern plateau.

The axial direction of the Ethiopian rift is characterized by right offset of en echelon faults and volcanic centers. These volcanic centers are either take the form of volcanic complexes (e.g., Aluto and Bora) or calderas such as Corrbetti, Tulu Moye, Gedemsa, Dofen and others located further north in the MER (Fig. 2.6). Some of these geologic features are considered to be volcanic segments initiated by magma injection in the form of dikes (Ebinger and Casey 2001; Kendall et al., 2005).

2.4 Geophysical Data

Previous wide-angle refraction seismic studies carried out in Afar indicated a very thin crust (Berkhemer *et al.* 1975; Makris and Ginzberg 1987) with sub –Moho velocities 7.4 -7.5 km s^{-1}. Teleseismic, seismic anisotropic and tomographic studies (e.g. Bastow et al. 2005, Kendal, et al., 2006) have revealed anomalous crustal structures in Afar and along the northern MER. All these studies interpreted this anomalous crust due to high temperature upper mantle material.

The physiographic expression of the rift is very strong so a good digital elevation map was important in this study. Thus, digital topography data were downloaded from the publicly available Shuttle Radar Topographic Mission 90m data (SRTM90) (http://edcftp.cr.usgs.gov/pub/data/srtm) and locally from 900m Digital Elevation Maps (DEM). In

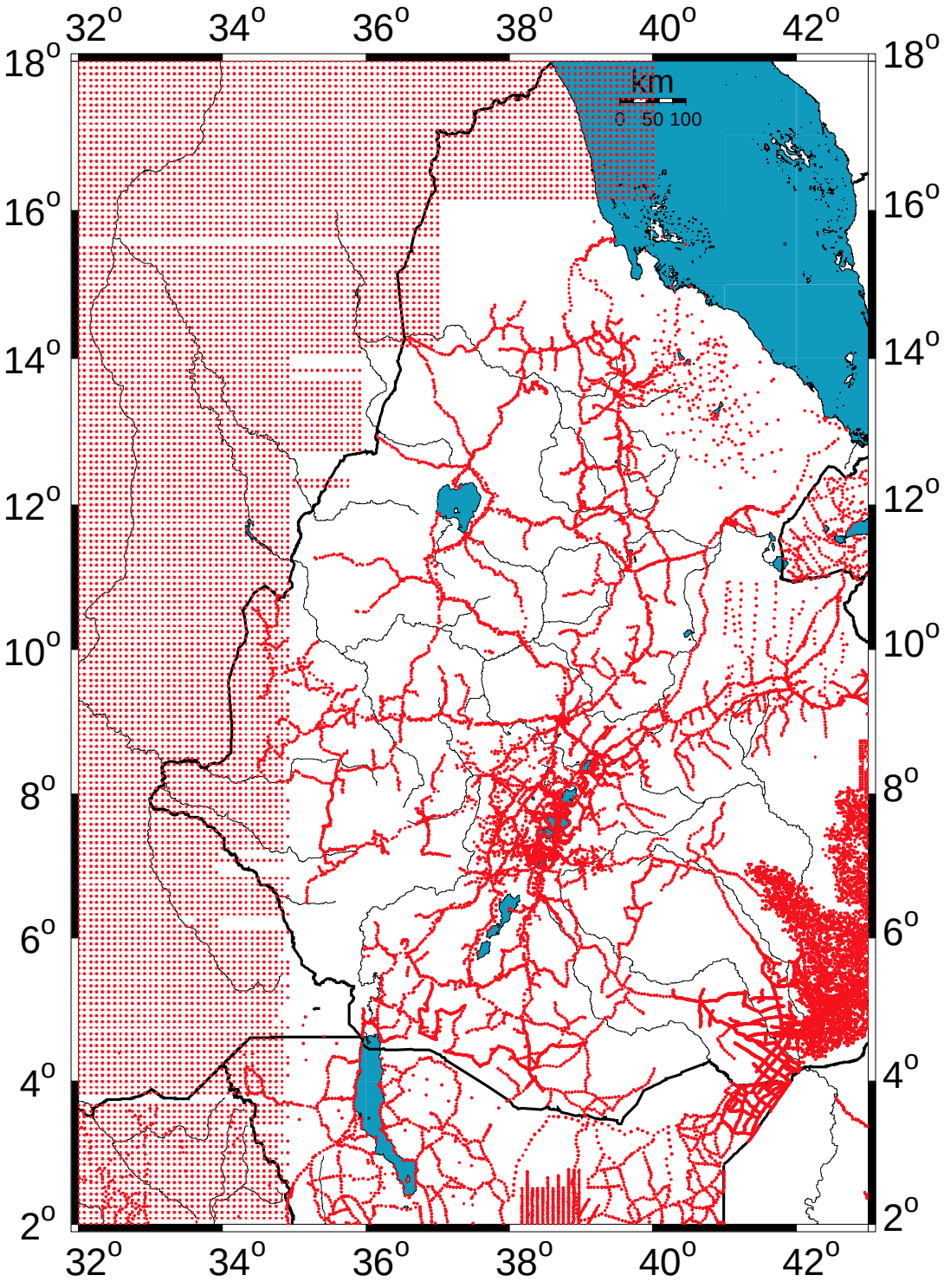

Figure 2.6: Map of the East African region showing the distribution of gravity point data and gridded data (red dots). The gridded data are shown as regularly spaced distribution, whereas the point data distribution is uneven and follows main roads, trails and sometimes based on profiles.

addition, satellite imagery is useful in helping define structural trends and spatial relationships. Thus, Landsat 7 ETM+ obtained from USGS is used to define fault zones and magmatic segments.

The EAGLE and KRISP seismic experiments provided crucial constraints for our modeling effort. Analysis of the EAGLE seismic refraction data for the axial profile indicate that the Moho depth varies from ~40 km to 26 km (Keller et al., 2004; Maguire et al., 2006) between the MER and the southern Afar region, respectively. The mantle P-wave velocity is ~7.5 kms^{-1} along this profile and crustal velocities vary from <5 kms^{-1} in the sediment/volcanic cover to 6.0-7.2 kms^{-1} in the crystalline crust. These are in general agreement with the results of previous refraction survey studies (e.g., Makris, 1978) in the Afar region and also the receiver function results of Dugda et al. (2005).

A wide range of geophysical data was employed in this study, but gravity data are stressed, and gravity modeling was used as mechanism to integrate as much data as possible into our analysis. Thus, a major effort in this study was to compile gravity data from several sources into a database and conduct a quality control effort to remove questionable data. For this study, gravity data from the Geological Survey of Ethiopia, Petroleum Operations Department (Ministry of Mines and Energy) were primarily employed. Some of these data are confidential, because they were acquired by petroleum companies in some of the basins. Since our interests spanned a large region of East Africa, gravity data from the neighboring countries in the form of grid and point data were obtained from various sources (e.g., National Geospatial-Intelligence Agency, GETECH). Much of the East African data were obtained from database compiled at the University of Texas at El Paso and most of these data are available as point measurement with all principal facts.

This database effort started with the Ethiopian National Regional Gravity Survey Project (ENRGSP) that started in the late 1980s. The main goal of the project is to cover the whole of Ethiopia with an improved and quality gravity data that can be used for various geoscientific investigations of the region. As part of the ENRGSP, a significant amount of data has recently been collected with improved position and elevation accuracy. However, a significant amount of older data acquired by various researchers, institutions and private companies are also available. The similarity and differences of these data need to be investigated as to use for accurate applications in various geoscience studies. Improvements in the data have been attained by the use of GPS instruments and Digital Elevation Maps (DEM) of various accuracies. Merging the older and new data require knowledge of each survey. However in many cases, there are no metadata established as to how the older data were acquired. The quality of much of the regional survey of the country is known fairly well since many of the project participants are still available and well known to the author who was personally involved in many surveys. Thus, I was able to prepare a considerable amount of informal metadata for this study.

During the early stages of the ENRGSP gravity data acquisition, topographic maps (1:50,000; contour interval 20m) produced by the Ethiopian Mapping Authority (EMA) were used for navigation and station location purposes, and elevations were determined using groups of altimeters with a maximum error of 3 meters. Other data (from geothermal projects for example) were obtained from localized surveys using optical leveling instruments. Information is available in some of the annual reports of the Geological Survey of Ethiopia (e.g., Woldetinsae, 2005 and references therein). Elevation calibration of survey base stations was accomplished via ties to triangulation stations and leveling benchmarks. Thus, most of the gravity readings are reliable in terms of elevation accuracy.

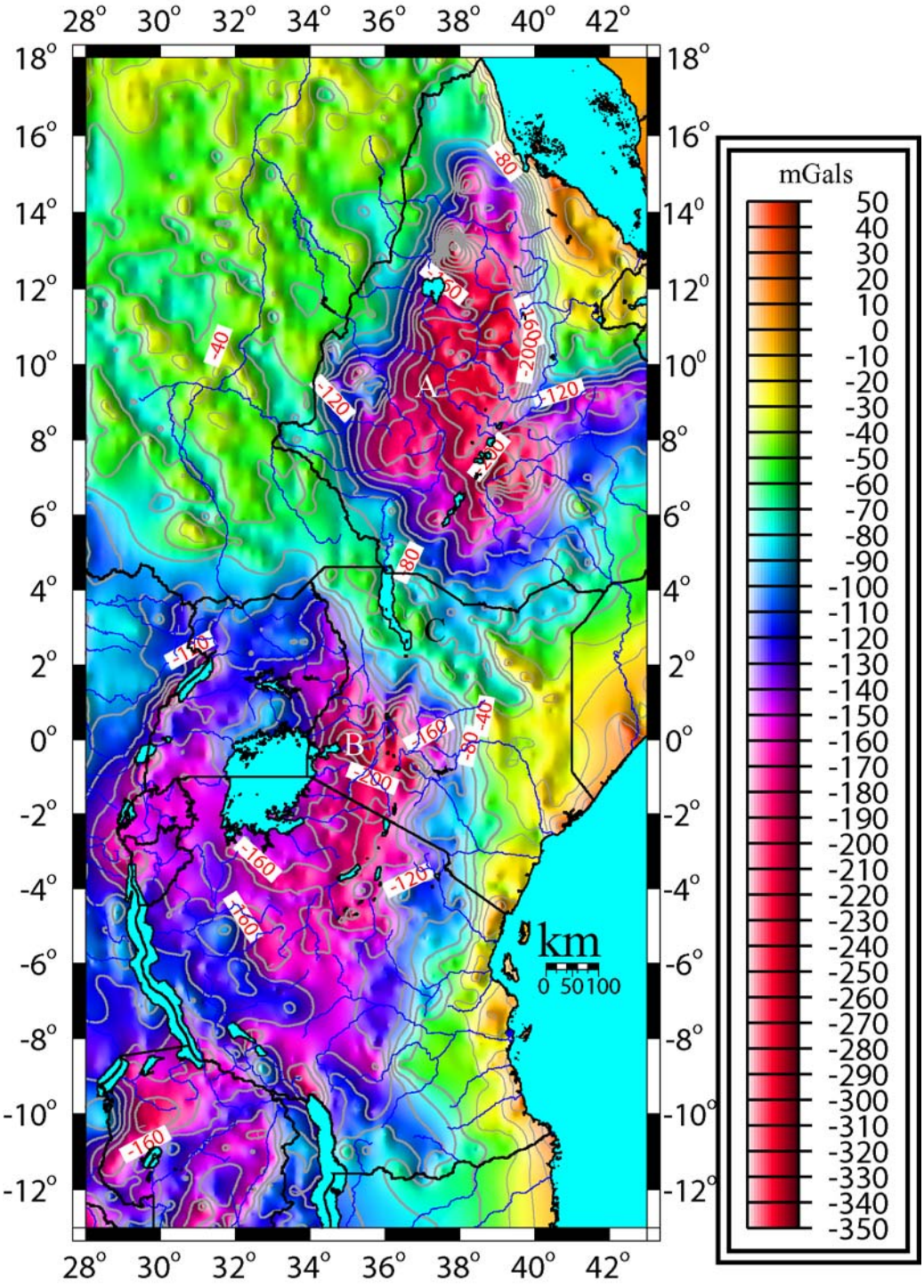

Figure 2.7: Bouguer gravity anomaly map of the East African region from -13° south to 20° north latitudes and from 28° east to 43° east longitudes. Color codes show the gravity values and contour intervals.

The ENRGSP gravity data are connected to the IGSN71 base station at Addis Ababa University via sub-base stations. Other IGSN71 stations with appropriate locations were also employed. In the rift valley region, some older data (~100 readings) were recovered from hard copies but only had coordinates (x, y, z) and simple Bouguer.

In addition to the ENRGSP database (~12,000 readings), about 500 readings were collected as part of the EAGLE project (~500 stations) using GPS instruments such as the Trimble 4000SSE and SSI with sub-meter accuracy in elevation. These stations were at close spacing (1 to 2 km) along the MER and the northern MER in the axial direction and were also added to the database.

In the Ogaden basin region, a large amount of industry data (~23,000 readings) was available on a proprietary basis. These data were also tied to the IGSN71 ((Morelli, 1974) base station at Addis Ababa University via sub-base stations and had high-quality elevation values. With the addition of these industry data, the database for Ethiopia totaled about 40,000 readings.

In addition to the database for Ethiopia created as part of this study, additional data for my regional analysis comes from the University of Texas at El Paso (UTEP) database that is comprised of more than 60,000 data points from East Africa. Also, gridded data for the Sudan region were obtained from GETECH. We ensured that all these data were tied to IGSN71 stations in each of the countries where data were obtained (e.g., Mariita and Keller, 2007). In total over 120,000 points and gridded data were used for our regional analysis.

It is obvious that a gravity database such as created here contains some data that produce artifacts that are not true anomalies due to geologic features. These spurious values may be caused by a number of factors, and prior to any analysis, it is essential to understand them and correct them if possible. The major source of error in this database can be attributed due to error in elevation measurements (Altimeters, GPS and optical leveling were employed in most of the

data point measurements), and other sources of errors include calibration and meter drift (Worden gravity meter, Lacoste and Romberg, GNU-KV, GAG-2, GAG-10 and Scintrex were employed in Ethiopia), instrument reading error, and typographic or computational errors.

To the extent possible, the data we compiled were revised regarding the underlying sources of errors when they could be identified and reference system. Almost all of the data were tied to the IGSN71 (Morelli, 1974), and only data that could be related without any doubt to this reference system were included in the database. The data were assigned a unique identification number based on the source of the data. Environment Systems Research Institute, Inc. (ESRI) Geographic Information System (GIS) and mapping software was used for analyzing the discrepancies and similarities of the datasets individually as well as together. Shape files were prepared for plotting based on database attributes. These attributes are the longitude, latitude, elevation, observed gravity, free air anomaly, simple Bouguer anomaly, terrain correction and complete Bouguer anomalies. The Geostatistics analysis and 3D spatial analyst tools were used to plot the stations and evaluate the statistical variation in the dataset. Assuming normal distribution in the data, frequency histograms were generated for the dataset and discrepancies outside the minimum and maximum value of the plot were regarded as inhomogeneous. These data were then selected and exported as a different dataset for further analysis. As expected, many of these selected data were found to have either too low values or to high values relative to the trusted data in a particular location. Again these data were plotted at their respective locations and analyzed consistency with digital elevation data and known geology. Much of the problem was with the Ethiopian regional gravity data that contains different sources but no metadata. Therefore it was necessary to analyze each source of data separately before merging.

By checking and editing the data based on root mean square error (RMS) values, it was possible to compare the unedited and edited data. RMS error values that were as high as 45

mGals were reduced to 2.14 mGals after editing spurious values. The evaluation process was mainly carried out on attributes such as observed gravity values, elevation values and complete Bouguer values and compared with adjacent values that were considered as trusted data. Also, gridding and contouring using the spatial analyst tools of ArcGIS were employed to identify problematic data areas by examining areas with isolated dense contours. The quality of the data was checked again by regridding and contouring after editing.

Data close to the boundary between regional data and the Ogaden data from industry were examined. Differences ranging from ±2 to ±13.4 mGals were observed. Spurious values in the ENRGSP were edited out and the statistical evaluation was made again. When lower RMS values resulted, the edited data were output into a new database which was used to generate the grids and maps used in this study. Our analysis shows inconsistency in the data is mainly due to elevation determinations. However, this editing effort resulted in the removal of ~250 readings from the new merged database for Ethiopia and the final distribution of data is shown in Figure 2.6.

The Bouguer gravity anomaly values employed in this study were prepared using the 1967 international gravity formula (Morelli, 1967) with sea level as a datum and a reduction density of 2670 kg m^{-3}. Terrain corrections were performed using Hammer charts (Hammer, 1939) and tables to outer zone M manually at the outset of the ENRGSP project. The terrain correction process was later verified using the Geosoft terrain correction software based on SRTM90m DEM data. Most of the corrections were below 1 mGal with the exception of mountainous regions that attain a maximum of 10 to 20 mGal.

Since our data are in the form of distributed points and lines, we employed the minimum curvature technique for the gridding process (e.g. Briggs, 1974). The contour interval of the

maps produced by this study is 10 mGal, and the resulting Bouguer anomaly map is shown as Figure 2.7.

The gravity points used to construct the gravity profiles for modeling were extracted from the database using a program developed at UTEP. A search radius of 10 km was employed to extract the data. The data points extracted were edited as to favor those points that were closest to the straight-line profile between the starting and end points entered.

2.4.1 Regional Gravity Field

The regional gravity data in the EARS (from Kenya to Ethiopia) and the adjacent plateaus have been compiled by a number of authors (e.g., Alemu, 1992; Fairhead, 1976; Woldetinsae, 2005; Mahatsente, 1999; Tessema, 2004; Simiyu and Keller, 1997; Mickus et al., 2007; Mariita and Keller, 2007) to some extent either for particular region or in smaller areas and with small amounts of data. Our compilation is based on a larger database and includes large areas throughout East Africa and the Horn of Africa including the southern part of the Red Sea rift. Figure 2.6 shows the gravity data distribution within the study area. Figure 2.7 shows the regional Bouguer gravity anomaly map of the entire EARS and its adjacent plateaus. In this regional context, the main anomalies are classified as the Ethiopian dome (A), the Kenyan dome (B), the Afar triple junction, and the Anza graben area (C) (Fig. 2.7).

The highest amplitude (≤-300 mGal) Bouguer gravity minimum observed in the region coincides with the Ethiopian dome (Fig. 2.7). This gravity low is correlated with the Ethiopian dome where the outline of the high altitude in the region exists (Figs. 2.2 and 2.3). This gravity low coincides with large parts of the western part of the Ethiopian dome, located northwest of Lake Tana. In general the gravity low coincides with both the western and eastern plateaus of Ethiopia. The gravity low associated with the plateaus suggest that either the region was uplifted

as a result of a mantle plume impingement beneath the high topographic feature (e.g., Ebinger and Casey, 2001; Rogers, 2006; Furman, 2006; Pik et al. 2006) or that the uplift may be due to an intrusion complex (e.g., Kieffer et al., 2004), contributing to low-density crustal features.

The other distinct gravity minimum observed in the Bouguer gravity anomaly map is associated with the Kenyan dome, part of Uganda and most of Tanzania (Fig. 2.7), including the region around Lake Victoria. This gravity anomaly is also the area associated with the southern part of the Western and Eastern arms of the EARS. This long wavelength gravity minimum has been suggested to be due to a typical mantle feature with superimposed short wavelength anomalies in the crust (Swain et al., 1994) that resulted in a modified crust.

One of the basic problems in interpretation of the Bouguer gravity anomaly lies in the separation of the regional component, a long wavelength anomaly commonly caused by a deep density contrast. Furthermore, in order to enhance gravity anomalies of interest, filtering techniques can also be employed. Regional-residual separation is one of these commonly applied filtering techniques. Thus, in order to separate those short wave length anomalies caused by shallow structures or features, we applied a regional-residual separation method. There are a number of regional residual separation techniques. These include, polynomial fitting, wavelength filtering, spectrum and upward continuation methods. We experimented with all of these techniques and found that upward continuation worked adequately. Residual gravity anomaly maps were produced by subtracting the upward continued grid from the Bouguer gravity anomaly grid. The final results are presented as grid contour maps, which are included in the following sections.

Produced from existing data, the residual gravity anomaly field for Eastern Africa is shown in Figure 2.8. In the residual gravity anomaly map, the EARS is clearly distinguished

from the surrounding regions. In this map most of the subdued anomalies are clearly depicted and are coincident with the regional structural grains. The Anza graben, with a northwest southeast trending anomaly, appears as a regional positive anomaly compared to the Ethiopian and Kenyan domes. The Afar triple junction is marked by a funnel shaped positive anomaly associated with a high-density thin crust of mostly basaltic composite due to asthenospheric upwelling. There exist relative low residual gravity anomalies in places in Afar, which may be due to localized sediment accumulation. Drilling results from Tendaho graben (central Afar) and Red Sea indicated sediment thickness exceeds 1.5 to 3 km intercalated with lava flows (e.g. Bosworth et al., 2005). Recent assessment of young rift evolution due to asthenospheric upwelling beneath the Kenyan and Malawi rifts attests to the existence of thick sediments (Chorowicz, 2005), where both rifts are demonstrated to contain up to 3 km thick sediment.

The coastal region of east Africa is characterized by a gravity high that merges with the Anza graben gravity high in the area of the Lamu embayment of eastern Kenya (Figs. 2.7 and 2.8). The positive anomalies along the coastal margin (Fig. 2.8) are primarily due to a thin crust that was attenuated during the rifting processes related to the break up of Gondwanaland during the Permo-Triassic.

2.4.2 Gravity Field of the Ethiopian Region

The main focus of this study is a relatively detailed analysis of the gravity field of the region between 2^{o} to 18^{o} north and 32^{o} east to 43^{o} east. A detailed Bouguer gravity anomaly map

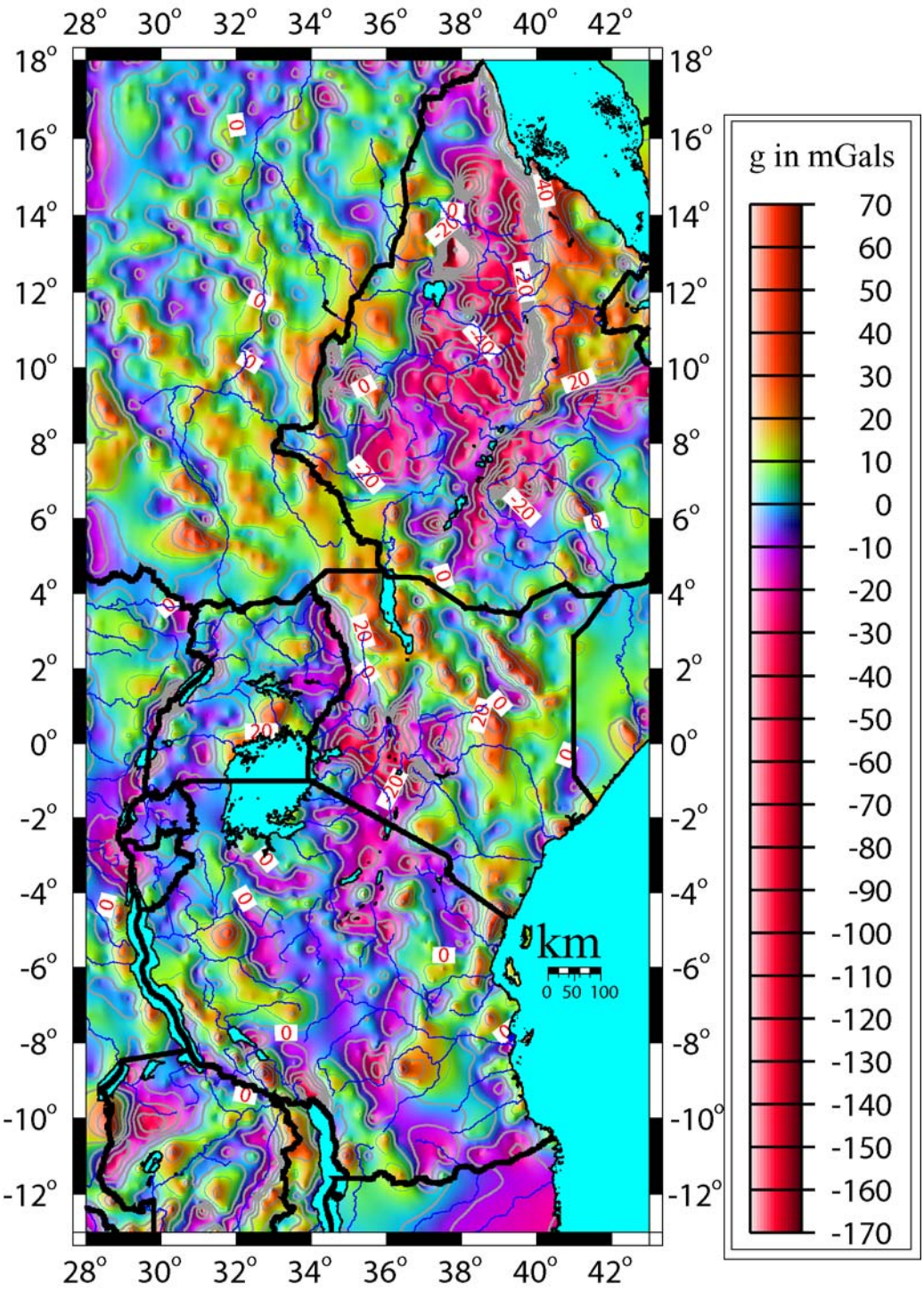

Figure 2.8: Residual gravity anomaly map of East African region, showing local structures with shortwave positive anomalies that are associated with volcanic centers.

of the region is shown in Figure 2.9. This map shows that a large part of the western plateau in Ethiopia is characterized by a long wavelength gravity low. It encompasses a large area of Ethiopia from Chencha (at about 37^{o}E and 6^{o}N) in the southern part of the western plateau along the Gurage highlands (at about 38^{o}E and 8^{o}N) within the western margin of the MER, and the Blue Nile area further north of Lake Tana. The western plateau is depicted as a northeast-southwest trending elliptical gravity low following the plateau elevation. The other distinct low gravity anomaly is associated with the eastern plateau. Much of the elevation are more than 3000 meters above sea level, are associated with a broad negative anomaly. The area of the eastern plateau is smaller than the western plateau; however, the gravity anomaly, with an amplitude value of <-240 mGals, is nearly comparable to the central part of the western plateau gravity anomaly values. Figure 2.11 shows the residual gravity anomaly map of the Ethiopian rift and adjacent areas. The upward continued map produced for the region using a cut-off wavelength of 50 km, is shown in Figure 2.10. The residual gravity anomaly map of the region (Fig. 2.11) is produced by subtracting this upward continued grid (Fig. 2.10) from the Bouguer gravity grid (Fig. 2.9). The Sudan area is largely dominated by northwest-southeast trending short wavelength relative gravity lows and highs. Relative shortwave length gravity low anomalies within the Sudanese plain are associated with Cretaceous rift basins.

For a better understanding of lithospheric scale and crustal structure variations, it was necessary to apply filtering to the Bouguer gravity data. Among the filtering techniques applied to this data are band pass filtering and low pass filtering. The term filtering can be applied to any of the various techniques that are used to separate anomalies on the basis of their wavelength or trend (e.g., Blakely, 1996). The Bouguer gravity grid was prepared for the analysis using fast Fourier transform (FFT). The data were transformed from the space domain to the wave number domain (frequency). A filter was designed based on to either pass or reject the desired anomaly.

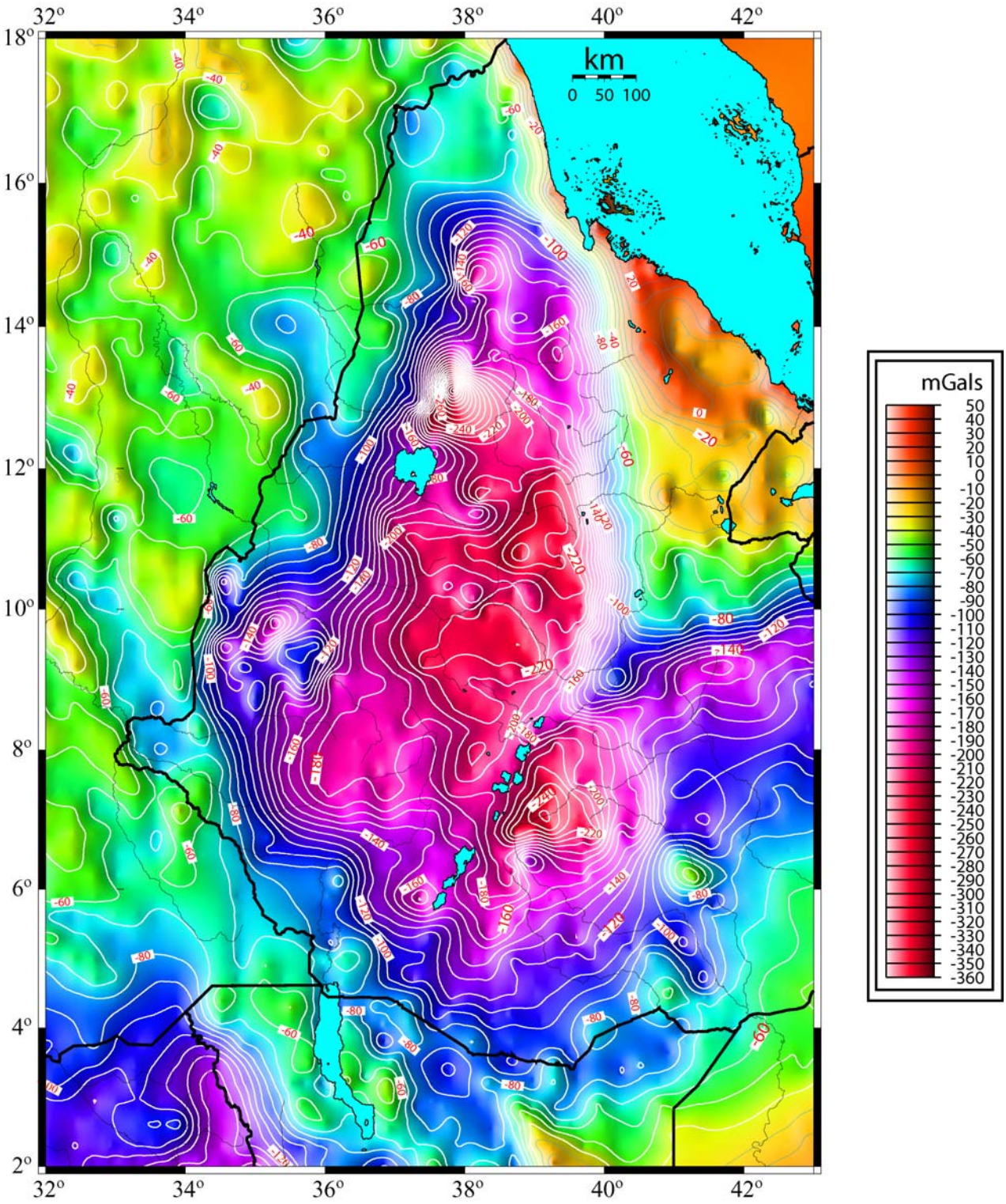

Figure 2.9: Bouguer gravity anomaly map of the Ethiopian rift and adjacent plateaus including the Turkana region and Afar triple junction. The two plateaus are shown as gravity lows compared to the rift regions and the Sudan rift basin

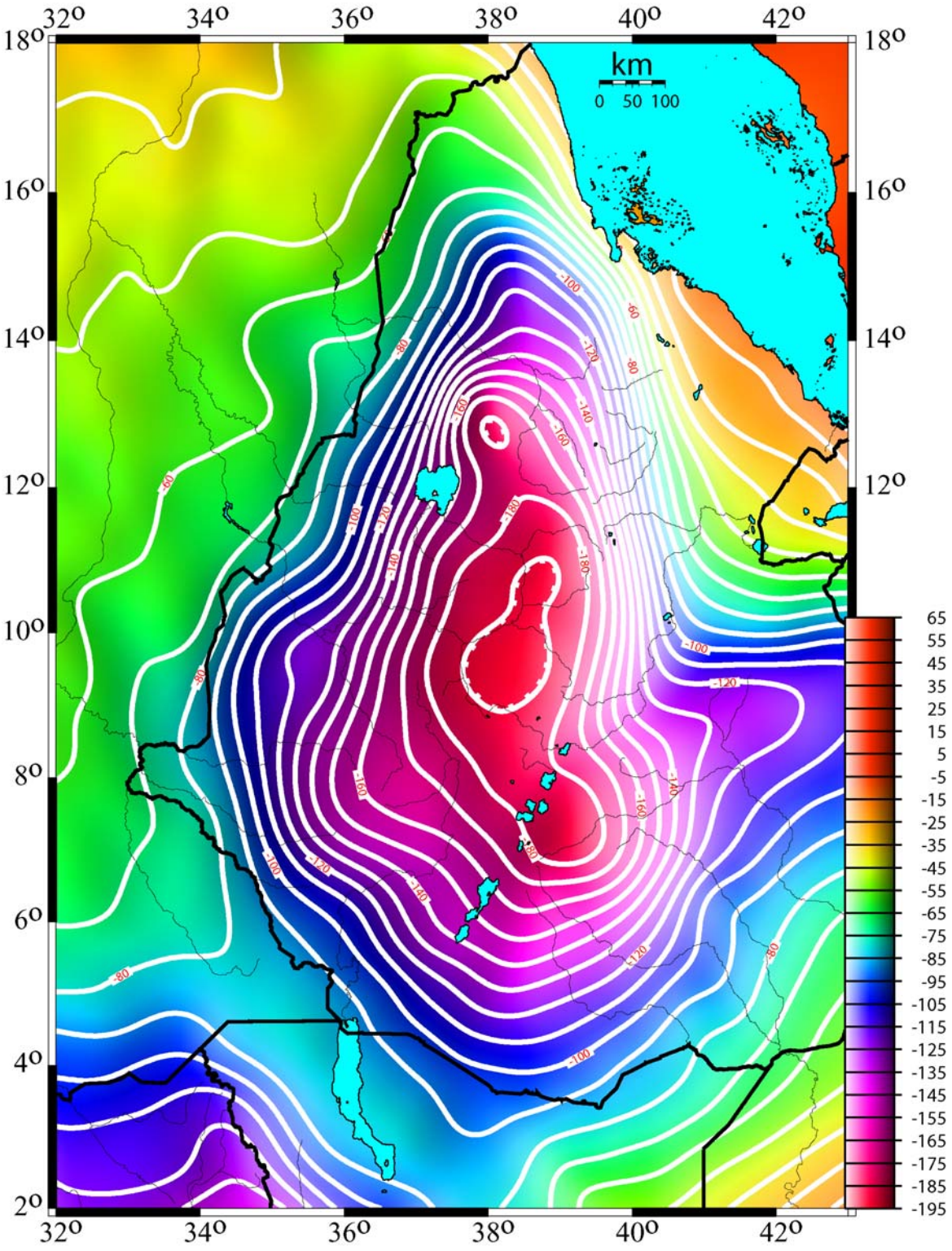

Figure 2.10: Upward continued gravity anomaly map of the Ethiopian rift and adjacent plateaus showing a broad low wavelength anomaly associated with the western and eastern plateaus and the MER. The cut-off wavelength is 50 km.

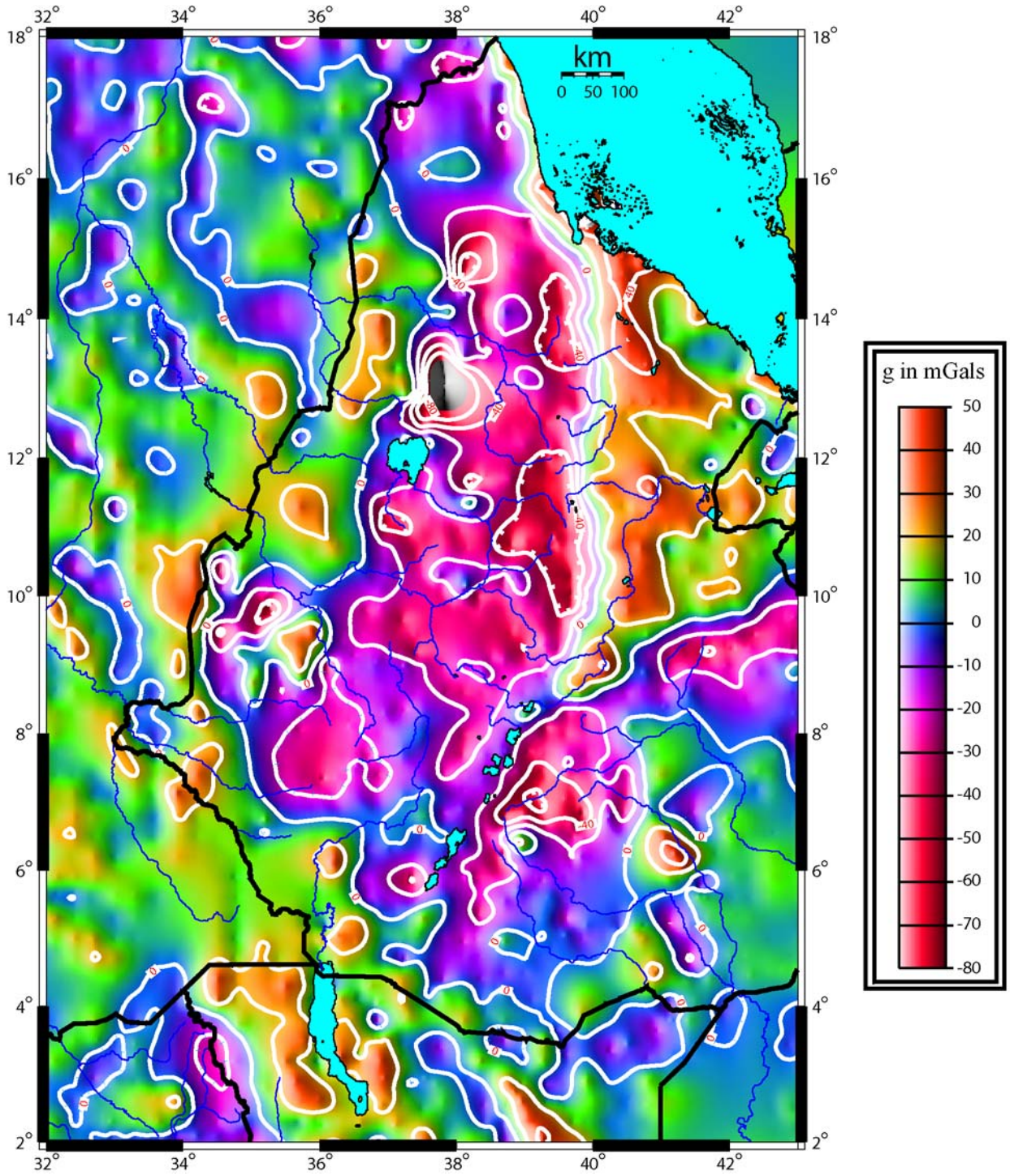

Figure 2.11: Residual gravity anomaly map of the Ethiopian rift and adjacent plateaus, clearly showing the segregation of the rift areas from the plateaus.

The result was then transformed back to space domain. Figure 2.12 shows a band pass filtered anomaly map of the study area. The wavelengths that were allowed to pass vary between 50 and 1000 km. Anomalies above 50 km tend to emphasize shortwave length structures associated with crustal features. Anomalies associated with longer wavelengths of ≥1000 km are due to deeper features associated with the upper mantle and Moho topography. Figure 2.12 emphasizes many features in the region. The western plateau is associated with low values with a northeast-southwest elongation. High amplitude negative gravity anomalies appear to be coincident with the mountainous regions in the southwestern part of Ethiopia, the Blue Nile (Abbay basin) east and northeast of Lake Tana, which all are associated with gravity minima. The rift is outlined by troughs of contour lines that are open towards Turkana in the SER area and the Afar regions in the NMER. The apex of these anomalies coincides with the MER in the lakes region. Though smaller in extent compared to the western plateau, the eastern plateau is associated with a negative anomaly comparable to the Western plateau anomaly in magnitude.

The Afar triple junction shows large positive anomalies in a northeast-southwest trend coincident with the Ethiopian rift section in this area. The Erte Ale (EA) region is shown as a positive anomaly with a north-northwest south-southeast direction and is separated from the southern Afar anomaly by a subdued region. This subdued gravity anomaly in the southern Afar may mark the termination of the Red Sea rift in this region. The Danakil horst is shown as a relatively negative anomaly in the region between Erte Ale and the Red Sea. The other relative positive anomaly lies within the Turkana rift and shows nearly a north-south positive anomaly coincident with Lake Turkana. The other interesting feature is the relatively positive anomalous region with a northwest–southeast trend starting from the Ogaden basin along the Wabi Shebele river basin. This may be an older structure that may extend into the Abbay basin on the northwestern part of the western plateau before it is modified by the recent Ethiopian rift.

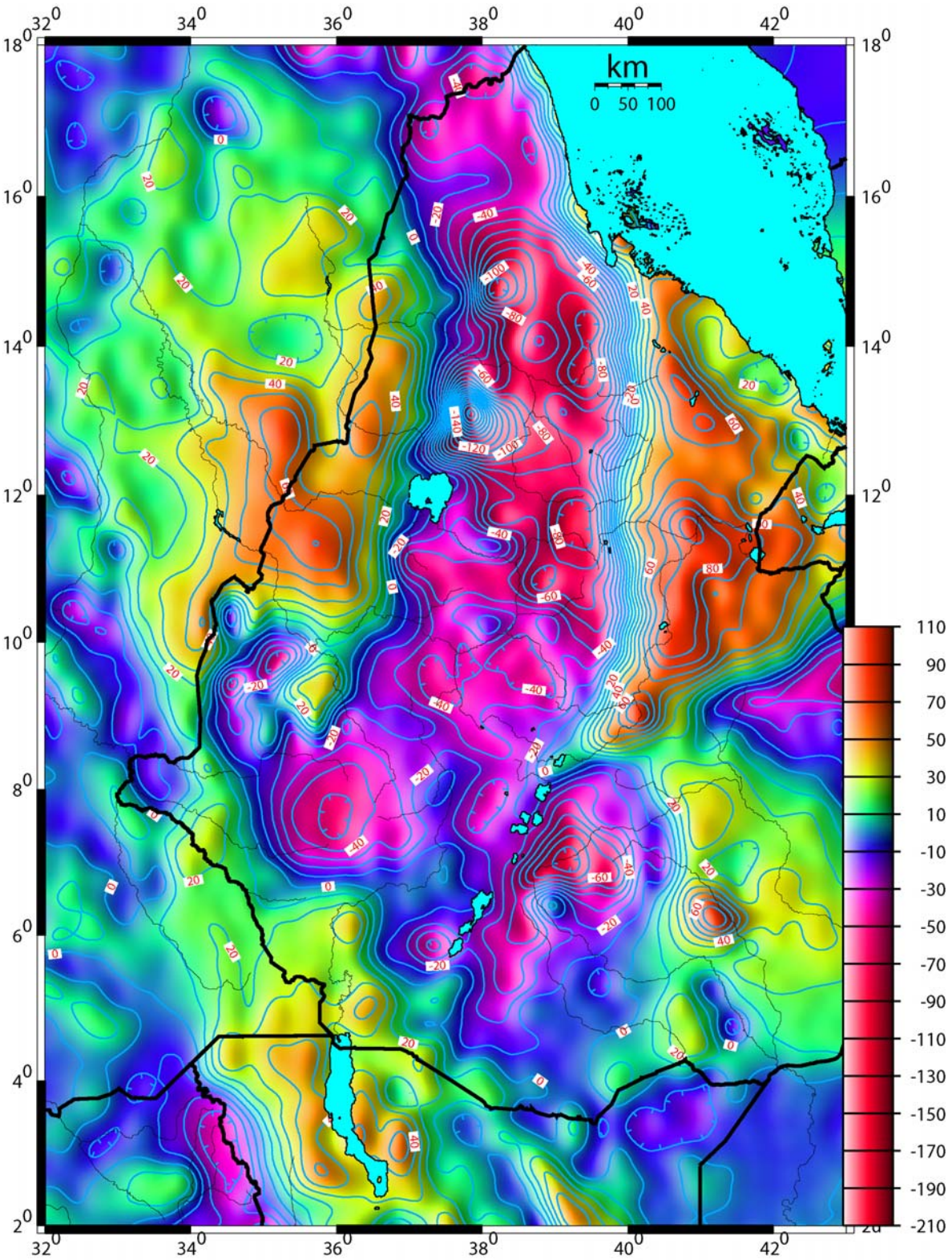

Figure 2.12: Band pass filtered anomaly map of the Ethiopian rift and adjacent areas. The bands are between 50 and 1000 km.

Figure 2.12 shows a band pass filtered map of the study area with a bandwidth of 50 to 1500 km. In this map, most of the major features, such as the western and eastern plateaus remain segregated from the relatively positive anomaly regions of the Afar triple junction and the Turkana region and/or the Anza graben. The high amplitude anomalies shown in Figure 2.13 are masked by the effects of deeper structures as shown in Figure 2.12.

Low pass filtering techniques are another aid in recognizing deeper structural effects. Therefore, we tested various cut-off wavelengths for the Bouguer gravity anomaly data in order to analyze the effect of deeper structures. Figure 2.13 shows a low pass filtered map of our study area with a cut-off wavelength of 200 km. Figure 2.13 highlights the broad long wavelength negative anomalies associated with much of the western plateau. However, the eastern plateau is shown as a broad negative gravity anomaly with near equal amplitude to the western plateau. The MER is depicted as trends of coherent gravity contours open to both the Afar and Turkana regions with an apex at about the central portion of the MER near Lake Koka. Superimposed on the long wavelength negative anomalies are high amplitude short wavelength negative anomalies associated with the Gurage highlands (GH) near the MER, the Chencha (CH) area in the south, and on the eastern plateau associated with the Bale (BA) mountains. Further to the northwest near Lake Tana the high elevation region is associated with the apex of negative anomaly in the region. The other interesting feature of the eastern plateau is the relatively elongated, nearly east-west trending negative anomaly associated with the eastern plateau south of Afar. The Afar triple junction area and the Turkana rift are depicted as short wavelength positive anomalies. However, the Afar region shows a maximum positive amplitude in the region associated with the Erte Ale (EA) volcanic region and/or the Danakil depression. The Anza graben shows a similar anomaly to the Sudan basins, which may indicate that they are simultaneous rift structures with similar lithospheric characteristics.

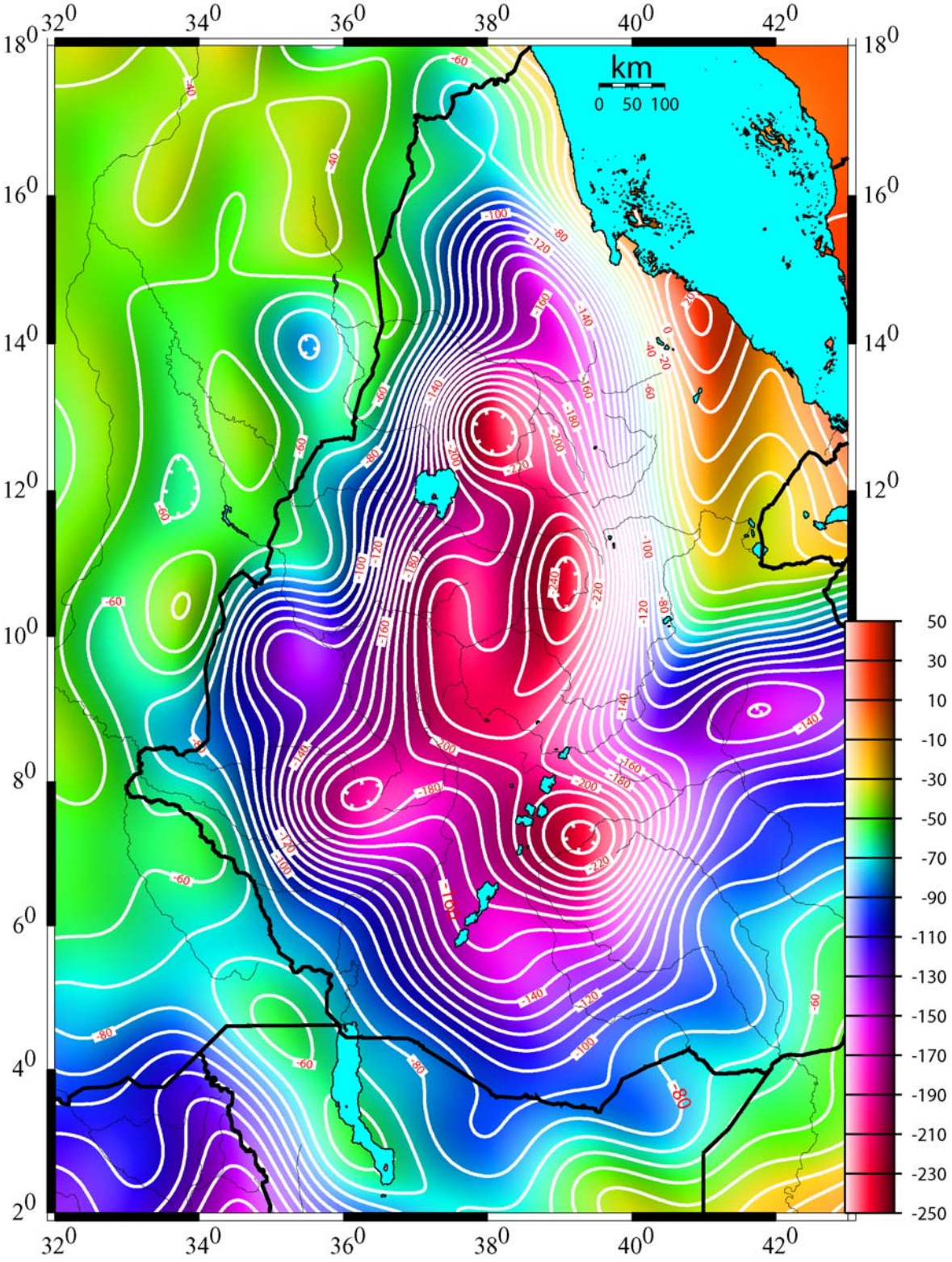

Figure 2.13: Low pass filter map of the study area with a wavelength cut-off of 200 km.

To further investigate the deeper effect, we constructed several low pass tests for our analysis. Figure 2.14 shows one of the low pass filtering results with a cut off wavelength of 500 km. In this map much of the Ethiopian dome is characterized by a nearly north-northwest and south-southeast concentric negative anomaly. The apex is associated with the central part of the western plateau. This minimum gravity apex indicates that deep effects associated with the Ethiopian dome comprise a large area. The Anza graben and the Red Sea area appears to be a structural divide for the Ethiopian dome and its surrounding areas. To the west the Sudan basins appear as a relative positive with a slight anomaly variation across the region. These relative positively anomalies associated with the Turkana and Afar regions could be the expression of a thin crust, resulting from crustal attenuation due to deeper mantle effects.

For detailed discussion we have divided the rift valley region into three sections that are explained in turn below.

2.4.2.1 The Afar Triple Junction

The Afar triple junction, commonly known as the Afar Triangle, is a funnel shaped region characterized by recent volcanism and located at the intersection of the three great rifts: Red Sea rift, the Gulf of Aden rift and the Ethiopian rift (Figs. 2.1, 2.2 and 2.3). The splitting away of Saudi Arabia from Africa formed the two rift systems: the Red Sea, with a northwest trend, and the Gulf of Aden, with a northeast southwest trend, and developed ocean floors in both. From a plate tectonic point of view, these three rift zones are a continuation of the break up of Gondwanaland, justifying extensional processes as studied by various authors (Chu and Gordon, 1999; Bilham, 1999; Fernades et al., 2004).

The gravity field of the Afar triangle is marked by a broad positive anomaly with an amplitude of ≥40 mGals, and its apex is centered on the Erte Ale or Afar depression zone (Fig.

2.14). This broad positive anomaly in the triple junction widens towards the ridges in both directions (west and southeast), creating a funnel shaped anomaly, which narrows towards the Ethiopian rift. The Afar triangle is a wonderful region to examine uplifted asthenospheric upwelling and zones of incipient volcanism (e.g., Tiberi et al, 2005; Ritsema and Van Heist, 2000). The Afar triangle is bounded by distinct topographic high areas of the northern part of the western plateau and includes the Danakil horst located on the western part of the southern Red Sea. These regions are areas of seaward dipping volcanic rift margins, which bound the Oligocene Red Sea rift from the west as an escarpment (Wolfenden et al., 2004). The coastal region of the Red Sea exhibits a relative regional gravity high coincident with the coast. The Erte Ale (EA) or Danakil depression and the coast of the Red Sea are separated by the Danakil horst, which is characterized by a relative gravity low. This gravity low in the region of the horst could be attributed to low density materials within the horst and its relatively thicker crust compared to the adjacent regions (Earte Ale and Red Sea). The Danakil horst exhibits basement outcrops and has a relatively low-density contrast compared to the volcanics in the region (Fig. 2.15). Thus, this density difference in the region exhibits a crustal structure variation between the nearby basaltic/igneous rocks and the crystalline basement associated with the horst.

The maximum positive gravity anomaly in this particular region lies along the Afar depression or the Erte Ale active volcanic region. This region coincides with the actively spreading center of the Southern Red Sea rift zone. This anomaly zone coincides with the spreading zone suggested by Bosworth et al., (2005) as the new direction of the Red Sea rift axis to join with the Gulf of Aden rift. Present earthquakes (since September 21, 2005) in this region formed a 60 km long and more than 1.5 km vertical displacement, attesting to the active rifting coincident with the Red Sea rift axis onshore in the Afar region.

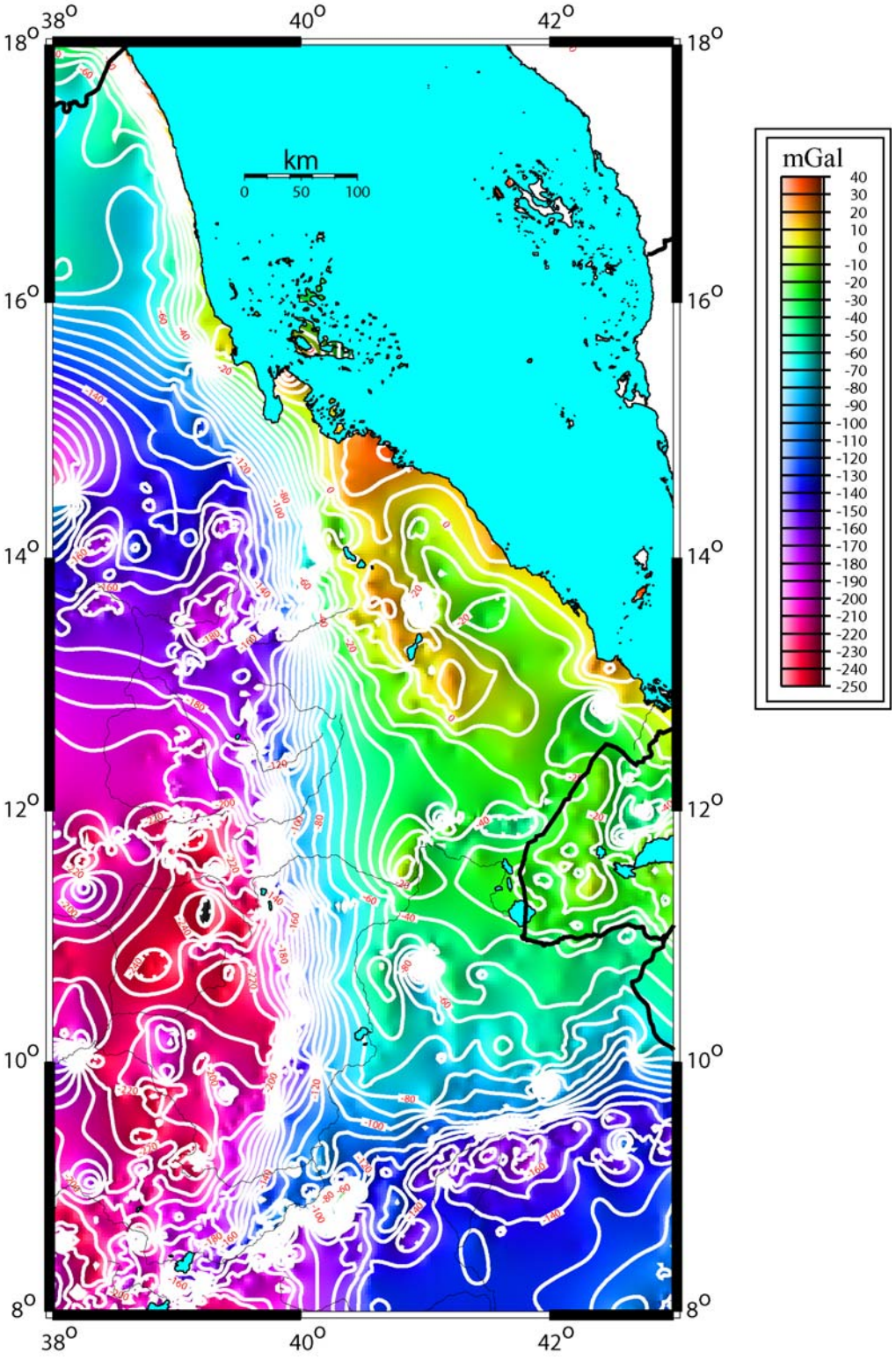

Figure 2.14: Bouguer gravity anomaly map of the Afar triangle region and adjacent plateaus.

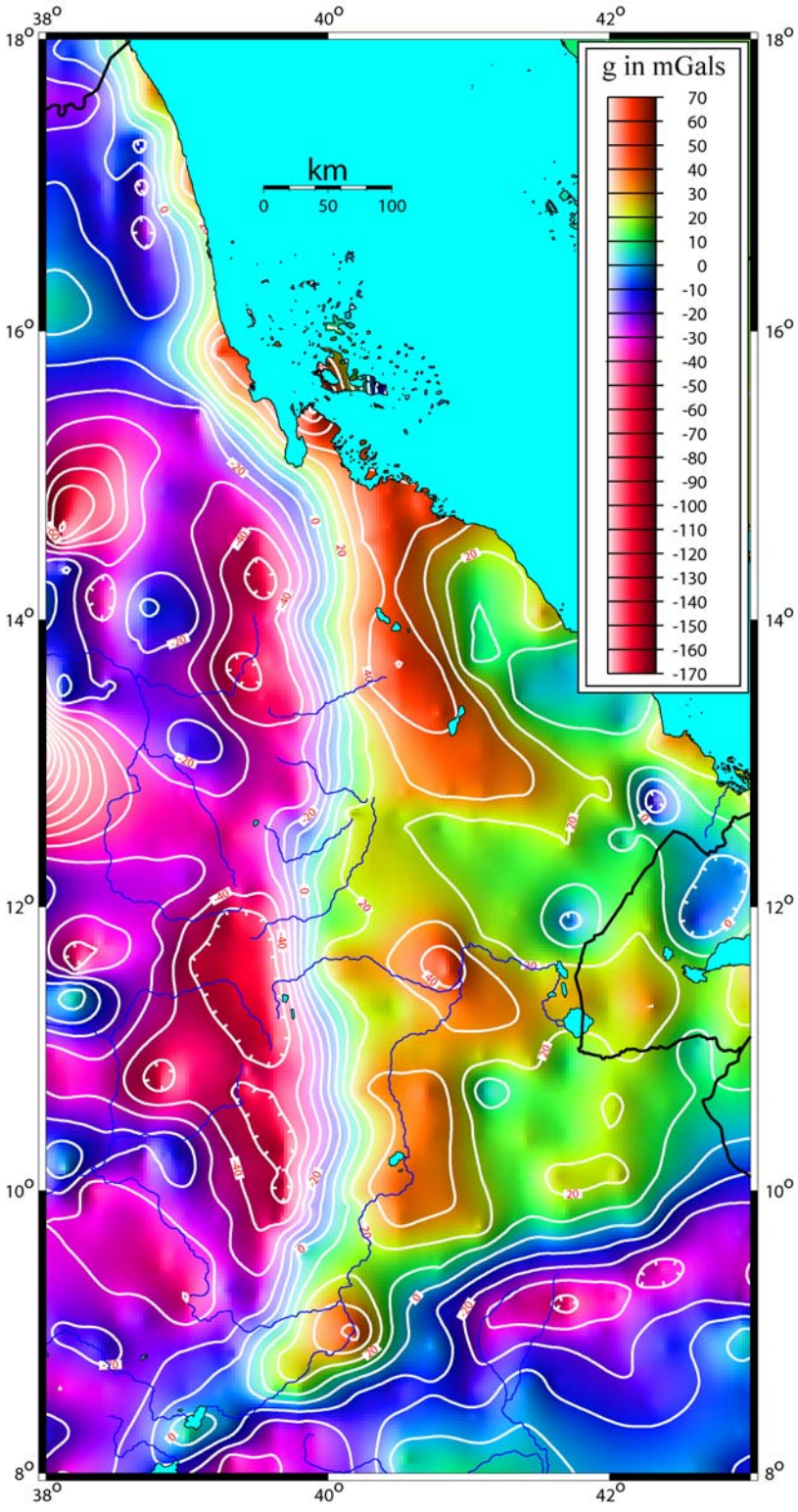

Figure 2.15: Residual gravity anomaly map of the Afar triangle region and adjacent plateaus.

The residual gravity anomaly map for this region (Fig. 2.15), clearly defines both the rift flanks and the different volcanic segments. The Erte Ale (EA) region, with a maximum local gravity high, lies to the north of the triple junction. Towards the southern section of the region, two areas of short-wavelength positive gravity anomalies are clearly delineated. These regions are associated with the magmatic segments in the Afar triangle region. These short wavelength positive anomalies coincide with the different NNE trending volcanic segments marked on the Landsat image (Fig. 2.5) as zones of distinct linear features. These areas have recent volcanic edifices and prospective geothermal potential in the region. To the south, a relative gravity minimum is superimposed with high-density nearly parallel contours with a northeast southwest trend that coincides with the eastern rift flank south of the Afar triple junction. This relative gravity anomaly with a sharp gradient increasing in value from the plateau down to the rift floor marks the uplifted rift flank in this part of the study area.

2.4.2.2 The Main Ethiopian Rift (MER)

The area of the main Ethiopian rift and adjacent plateaus considered for our detailed analysis lies between 5^{o} to 9^{o} N latitudes and 37^{o} to 39^{o} E longitudes (Figs 2. 16 and 2.17). Major structural features of the western plateau considered in this study include the Gurage highlands (GH), the Wenchi Lake (WL) region, and the Gibe River valley. This river is also known as the Omo River in its lower course. The Addis Ababa embayment (AE) and the volcanic features in the Debrezeit region are also included in this region.

The MER has been studied by many researchers (e.g., Alemu, 1992; Mahatsente, 1999; Tessema, 2003; Woldetinsae, 2005). As part of the EAGLE project, we added new gravity data with high precision GPS elevation control. In this effort, our goal was to acquire data at closer spacing to improve the resolution of local anomalies depicted in this region.

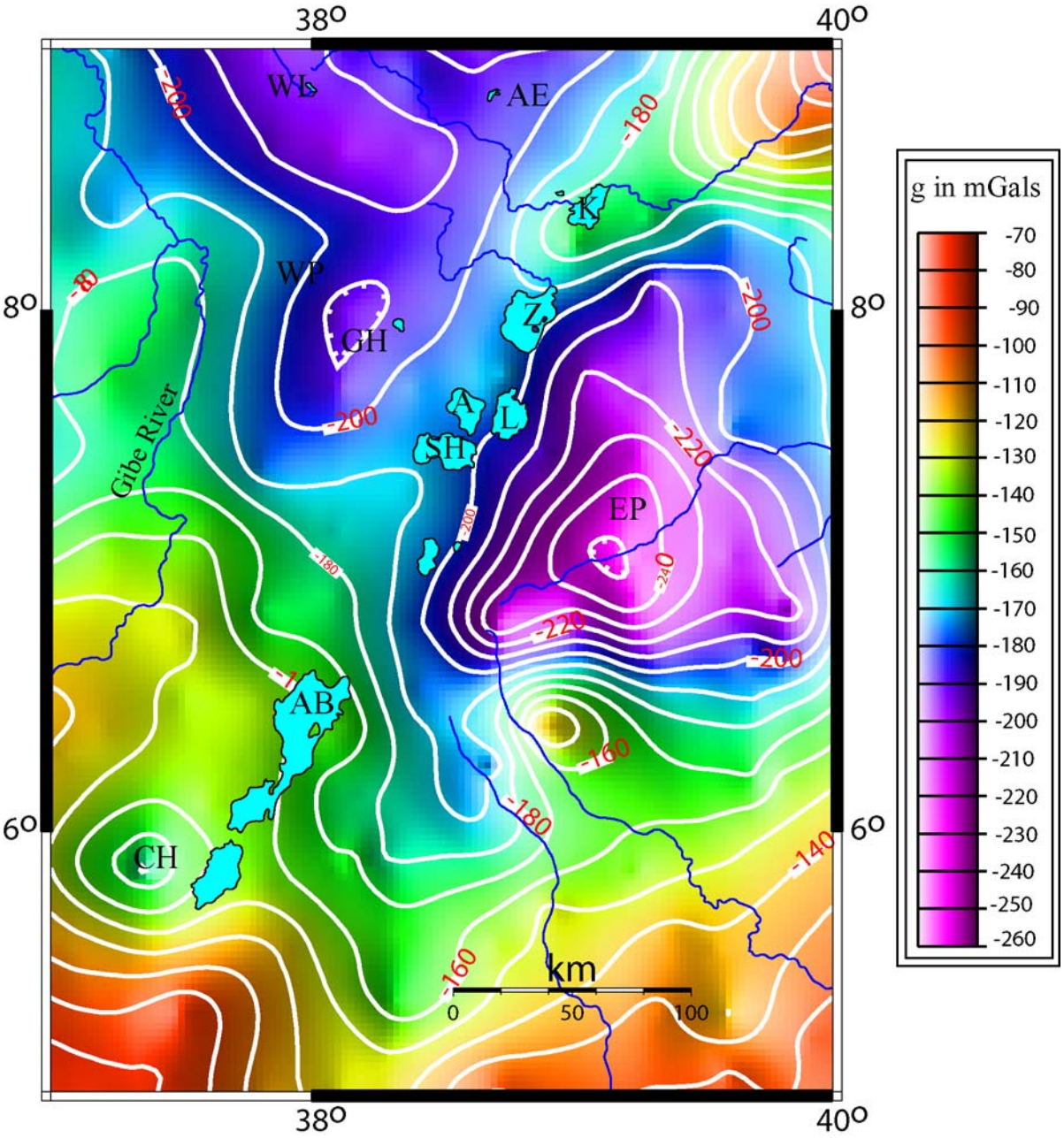

Figure 2.16: Bouguer gravity anomaly map (smoothed) of the Main Ethiopian rift and the western plateau (WP) and eastern plateau (EP), showing the different anomalies associated with Addis Ababa Embayment(AE), Wonchi Lake (WL), Gurage Highlands (GH) and Chencha area (CH). The lakes region includes Lake Koka (K), Ziway (Z), Langano (L), Abijata (A), Shalla (SH) and Abaya (AB).

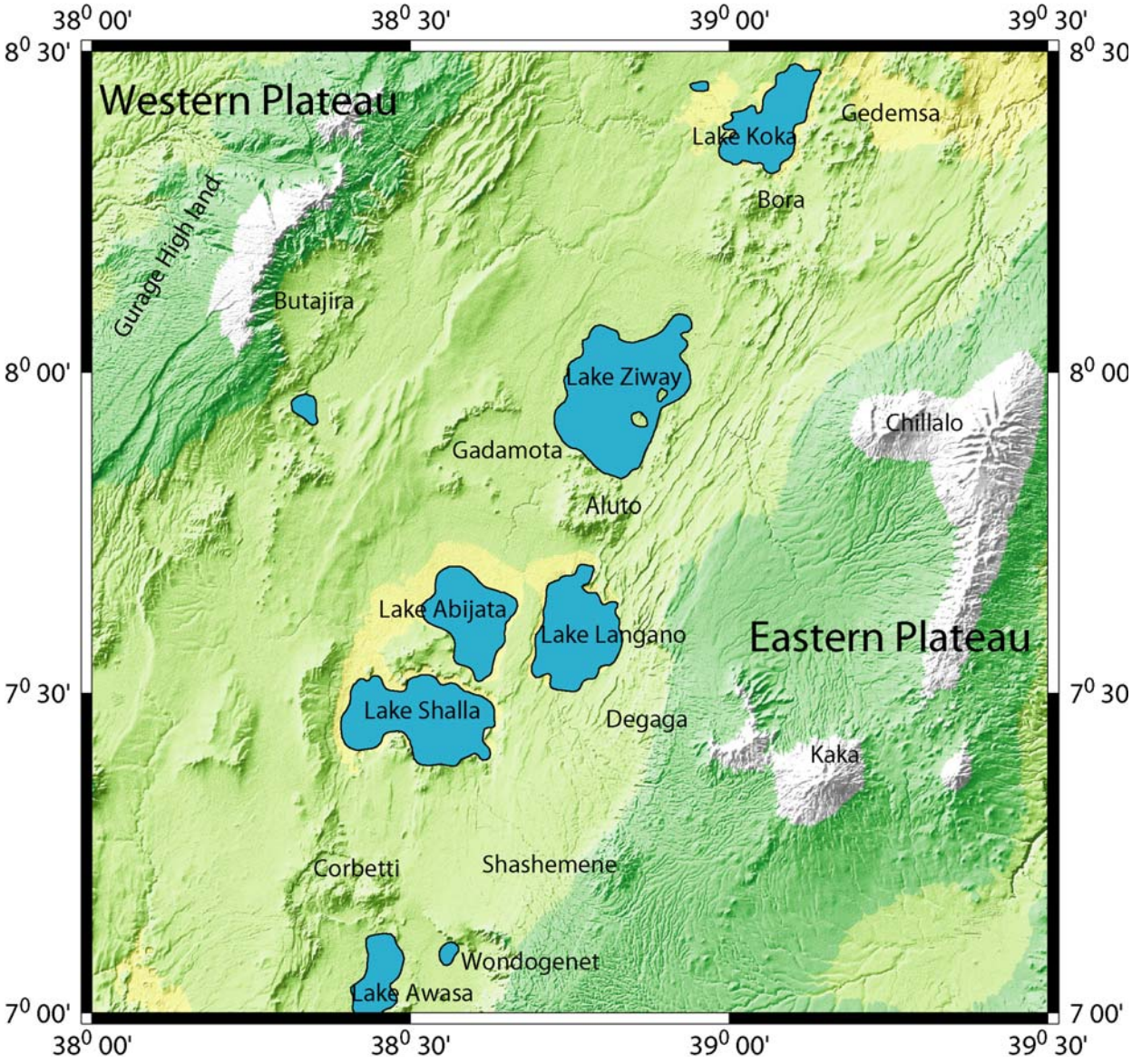

Figure 2.17: Topographic shaded relief map of the main Ethiopian rift showing the western and eastern border faults and the different lakes, and volcanic centers, such as Aluto, Gadamota Caldera, Gedemsa, and Bora. The volcanic centers Chillalo and Kaka on the eastern plateau and Gurage highlands on the western plateau are also shown.

The Bouguer gravity anomaly map of the MER shows various distinct anomalies. A broad northwest-trending gravity low is located in the northwestern part of the region (Fig. 2.16). This relative gravity low is associated with the maximum elevated region of the Wenchi crater area having an apex close to the crater. The Wenchi crater is a region dominated by volcanic ash and recent sediments that could be a reworked volcanic product of low-density material creating a low-density contrast when compared with the surrounding volcanic rocks. The other noticeable distinct relative low gravity anomaly is associated with the Gurage highlands (GH) close to the western rift margin. In this region the MER is bounded by a major border fault that extends from north of Hosaina to south of Debrezeit. Physiographically, this region is clearly separated with its high elevation (>3000m) from the rift floor around Butajira area, exhibiting an arcurate shape fault zone (Fig. 2.17). As a whole the plateau region associated with a broad gravity extending to the southwest until the faulted margin dies out into a low elevation ridge and turns into a gentle slope. In general, this broad negative gravity anomaly on the western side of the MER coincides with the high elevation regions such as Gurage highlands. The strong negative anomaly indicates that the region has a relatively thicker crust than the rift, which is mainly dominated by relatively high-density volcanic products and volcanic centers such as the Gadamota caldera and the Aluto volcanic complex. According to WoldeGabriel et al. (1990), the volcanics in this region are younging towards the rift axis. However, a recent assessment by Keiffer (2004) indicated that some shield volcanoes in the region have different ages and compositions. The relative age and composition variations lead to relative small differences in density. This could be one of the reasons we see localized high gravity anomalies close to the western side of the Abbay basin, which could be associated with nearby shield volcanoes.

The MER is distinguished from the remaining areas by its northeast to southwest trending relatively positive anomaly situated in between the broad negative Bouguer gravity

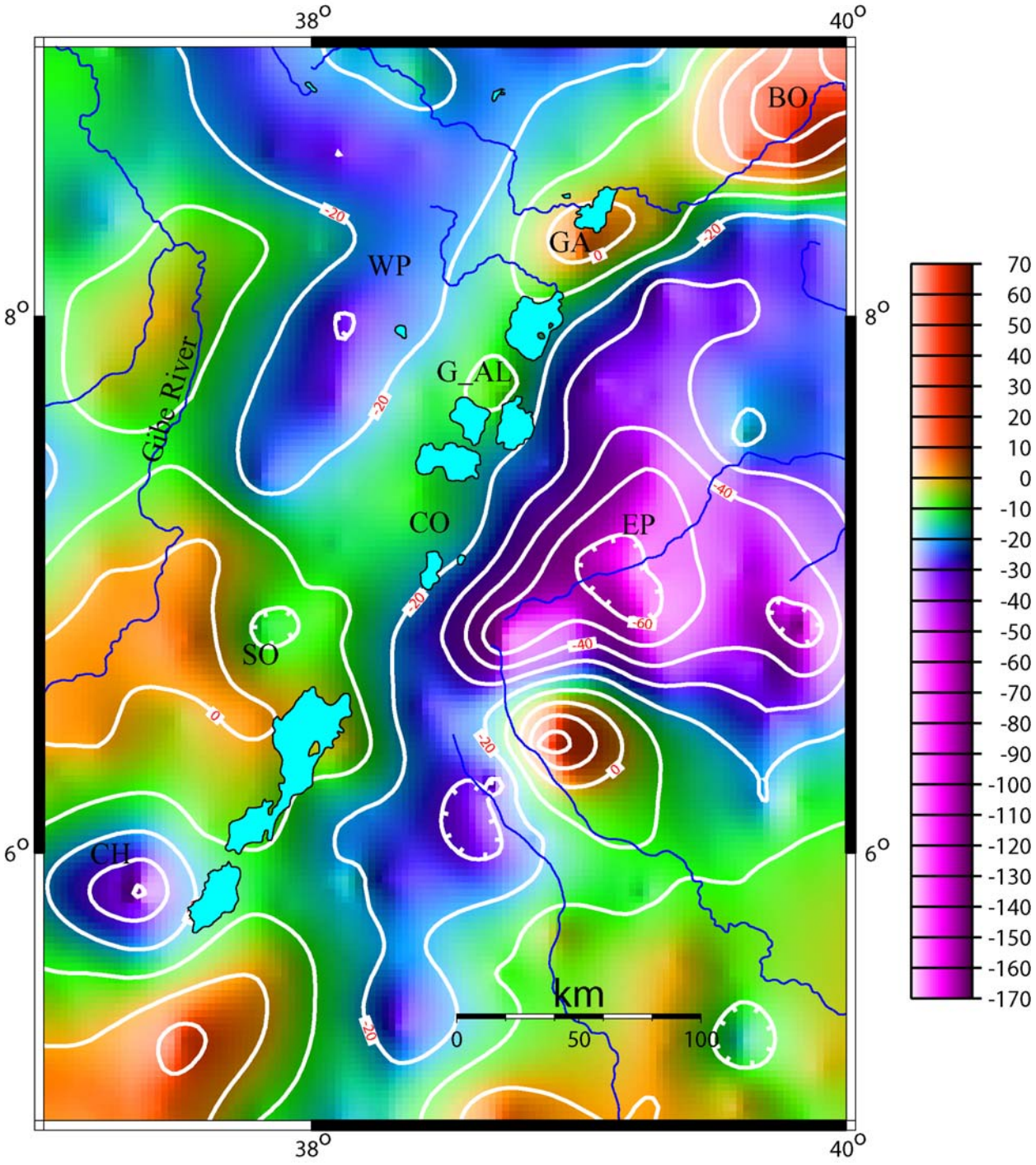

Figure 2.18: Residual gravity anomaly map (smoothed) of the Main Ethiopian rift and adjacent plateaus, showing the different volcanic centers as short wavelength positive anomalies. These are Boseti, (BO), Gadamota-Aluto (G_AL), Gedemsa (GA), Corrbetti (CO), eastern plateau (EP) and western plateau (WP).

anomalies that are associated with the western and eastern plateaus (Fig. 2.18). On the northeastern part of this rift there is a prominent relative gravity high with a northeast-southwest trend. This gravity high is the region where the Wonji fault belt, the Gedemsa Caldera and numerous northeast-southwest trending en echelon fault zones exist. The Wonji fault belt (WFB) (Mohr, 1962), is associated with the spreading center of the MER extension. The zone of crustal thinning associated with sea floor spreading and may be controlled by asthenospheric processes with magma supply in the crust by axial diking (e.g., Ebinger and Casey, 2001). Other relatively positive anomalies within the rift are associated with the volcanic centers of the Bora, Aluto-Gadamota, and Corrbetti areas (Fig. 2.18).

The eastern plateau is characterized by a broad negative gravity anomaly with a north south trend (Fig. 2.18). A sharp gravity gradient with a northeast-southwest trend east of the rift valley lakes marks the eastern border fault of the MER. Physiographically, this border fault is one of the remarkably clear fault lines that extends from south of Digelu to Degaga, east of Lake Langan, until it dips into a gentle slope northeast of Shashemene (SH) (Fig. 2.17 and Fig. 2.18). The long wavelength negative gravity anomaly to the southeast of the rift coincides with high altitude regions of the eastern plateau that include the Chillalo, Kaka and Bale Mountains regions further east. The minimum gravity anomaly observed in this region is located on the eastern plateau rather than the western plateau. This broad gravity low may indicate that the eastern plateau has a thicker crust than the western plateau in this locality (Tadesse et al., 1986; Mahatsente, 1999; Dugda et al., 2007 (in press).

The other prominent feature is Gibe River valley region (Fig. 2.17). This region is characterized by a positive gravity anomaly starting from the northern part of the Gibe River, following the course of the river and widening towards the south in the direction of the lower course of the river, which is known as the Omo River valley. This structural feature joins with

the southern rift valley north of Lake Turkana and occupies a long structural feature, which is elongated in a north-south direction. This positive gravity anomaly, which coincides with the Gibe River valley, could be a possible indication of aborted rift propagation into the western plateau, or a fracture zone associated with the Omo rift valley.

The residual gravity anomaly map of the MER exhibits interesting results (Fig. 2.18). The rift margins or border faults are clearly marked and segregated from the plateau regions by long contour lines that are coincident with the border fault zones along both the eastern and western sides of the rift flank. Central volcanoes, such as the Aluto-Gadamota (G_AL), the Gedemsa caldera, Boseti, Bora and Corrbeti-Shalla and northern part of Lake Abaya (AB), are clearly marked by local positive anomalies (Figs. 2.16, 2.17 and 2.18). Surface observation in the region reveals that these regions are prospective geothermal areas that are associated with fumaroles and hot springs. These areas are best delineated in the residual gravity anomaly as short wavelength relative positive anomalies. One of the more striking anomalies, which is depicted as a zone of relative positive on the residual gravity anomaly map of the MER region, is the NW-SE trending feature located between the Sodo (SO) and Chencha (CH) plateau (Fig. 2.18). This anomaly extends from the northwestern part of Lake Abaya to the Omo River valley to the northwest. Although this structural significance is not explained some researchers (e.g. WoldeGabriel et al., 1990) call this northwest-southeast trending feature the Bonga lineament. This can also be clearly seen on the DEM and Landsat images (Figs. 2.2, 2.3 and 2.6) as a NW-SE trending structure.

2.4.2.3 The Southern Ethiopian Rift (SER)

The Southern Ethiopia rift (SER) and the Turkana region is one of the most complex geological features at the junction of the southern part of the Ethiopian rift system and northern

part of the eastern East African rift system and Anza graben (Fig. 2. 19). The region is affected by multiple episodes (Ebinger and Ibrahim, 1994) and exhibits complex geologic structures with various geologic formations composed of various lithologies, ranging from Precambrian rocks to recent alluvium.

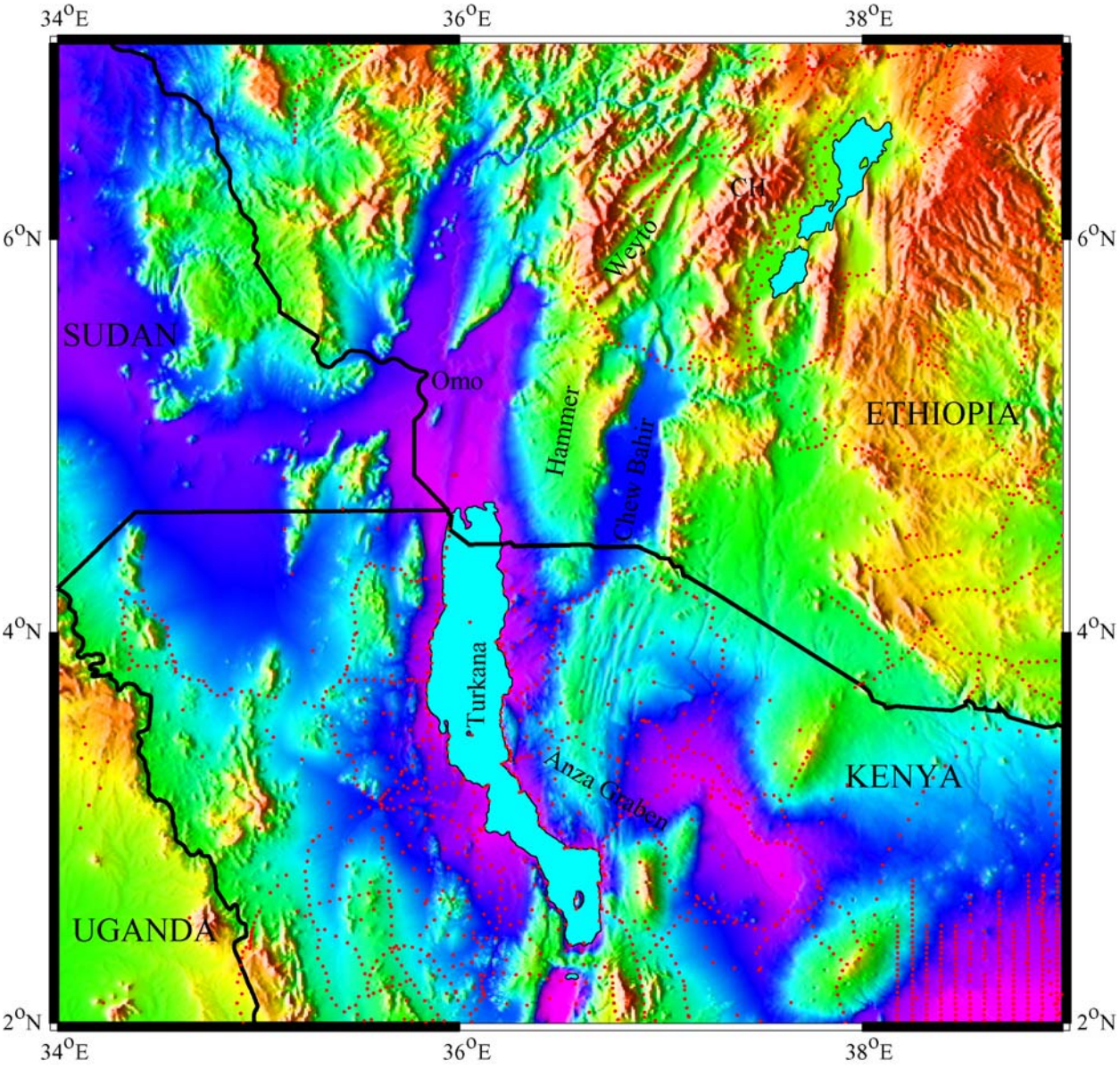

Figure 2.19: Shaded relief topographic map of the Southern Ethiopian rift, Turkana rift and Anza graben, showing the different fault zones and rift basins in the region. Red dots are gravity stations.

The multistage faulting that bounds the rift is characterized by a number of sedimentary basins flanked by deep escarpments. The basins are bounded along one or both sides by normal faults with large vertical displacements. The three rift floors, which are covered by Quaternary sediments, are the Omo rift on the west and the Chew Bahir and Weyto basins on the east. Crystalline basement rocks are exposed along uplifted horsts such as the Hammer block that is located on the eastern side of the Omo rift and serves as western boundary of the Chew Bahir rift (Fig 2.20). These rocks are subjected to different phases of deformation that belong to Pre- and Post-rift structures. These rocks are predominantly amphibolites with rare granulites of uncertain age that were overprinted by the Pan-African orogeny (Davidson, 1983).

In a regional geology context the Anza graben is part of the Cretaceous rift system of southern Sudan basins. The wide tectonic scene of this complex region is better envisaged by projecting it into the central and the western African Cretaceous rift system (Fig. 2.20). The central African shear zone (CASZ) is one of the major structural grains in the region where the opening of the central and western African rift system originates at the Benue trough in Nigeria. The Benue trough is the focal point or triple junction of the southern Atlantic Ocean and the equatorial fracture zone (Fairhead, 1987). It is a zone split again into the south Sudan and White Nile intracontinental rift zones (Fairhead, 1987), reaching up to the east coast of Africa around the Lamu embayment in Kenya.

The Paleogene rift system, which is controlled by NW-SE trending normal and strike-slip faults in the southwestern Ethiopia, is linked with the White Nile rift system in the Sudan (Browne and Fairhead, 1985). The depth and lateral continuity of these geologic successions is known from the refraction seismic studies of the Kenyan Rift International Seismic Project (KRISP) (Mechie et al., 1994; Keller et al., 1994).

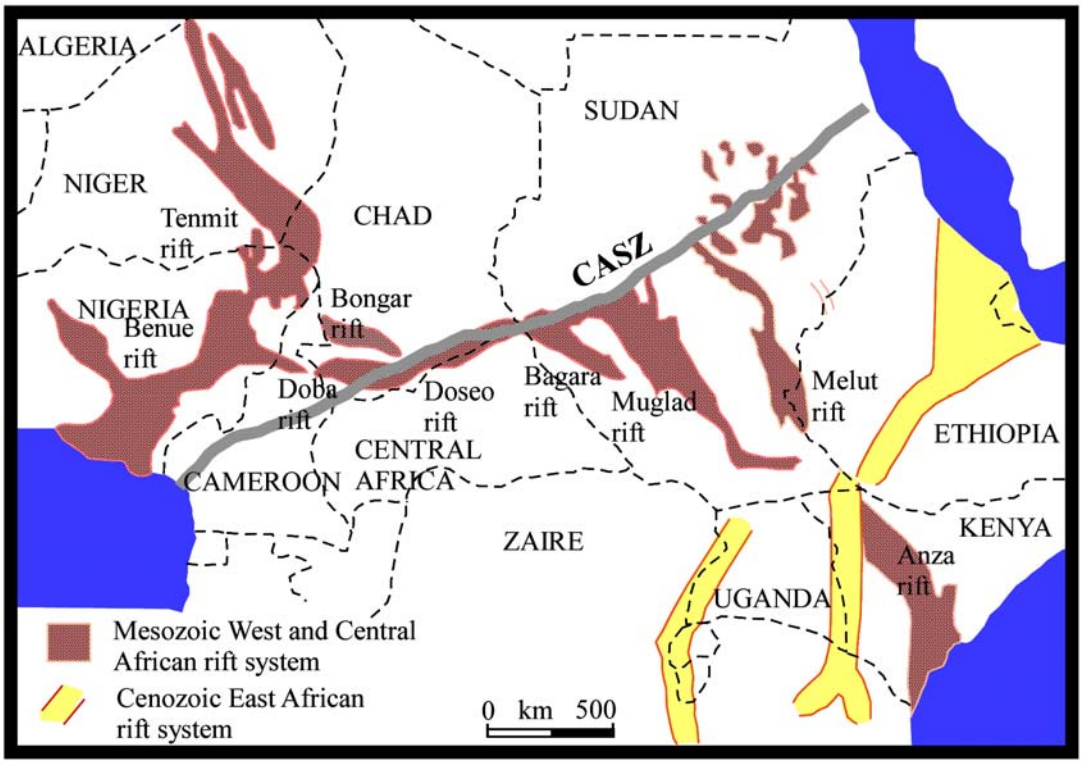

Figure 2. 20: Cretaceous Structural features of central Africa, and western Africa in relation to the Anza graben (Modified from Ebinger and Ibrahim, 1994).

In Kenya, part of the Paleogene rift is concealed by Tertiary volcanics, and there is an overlap with the Neogene rift at the northern tip of Lake Turkana, which is trending in NNE and SSW direction. In part of Kenya and southwest Ethiopia, the Paleogene rift is covered by a thick succession of trap series and Quaternary sediments (Fairhead, 1992). The NW-SE trending Anza graben is one of the oldest structural features and is comprised of highly faulted depocenters containing as much as 7 km of sediments that are Neocomian to Paleogene in age (Bosworth and Morley, 1994).

The southern Ethiopian rift basins, the Omo and Chew Bahir basins contain sedimentary rocks ranging from the Oligocene through the Miocene and the Early Pliocene age (Davidson, 1983; Fleagle et al., 1991) and are the northern extension of the Turkana rift system. These two features are located near the Ethiopian-Kenyan boundary and contain two graben systems. The western one is the Omo rift system that is wider and longer than the Chew Bahir graben, and they are separated by the Hammer horst (Figs. 2.19, 20 and 2.21).

A detailed Bouguer gravity anomaly map for this region is shown in Figure 2.22. The Anza graben is clearly marked by a northwest- southeast trending positive gravity anomaly superimposed with relative negative anomalies. Much of the short wave length positive anomalies are associated with the Turkana rift, which is close to Lake Turkana. Further to the southeast within the Turkana graben, a strong, short wavelength, positive gravity anomaly occurs. This positive gravity anomaly may be due to thin crust associated with features related to the coastal margin as a result of an older structural development. The breakup of Gondwanaland, which resulted in the development of rifts and ocean floor processes, could be the reason why this coastal region exhibits such a high gravity anomaly.

A northwest-southeast trending gravity low is located between Turkana and eastern Anza graben and is associated with thick Cretaceous rift basins. The gravity anomalies also delineate a

series of N-S trending half graben structures present in the Turkana region (e.g., Lokichar and northern Kerio basin) associated with large negative anomalies that are separated by a gravity high (Mariita and Keller, in press); Simiyu and Keller, 1997). The residual gravity anomaly map clearly delineates local anomalies. The relatively positive, high amplitude anomalies close to Lake Turkana (Figs. 2.22 and 2.23) may be associated with recent volcanics related to the modern rift. Local negative anomalies may be the result of thick sediments. The Chew Bahir and Omo rift basins are depicted as relative negative anomaly troughs opening towards the Anza graben.

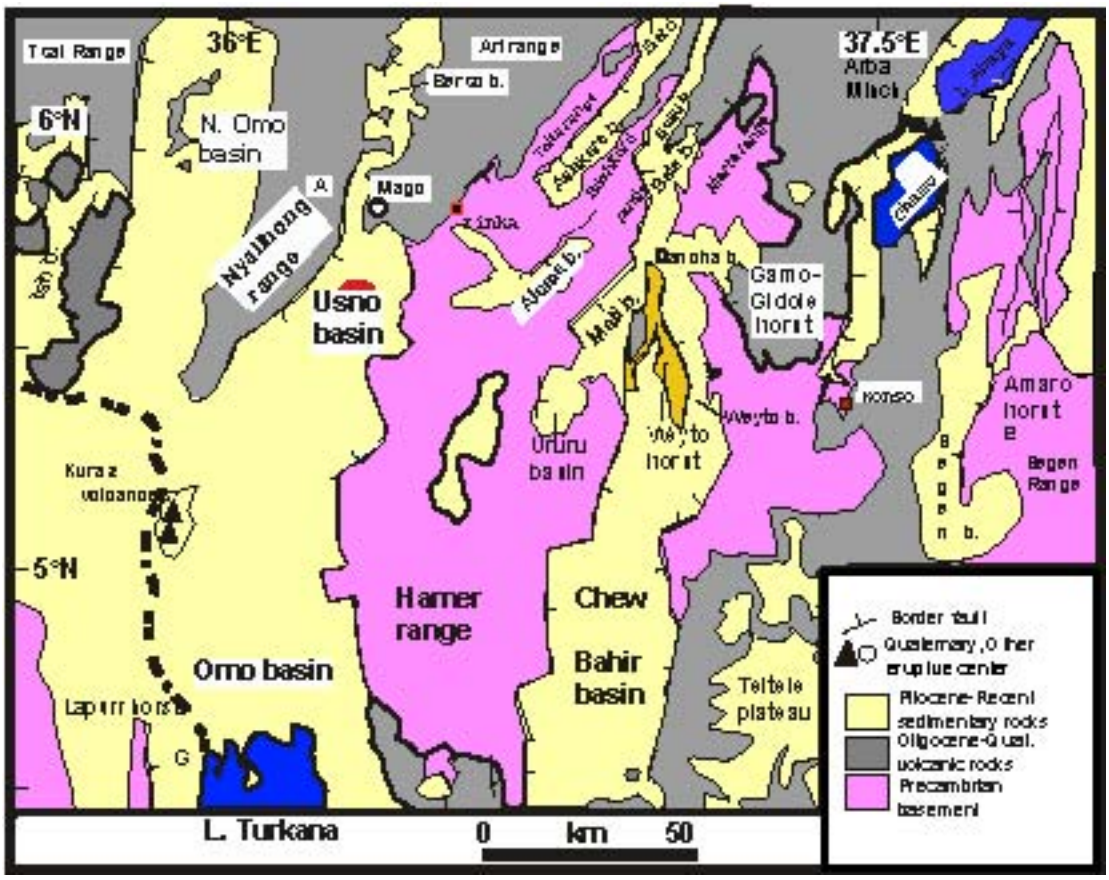

Figure 2.21: Geological map of the southern Ethiopian rift basins, modified from Tefera et al. (1996).

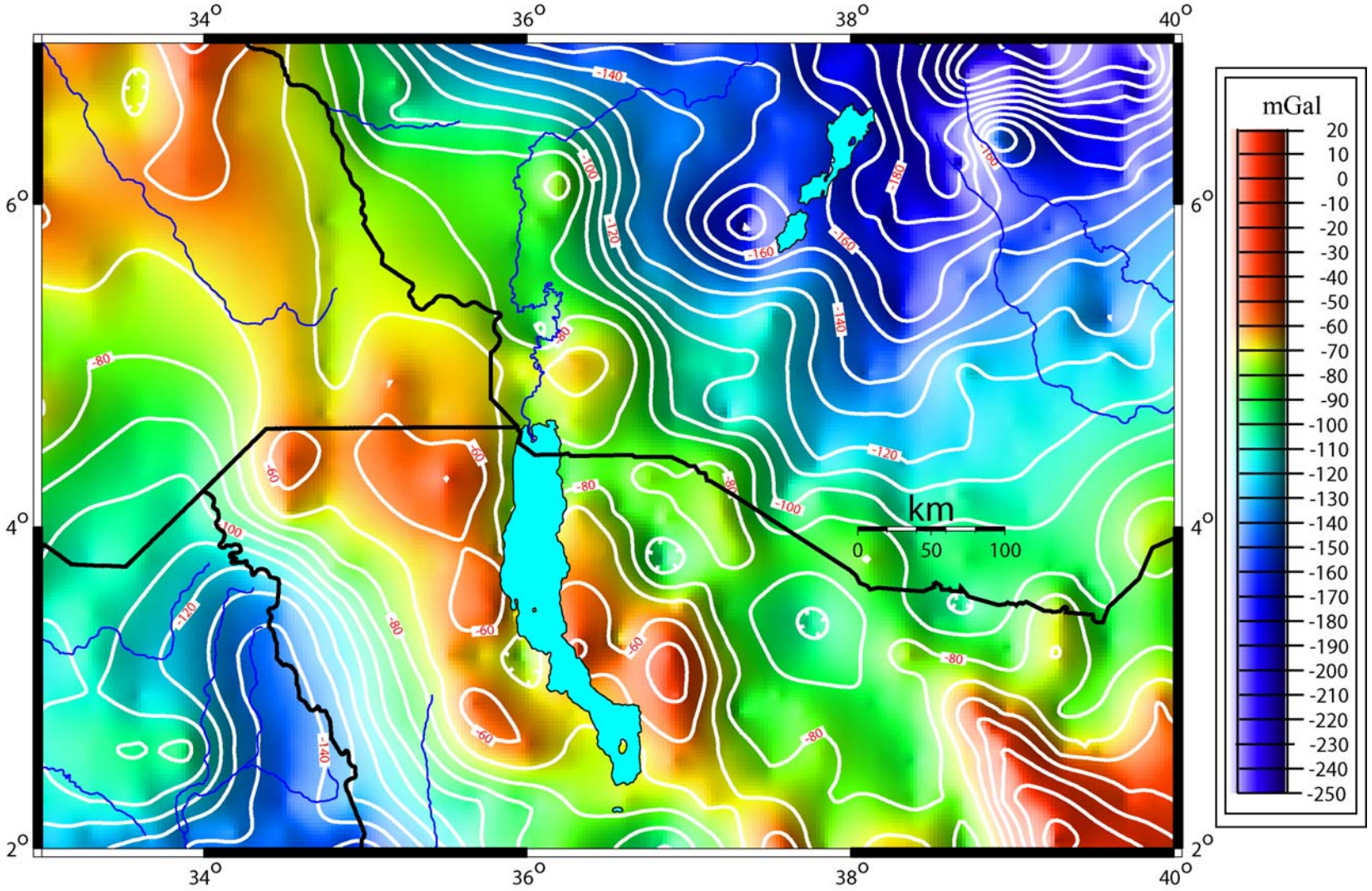

Figure 2.22: Detailed Bouguer gravity anomaly map of the Southern Ethiopian rift, the Anza graben, and Turkana rift.

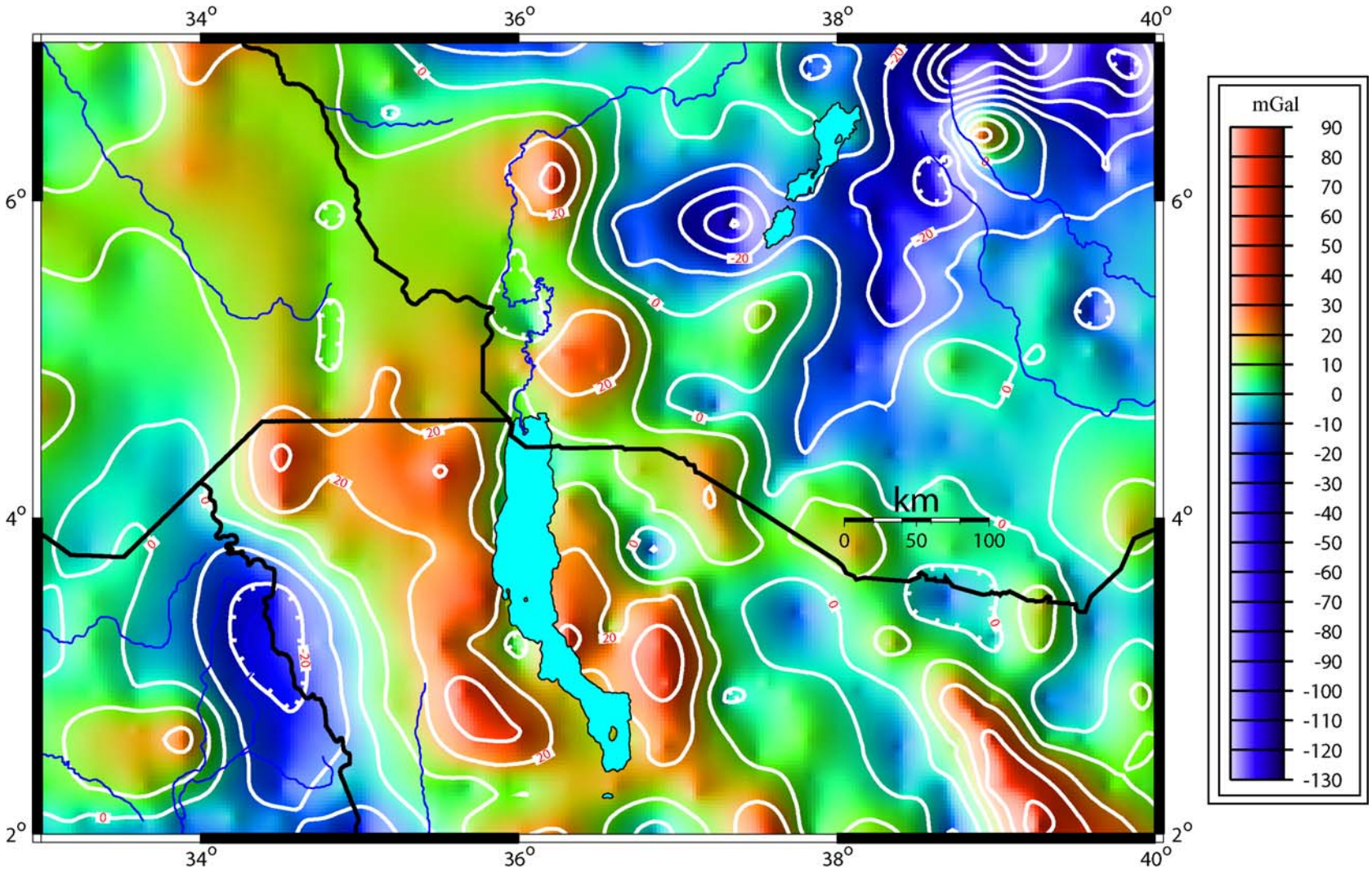

Figure 2.23: Residual gravity anomaly map of the Southern Ethiopian rift, the Anza graben and Turkana area.

2.5 Geophysical Data

The EAGLE and KRISP experiments produced detailed information about the crustal structure of the Ethiopian and the Kenyan (Eastern) rifts, respectively. These regional models across and along the axial direction of the great east African rift provide geophysical and geological constraints in order to determine the nature of the crust as well as the lithosphere beneath and across the rift system. To analyze the crustal structure of the ERS, we constructed interlocking gravity profiles, forming a network across and along the axial direction of the rift. Figure 2.6 shows the location of the data points used for our analysis. The location of our profiles is shown in Figure 2.25. We used the available seismic velocities and data compiled from other sources such as drill holes (e.g., Simiyu and Keller, 2001) to constrain these models. These models reveal the subsurface structure of the crust across the rift and along the axial direction of the rift as discussed in the following sections.

For our modeling we chose anomalies of interest along five profiles (Fig. 25). The criteria for choosing these profiles are density of point data along the profiles, seismic constraints for velocity and depth, and their relative position to key geologic features.

Refraction seismic results from the EAGLE survey indicate that the crust thins towards the northern MER and into the Afar triple junction (e.g., Keller, 2004; Maguire et al; 2006, Tadesse and Keller, 2006). From this profile we can also see that the upper mantle is at shallower depth beneath the Afar triangle.

In some cases modeling is based on a residual gravity anomaly, using different regional residual separations. The modeling algorithm is based on a standard 2.5D modeling program following the approaches of Cady (1980) and Talwani (1959). Geologic cross sections were

approximated by arbitrary polygonal shapes in such a way that they mimic the nature of the geologic feature.

2.5.1 Densities

The Geological Survey of Ethiopia (GSE) archived some measured densities from surface and deep borehole samples obtained from geothermal wells in the Ethiopian rift. Many of the samples were acquired from the northern MER. In the process of modeling gravity profiles, estimation of densities plays a key role. For shallow structures and sediments, measurements carried out by the GSE and lithologic information from field mapping provides important constraints and density values. In the Kenyan part of the EARS, density information comes from deep wells and stratigraphic information. This information was used to constrain the upper 3 km of the model (e.g., Mariita and Keller, 2006 in press). Densities and seismic velocity are related through an empirical relationship (e.g., Nafe and Drake, 1957). Densities for the deep crustal and upper mantle units were estimated based on P-wave velocities from the KRISP and EAGLE refraction seismic profiles. The axial seismic refraction profiles from both countries were used for constraints in the gravity modeling

Crustal thickness and densities for the northern MER and adjacent plateaus were determined using the cross rift refraction model of McKenzie et al., (2005), as well as information based on Maguire et al, (2006); Keller, et al. (1994); Keller et al. (2004) and Dugda et al., (2005). Most of the density information comes from seismic velocities derived from refraction surveys along the axial direction in the Eastern rift in Kenya for the southern section of the axial profile model (Table 1.1).

Table 2.1: Density values inferred from seismic refraction studies of Mechie et al., (1994); Keller et al., (1994); Simiyu and Keller, (1997); Keller et al.(2004); Mariita and Keller, (2007). Where ρ is density and V_P is P-wave velocity.

Table 2 .1: Summary of density measurements in from the Kenyan rift.

Lithology	Region	Vp ($kmsec^{-1}$)	ρ ($kg\ m^{-3}$)
Sediments	Turkana region	2.0-3.10	2350
Sediment	Lokichar-Baringo area	2.0-4.15	2450
Upper-Crust	Turkana-Baringo	6.10-6.30	2700
Lower Crust	Turkana	6.4	2850
Upper crust	Tanzania Craton	6.00 – 6.2	2680

Table 2.2: Summary of measured densities of outcrops from the Ethiopian rift and adjacent areas.

Rock Type	Samples	Minimum	Maximum	Mean	SD
Basalt	277	1540	3060	2310	403
Granite	9	2310	2830	2570	162
Granite gneiss	10	2330	2970	2770	185
Ignimbrite	137	1700	2970	2280	258
Limestone	31	1440	2690	2350	468
Marble	8	2640	2980	2720	125
Obsidian	27	1900	2490	2350	118
Pumice	12	1110	2400	1810	449
Pyroclastic	38	1990	2870	2380	192
Tuff	172	1140	2700	2030	378

Source (Woldetinsae, 2005)

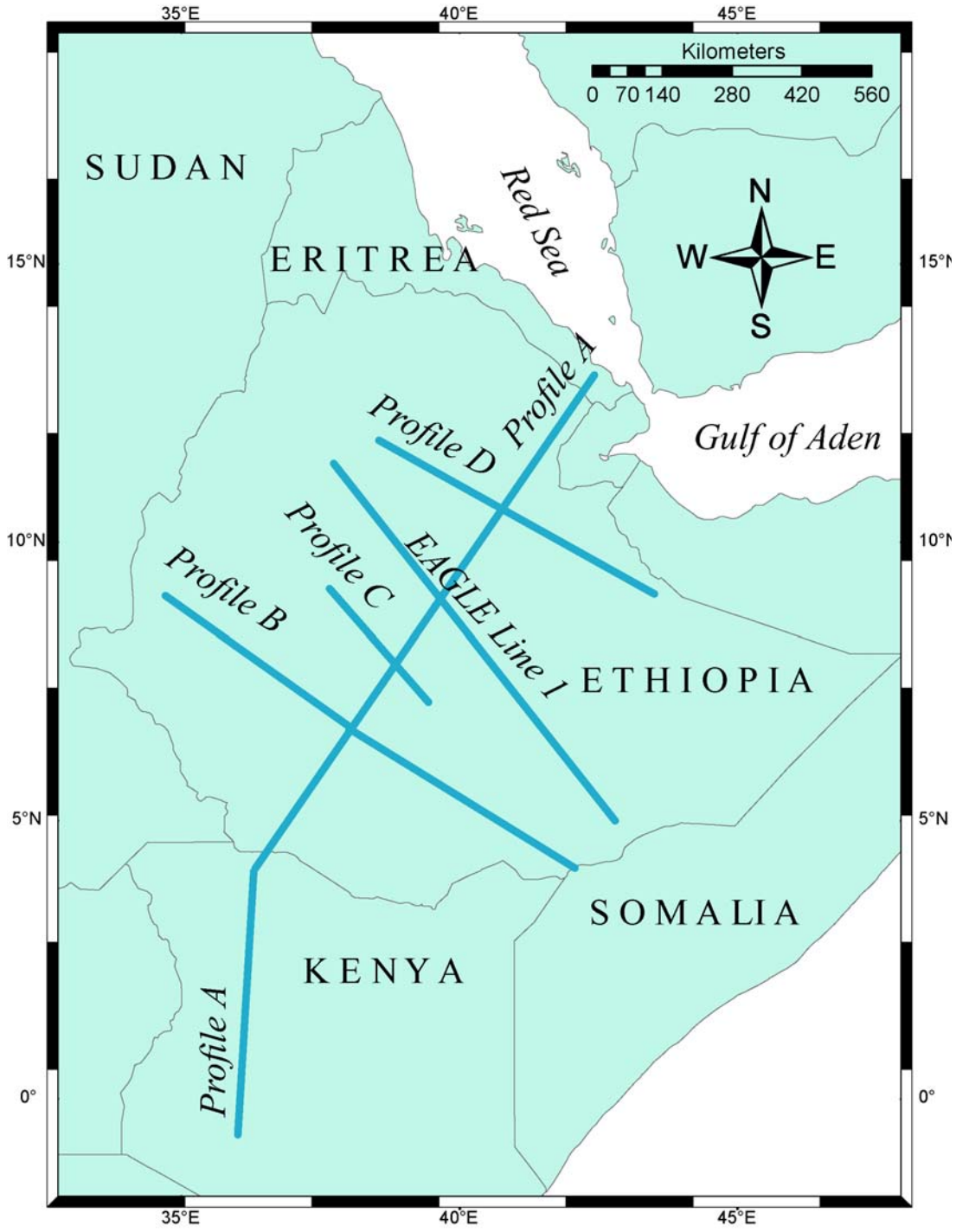

Figure 2.24: Gravity profile index map across and along the Ethiopian rift.

2.5.2 The Cross Rift Profiles

Four profiles were extracted across the Ethiopian rift (Fig. 2.24). The orientation of these cross profiles are almost orthogonal to the rift axis, which is north-northeast-south-southwest oriented. The longest profile extracted in the axial direction of the Eastern rift (from Kenya and the Ethiopian rift up to the Afar triple junction) cuts across all the cross profiles along the rift in the axial direction (Fig. 2.24). The axial profile is close to the KRISP axial rift direction refraction seismic profile from -0.59^{o} N latitude and 36.19^{o} E longitude to 12.9^{o} N latitude and 42.58^{o} E longitudes. This profile is close to the EAGLE axial refraction survey profile in Ethiopia that starts just north of Lake Awasa in the MER and ends at Gewane in the Afar (Fig. 2.24). Obviously, the structures along the axial profile may be more complex than presented here. However, our model provides an integrated regional interpretation of the crust beneath each profile. The thickness and densities from previous studies (Table 2.1 and 2.2) were compared, and average values were taken. However, since profiles were not exactly coincident with the seismic profile and density-velocity relationships are not exact, model parameters were varied and adjusted slightly to fit the observed gravity data.

2.5.2.1 The Southern Afar Profile

The profile across the southern Afar is designed to pass from the western plateau across the rift and continue to the eastern plateau where maximum data coverage is available (Fig. 2.6 and 2.24). The profile starts at 11.76^{0} N latitude and 37.88^{0} E longitude in the northwestern part of the western plateau and crosses the southern section of the southern Afar rift. From the southern Afar, it continues to the eastern plateau at about 9.084^{o} N latitude and 43.48^{o} E longitude on part of the eastern plateau.

This profile is important because it contains the maximum number of data points acquired along the main roads of both on the eastern and western plateaus. A fair amount of good point data coverage, with a reasonable spacing on this section of the rift floor, is also available,

thus allowing us good data point extraction for modeling purposes. Within the Afar triangle, the profile shows a 300 km wide gravity high that is associated with the rift floor until it nears the border faults on both sides of the rift. This gravity high could be due to crustal thinning in the region and/or possibly to a high-density oceanic crust (Kendal et al., 2005) or to the existence of a mantle plume at a relatively shallow depth (Montelli et al., 2004; Ebinger, 1989; Ritsema and Van Heijst, 2000). This northwest-southeast trending profile is about 600 km long and connects the two plateaus. The gravity anomalies on the two rift flanks are similar. Both sides of the rift flanks are associated with a negative gravity anomaly; however, we can observe that the existence of a relative gravity minima on the western section of the rift flank for part of the western plateau. These gravity minima on both sides on the rift flank could be associated with a thicker crust beneath the plateaus.

Compared to the MER profile, the southern Afar profile shows a gravity increase with a broader wavelength. The gravity high observed in this profile has much higher amplitude than the MER profile. A lithological investigation of the area reveals that the western part of the rift flank and its adjacent areas are associated with voluminous flood basalts (Ayalew and Yirgu, 2003); whereas, the eastern rift flank is associated with a minimum basaltic cover associated with crystalline basement and carbonate sequences (Bosselleni et al., 2001). This gravity minimum on the western part of the profile suggests that the western rift flank has thicker crust overlain by flood basalts compared to the eastern rift flank that is associated mainly with uplifted basement rocks and thinner basalts which outcrop just north of the Ogaden basin.

The upper most section of the Afar rift floor is represented by a thin section of sedimentary basin fill with a thickness of ~2 km. A density value of 2500 kg m^{-3} was found appropriate for modeling this section of the rift (Fig. 2.25). Also, the area is known for its sedimentary deposition. The other evidence comes from geothermal drilling. Further northeast of

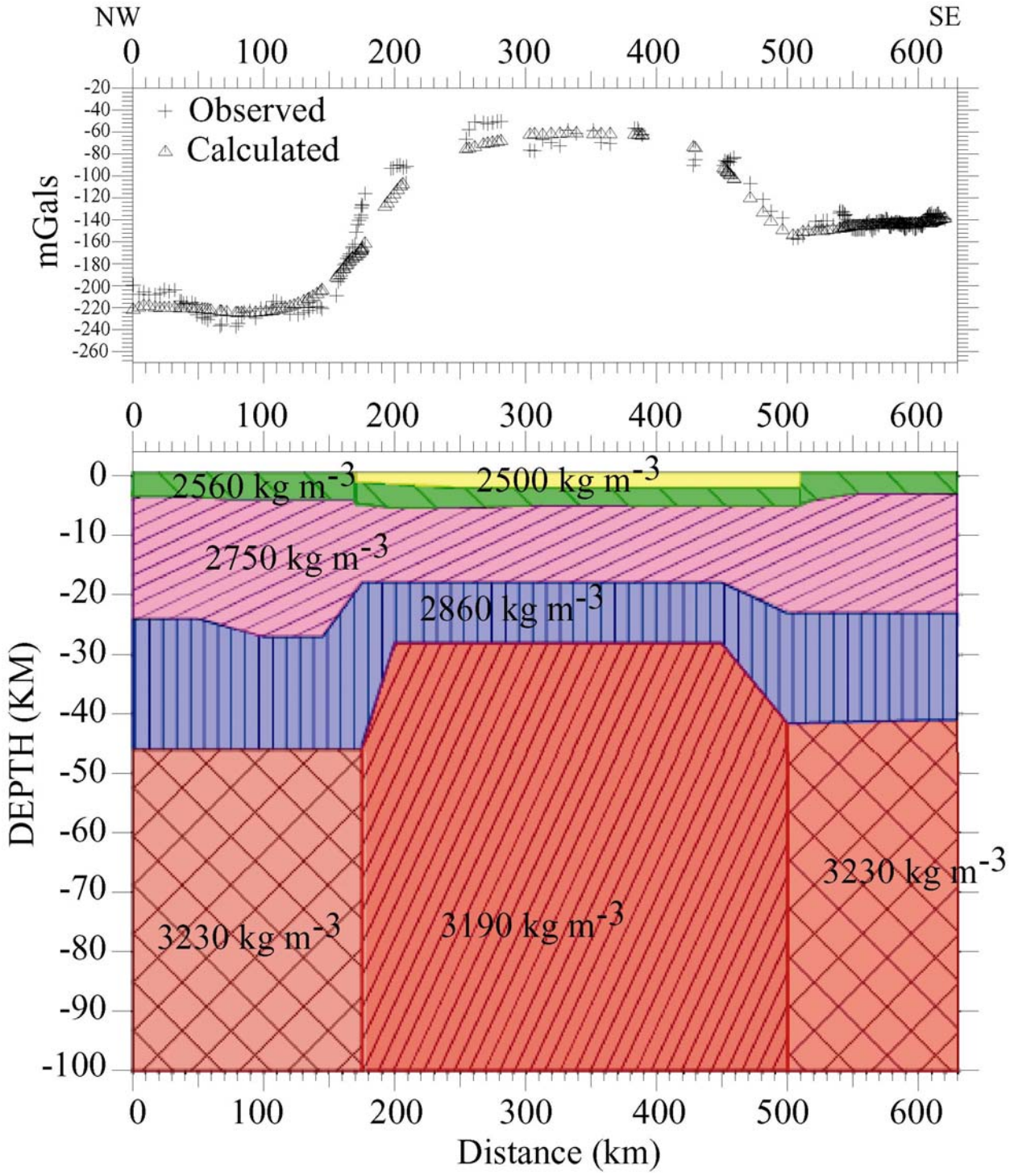

Figure 2.25: Gravity profile across the southern Afar.

the region, the Geological Survey of Ethiopia conducted deep drilling to tap the geothermal resources of the Tendaho graben. It is reported that there are more than 1400 meters of sediment intercalated with lava flows (Tadesse Mamo, personal communication). Our model shows a relatively thin crust divided into an upper and lower crust. The plateau on the western and eastern side of the rift shows low densities compared to the rift mainly associated with the upper mantle.

2.5.2.2 The Profile across the main Ethiopian rift

The MER cross profile extends from the western plateau starting approximately at 8.74^{o} N latitude and 37.88^{o}N latitude, through Gadamota –Aluto volcanic complex (G-AL) in the MER to 6.94^{o} N latitude and 39.29^{o} E longitude on the eastern plateau. This profile crosses a well-studied region of the Ethiopian rift section (Fig. 2.19 and 2.26). Much of the geological and geophysical studies of the Ethiopian rift come from this region. These studies address issues such as rift evolution, geochronology, elastic thickness, extension direction, thickness of the crust, and segmentation styles (WoldeGabriel, et al, 1990; Alemu, 1992; Tessema, 2004; Woldetinsae, 2005; Mickus et al. 2006; Ebinger, et al., 1989; Mahatsente, 2000; Acocella and Korme, 2002; Boccaleti et al., 1998). This profile is about 257 km long and crosses the geothermal potential area of the Aluto volcanic complex. It is characterized by a gravity minimum over the western and eastern plateaus and a gravity maximum over the Gadamota caldera and the Aluto geothermal field. Comparing the two plateaus considered in this section, it is possible to observe that the eastern section exhibits a more intense regional minimum than the western plateau in the proximity of the MER. This gravity profile is important because it crosses the western physiographic rift margin, with the Gurage highlands on the west, which clearly marks the western border fault for the MER (Fig. 2.19). Also, this profile crosses the eastern boundary fault east of Lake Langano

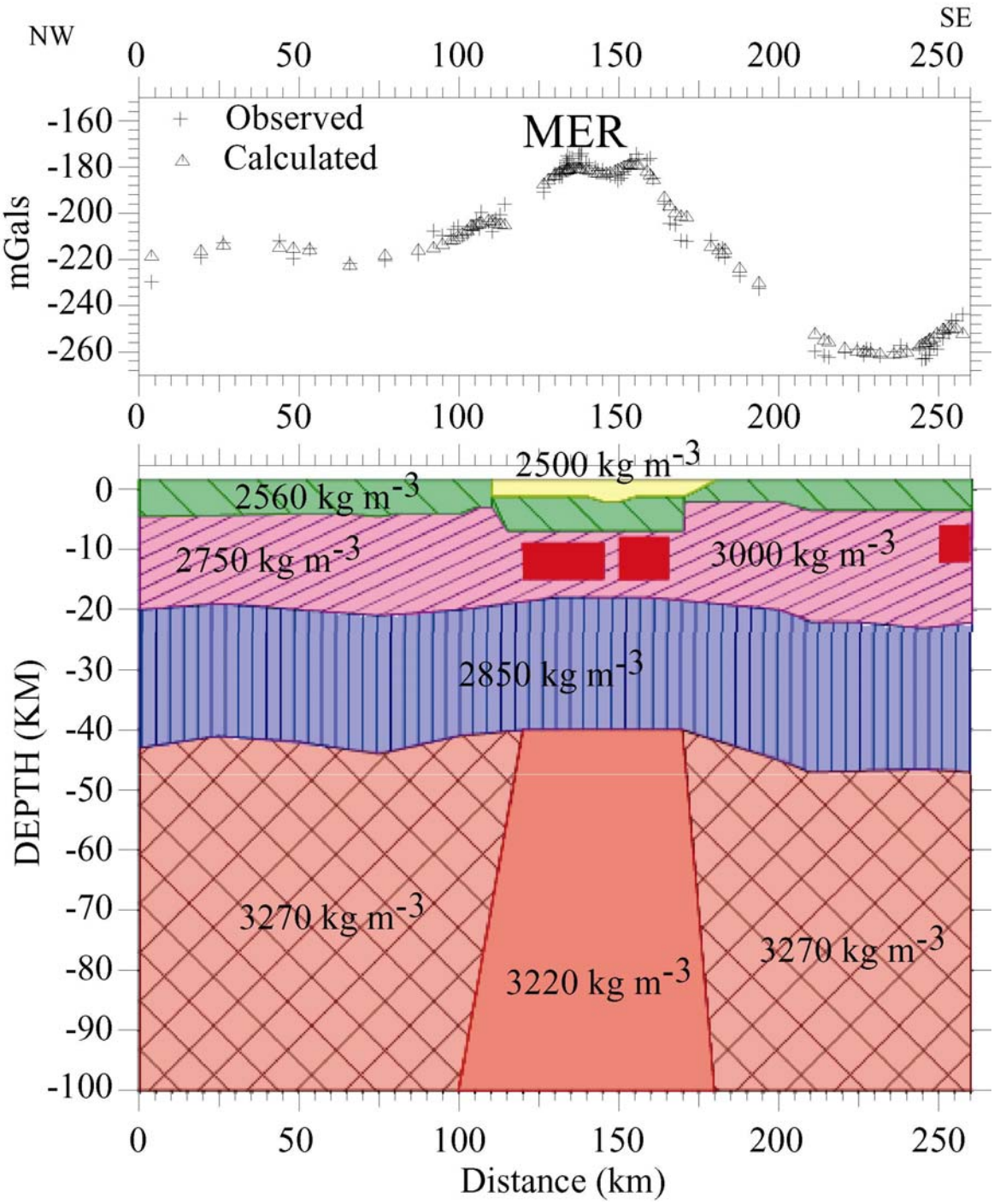

Figure 2.26: Gravity Profile across the MER.

in the Degaga region; thus, the rift structure is clearly shown by the eastern and western border faults and the rift as a graben with its low elevation (Fig. 2.19 and 2.26). The Kella horst, a basement outcrop on the rift floor close to the western rift margin, is located just a few kilometers north of this profile, (WoldeGabriel et al., 1990). This suggests the lithology in the region varies from sediment on the top, volcanics and volcano sediments, followed by basement formation in parts of the upper crust.

This profile model indicates that a part of the western plateau is dominated by volcanics and volcano sediments about 2 km thick. Field examples show that areas like the Wonchi crater lake are characterized by such depositional lithologies. Similar lithologic units with a thickness 3 km and a similar density value of 2560 kgm^{-3} provided a reasonable fit to the model. A thin layer of sediment with a density value of 2500 kg m^{-3} was required to obtain an accurate fit in the rift section. This is in fact indicated in the refraction seismic model in the axial direction (Keller et al., 2004; Maguire et al., 2006). A field visit to the region proved that it is possible to obtain such layers as the profile crosses the Lake Ziway (Ebinger and Casey, 2001) (Fig. 2.19). The upper crust, mostly comprised of basement rocks, is assumed to have a density of 2750 kg m^{-3} and extends to a maximum thickness of 20 km.

The lower crust, usually characterized by basaltic units, extends to a depth of 40 km in this part of the rift. The density of this unit is 2850 kg m^{-3}. This section of the lithologic unit is much thicker on the eastern side of the rift flank. This in turn indicates that the eastern rift shoulder may be thicker than the western rift shoulder in proximity of the MER.

Two intrusive bodies with a density of 3000 kg m^{-3} each are required to fit the gravity high anomaly depicted in this section of the rift. This is also known from the outset, as the profile was designed to pass through the Gadamota caldera and Aluto volcanic complex resulting in local positive gravity anomalies. Therefore, it was necessary to use intrusive bodies with the

indicated density values. With a thickness of 15 km and width of 20 km, these intrusive bodies provide a reasonable fit in this section of the profile. Aluto is known for its geothermal potential and complex volcanic activity. The upper mantle beneath both plateaus is modeled using a density 3270 kg m^{-3}; whereas, the mantle below the rift is modeled using 3220 kg m^{-3}.

2.5.2.3 The Cross profile along EAGLE Line 1

This profile crosses the northern MER along the controlled source seismic experiment EAGLE line 1 (Fig. 2.24). The original 325 km long profile out of the 400 km seismic line was modeled by Cornwell et al., (2006). We extended this profile by adding more data to the northeast and southwest direction from both ends of the profile to better assess the lithosphere. After we add available regional data, the total length of the profile is 725 km. The profile begins at about 11.55^{o} N latitude and 37.37^{0} E longitude south of Lake Tana on the western plateau. It crosses the Abbay river gorge to the southeast north of Addis Ababa. When it reaches the northern part of the main Ethiopian rift, it passes through the Bosseti magmatic segment and a possible intrusive body as suggested by a relative positive gravity anomaly south east of Boseti. On the eastern plateau it passes northeast of Mt. Chillalo towards Bale and reaches the Ogaden basin at about $6.23\ ^{0}$N latitude and $41.19\ ^{0}$E longitude. The profile shows a typical rift anomaly with a general broad negative anomaly associated with the rift. However, the rift section also contains relatively positive short wavelength anomalies associated with volcanic intrusions or complexes. As a result we can see an underplated layer modeled on part of the EAGLE profile 1 refraction seismic result beneath the western plateau (Fig. 2.27). The relatively high elevation along the profile on the western plateau provides further evidence of this under plating. The upper and lower crusts are similar to the rest of the cross profiles with the exception that they are thicker than the southern Afar cross profile. In this section the upper mantle beneath the rift is less dense than the region beneath the plateaus. However, the width is less than the south Afar profile and greater than the MER profile. The Boseti magmatic segment is modeled with a 5 km top width and a wider base. A density of 3000 kg m^{-3} is assumed for this mafic body. Beneath

the eastern plateau we see a similar density variation and four layers with characteristics similar to the other cross profiles.

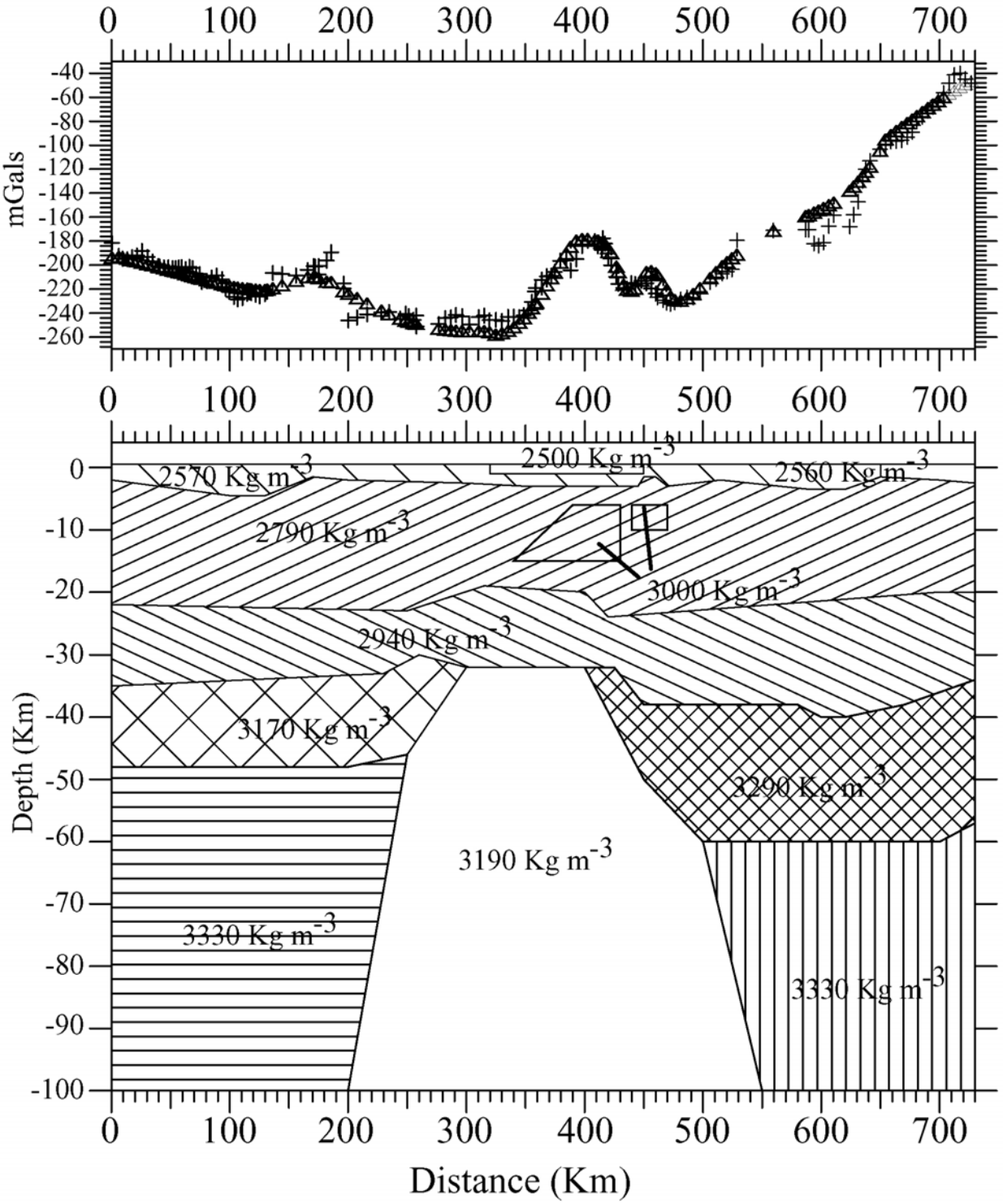

Figure 2.27: Gravity Profile across the Northern Main Ethiopian rift (EAGLE line1)

2.5.2.4 Southern Main Ethiopian cross rift profile (B-B')

Profile B-B' (Fig. 2.25 and 2.28) passes across the southern part of the MER. It starts at 34.86^{o} E, 9.05^{o} N in the western part of Ethiopia, crosses the Bilate River north of Lake Abbaya in the rift valley and ends in the Ogaden basin. This profile samples a great variety of topography from the northwest across the southern part of the MER towards the Ogaden Basin. The elevation along this profile ranges from 500 m in the Ogaden region to 300 meters on the western plateau margin. The lowest elevation in the rift is a little less than 1000 meters; whereas, in the volcanic mountains the elevation is as much as 2000 meters (Fig. 2.3 and 2.4). The length of the profile is about 964 km. The rift is about 80 km wide in this section of the MER. According to Bosworth (2006) the MER ends at Lake Awasa. However, others consider the MER to extend to the south of Lake Abaya (e.g., Tessema, 2004; Mahatsente, 1999; WoldeGabriel et al., 1990). We consider the MER to extend to the southern part of Lake Abaya in our study. Within the rift itself, the elevation increases from northwest (~1000 m) to the southeast (~1700 m). This profile is important because it samples the Precambrian outcrops in western Ethiopia and on the eastern plateau before it reaches the Ogaden basin. Much of the other section of the profile is covered by a series of flood basalts on the western and eastern part of the plateaus. Quaternary sediments within the rift cover the top of the rift; whereas, a thick Paleozoic to Cenozoic sediment covers the Ogaden basin. This variation attests to the existence of greatly varying densities in the formations along the profile. The surface lithologic expression can also indicate a variation in the upper crust and upper mantle structures of the region, which results in undulating gravity profile in some places.

The western extreme part of the profile is characterized by a relatively positive gravity anomaly. Geological data indicate that there are Precambrian outcrops in the northern and southeastern parts of the profile, which are associated with the high grade metamorphic belts of western Ethiopia and the Mozambique belt, respectively. Overall, characteristics of the profile indicate that the rift region, as a whole, is associated with a long wavelength gravity anomaly. Two short wavelength relative gravity positive anomalies are superimposed on the long

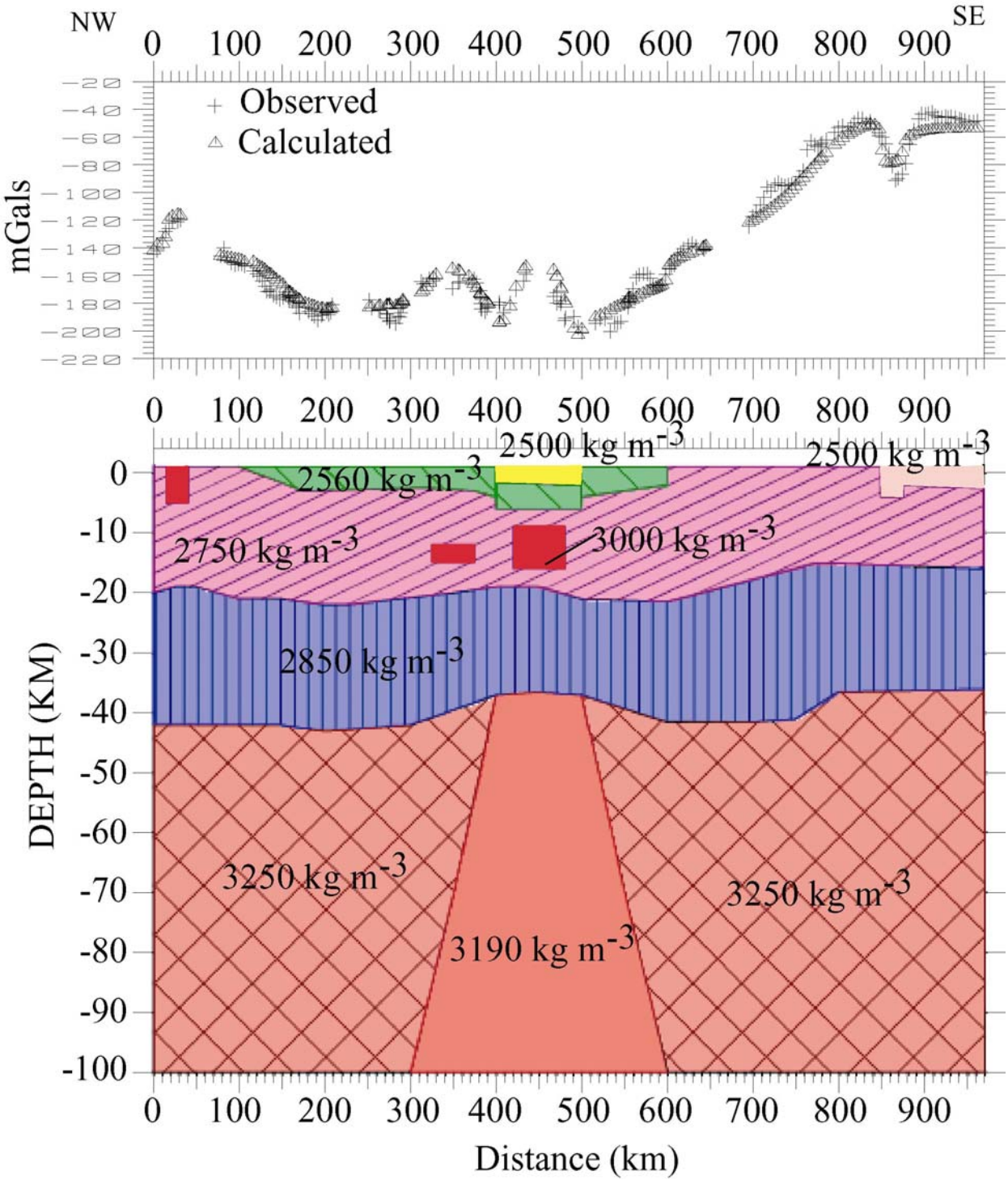

Figure 2.28: Gravity Profile across the southern part of the MER

wavelength gravity low. These short wavelength positive gravity anomalies are associated with volcanic centers in the rift floor. The long wavelength positive gravity anomaly is associated with the southeastern part of the profile because of the Mozambique belt zone in the southeastern Ethiopia region and passive margin of the coastal East Africa. Geological data indicate the presence of Precambrian rock outcrops and the region of east African passive margin. Thus these geologic phenomena could be responsible for the broad positive gravity anomaly. Local minima are present in parts of the Ogaden basin. Because of the presence of Karroo rifting, these features suggest grabens filled with sediment.

The upper part of the rift is modeled using a 2500 kg m^{-3} density for the Quaternary sediments. There is about 2.0 to 2.5 km of sediment. The basaltic formation and volcanic sediments have a density of ~2560 kg m^{-3} and are thicker at the western and eastern flanks of the rift. The upper crust appears to be thicker on the two plateaus, especially close to the rift flanks. The lower crust which is modeled as a 2850 kg m^{-3} layer has a fairly uniform thickness that slightly rises towards the southeast. The upper mantle, which follows the topography of the Moho, reveals a shallow mantle beneath the passive margin.

The narrow positive anomalies within the rift are modeled using 3000 kg m^{-3}, which indicates volcanic intrusive bodies within the upper crust. The Moho appears deeper on the western plateau. As in the northern part of the rift, this profile also indicates a thicker crust ~38 km within the rift.

2.5.3 The Axial Profile

The axial gravity profile, about 1800 km long, (Fig. 2.29) was constructed to assess the along-axis crustal variation of the Ethiopian rift and to tie the modeling done in this study to the previously studied northern part of the eastern rift in Kenya. Another purpose of this profile is to tie the profiles that cross the southern Afar and the main Ethiopian rift (Figs. 2.25, 2.26, 2.27, 2.28 and 2.29). The profile starts in the central part of the eastern rift in Kenya just south of the

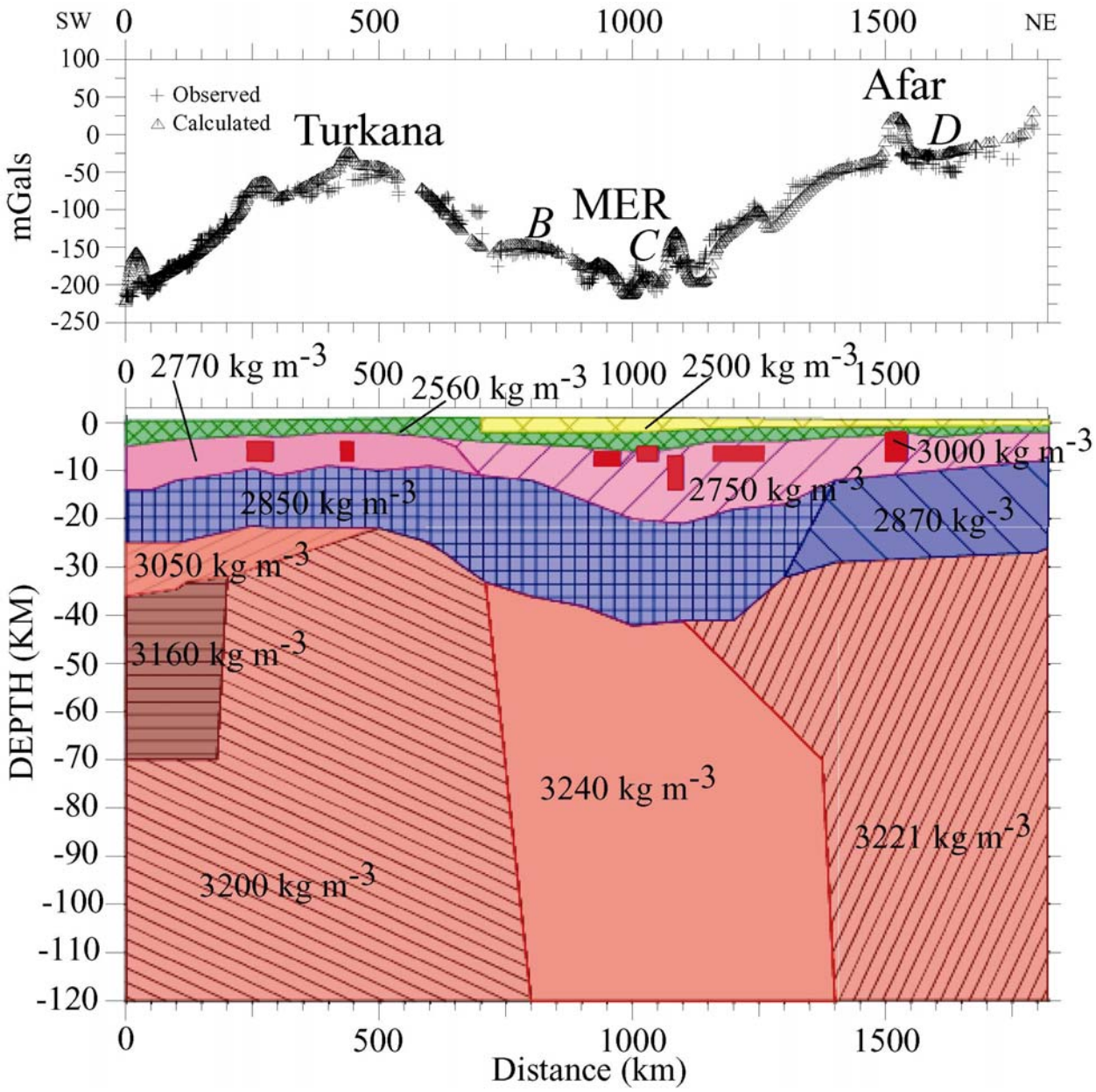

Figure 2.29: Gravity Profile along the axial direction of the East African Rift

Equator at -0.59°S latitude and 36.19°E longitude and passes through the Lake Turkana region into the southern part of the Ethiopian rift. This profile continues further to the northeast, close to west of the Lake Abaya area towards the Lake Awasa region into the main Ethiopian rift. This profile crosses a number of rift basins and rift segments (Rosendahl, 1987; Hayward and Ebinger, 1996; Ebinger and Casey, 2001), including Lake Turkana, the Omo Valley, the Lake Abbaya region, Shalla and Ziway. Further northeast, this profile crosses the Aluto volcanic complex, the Gedemsa caldera, through the Kereyu basin into the Afar triangle close to Red Sea at about 13.95°N latitude and 40.99°E longitude.

The main advantage of modeling this profile is the availability of constraining parameters. Because it is designed to pass close to the axial refraction seismic lines acquired for EAGLE and KRISP in Ethiopia and Kenya, respectively, along the axial direction. Therefore, constraining model parameters benefited from the data of these two surveys. The KRISP90 line for the northern part of the eastern rift up to Lake Turkana (Mechie et al., 1994, Keller et al., 1994) is used for model parameter control (layer thicknesses and densities) in the southern section of the profile. The EAGLE refraction profile (Keller et al., 2004, Maguire et al., 2006) along the axial direction starting from Lake Awasa to southern Afar was instrumental in constraining the northeastern section of this model. No seismic survey has been conducted in the area between Turkana and Lake Awasa, and our model depends solely on the geologic information and extrapolation between the two fundamental, along axis, refraction surveys conducted in Ethiopia and Kenya.

The axial profile model can be divided into four major areas. The first section is the southern extreme which is associated with the central part of the Kenyan rift and which has a relative negative Bouguer anomaly. This section of the rift has a crustal thickness of 35 km. Based on seismic results in the Kenyan section of the rift this portion of the profile has been

interpreted (Keller, et al., 1994; Mechie et al., 1994; Hay et al, 1995b) as having low velocity seismic material underlying the base of the lower crust, the Moho, that has modified and thickened the lower crust by magmatic intrusion or underplating.

The Turkana area is the second region characterized by a relatively positive anomaly in the southern section of the profile. The crustal thickness in this region decreases from about 35 km in central Kenya to 22 km beneath the Turkana area. The Turkana region is known for its multiple episodes such as the possible Mesozoic rifting and the Cenozoic greater extension (Ebinger, et al., 1989; Hendrie et al., 1994; Morley, 1994). Morley (1999) further explains the multiple rifting episode scenario of the Turkana region, relating it to the extensive rift system that extends across central Africa from the west coast of Nigeria to the east coast of Kenya. The episodic activity of this major rift started in the Cretaceous and lasted into the early Tertiary (e.g., Shull, 1988; Bosworth and Morley, 1994).

The third region is associated with the proper Ethiopian rift. The gravity anomaly just northeast of the Turkana and the southern Ethiopian rifts begins to decrease and reaches a minimum in the MER between Lake Koka and Ziway. In general, the MER is characterized by a gravity minimum observed along this profile. In our model the crystalline basement appears to consist of much of the upper crust and basement outcrop in between the Omo valley and Lake Abaya. This is also true from the geology of the area as explained in other studies (e.g. Davidson, 1983; Ebinger et, al; 1989; WoldeGabriel, 1990). In this region the profile across the MER shares the same crustal thickness (~40 km). The Aluto and Gedemsa volcanic centers are modeled as mafic bodies with a density of 3000 kg m^{-3}. Crustal thickness begins to decrease in both directions towards Turkana and the Afar triple junction.

According to our model much of the crustal variation is associated with the lower crust. The thickness of the lower crust increases beneath the MER. The crystalline basement appears to

vary in thickness in both directions towards the Afar triangle and the Turkana rift. The maximum thickness appears to exist beneath the main Ethiopian rift, which also coincides with the gravity minima in this area.

The fourth section of the profile is the Afar triple junction area. The maximum gravity anomaly observed along this profile occurs in this section. The upper and lower crust thin toward the end of the profile, attaining a thickness of 26 km, although the gravity anomaly of the Afar triple junction area is much higher than the Turkana area. The density of the lower crust must be greater and shallower than the rest of the rift section. This could be the result of the intensive volcanism and crustal attenuation beneath the Afar. The lower crust may be modified to attain slightly lower density variation values.

2.6 Discussion and Conclusions

Understanding the geodynamics and tectonics of the east African rift system requires knowing the crustal structure of the region along and across the rift. Gravity data, more widely available in this area than any other geophysical data, are the best tool to most accurately investigate these processes because they are also the only available geophysical data with fairly even regional distribution across and along the east African rift system. The gravity anomaly maps presented in this study show most of the major structural features such as the northwest-southeast trending Anza graben in northern Kenya. The north-south trending Turkana rift cuts the Anza graben and is characterized by a local gravity high. North of Turkana rift is the northeast-southwest trending Ethiopian rift, which divides the western and eastern plateau of Ethiopia. The boundaries of all these structural features are clearly delineated with parallel, closely spaced contour lines that are coincident with the border faults of the rifts indicating sharp gravity gradients. The Anza graben is depicted as a regional gravity high superimposed on a relative low. These relative lows may be associated with Cretaceous sediments deposited in the

region. Distinct gravity highs observed in the Turkana region may be associated with the recent volcanic centers as a result of the modification of the Anza graben by the Cenozoic Ethiopian rift as it propagates towards the south. The Ethiopian dome and the Kenyan dome are separated by this anomaly, and they are characterized by broad negative Bouguer gravity anomalies as well. The large negative gravity anomaly associated with the western Ethiopian plateau suggests that it has a thicker crust and/or a lower upper mantle density compared to the Kenyan dome. Possibly, the original plume uplift occurred beneath Lake Tana (e.g., Chorowicz, 2005), causing maximum uplift in the region. The cross profiles also suggest thick crust on the Ethiopian plateaus compared to Kenyan dome when compared with previous integrated interpretation in Kenya (Simiyu and Keller, 1997; Mariita and Keller, 2007), indicating that the Ethiopian dome has thicker crust and higher topographic expressions. This implies that there is a correlation between high topography, greater crustal thickness, and low gravity anomaly.

The models produced using integrated data from both the Ethiopian and the Kenyan rift surveys suggest that the MER is underlain by a thick crust. Because thick crust exists beneath the MER it suggests that the crust in this region may not be modified like the northeastern and southwestern sections of the rift in the Afar and the Turkana regions. We can also observe from the cross rift models that the mantle or the Moho has a smooth topography with a gentle rise under the MER and a dips towards the northwest and southeast beneath the western and the eastern plateaus respectively. This anomalous crustal thickness within the rift is also supported by teleseismic and tomographic results (e.g., Bastow et al., 2005), as shown by an elongated low velocity zone beneath the Afar region and northern MER from 75 km to 400 km depth.

The south Afar profile shows a strong positive anomaly across the rift flanked by the two negative anomalies on the western and eastern plateaus. The crust in this region is thin which it may be attenuated either by immense volcanism or an uplift. The shallow occurrence of the

Moho or the mantle structure beneath this region may be the result of a mantle plume impact as suggested by various studies (Montelli, 2004; Ritsema et al., 1999; Courtillot, 1999; Corti et al., 2005; Furman, 2006). Thus, our study consistently supports previous assumptions. The regional extension is also immense (Bilham, et al., 1999; Fernandes et al, 2004). The mantle material appears broad and shallower in this region.

The cross profile along the EAGLE controlled source experiment profile 1 indicates that an underplated layer exists beneath the western plateau, which is also supported by the EAGLE line 1 seismic refraction model (e.g. McKenzie et al., 2005) and high topography.

The gravity anomaly maps and the axial gravity profile show that the crustal thickness in Afar is thicker when compared to the Turkana region. Although the Afar region is still one of the active spreading centers affected by the tri-radial rift systems (the Red Sea, the Gulf of Aden and the Ethiopian rifts), the geodynamics can be considered as single impact. The deformation of the brittle part of the crust is difficult to quantify, based on a single kinematic model. However, some have proposed that a layer is thinned by an amount proportional to its extension (Keen, 1985). If this is the case, it suggests that Afar is more extended than the MER. However, due to multiple rifting episodes, the Turkana region has had the highest amount of extension and thinning to attain the thinnest crustal thickness observed along the axial profile. Some suggest thin crust in the Turkana region is due to plume and ambient mantle source activities (Furman, 2006). However, based on the surface geology and tectonism, as well as our modeling and mapping results, multiple episode of rifting could be responsible for this wide area of crustal thinning.

The timing of rifting and volcanism gets younger as one progresses southwestward from the Red Sea rift, which is believed to be initiated before 30 Ma (Wolfenden, et al., 2004; Ebinger, 1989). This fact, together with the existence of a progressively thickening crust towards

the Main Ethiopian rift along the axial profile (Fig. 31), suggests that the rifting phenomena is younging towards the southwest up to the MER. The axial profile shows a reduction in the crustal thickness as one progresses southwest to the southern Ethiopian rifts and the Turkana region. The oldest volcanic rocks (~40Ma) are found in the southwestern section of the Ethiopian plateau close to the southern rifts (Ebinger et al, 2000). Precambrian rocks, such as the Hammer horst, are widely exposed in this region (Davidson, 1983, WoldeGabriel et al., 1990; Asrat et al., 2001; Teklay et al., 1998). Just as in the case of the eastern rift in Kenya and Tanzania that has propagated southward for the last 15 Ma (e.g., Simiyu and Keller, 1997), we see a similar trend in the southern part of the Ethiopian rift towards Turkana.

The crust beneath the plateaus is generally thicker, exceeding 40 km, than in the surrounding regions. The cross profile in the MER suggests that the crustal modification is less in this region than in the Afar and Turkana areas. The eastern rift flank shows a thicker crust near the area of the MER. However, in the southern Afar profile, we see a much thicker crust in the western plateau, which is close to the topographically high region of Ethiopia (Lake Tana region). The thick crust, coupled with the high elevation of the region, may indicate that the western plateau has a much thicker crust and occupies the largest part of Ethiopia. The basement rock outcrops of the MER in the area of Kella (north of Butajira) may indicate the existence of a less modified crust beneath the MER.

The cross profile results indicate a general topography high for the Moho within the rift. Also, the width of the elevated Moho within the rift is greater across the southern Afar area; however, it is less subdued along the MER. One of the longest profiles across the southern part of the MER indicates a much shallower Moho beneath the western and eastern parts of the profile. The eastern elevated Moho depth may be due to its proximity to the eastern passive margin beneath the Somalian and northeastern Kenyan coastal margin. Further to the west,

metamorphic outcrops that are part of the Mozambique belt may be the cause of the broad gravity high of the region. In general our modeling indicates a five-layer structure exists. The layers are: i) an upper thin sedimentary section; ii) a volcanic and volcano-sediment layer; iii) an upper crust mostly characterized by crystalline basement iv) a lower basaltic crust; v) a part of the upper mantle exhibiting a shallow depth in the region of the Turkana rift and the Afar triangle, and a thicker depth within the main Ethiopian rift. In addition to these large structural features, intrusive bodies associated with central volcanoes within the rift floor are exhibited. These intrusive bodies are intruded within the upper crust. The gravity, seismic and geologic information available for the region was integrated to produce the model generated along each profile. These models are as simple as possible, yet they still honor the available constraints. The models contain no lateral changes in most of the layers; however, varying the topography of each horizon produces a reliable fit to the observed data. Also, the underplated section beneath the western plateau is unique on the cross profile along EAGLE line 1. The mantle layer shows low density underneath the rift and relatively high densities beneath both plateaus.

In each model, the short wavelength positive gravity anomalies associated with intrusive bodies correspond to the existing major volcanic centers in the rift. These mafic bodies are the result of diking within the upper crust or beneath the different volcanic segments in the rift. Other gravity high anomalies correlate well with outcrops of Precambrian zones or metamorphic belts. A zone of high-density mafic bodies exists beneath the Aluto volcano along the MER profile, as well as under other volcanic centers. These volcanic centers could be regions of intense magmatic intrusion.

A general relationship appears to exist between topography and crustal thickness. Topographic highs associated with the plateaus result in gravity low anomalies and thicker crustal structures. Along the axial profile model, an exact correspondence occurs between the

topographic variation and the gravity anomaly. The high topography within the MER and Kenyan rift indicate thicker crustal structures when compared to the low elevation and crustal thickness attained via underplating in the Afar triple junction and Turkana rifts, resulting in thinner crustal structures and relatively positive gravity anomalies. On a broader scale the Ethiopian rift shows wide negative Bouguer gravity anomaly. However, superimposed on the broad negative anomaly are short wavelength positive anomalies associated with volcanic centers (e.g., Figs. 2.26, 2.27, 2.28 and 2.29).

Taking the all cross profiles together, a zone of low density material in the axial direction is observed. These low density anomaly in the southern main Ethiopian rift is narrower and it widens towards the north beneath the Afar triple junction. The cross profiles show rift basins filled with low density sediments and volcanic sediments in almost all profiles within their upper most layers. These sediments may be important exploration targets and further detailed study needs to be conducted in Afar and Southern Ethiopian rifts.

Chapter 3: The Abbay (Blue Nile) Basin

3.1 Introduction

Today, petroleum companies are searching the world over for new exploration targets. High oil prices, the peak world oil production scenario, and the scarcity of petroleum itself are creating an avenue for marginalized and challenging exploration areas to be considered. To locate new targets in this environment, all potential source and reservoir rocks have to be investigated, in addition to analyzing the tectonic setting and basic petroleum occurrence conditions. The Abbay basin in the central northwestern part of Ethiopia is little known from both a tectonic and exploration point of view and is the target of this study (Fig. 3.1). One motivation for investigating this area is the existence of oil seep in the Were Ilu region on the northeastern part of the basin. This is a possible indication of the existence of commercially

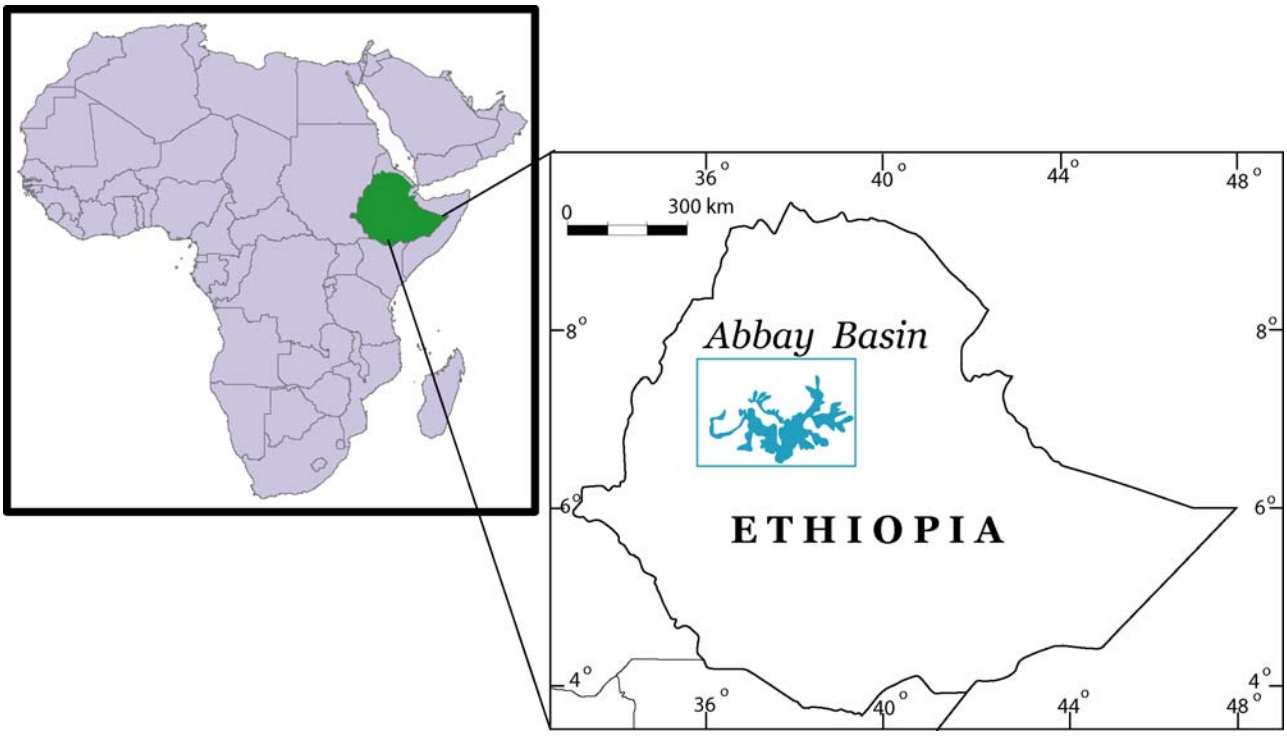

Figure 3. 1: Location map of the Abbay basin. The light blue colored section is the area where the sedimentary rocks outcrop. The inset shows the location of Ethiopia in green.

attractive hydrocarbons trapped in the sedimentary formations, which are buried a few kilometers under the flood basalts of the Ethiopian Plateau.

The Abbay basin is located in the northwestern part of Ethiopia and lies beneath the western Ethiopian plateau. It covers an area of about 70,000 km^2 (Fig. 3.1). The physiography is characterized by incised rivers, extensive plateaus, and volcanic mountain edifices rising up to 4620 meters above sea level. The Abbay (Blue Nile) River is the outflow from Lake Tana (Fig. 3.2). It flows into a deeply incised canyon, initially flowing southeastward. After about 100 km, the river turns westward around the Choke shield volcano. The Abbay River then leaves the Ethiopian plateau and flows into the Sudan plain in a northwest direction. This drainage pattern is suggested to be a result of uplift in the region (e.g., Chorowitz et al., 1998).

The Abbay basin region is underlain by over 3 km of Paleozoic and Mesozoic sedimentary strata that are exposed along the Abbay River gorge (Fig. 3.2). However, most of these strata are covered by flood basalts that are widely believed to have erupted as a result of the initiation of a mantle plume beneath the Afar triple junction region. The stratigraphic and lithologic similarities that exist between the Abbay basin and Ogaden basin in the southeastern part of Ethiopia are based on information from deep exploratory wells in the Ogaden basin, some of which were oil and gas discoveries. The source and reservoir rocks of the Ogaden basin are also similar to the Abbay basin (Wolela A. 1997; BEICIP FranLab, 1998). Age equivalent sedimentary basins in neighboring countries such as Sudan, Yemen and other East African countries contain important hydrocarbon discoveries in similar context. Thus, a better understanding of the evolution of the Abbay basin is not only important from a tectonic and regional geology point of view, but is also important to understanding its hydrocarbon potential.

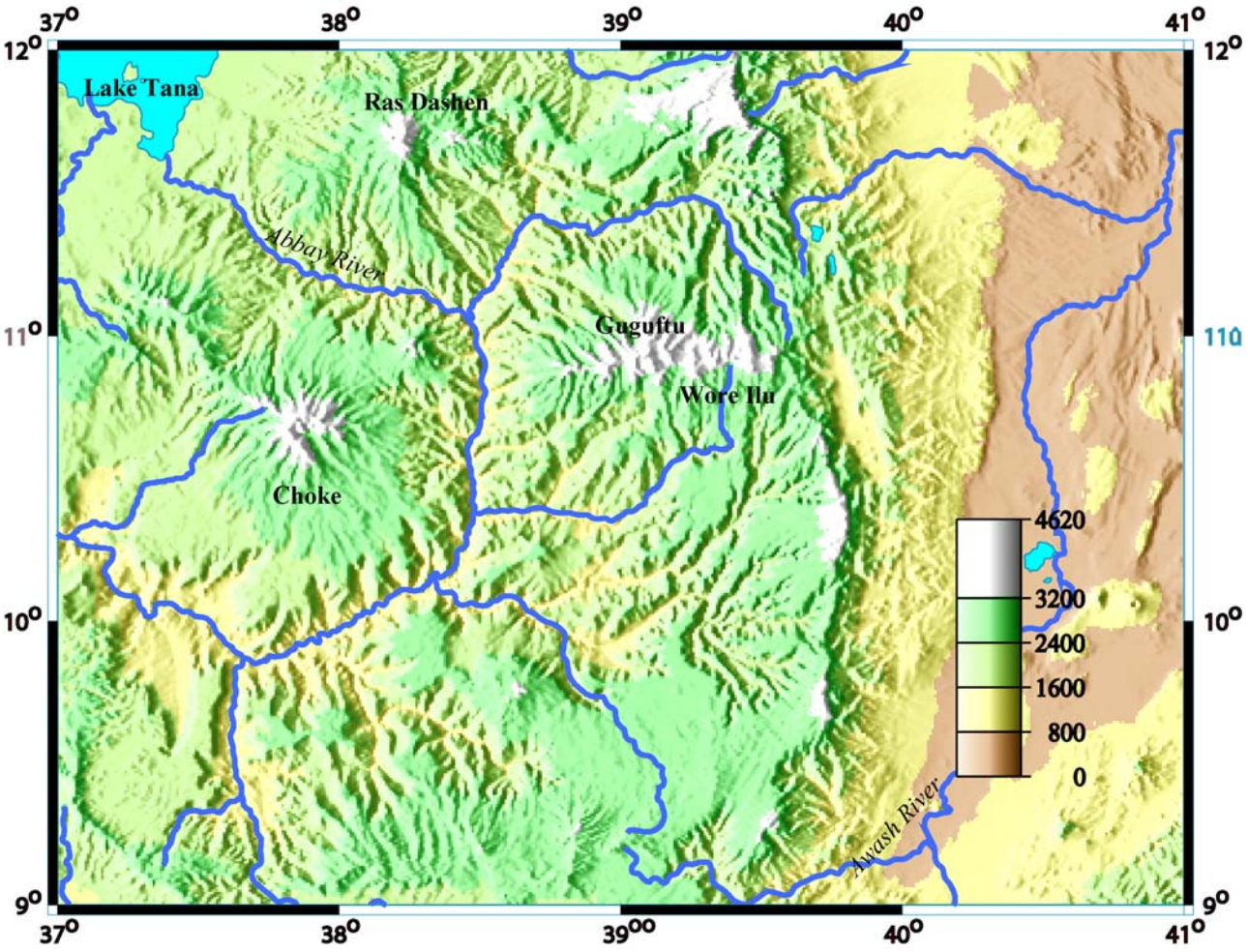

Figure 3.2: Topographic map of the Abbay (Blue Nile) basin, and its surrounding areas, showing the Abbay (Blue Nile River) along with its tributaries cutting deep gorges.

Since more than 3 km of Paleozoic and Mesozoic strata outcrop along the Abbay (Blue Nile) gorge but the remainder of the area is covered by the flood basalts, this area is an ideal

target for the integration of a variety of geological and geophysical techniques for delineating the subsurface of these strata. In this study, gravity data, gravity models, geologic cross sections, surface geologic structures, remote sensing and Digital Elevations Model (DEM) analyses have been carried out for better understanding of the evolution, structural configuration and geometry of the Abbay basin.

3.2 Geologic Setting

3.2.1 Regional geology

The regional geology and stratigraphy of the Abbay basin has been documented by a number of authors [e.g. Blanford (1869); Aubry (1886); Elewarth, 1960; Jepson and Athearn (1961, 1964); Mohr (1962); Shumbro (1968); Greitzer (1970); Kazmin (1972, 1975); Rabben et al., 1979; Getaneh (1979, 1980, 1981 and 1991); Russo et al., (1994); Wolela et al. (1994); Wolela (1997)]. After development of the Neoproterozoic East African orogen (Stern, 1994) there is little evidence of sedimentation in the region of Ethiopia until the Late Paleozoic.

The Breakup of Gondwanaland, which began in Late Paleozoic and persisted up to Jurassic time, produced rift basins around the border of the super continent. In East Africa, these basins are largely fault-bounded, and are in-filled with thick successions of continental Karroo and marine sediments. In the Abbay basin, the Paleozoic and Mesozoic sediments are covered by Tertiary basalts. The K/Ar ages of basalts from volcanic piles of the Abbay basin are 31.0 -27.4 Ma. This suggests the existence of Aiba and Alaje Formation of the Ashangi (Fig. 3.3) Trap domain (Zanettin et al., 1980; Ukstins et al., 2002). The Trap series are the earliest group of volcanic rocks which were erupted from fissures during the Tertiary. The other volcanic cover in the region comes from the shield volcanoes in the area and is younger.

3.2.2 Stratigraphy of the Abbay basin

The general geology and stratigraphy of the Abbay basin and adjacent areas (Fig. 3.3 and Fig. 3.4) has been studied by various researchers, but since no deep wells have been drilled in the Abbay basin, very little information is available on the subsurface geology of the basin. Most of the current information available in documents comes from surface geology exposed along walls of river canyons and gorges (Figs. 3.2 and 3.3). The thickness of the overlying basalts is not known everywhere and the common estimate of 1-2 km (Getaneh, 1979; Wolela, 1997) comes

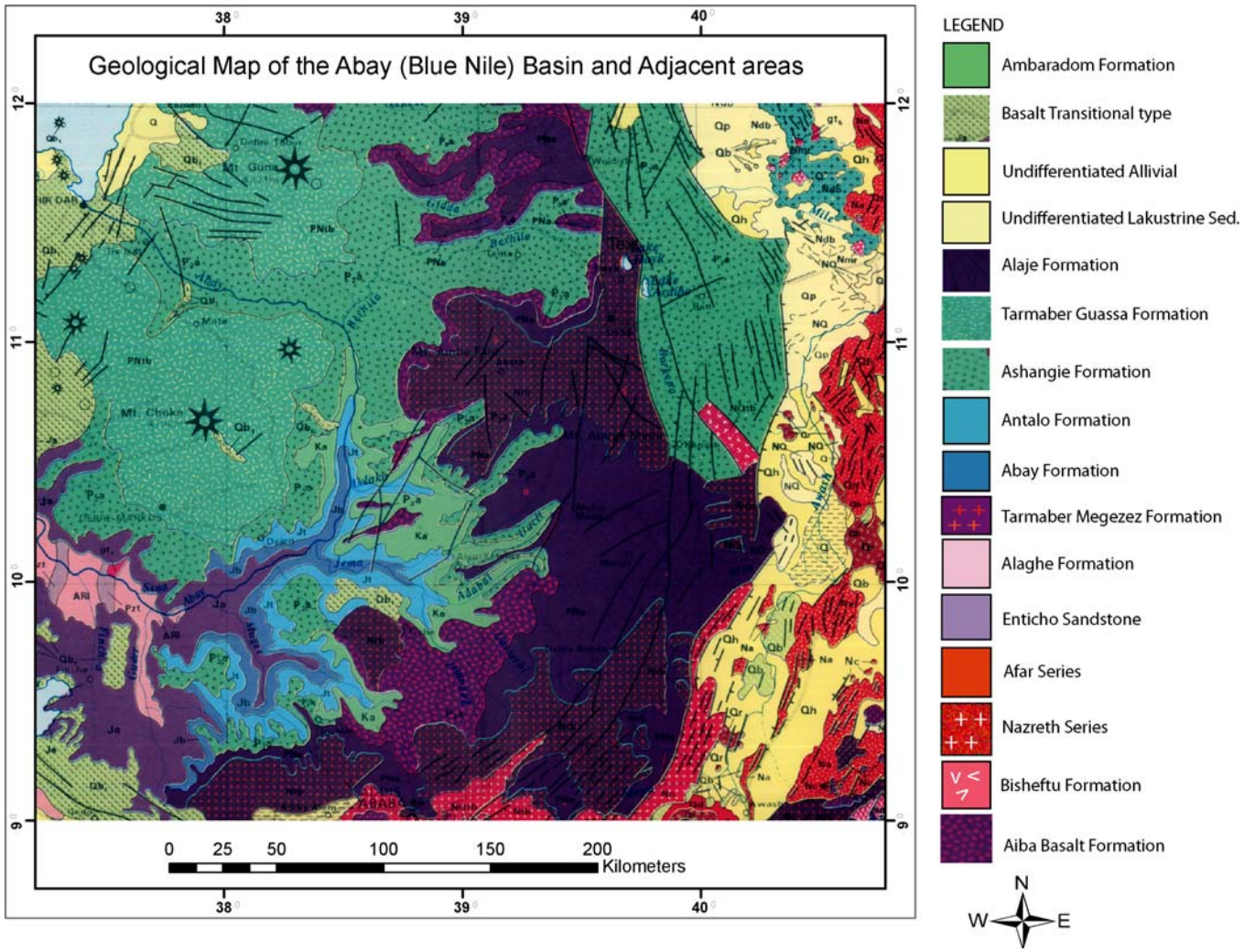

Figure 3.3: Geological map of the Abbay basin and adjacent areas, showing the central part of the Abbay basin where the Mesozoic sediments outcrop and the extent of the volcanic cover of varying ages (modified after Tefera, et al., 1996).

from surface exposures. However, various authors have established different measurements and estimates of the stratigraphy of the Abbay basin (e.g., Aubury, 1886; Jepsen and Athrean, 1964; Kazmin, 1972; Mohr, 1971; Getaneh, 1979, 1979, 1980, 1981 and 1991; Wolela, 1997).

From the standpoint of petroleum exploration, the Urandab Shale in the Ogaden basin (southeastern Ethiopia) has attracted recent attention as a potential petroleum source rock because of its high total organic content. The equivalent of Urandab Shale in the Abbay basins is the Upper Hamanlei Formation. The Upper Hamanlei Formation (limestone and shale intercalations) in the Abbay basin has equivalent TOC to Urandab Shale which is in the range of 1.9 to 6.8 %. This important source rock (the upper Hamanlei Carbonate) coupled with excellent reservoir rocks, the Adigrat Sandstone, and the Debrelibanose Sandstone (Fig. 3.4), overlying this source rock and the basalt top seal comprises a challenging and interesting petroleum system in the Abbay (Blue Nile) basin.

3.2.2.1 Precambrian

Precambrian rocks are exposed in several areas of Ethiopia. The Precambrian rocks of Ethiopia contain a wide variety of sedimentary, volcanic and intrusive rocks that have been metamorphosed to varying degrees (Kazmin, 1972; Getaneh, 1991). The Precambrian rocks of Ethiopia represent part of the Pan African orogenies. Classification of the Precambrian rocks composition and distribution in Ethiopia are described by various researchers (e. g., TekleWold and Moore, 1989; Tefera et al., 1996; Asrat, et al., 2001; Teklay, et al., 1998). The Precambrian basement rocks of the Abbay basin (Fig. 3.3) are part of the high-grade metamorphic rocks of the Geba Domain (TekleWold and Moore, 1989), which are classified as being part of the Alghe Group (Tefera et al., 1996).

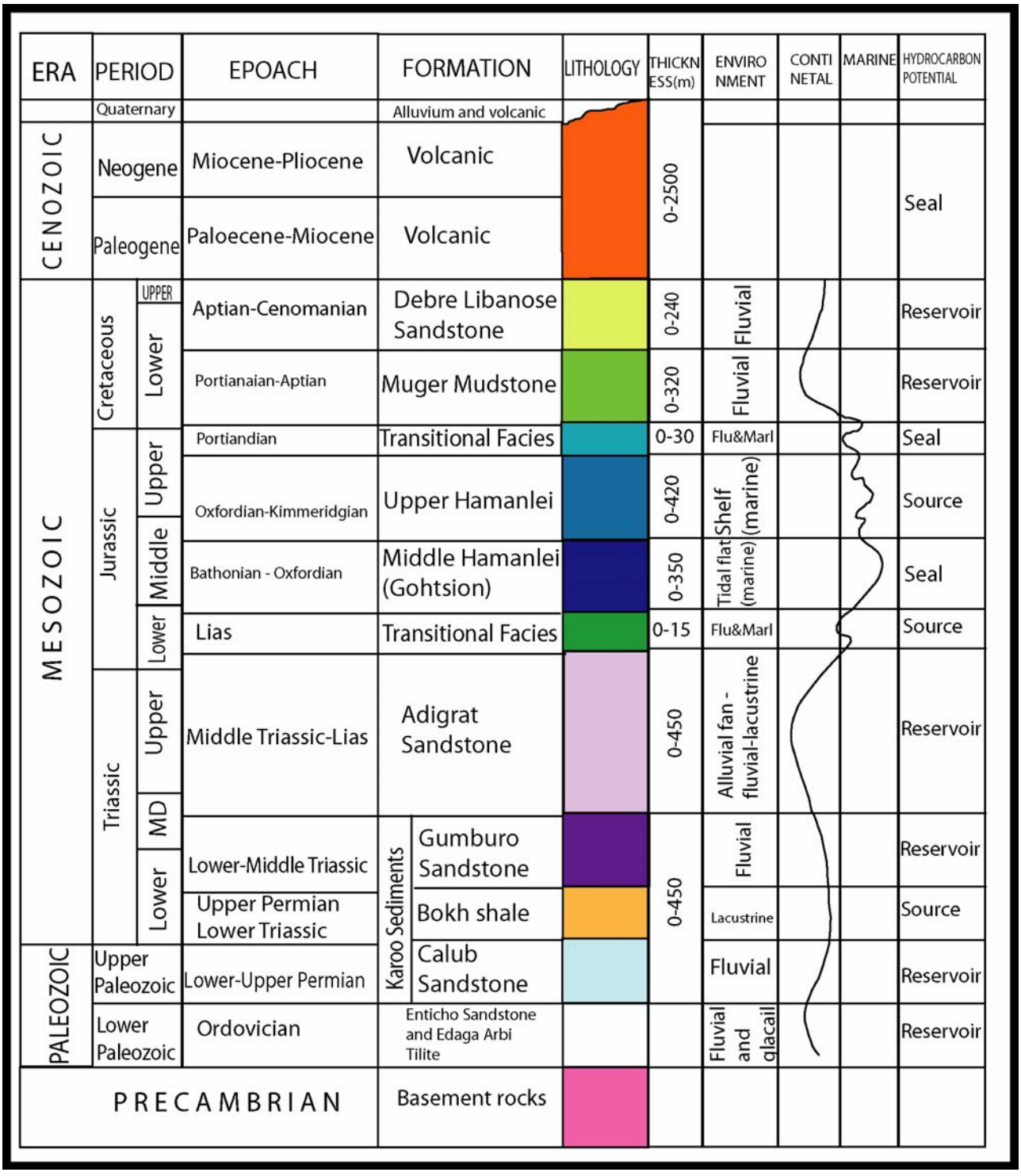

Figure 3.4: Stratigraphic column of the Abbay basin area.

3.2.2.2 The Paleozoic Sediments

The oldest unmetamorphosed Paleozoic strata of Ethiopia are the Enticho Sandstone and Edaga Arbi Tillites found in northern Ethiopia (Fig. 3.4). These formations are named after the localities where the type sections were first found. Presence of Karroo strata in the Abbay basin is not yet confirmed. Geological studies confirmed that a 135 m thick layer of lower Paleozoic strata is found in the southwestern section of the Abbay basin (Asnake, 1989). Fossil studies of these strata have indicated that they are Silurian and upper Ordovician in age.

3.2.2.3 Karroo Sediments

During the Permo-Triassic the break up of Gondwanaland was initiated in present day South Africa and propagated northward (modern coordinates) to form the continental margin of East Africa and associated rift zones. Structural features associated with this rifting are known in parts of South Africa, Mozambique, Tanzania, Kenya, Somali and Ethiopia including Madagascar (Flores, 1973; Canon et al., 1981; Worku, 1988). In the middle of Abbay basin there are three extensive patches of sedimentary rock that are largely composed of light to dark grey sandstones and shales that underlie the Adigrat Sandstone (Jepson and Athearn, 1964; Mohr, 1962; Raaben et al., 1980). Kazmin (1975) has documented the presence of channel filling siltstones south of Lake Tana, which possibly represent the Upper Carboniferous to Lower Mesozoic interval. Erosion has removed a considerable part of these strata. Karroo strata in the Ogaden basin have been confirmed to have a thickness in excess of 1200 meters based on deep drilling results (Worku, 1988).

The Karroo strata in the Ogaden basin include the alluvial or fluvial Gumburo Sandstone, the lacustrine Bokh Shale and the alluvial or fluvial sandstone and conglomerate of the Calub Formation (Raaben et al., 1972; Worku, 1988; Worku and Austin, 1992).

3.2.2.4 Adigrat Sandstone

The Karroo rift system favored the deposition of fluvial and debris flow dominated proximal-mid alluvial fan sedimentation. The Adigrat Sandstone in the Abbay basin attains a thickness of 100 meters in the Jemma River section (Mohr, 1962). The Adigrat Sandstone is a widely available formation in Ethiopia. The thickness of this formation ranges from 120 to 800 meter within the Abbay basin (e.g., Wolela, et al., 1994; Tamrat and Tibebe, 1997). This formation has a thickness of 450 meter in the Ogaden basins in the subsurface and about 700 m outcrop in northern Ethiopia (Mekele).

After the deposition of Calub Sandstone formation, the Bokh Shale and Gumburo Sandstone Formations in the Karroo rift system, the Adigrat Sandstone formation overstepped the Karroo rift and is widely distributed beyond the Karroo graben. It extends westward as far as Arjo in western Ethiopia (Asseffa and Wolela, 1996). The Adigrat sandstone is one of the potential reservoir rocks in the Abbay basin (Wolela, 1997).

3.2.2.5 Hamanlei Limestone

The Horn of Africa was marked by a major Mesozoic transgression initiated by thermal subsidence. The Hamanlei Limestone represents the main transgressive phase of Mesozoic strata in Ethiopia. This unit attains a thickness of 750 m in the Abbay basin, 800 m in Mekele (Northern Ethiopia), 1558 m in the Ogaden basin, and 1480 m in the Denakil Alps in Afar (Beyth, 1972; Kazmin, 1972; Walsh, 1981, Habtezgi, 1989)).

3.3 The Geophysical Database

For our analysis we used a variety of geophysical data that are available for the Abbay basin and were compiled for this study. These data include digital elevation data, gravity readings, and Landsat7 ETM+ orthorectified and georeferenced images. The Landsat data were

processed using a variety of image processing techniques to map the geologic units and their extent. These data were acquired in 2004.

Shuttle Radar Topography Mission digital elevation data (SRTM90, 90 meters) were acquired from the publicly available USGS website (http://edcftp.cr.usgs.gov/pub/data/srtm) for inclusion in our integrated analysis. These data were used to generate topographic images for analyzing this remote region. Soft rock formations and hard rocks can be viewed from these images by considering the prevalence of incised valleys and river gorges. Also, terrain corrections for the gravity readings were calculated using these data. These data provide effective displays (Fig. 3.5) that were an instrumental part of our analysis.

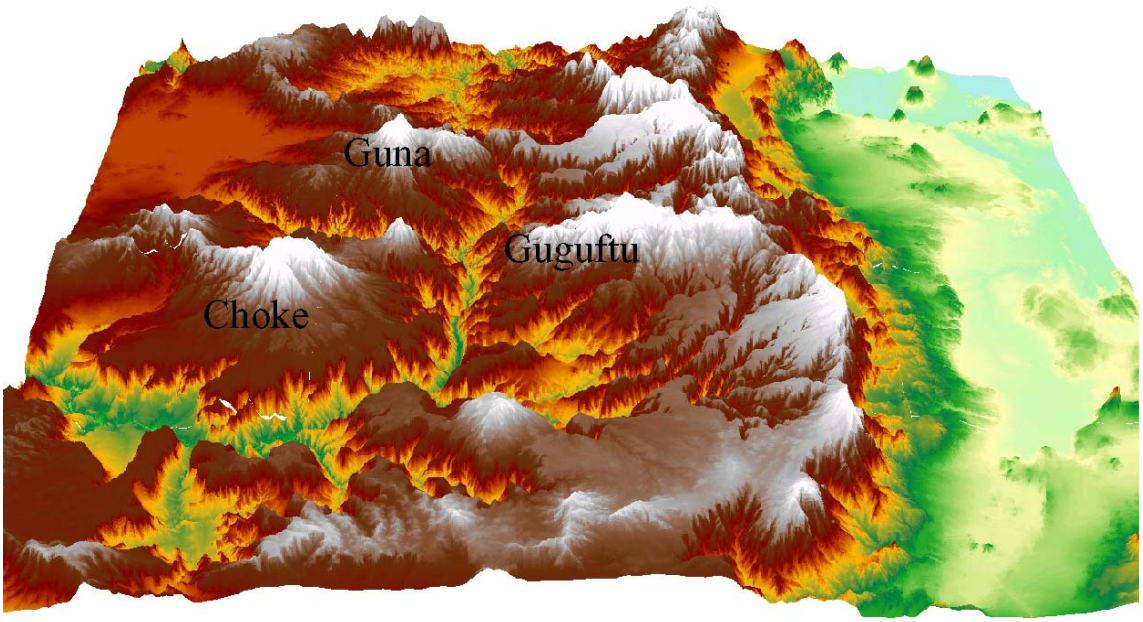

Figure 3.5: Perspective view of the topography of the Abbay basin region based on SRTM90m digital elevation data

Gravity measurements in the Abbay basin region were made as early as 1970 (Searle and Gouin, 1972). However, these measurements were only along the main roads to major cities in the northwestern part of the country. Gravity data acquired by the Petroleum Operations

Department (POD) of the Ministry of Mines and Energy of Ethiopia were the main resource for this study. However, additional data from the National Regional Gravity survey project that were acquired by the Geological Survey of Ethiopia were also included. For regional comparison purposes, data from Afar region that were acquired by University of Hamburg in the late 1960s were also included.

Nearly 3000 data points (Fig. 3.6) were used in this study to generate a Bouguer gravity anomaly map of the Abbay basin region. The Bouguer gravity values were compiled using a density of 2670 kgm^{-3} and the 1967 reference ellipsoid. Sea level was taken as the reference height. The distribution of gravity data in the basin is uneven due to its topography and

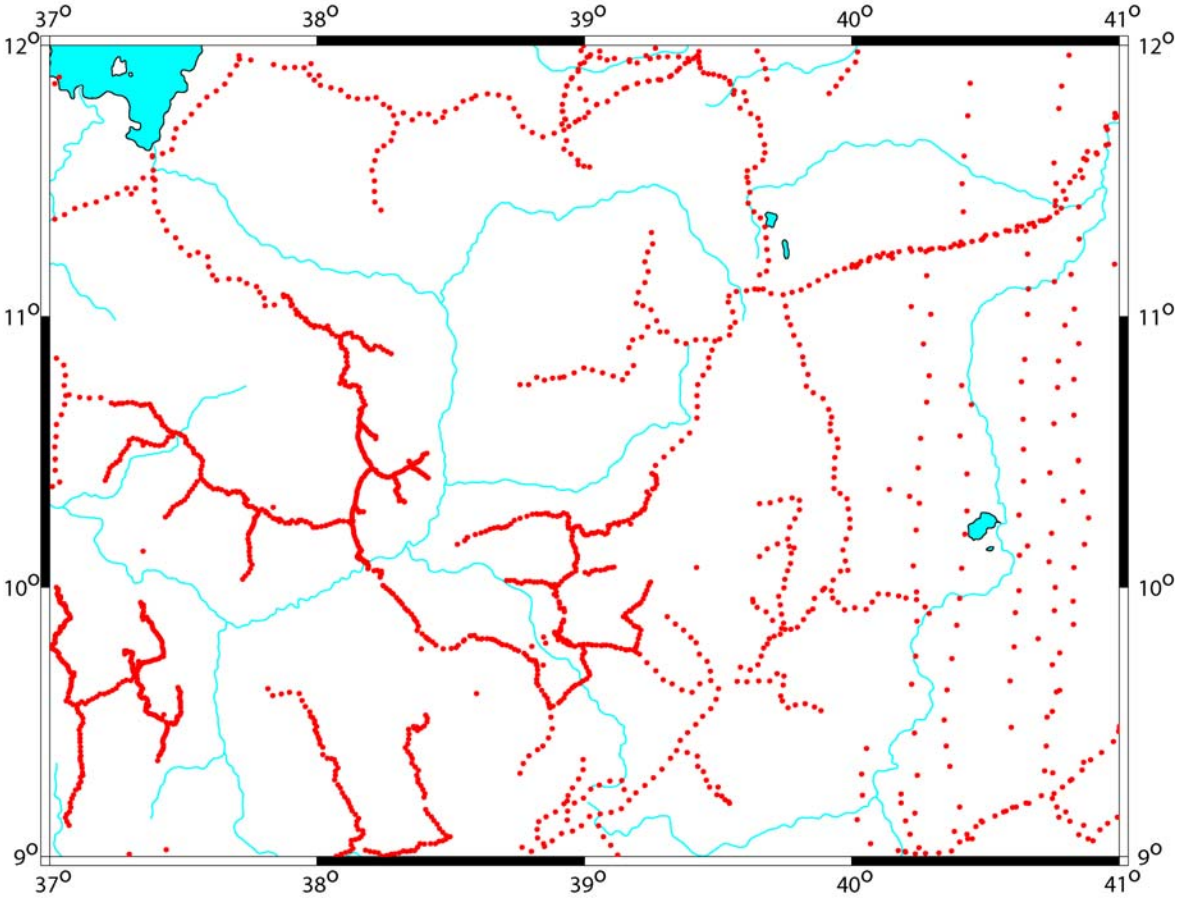

Figure 3.6: Gravity stations location map of the Abbay basin. Red dots are gravity stations, and cyan lines represent rivers.

remoteness. Earlier gravity measurements were made using altimeters for elevation control. The data acquire by the POD are based on Global Positioning System (GPS) locations which have higher accuracies, especially in latitude and longitude values. Terrain corrections for the gravity stations are a must in this topographically complex region. Therefore, we calculated terrain corrections for each station using the SRTM90m data for the regional topographic grid. Local grids were generated using the local elevations obtained for each station, which are determined using high precision GPS instruments such as Trimble 4000SI units. Using these two grids, the terrain correction for each station was computed based on the Hammer technique up to zone M (Hammer, 1939), which considers the terrain effect within a radius of about 21 km. Using Geosoft Oasis Montaj software, this terrain correction was extended up to 21 km to account for the effect of topography in the region. Inner zone terrain corrections were done during field data acquisition up to 170 meters from the station location.

3.4 Landsat Image Processing for Abbay basin

Because of the remote and difficult terrain in the Abbay basin region, Landsat7 ETM+ images were employed to analyze the regional geology and proved very useful. Most remote sensing data are recorded in digital format and virtually all image interpretation and analysis involves some element of digital processing. Digital image processing may involve numerous procedures including formatting and correcting of the data, digital enhancement to facilitate better visual interpretation, and even automated classification of targets and features. The most common image processing methods can be summarized as: Image Enhancement, Image Transformation and Image Classification, and Image Analysis. Image enhancement operations are performed solely to improve the appearance of the imagery in order to assist in visual interpretation and analysis. Examples of enhancement functions include contrast stretching to increase the tonal distinction between various features in a scene and spatial filtering to enhance

(or suppress) specific spatial patterns in an image. Spatial filters are used to enhance the appearance of an image. They are designed to highlight or suppress specific features in an image based on their spatial frequency so as to generate a "new" image.

3.4.1 Pre-Processing

Various factors such as drift of the sensor, radiometric calibration, atmospheric, and topographic effects affect the signal measured at the sensor. Corrections for these effects must be made for accurate remote sensing image analysis. The Landsat7 product is formatted in such a way that it is readily compatible with the ENVI image processing software that is licensed to UTEP. Figure 3.7 shows the original image (a) and a zoomed in version (b) shown as the red box in (a). The wavelengths for each band are given in Table 3.1. The six key bands that have the same spatial resolution (28 m pixels) (i.e., bands 1, 2, 3, 4, 5 and 7) were used in this study. Since the image data are orthorectified, we can assume that the data are corrected to remove

Table 3.1: Wavelength values for each Landsat ETM+ Image and the respective pixel resolution.

Band Number	Wavelength in micrometer	Resolution in m
1	0.45-0.52	30
2	0.53-0.61	30
3	0.63-0.69	30
4	0.78-0.90	30
5	1.55-1.75	30
6	10.40-12.50	60
7	2.09-2.35	30
8	.52-.90	15

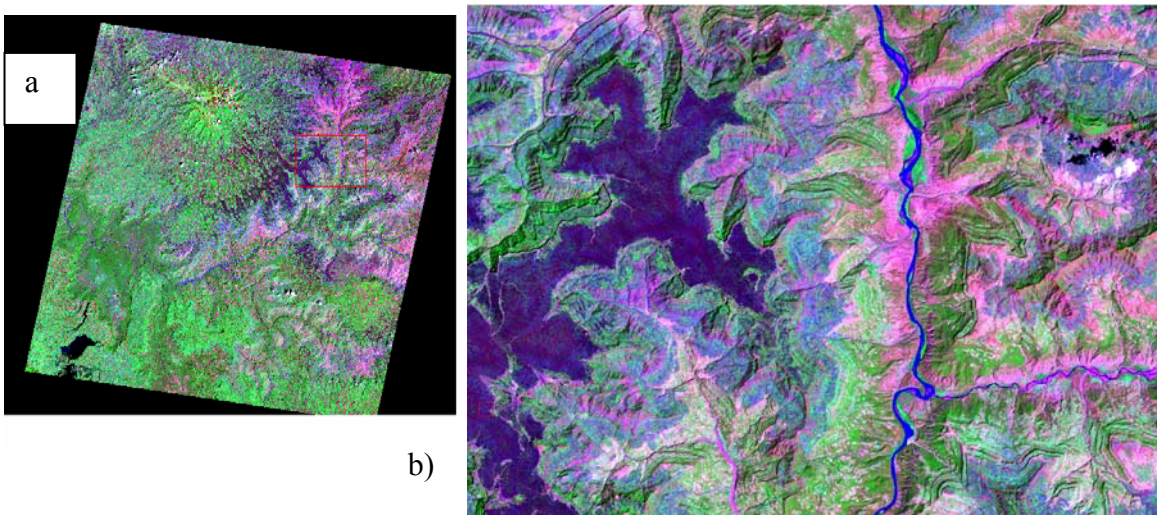

Figure 3.7: The original image displayed using bands 7, 4, and 2 (a) and (b) shows the zoomed version of the area in the red box inside (a)

topographic effects. For the radiometric corrections, I have applied Internal Average Relative Reflectance Calibration (IARRC), which is the best way of correction when there is minimal ground truth data. An average spectrum calculated from the entire scene is used as the reference spectrum and is then divided into the spectrum at each pixel of the image (ENVI User's Manual 2004). Comparisons of the spectral plot before and after radiometric correction are shown in Figure 3.8.

3.4.2 Contrast Stretching

An image can be significantly improved by applying one or more of the many enhancement methods, and the most commonly employed method is contrast stretching. This method systematically expands the range of the digital number (DN) values to the full limits determined by the byte size in the digital data. For Landsat this is determined by altering the distribution to span the entire range of 0 to 255 DNs. The reassignment of DN values is based on the particular stretch algorithm chosen. Commonly, the distribution of DNs (gray levels) can be

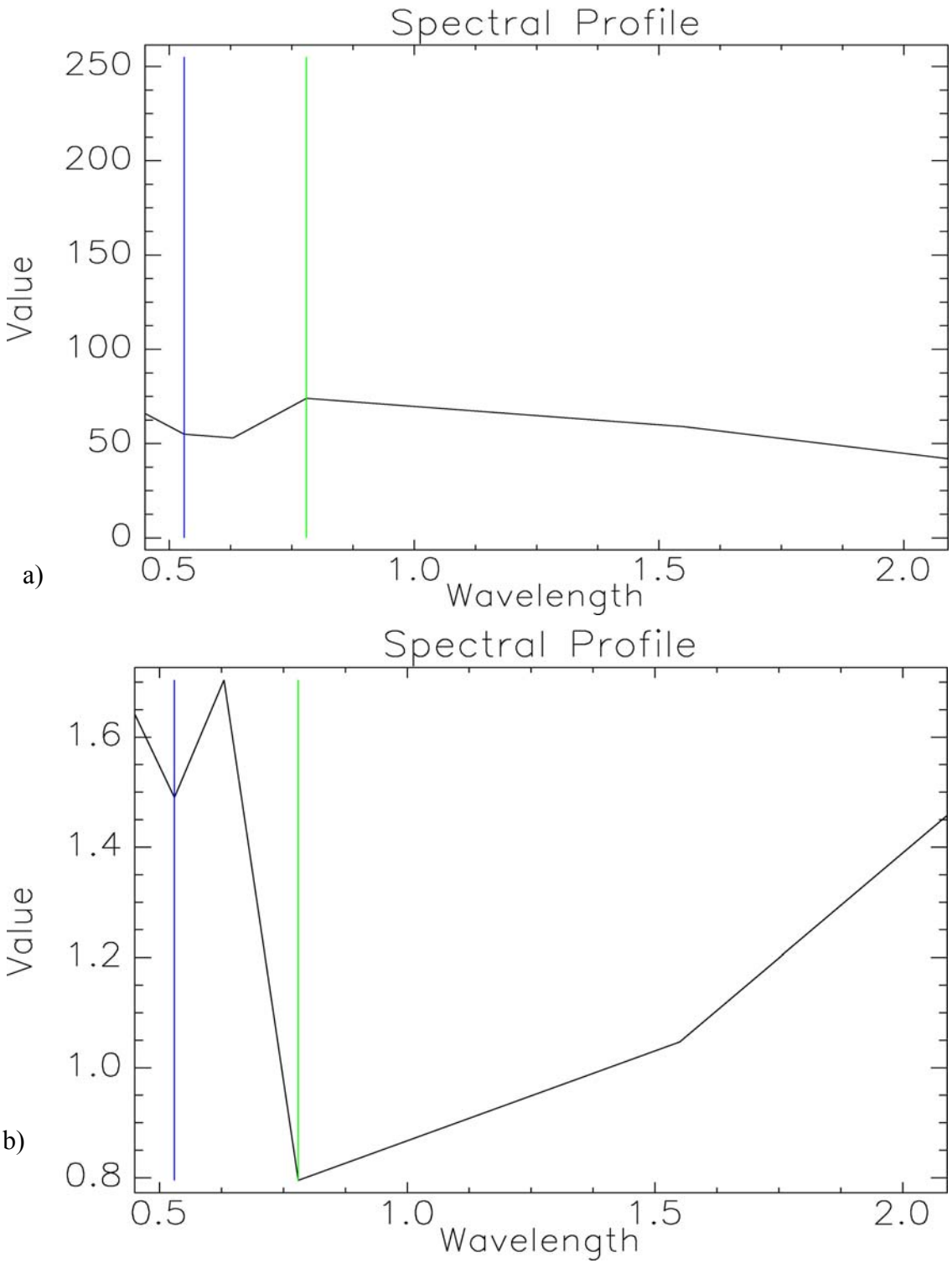

Figure 3.8: Spectral plot comparison before (a) and after (b) internal average relative reflectance (IARR) calibration.

unimodal and may be Gaussian in nature (distributed normally with a zero mean), although skewing is usual. Multimodal distributions (most frequently, bimodal but also polymodal) result if a scene contains two or more dominant classes with distinctly different (often narrow) ranges of reflectance. Upper and lower limits of brightness values typically lie within only a part (30 to 60%) of the total available range. Usually the few values falling outside 1 or 2 standard deviations may be discarded without serious loss of primary data. This trimming allows the new, narrower limits to undergo expansion to the full scale (0-255 for Landsat data). Linear expansion of DN's into this full scale is a common option. Prior to the application of contrast stretch, the histogram of the input and output images was analyzed (Fig. 3.9). Figure 3.10 shows the contrast stretch result of the Landsat scene used for this study. As expected, the contrast between features and their background increases, so that we can see the different lithologies clearly to the west and east of the Abbay River and its tributaries.

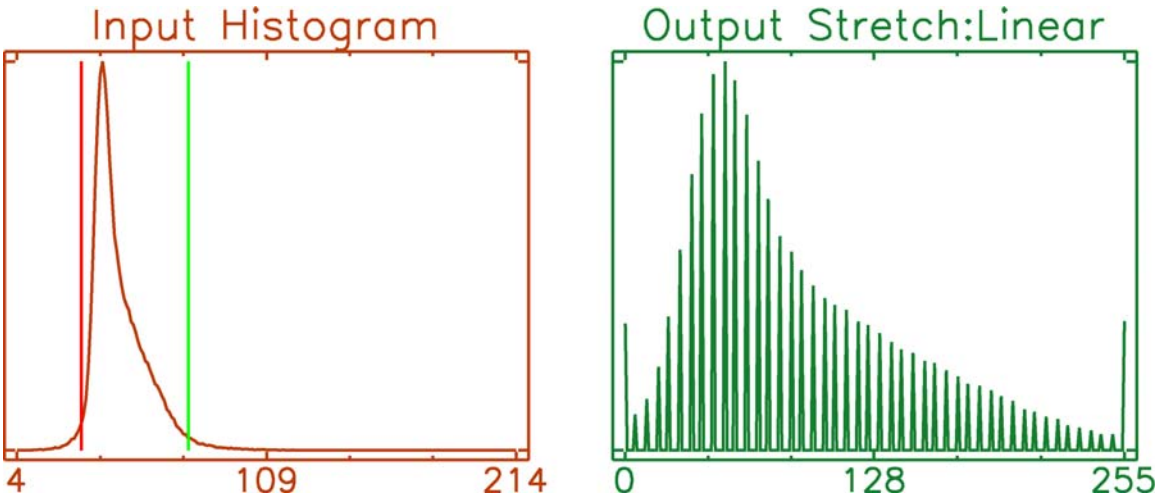

Figure 3.9: Histogram plot of input and output results displayed interactively before applying the contrast stretch.

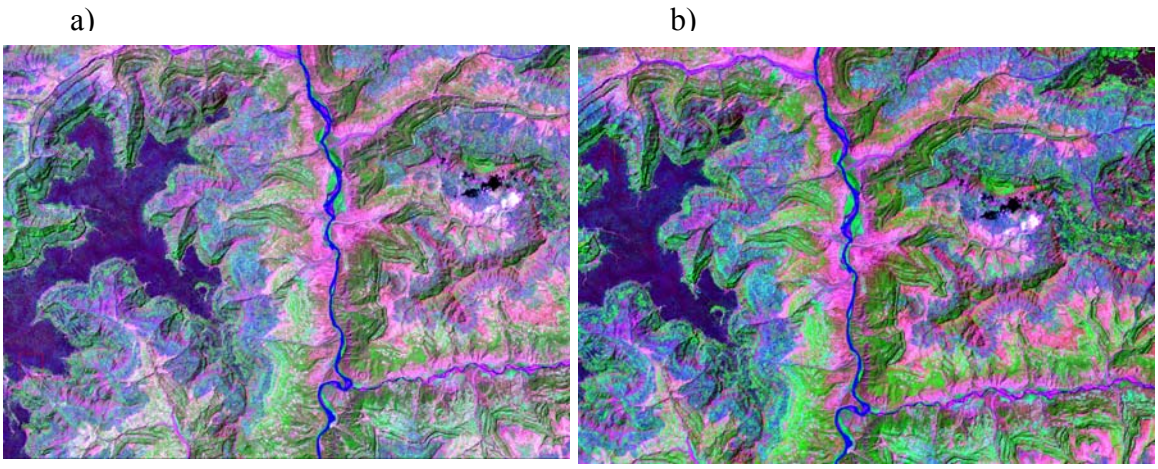

Figure 3.10: Comparison of the original image (a) and contrast stretch with 2% linear cut of enhancement applied image (b) both displayed using bands 7, 4, 2 in RGB. The contrast stretched image shows more color distinction than the original image.

3.4.3 Classification

Another type of image enhancement is classification. In ENVI, there are a number of algorithms that can handle classification. Prior to undertaking a classification, I identified lithologic units that represent the key geologic formations based on regional geologic maps. These units could be the basalt on top (magenta), the upper sandstone and mudstone units (yellow and black), carbonate units (above white), the lower sandstone units (below white) (Fig. 3.11). Figure 3.11 shows the lithologic units that I identified in the Landsat image. These lithologic units were then assigned to different classes. I applied many classification algorithms, and most of them produced virtually the same result. The best class representative analysis was obtained by using the Spectral Angle Mapper (SAM) classification algorithm. SAM is different from the other standard classifications methods because it compares each pixel in the image with every end member for each class and assigns a ponderation (weighing) value between 0 (low resemblance) and 1 (high resemblance) (Girouard et. al., 2004). The Spectral Angle Mapper

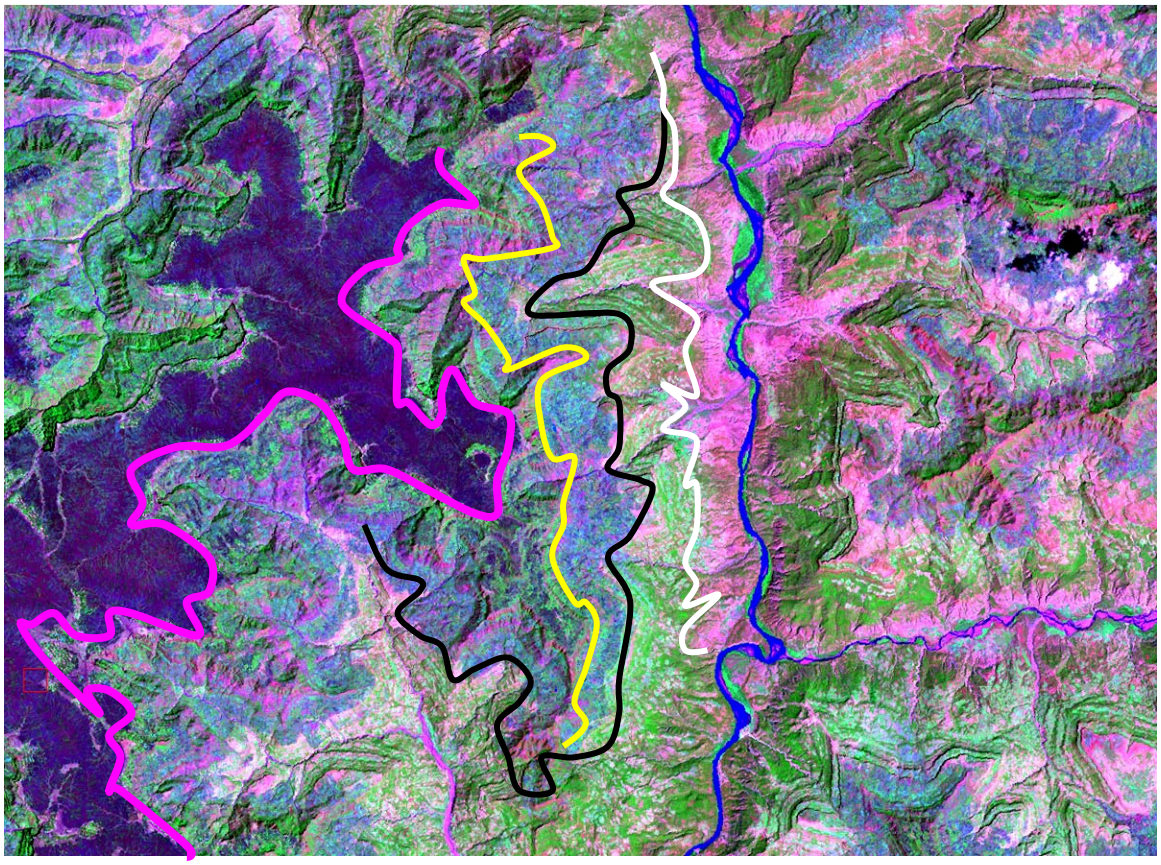

Figure 3.11: Lithologic units that can be traced as a result of the Landsat image processing. Possible units such as basalt (magenta), upper sandstone units (yellow), carbonates (black), lower sandstones (white).

Classification (SAM) is an automated method for directly comparing image spectra to a known spectrum (usually determined in a lab or in the field with a spectrometer) or an end member. This method treats both the questioned and known spectra as vectors and calculates the spectral angle between them. However, this method is insensitive to illumination since the SAM algorithm uses only the vector direction and not the vector length. Figure 3.13 shows the SAM result using 5 spectral classes for the Abbay basin area. These spectral classes can be assigned as basalt (magenta), upper sandstone and mudstone (cyan and yellow), the carbonates (blue), the lower sandstone unit (green) and the river (red). In this figure, we can see that most of the different

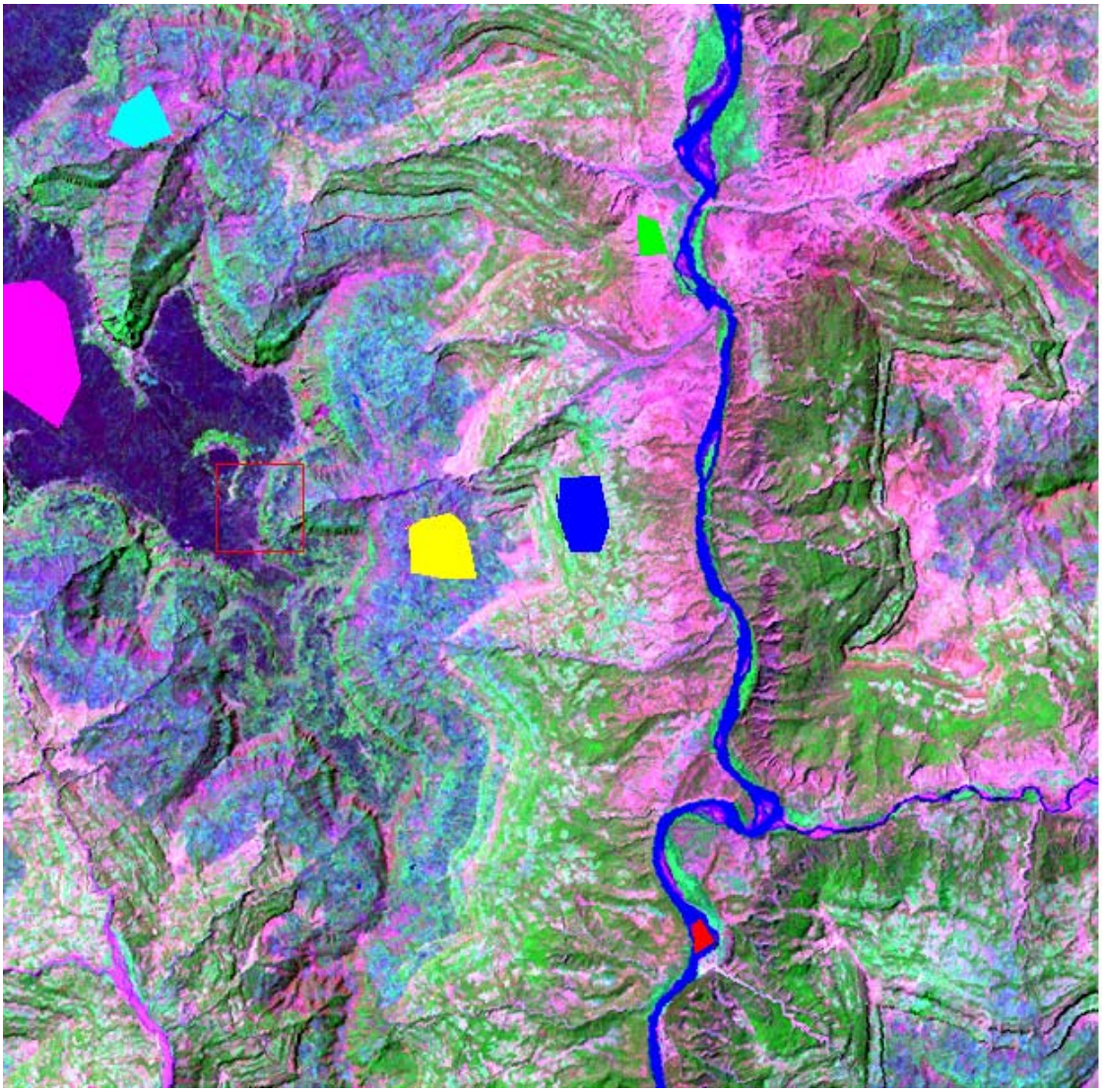

Figure 3.12: Region of interest defined to train the classification algorithm, red is river, green is the deepest formation close to the river, blue is a formation above the layer close to the river, yellow is another layer sequence on top of the blue, and magenta is the top layer overlying the yellow class.

colors that are assigned for the classes are depicted accordingly, which indicates that the different lithologies have distinct spectral signatures.

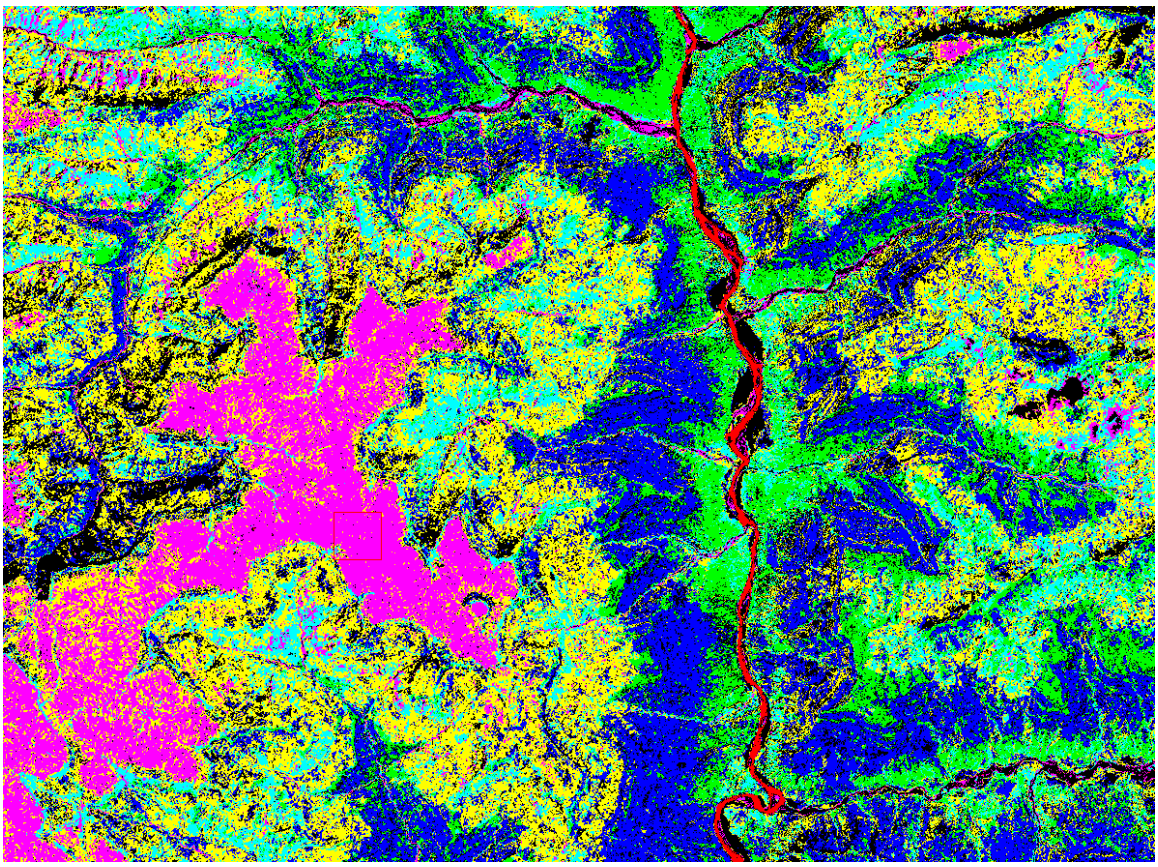

Figure 3.13: Result of SAM classification based on the five regions of interest showing the different lithologic successions in green (lower sandstone), blue (carbonate units), yellow and cyan (Upper sandstone and mudstones) and magenta (basalt). The river is classified as red and black is unclassified.

3.4.4 Principal Component Analysis

Another commonly used image enhancement technique is the Principal Component Analysis (PCA). The objective of this transformation is to reduce the dimensionality (i.e. the number of bands) in the data, and compress as much of the information in the original bands into fewer bands. The "new" bands that result from this statistical procedure are called components. This process attempts to maximize (statistically) the amount of information (or variance) from all the original data into the least number of new components.

When images for the individual bands are generated, they have appropriate, though subtle, contrasts. The images have similar tonal variations for the ground classes, because most of the features have approximately the same relative differences in reflectance in each band. But, their actual reflectance values (partially embodied in their DN's or digital numbers) vary more from one band to the next. Thus, a green reflector may have a higher average DN value in Band 2 than in 1 or 3 and this will contribute more effective brightness to the green component of a color composite.

PCA is thus a procedure for transforming a set of correlated variables into a new set of uncorrelated variables. This transformation is a rotation of the original axes to new orientations that are orthogonal to each other, and therefore there is minimum correlation between variables. Since the rotation is a linear combination of the original measurements, if all of the axes are included in the rotation, no information is lost. "No information is lost" means that the original measurements can be recovered from the principal components. The PCA procedure reorganizes, by statistical means, the DN values from as many of the spectral bands as we choose to include in the analysis. In producing these values, I used all six bands and requested that all six components be generated. Several of the TM bands, especially 1, 2, and 3, are strongly correlated, which means that variations in one band are closely matched in the others. Thus, tonal patterns or grey levels may not show enough variation to separate features that have similar responses in each band. Principal Components Analysis gets around this by shifting the axes that show strong correlations to new spatial positions that cause significant differences (decorrelation) in grey levels from band to band and thus discrimination. The new images contain the influence of all bands being considered for cross-correlations.

Excluding band 6, principal component analysis was carried out for the six key bands. Figure 3.14 is a plot of the eigenvalues showing the PCs order of largest to smallest variance in

the data. There is deterioration as we move from the 1st PC to the 6th PC (Fig. 3.15). The PC1 image in Figure 3.15 is the best as it somewhat resembles an actual aerial photograph, and thus, it contains most of the pertinent information inherent to the scene. In particular, the darker layer became more prominent suggesting that it has a distinctive response compared to the other lithologies. As will be discussed below, this layer represents the basalts that lie on top of the sedimentary layers. It is possible to see the form of the strata and their corresponding layers winding across each tributary and the main river. The remaining PCs with the exception of 2 and 3 do not show useful information. The last component, which contains most of the noise, is also shown in Figure 3.15 for comparison with PC1, and it clearly contains little information. Figure 16 shows a color composite image formed from PCs 3, 2, and 1 as Red, Green and Blue respectively. Most of the sedimentary sections show purple and bluish green color signatures.

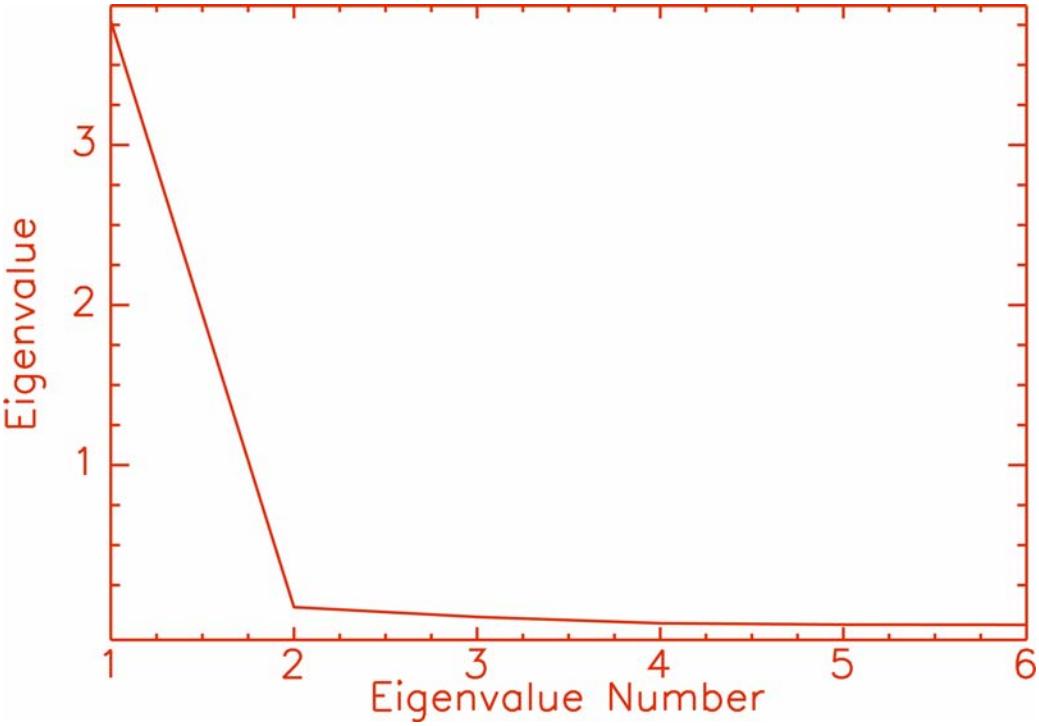

Figure 3.14: Plot of the eigenvalues showing that PCs 1, 2, and 3 have the most usable variance among the other components.

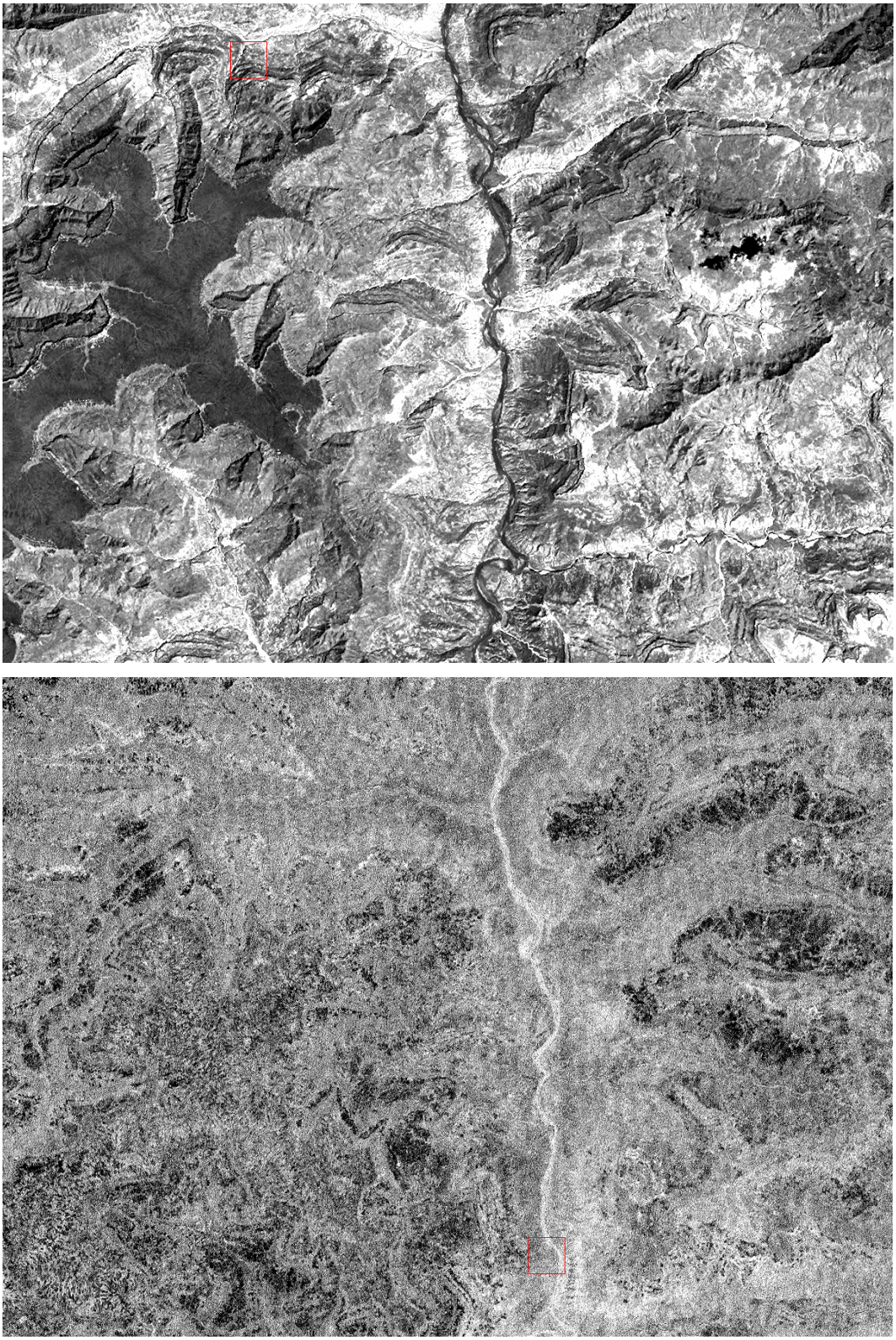

Figure 3.15: PCA analysis result showing that the maximum information is contained in PC1 while PC6 contains much of the noise. Top PC1, bottom PC6.

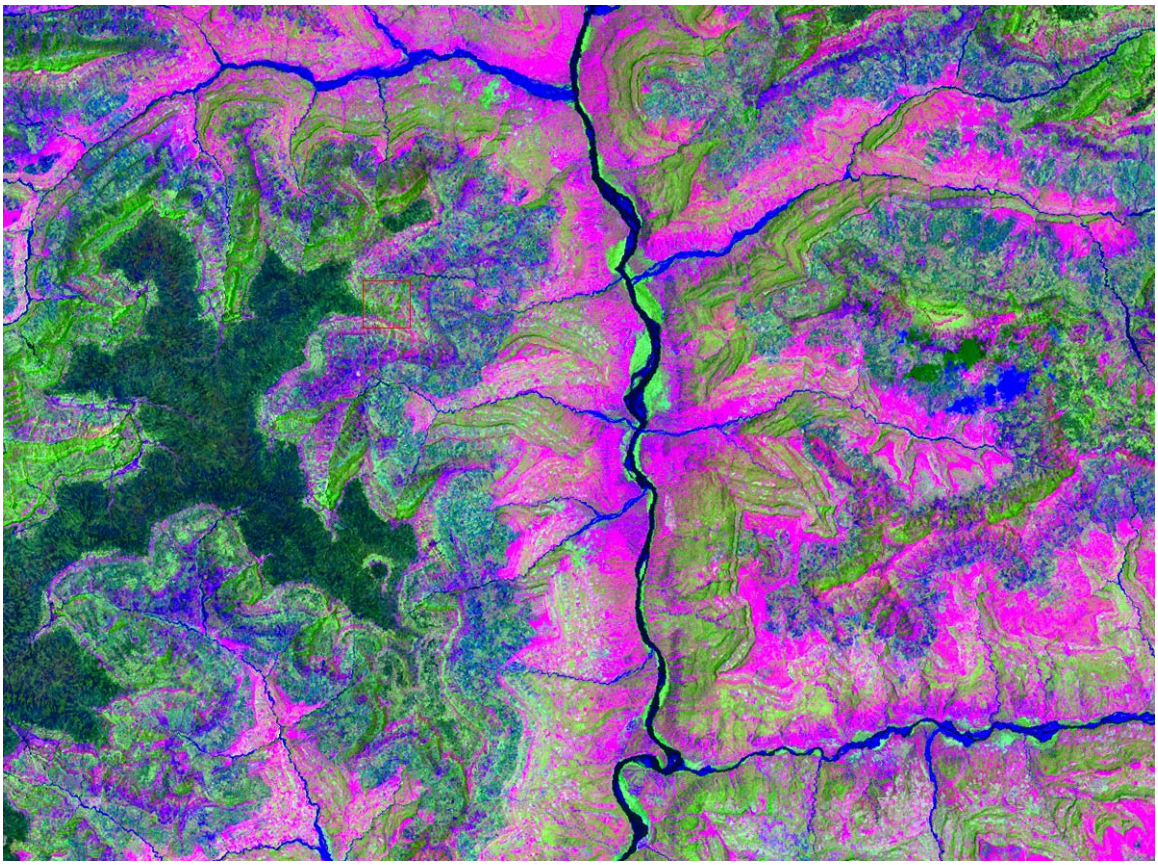

Figure 3.16: Principal component analysis result where PC1, PC2 and PC3 are combined as Bands 1, 2 and 3 in this RGB image.

3.4.5 Decorrelation Stretch

Another method to enhance the color composite image that I applied was a decorrelation stretch, which enhances color separation across highly correlated channels. The decorrelation stretch is applied to reduce the inter-channel correlation and stretch the dynamic range to the full extent, thus enhancing the color variation and improving visualization for interpretation (Gillespie et al., 1986; Gillespie, 1992). Figure 3.17 shows the image after applying decorrelation stretch using Bands 7, 4, 2 and a 2% linear decorrelation. The image appears to have a fairly distinct color for each lithologic unit identified during the earlier during classification.

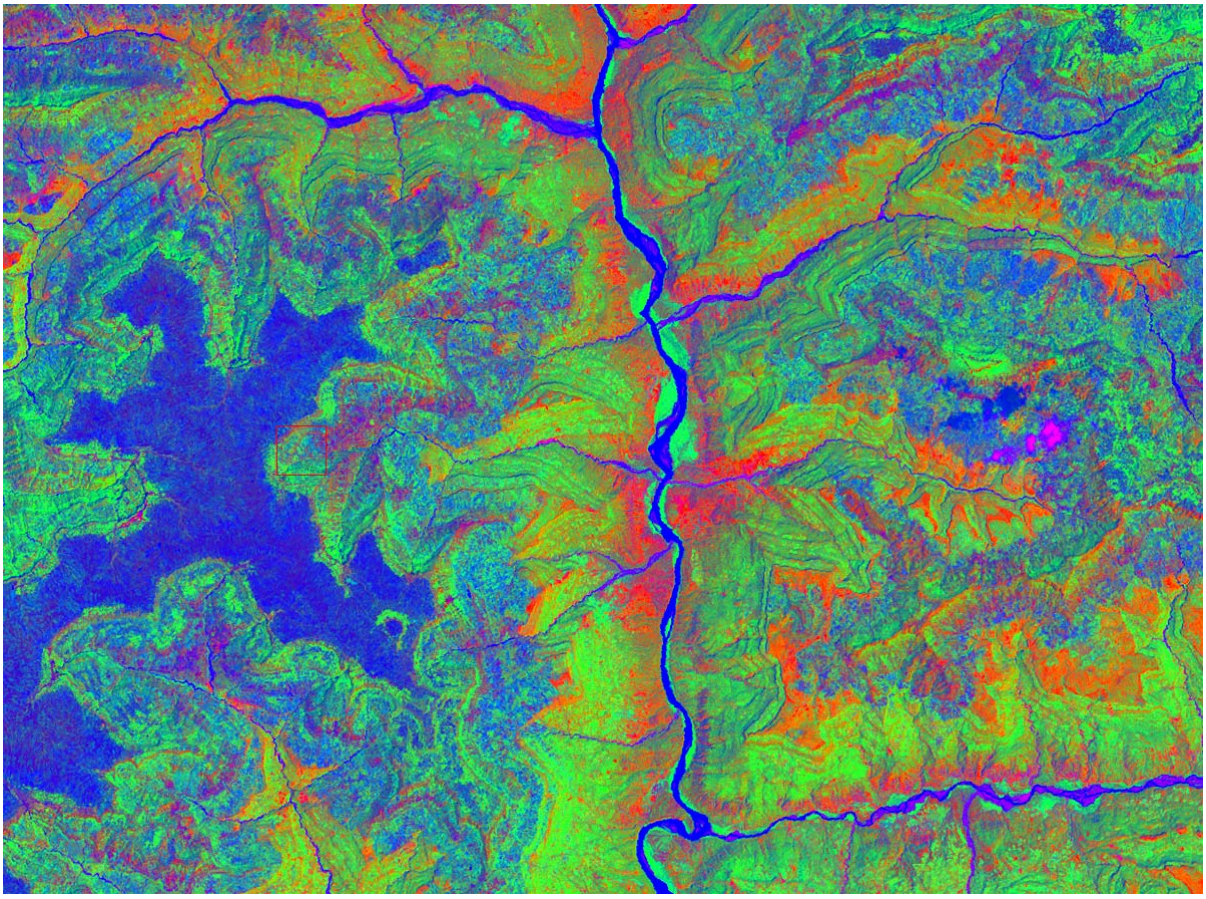

Figure 3.17: Image of the study area resulting from the application of decorrelation stretch showing separation of the correlated colors to consider the response of each lithologic unit. As expected, the different sedimentary sections are distinguished by their respective colors. This approximates a stratigraphic column with colors assigned.

3.4.6 Band Ratio Image Analysis

It is possible to use the DNs for two bands to calculate the ratios of one band with the other band so that another band can be obtained in order to create an output image different from the original. Band ratio images may be used to remove the influence of light and shadow on a ridge due to the sun angle. It is also possible to obtain certain band ratios which can enhance vegetation or geology. Figure 3.18 shows a band ratio of bands7/5, bands 4/3 and bands 3/2. The objective is to enhance sedimentary regions. As a result, the lithology on both sides of the river

appears to have equally enhanced colors implying that the ratios are not influenced by illumination direction or shadow effects.

Table 3. 2: Band ratios and their geological applications

Band Ratio	EM Spectrum	Application
Bands 3/2	Red/Green	Soils
Bands 4/3	PhotIR/Red	Biomass
Bands 7/5	SWIR/NIR	Sediments

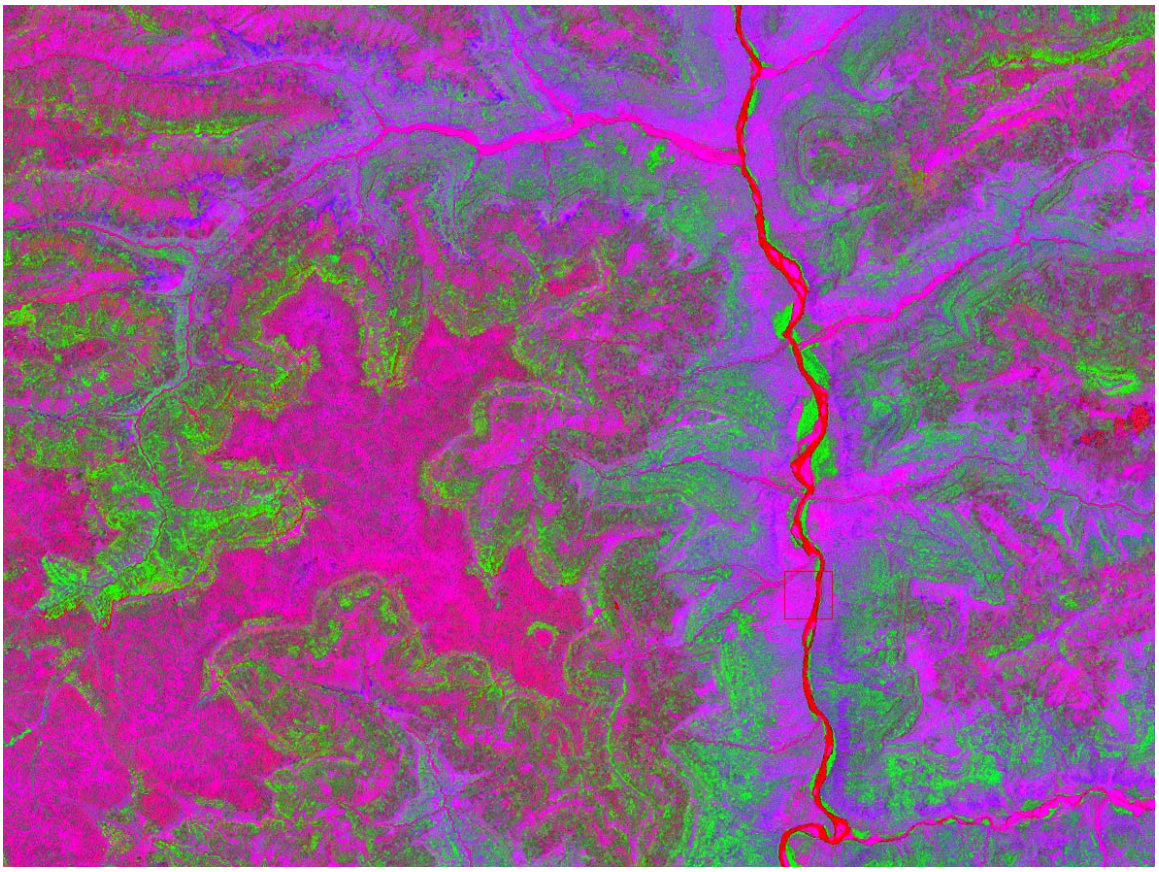

Figure 3.18: Image after a ratio is calculated for bands 7/5 (clay), 4/3 (biomass), and 3/2 soil to produce an image that is independent of shadow and illumination direction.

3.4.7 Interpretation

Based on all the analyses above, it is clear that making a detailed lithologic interpretation is possible. Figure 3.19 shows a mosaiked image selected for the study area (Fig. 3.1). An image of the area indicated by the red box is shown in Figure 3.20. Using the combination of processed images and existing geologic data (Fig. 3.3), I can map the lateral extent of the main lithologic units present. A basaltic unit lies on top of the high plateaus and is followed by the underlying sedimentary units. These units in turn are the basalt layer (white line), upper sandstone and mudstones (yellow), and the carbonates overlain by the lower sandstone units. Some faults can also be interpreted on the detailed image (Fig. 3.20), and there are a number of northeast trending features that suggest faulting is affecting the drainage patterns.

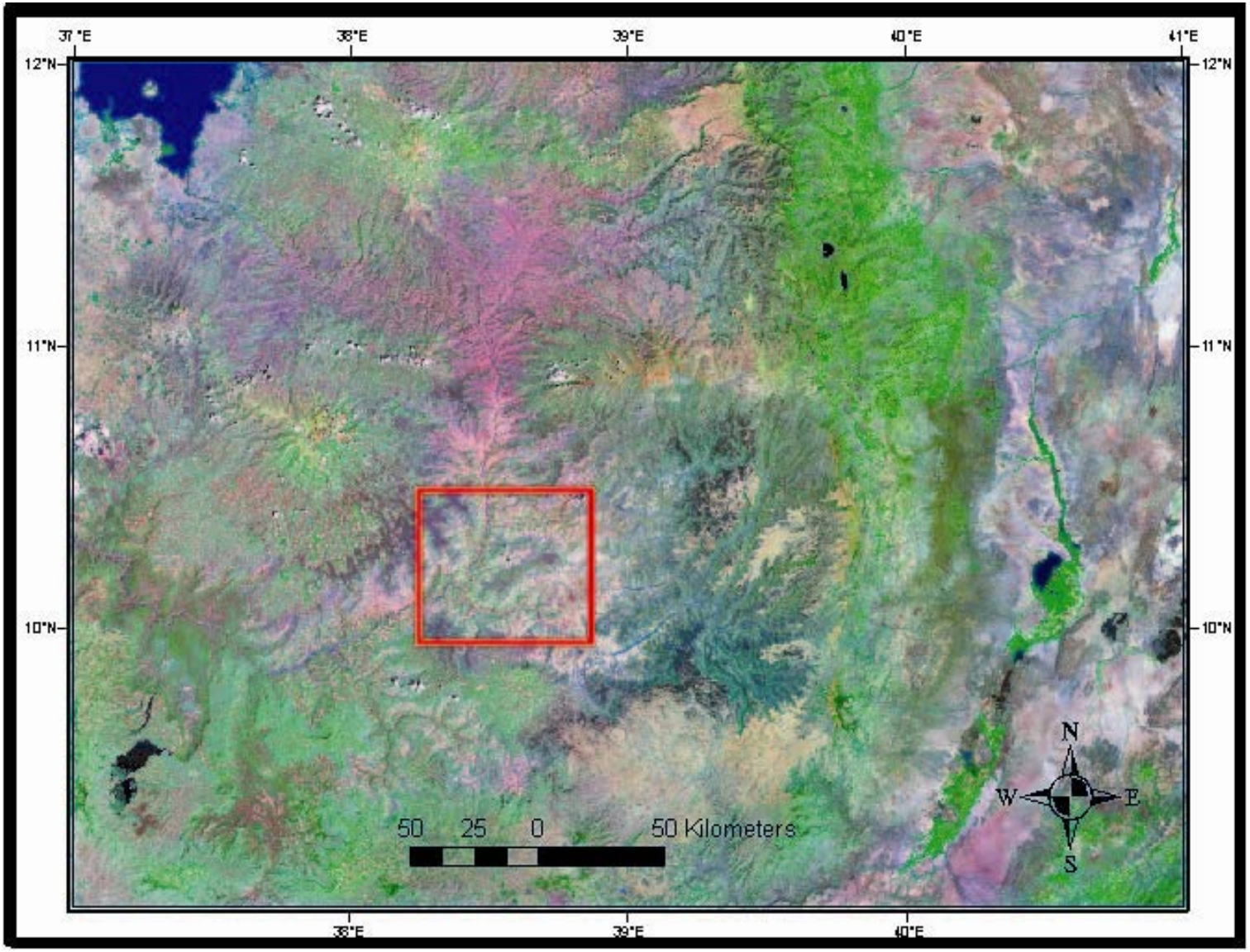

Figure 3.19: Mosaic ETM+ Landsat image in RGB display and selected area for detailed interpretation indicated in the red box.

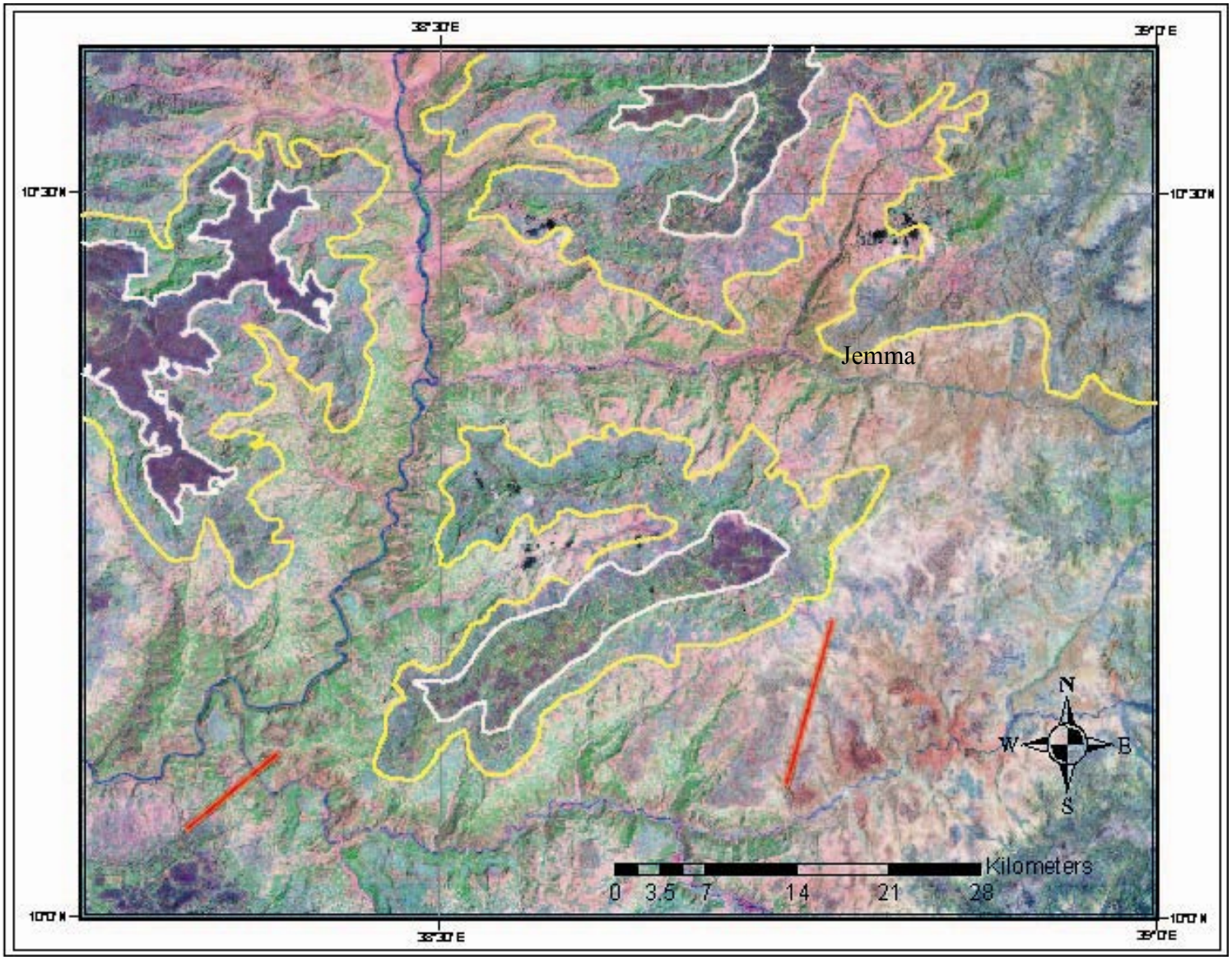

Figure 3.20: Detailed image interpretation of from the Abbay area. Red lines are faults interpreted in the region.

3.5 Gravity data processing and interpretation

3.5.1 Bouguer Gravity Expression of the Abbay Basin

Gravity anomaly interpretation, although non-unique by nature, is cost-effective and useful in approaching a variety of geological problems such as such studying sub-volcanic sedimentary basins and salt tectonics. Until recently geophysical techniques have played no role in the investigation of the Abbay basin. Past studies in the area have been generally confined to sedimentological, paleontological and stratigraphic analyses. Attention was given mainly to the flood basalts and shield volcanoes in the adjacent areas (e.g., Ayalew et al., 2003; Kieffer et al., 2004; Pik et al., 1999) and to the Afar triple junction and the Ethiopian rift.

In this study, gravity data available for the Abbay region were compiled, reprocessed and interpreted via the construction of a series of maps. Then computer models were constructed for two profiles to estimate the basalt and sediment thickness in the region.

A Bouguer gravity anomaly map of the region (Fig. 3.21) was produced using over 3000 gravity stations available for the region (Fig. 3.6). We used a grid interval of 5X5 km and a maximum search radius of 15 km to produce a grid for further processing. The general procedure for the gravity reduction and data quality control are outlined in section 3.0. Significant anomalies are evident in the gravity map (Fig. 3.21) as we proceed from west to east. The eastern section of the map which is characterized by gravity high (A) is the Afar area related to the thin crust and basaltic formation attributed to high density materials and thinner crust. The highest gravity anomaly (B) lies along the central Afar in the axial direction which is related to the local structures, possibly to the rift segments.

The western part of the Abbay basin region (C) is characterized by relatively high values compared to the central portion of the area. This may be due to the thinning of the sedimentary strata and/or the crust towards the Ethiopia-Sudan border. Inspection of the geologic map of the

study area (Fig. 3.3) reveals that there are outcrops of crystalline basement rock in the southwestern portion of the

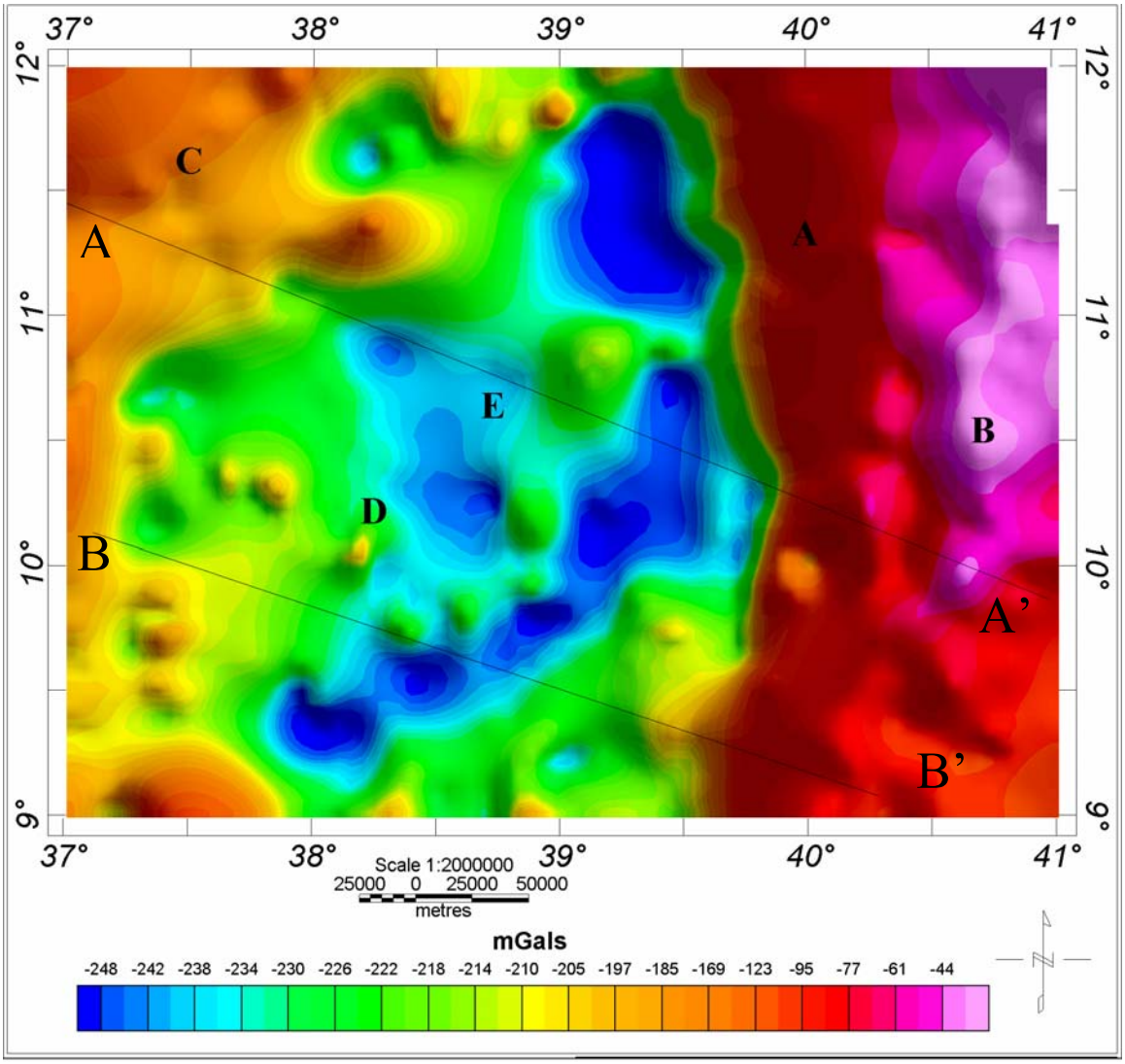

Figure 3.21: Bouguer gravity anomaly map of the Abbay basin and adjacent areas. A, B, C. D and E are anomalies of interest discussed in detail.

study area. It is also clear that the volcanic cover decreases in thickness and areal coverage westward. A good density of data coverage in some areas also allows us to distinguish high-density shield volcanoes close to the basin. The area of Choke Mountain (D) in the southwest portion of the basin is an example.

The most significant feature with respect to this study is the broad gravity low (E) associated with the central portion of the Abbay basin, which is characterized by two parallel series of linear anomalies that contain the lowest values. These large negative anomalies are very likely to be connected with low-density materials below the flood basalts. Some of these gravity lows coincide with the geologically identified sedimentary outcrops along the Abbay River gorge. Gravity lows are also associated with outcrops along tributaries of the Abbay River mainly towards the eastern and northeastern part of the area. These geologic units are known to be prevalent in these areas based geological studies and the remote sensing data analysis described in section 4.0. Therefore, these low gravity anomalies may be primarily due to thick sedimentary strata. Since the outcrops of sedimentary rocks are limited to the river gorges, the gravity anomalies present an important indication of the extent of the thick sections of sedimentary strata. The largest low gravity anomaly is situated between Guguftu shield volcano (F) in the northeast and Choke shield volcano in the southwest (D). In general, this gravity anomaly follows the sedimentary outcrops and extends further to the east into the main continental flood basalt region. This suggests that the strata are restricted to the areas where they are outcrop and that there are significant thicknesses of sedimentary strata beneath the flood basalts further to the east. This interpretation is also be supported by the existence of a sandstone unit (Adigrat Sandstone) along the Jemma River gorge (Wolela, 1997).

3.5.2 Residual Gravity anomaly

The underlying assumption in any regional study should be that the features not related to those of interest can be removed. Currently a number of regional residual separation techniques are available (e.g., Nabighian et al., 2006). For our regional residual separation technique, we opted for an upward continuation method because it is mathematically stable and physics-based. Therefore, we computed an upward continued anomaly grid for the region to 40 km, which is the average crustal thickness ~40 km in the region (e.g., McKenzie et al., 2006). Upward continuation smoothes the anomalies as if the observations were made at an elevation of 40 km above the surface (Fig. 3.22). We then subtracted the upward continued grid from the Bouguer gravity anomaly grid. The resulting difference was then taken as the residual to produce the map shown in Figure 3.23. The previously defined gravity high associated with the rift in the section of Afar triangle retains its characteristic pattern and has broad positive residual values. The other highs that are short wavelength are associated with the shield volcanoes identified earlier. In the residual map, they appear as larger and more clearly defined anomalies. Subtle local relative positive anomalies are clearly enhanced in the residual gravity anomaly map, suggesting that the residual gravity anomaly is an effective tool for enhancing the local structural effects.

The previously interpreted broad low gravity anomaly, which may be associated with the deepest part of the basin with thick strata, remains low in the residual anomaly map. This anomaly also coincides with the sedimentary outcrop region and the area of the oil seep in the Were Ilu region. The area of gravity lows extended further towards the east (A) suggesting that the main depocenter may be further towards the east. To the west, gravity minima (B, C) may represent localized sedimentary depocenters. A relative negative anomaly appears (D) east of the rift associated with part of the eastern plateau, which may be a continuation of the anomaly west of the rift, before it was disrupted by the Ethiopian rift.

3.5.3 Gravity Profile Modeling Results

Integrated models across the Abbay basin region where constructed for profiles A-A' and B-B' (Fig. 3.21) and were analyzed to obtain more specific information on the basin configuration. These profiles were extracted from the gridded data, and a $2^1/_2$ dimensional modeling approach was employed. The modeling was carried out using the Gravity and Magnetics Modeling System (GMSYS) software that is licensed to UTEP. In each of the models, five layers were deemed appropriate with the deepest one being the upper mantle. As indicated in the geological map and stratigraphic column (Figs. 3.3 and 3.4) that are documented by various authors (e.g., Getaneh, 1979; Wolela, 1997), the oldest rock unit exposed in the area is the Precambrian basement. Densities taken from surface sample measurements and literature were compared and average densities of 2400 kg m^{-3} for sediments, 2670 kg m^{-3} for crystalline basement rocks were used. The density of the basalt was assigned a typical value of 2900 kgm^{-3}. Thicknesses of the basalt layers are extracted from the geological studies (e.g., Getaneh, 1979; Wolela, 1997).

The model derived for Profile A-A' is shown in Figure 3.24. This model was constructed assuming the law of horizontality in relation to the Ogaden basin such that strata beneath the rift floor could be faulted and buried deeper below the volcanics. On the plateau there is better geological information about the thickness of the sedimentary strata, especially within the Abbay gorge. Accordingly, we have a layer of basalt with a maximum thickness of about 3 km to the west of the basin. In the central part of the basin, our model suggests more than 3 km sedimentary strata. Further to the east the volcanics thicken in the Afar triple junction, the crust thin and the sedimentary thickness reduces.

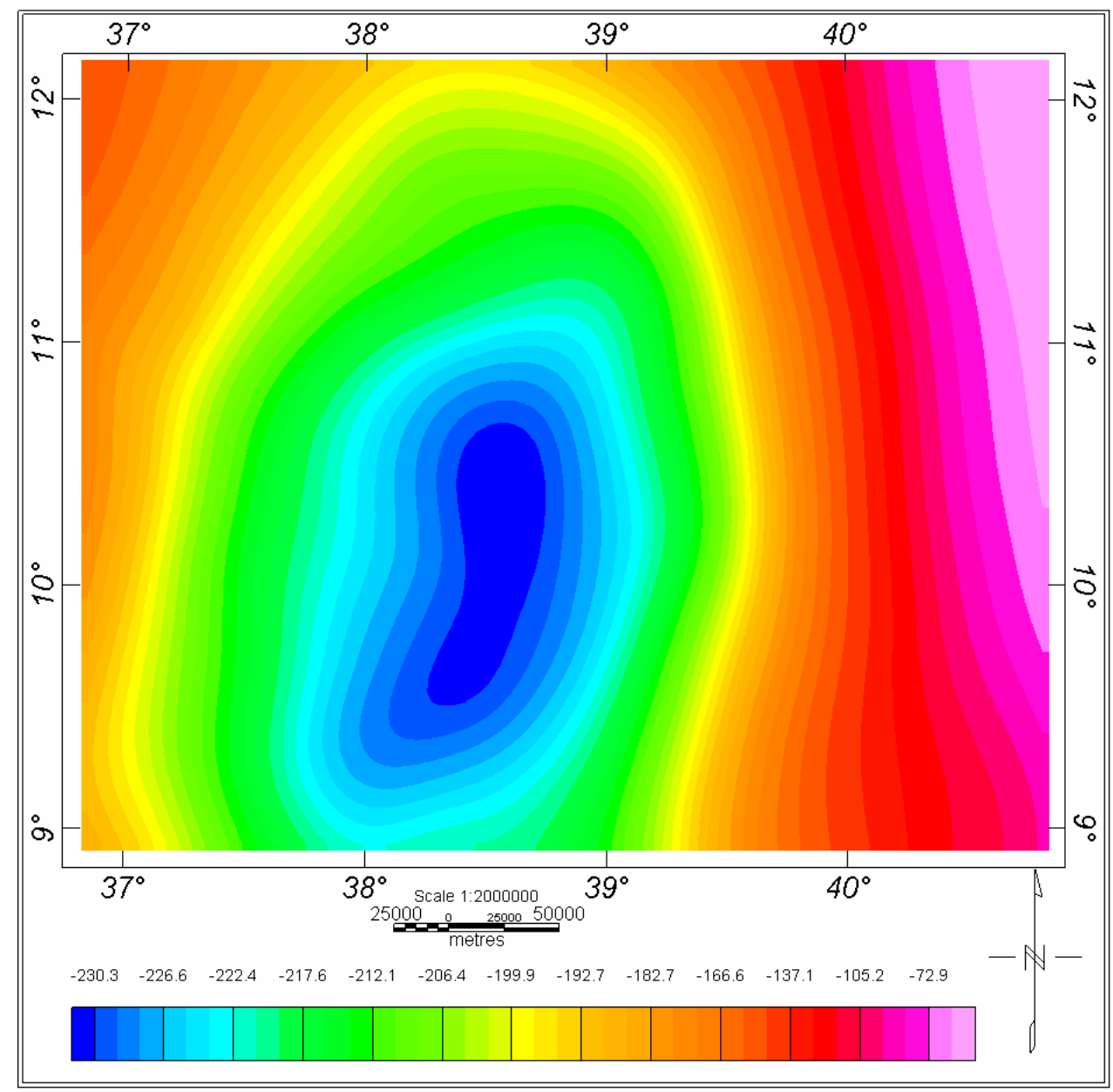

Figure 3.22: Map of upward continued (40 km) complete Bouguer anomaly values of the Abbay basin and adjacent areas

.

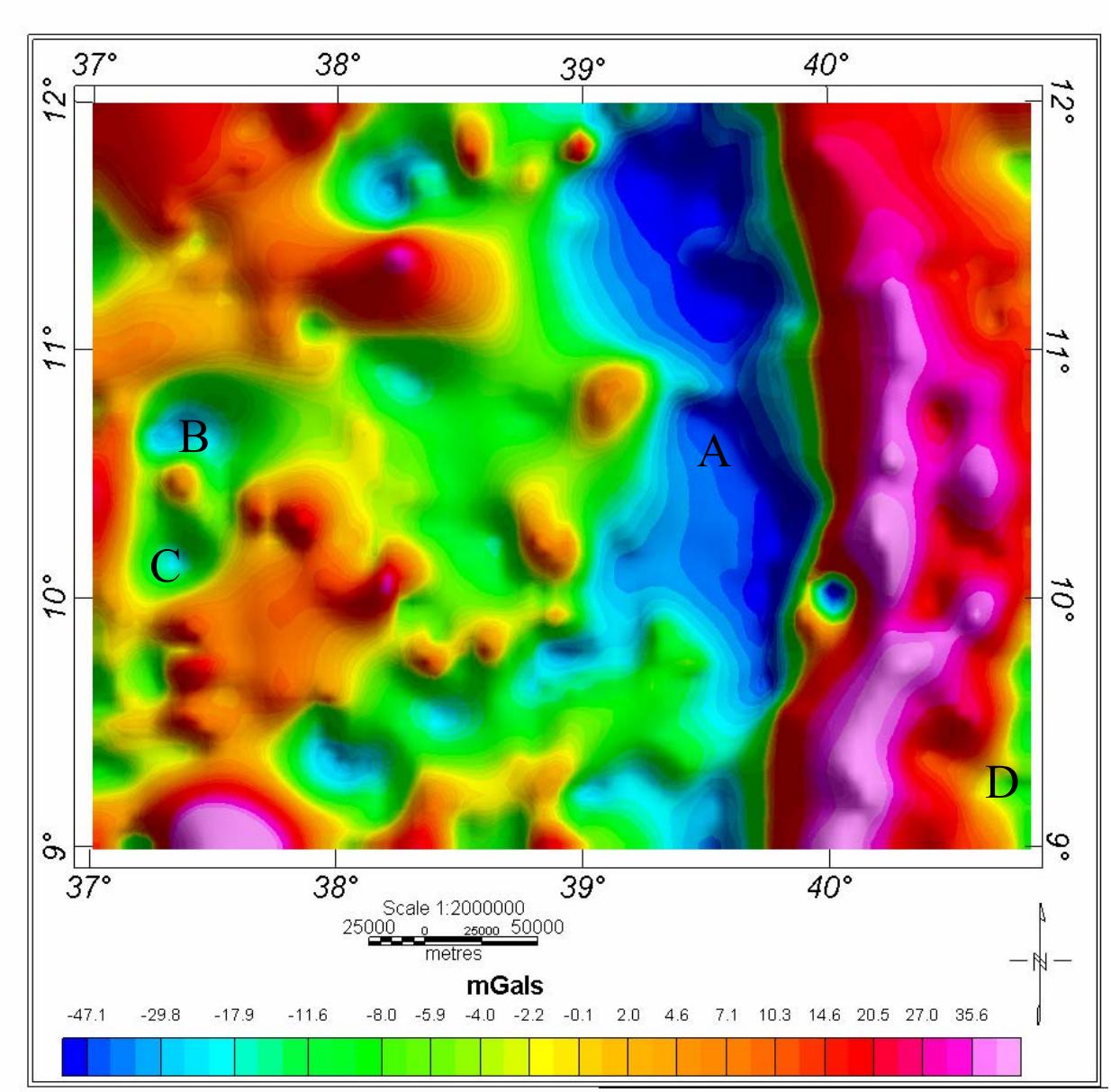

Figure 3.23: Residual gravity anomaly map of the Abbay basin and adjacent areas. A, B, C and D are anomalies of interest discussed in detail.

The model derived for Profile B-B' is shown in Fig. 3.25. The basaltic layer to the west of the basin has similar thickness as in profile A-A'. The sediment thickness appears to continue uniformly with minor undulating basement topography from west to east. In the central and eastern part of the basin the thickness of sedimentary layer increases. In general the modeling result reveals thicker sediment in the central part of the basin with similar thickness continuing to the east until it reaches the rift flank.

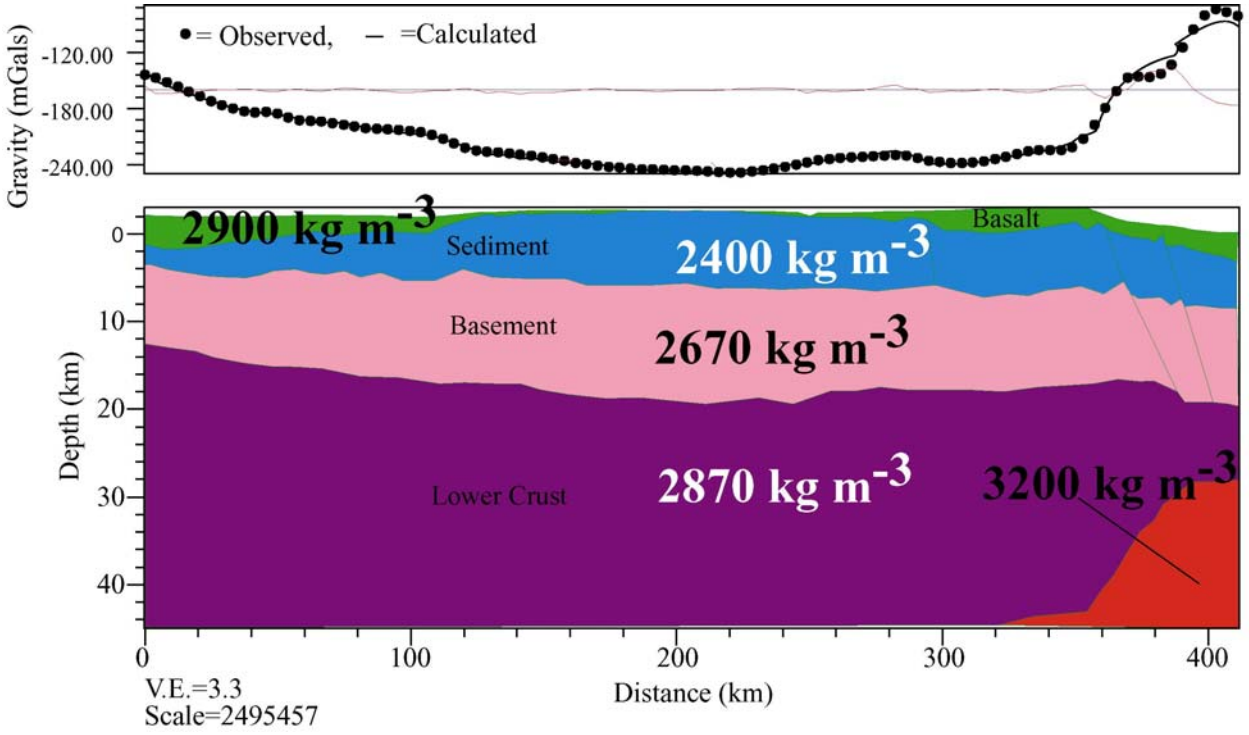

Figure 3.24: Two dimensional modeling along profile AA'

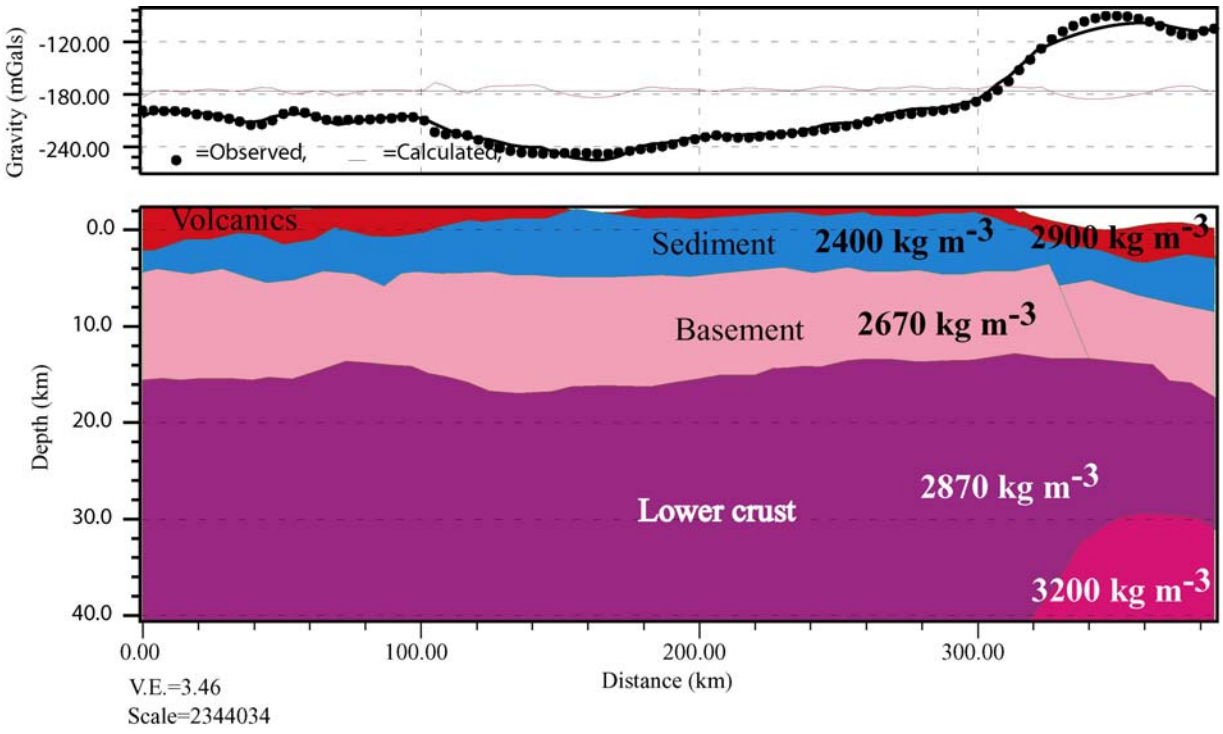

Figure 3.25: Two and half dimensional modeling along profile BB'

3.6 Conclusions and suggestions for further work

The remote sensing analysis, gravity maps and models, and integrated analysis in this study yielded more information on the geology of the Abbay basin. It is possible to make a lithologic interpretation of the strata and determine their lateral extent based on remote sensing analyses (Figs. 3.19 and 3.20). The gravity minima that we define as representing the Abbay basin coincides with these sedimentary outcrops but extends far beyond these outcrops to indicate the possible extent of the basin. The inferred basin appears to be deeper towards the east, probably indicating its relation with the Ogaden basin to the southeast. The presence of the strata within the rift cannot be defined; this can be due to the rift segmentation and localized volcanism modification and extensional processes that might have attenuated the strata beneath the rift.

The residual gravity anomaly indicated a clearer and narrower sedimentary basin compared to the Bouguer gravity anomaly. This could be due to the separation of areas of thicker crust from the signal due to the sediment beneath the flood basalts.

Two dimensional models (Fig. 3.24 and 3.25) show more than 3 km thick sediment mainly in the central part of the study area. This is in agreement with the geological observations.

Remote sensing data reveals the extent of the sedimentary strata that outcrop in the region. Some structures, mainly faults, are also indicated by the remote sensing results. In this study, the image analysis produced the following results:

1) Landsat7 ETM+ image analysis revealed detailed geologic units within the Abbay gorge that are subtle in the geological maps.
2) SAM is the best technique for classification and resulted in fairly distinct geologic unit identification.
3) Regional structures, mainly faults, are identified in different part of the study area. These structures could produce potential hydrocarbon targets provided that they are deep and sealed.

The results presented here show that there is a significant chance an extensive sedimentary basin lies beneath the flood basalts of the Western Plateau of Ethiopia. However, further work is needed in the Abbay basin and should include an aeromagnetic study and depth to basement estimation. The addition of gravity data will improve mapping and modeling results in areas that are sparsely covered now. Therefore, the basin area should be in-filled with closer spaced stations. A carefully designed controlled source seismic study could provide better imaging of the subvolcanic layer. More gravity modeling work could then been undertaken based on the seismic results. Magnetotelluric data may help with depth investigation and layer identification. Transient electromagnetic data could provide

additional deep electrical resistivity data that would help determine the sedimentary rock thickness and their extent beneath the basalt.

.

Chapter 4: The Ogaden Basin

4.1 Introduction

The Ogaden basin is the major structural feature in Ethiopia east of the Ethiopian rift. It covers a broad area (Fig. 4.1) and its deep structure is poorly known. Its origin has been traced back to the rifting, that broke-up Gondwanaland (e.g. Barnes, 1976; Coffin and Rabinowitz, 1988). However, as discussed in Chapter 3, the structural framework in the region may be more complex than generally recognized. Thus, I have undertaken a regional integrated analysis of the Ogaden basin region with the dual goal of understanding of its structural and advancing our tectonic history as well as its petroleum resources. In this study I have used new compilation of gravity and aeromagnetic data along with an analysis of over 1000 km of seismic reflection lines coupled with drill hole and regional geologic data in an integrated analysis.

From a geologic perspective, Ethiopia is best known for the Afar triple junction, the Ethiopian rift, and the related plateau basalts, but older features, especially basins, are the focus of this study. Precambrian rocks are exposed in various places where the younger formations are eroded. The Precambrian rocks contain wide varieties of metamorphosed sediments, volcanics and intrusive rocks with (Mohr, 1962; Kazmin, 1971, 1972b, 1978; Davidson, 1983) which outcrop in the southern, western and northern parts of Ethiopia (Fig. 4.1). There is almost no rock record of Paleozoic events. At the end of the Precambrian uplift associated with the East African orogen (Stern, 1994) was followed by erosion. As a result of the break-up of Gondwanaland, subsidence began in the Mesozoic (225 Ma) and a shallow sea spread across the southeastern part of Ethiopia, which extended to the north and west as the land continued to subside (Mohr, 1962). As a result of this, a sandstone unit commonly known as the Adigrat Sandstone was deposited (Blanford, 1870, Arkell, 1956). As the depth of a sea increased limestone deposition followed. Gypsum and anhydrite formations were deposited on intertidal

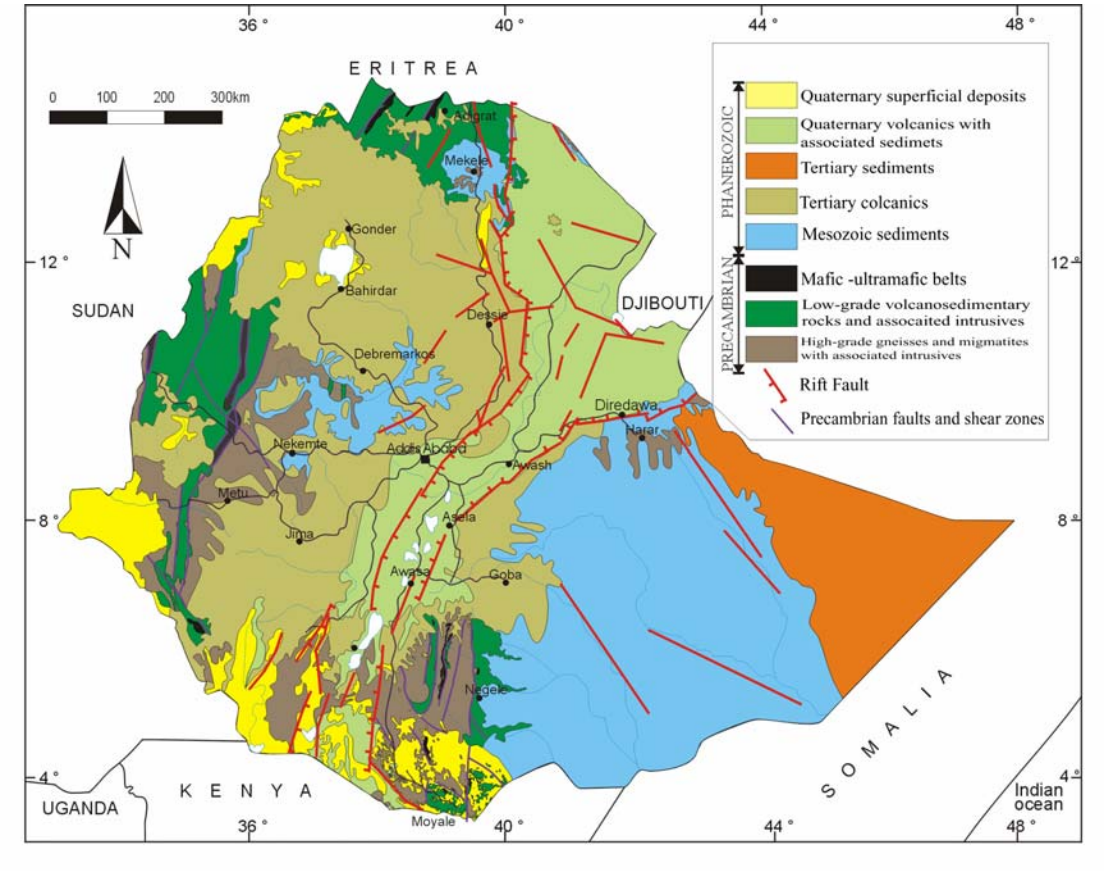

Figure 4.1: Simplified geologic map of Ethiopia showing regions of Precambrian outcrops, Mesozoic sediments and recent volcanics (Modified from Tefera et al. 1996).

flats as a result of sea regression (Habtezgi, 1989). Again a sea invasion occurred from the southeast direction depositing similar rocks mostly during the Late Mesozoic. During the Tertiary, the same cycle of deposition was repeated mainly in the southeastern part of Ethiopia (Hunegnaw et al., 1998).

Gravity and magnetic data are available for most of the region and can provide powerful constraints to validate tectonic, structural and stratigraphic models. When taken together with seismic and well data that are available in localized areas of the Ogaden basin, it is possible to come up with integrated and reliable models.

The benefits of an integrated analysis of these data include:

- Crustal thickness estimates beneath the region.
- Improving the assessment of the maximum sediment thickness
- Defining the structural framework of the basins and the regional paleogeographic evolution
- Improved assessment of potential reservoir and source rocks;
- Extrapolating of structural fairways and grain allowing initial estimate of prospect size distribution beyond seismic coverage; and

4.2 Evolution of the East African Continental Margin

According to plate tectonic theory the supercontinent Pangaea began to break up about 225-200 million years ago. Pangaea first broke into two large continental landmasses, *Laurasia* in the northern hemisphere and *Gondwanaland* in the southern hemisphere. Laurasia and Gondwanaland then continued to break apart into the various smaller pieces fragmenting into continents that we can see at present day. The large continent of Gondwanaland included Africa, South America, India, Madagascar, Antarctica, Australia, New Guinea, New Zealand, and assorted pieces now attached to other continents (Fig. 4.2).

The development of the East African Passive Margin (EAPM) is related to the breakup of Gondwanaland. Much of the history of the evolution of the EAPM comes from studies conducted by Barnes (1976), Coffin and Rabinowitz, (1983, 1987, 1988), and Bosellini (1986, 1989). When Gondwanaland broke up in Permo-Triassic time, fissures and faults were developed in the southern tip of present day South Africa (Barnes, 1976; Kent, 1974; Fairbridge, 1982; Tarling and Kent, 1976). Propagation of fracturing and rifting resulted in the drifting of the Madagascar, India, Australia and Antarctica plates. The development of most of the sedimentary basins in the region, such as the Ogaden basin, the Somalia basin, Mandera Lugh basin, and basins in coastal Mozambique, Tanzania and Kenya (Fig. 4.3) were related to these processes.

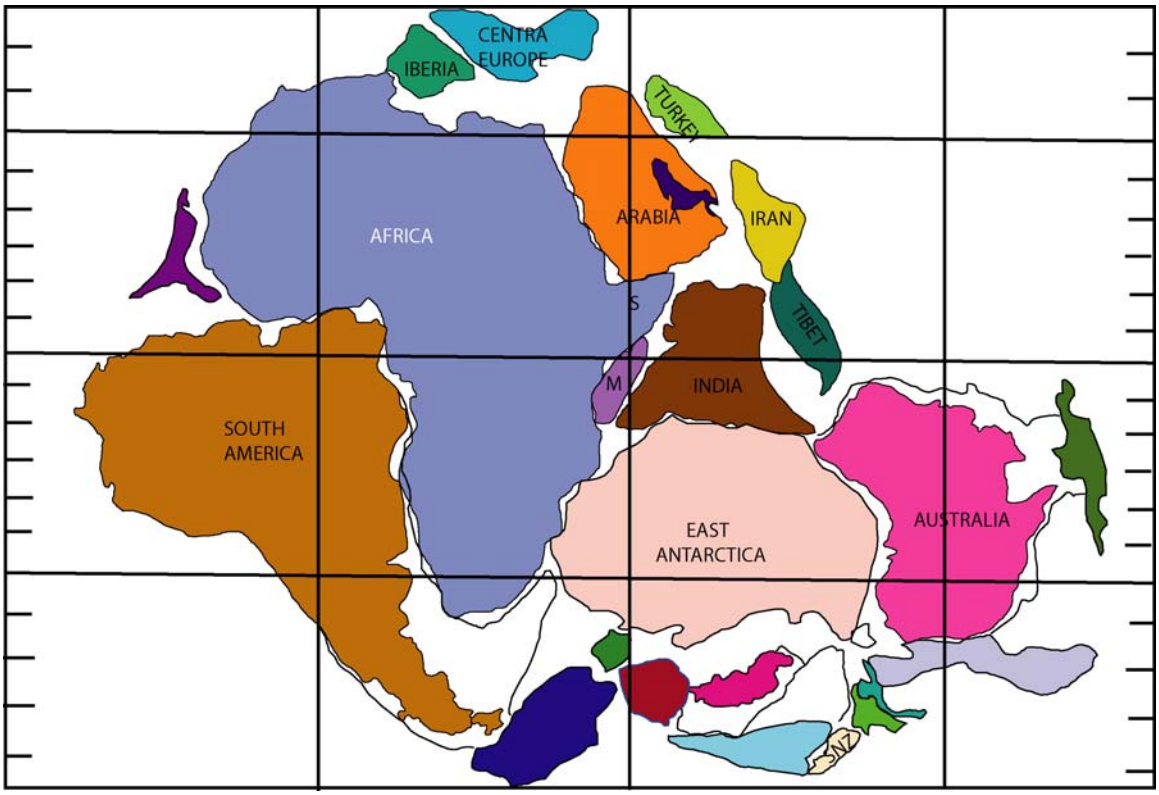

Figure 4.1: Plate reconstruction of Gondwanaland showing the positions of Madagascar (M) and the Somalian plate (S) close to the present day East African margin (Modified after Smith and Hallam, 1970). The Ogaden basin is location within the Somalian plate.

Studies by Bosellini (1987, 1988) have explained the development of the EACM to some extent in detail and divided the margin in to four regions (Fig.4.4). These are:

1. The continental margin bordering northern Mozambique, Tanzania, and most of Kenya, which was formed as a result of transform motion along the Davie Fracture zone between Africa and Madagascar.
2. The margins of northeast Kenya and southwest Somalia, which formed during the Jurassic period (150-160 Ma) as a result of rifting and separation of Madagascar from

Africa. This sector is related to the tectonic and depositional history of the development of the southwestern Ogaden basin of Ethiopia.

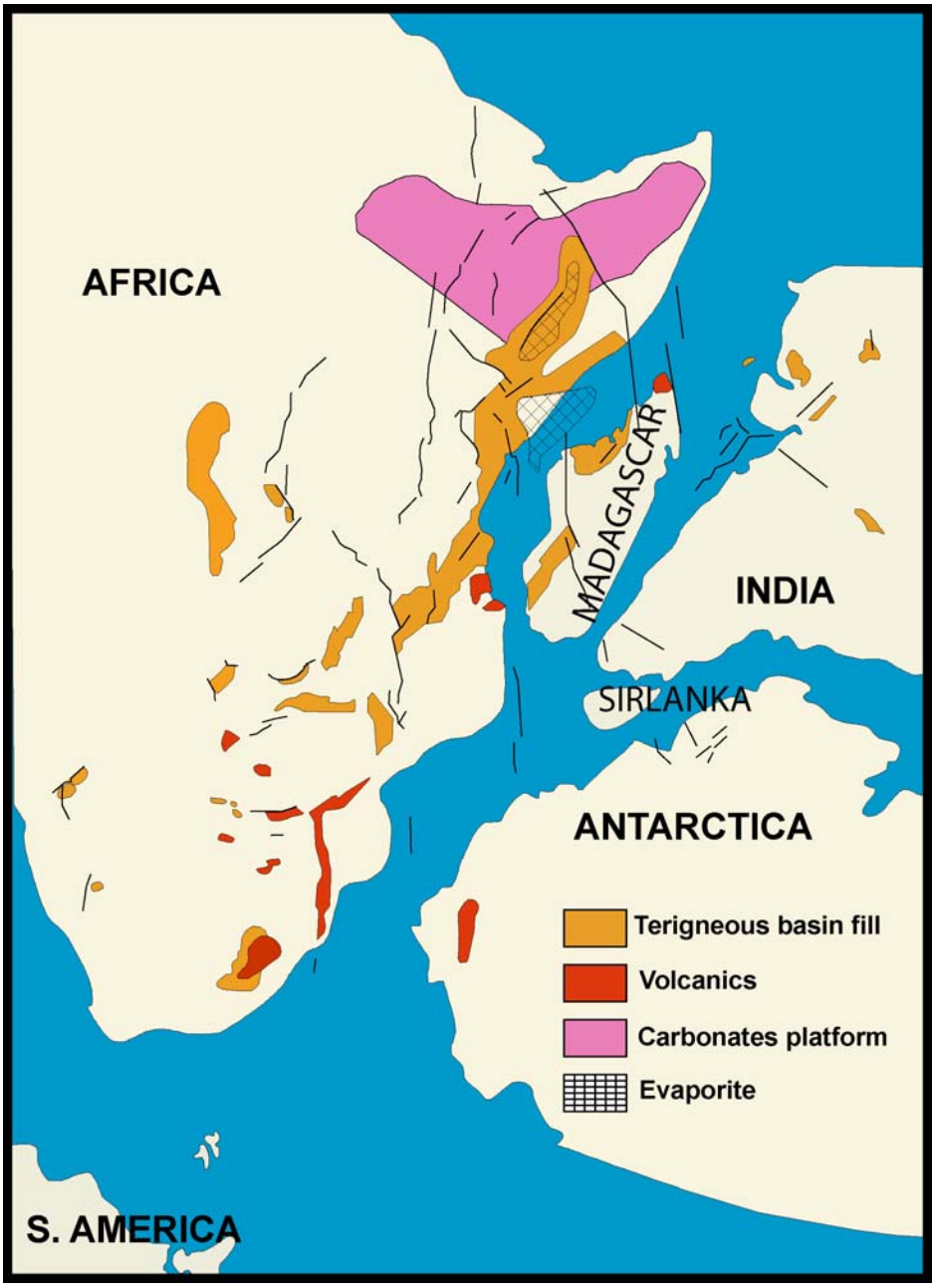

Figure 4.3: An interpreted map of the early break-up of Gondwanaland during Cretaceous time that developed rift basins, carbonate platforms and evaporites along the margin of East Africa (modified after Alconsult, 1996).

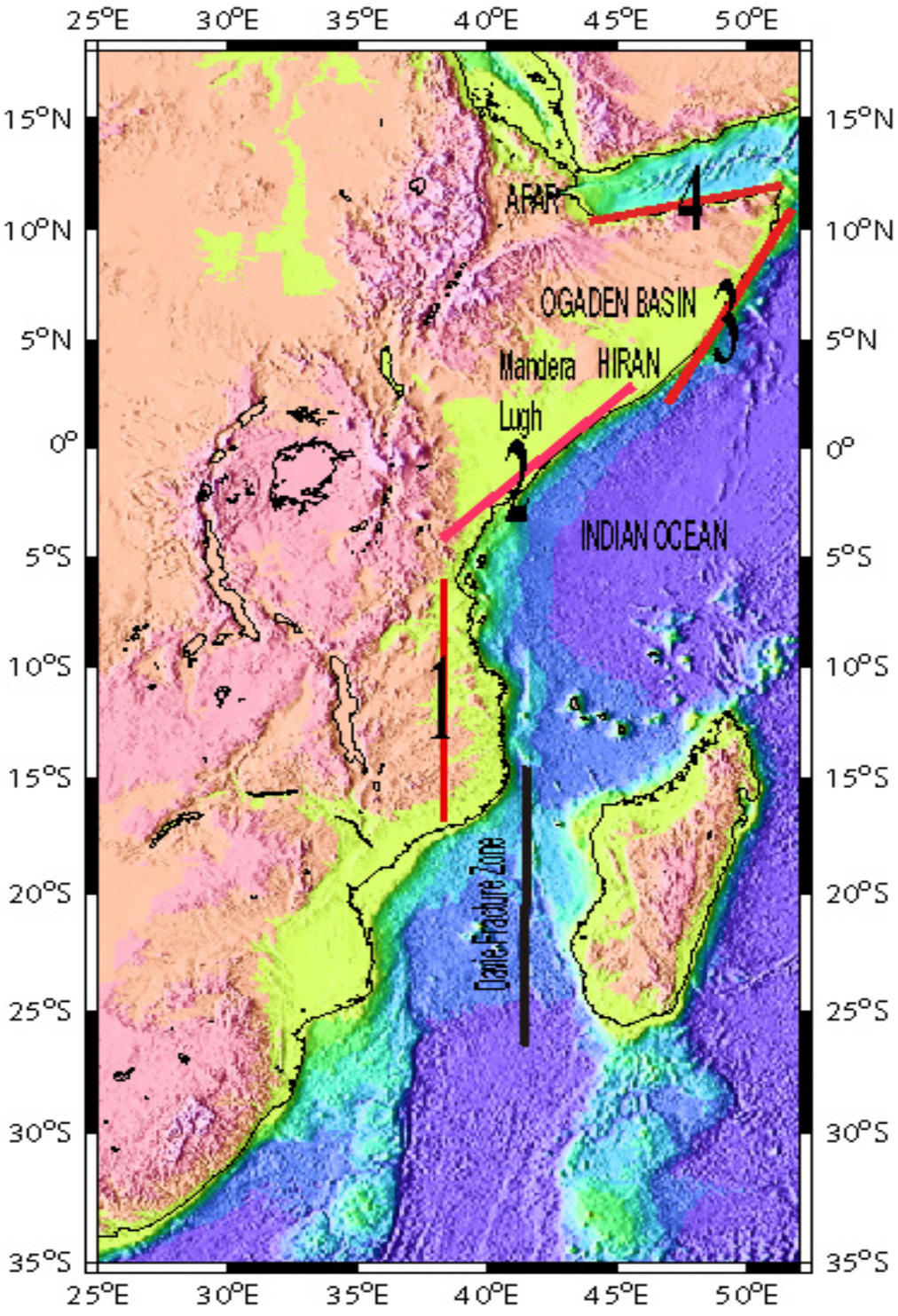

Figure 4.4: Topographic and bathymetric map of the East African margin showing the bathymetry, the Davie Fracture zone in relation to the Ogaden basin and adjacent structures.

3. The northeastern segment of the Horn of Africa (northeastern Somalia), which formed as a result of the separation of India from Madagascar forming the distinct northern Somalia sub-basin.
4. The northern Somalia margin bordering the Gulf of Aden, which is a Neogene feature formed as a result of rifting and separation of Arabia from Africa.

Bosellini (1986) conducted extensive research based on oil company data and fieldwork in Somalia to assess the Jurassic sediments and the Karroo rift system, which is believed to have developed during the Permo-Triassic along the east coast of Africa starting from South Africa up to Ethiopia. His studies show that the Karroo rifts reach only up to the Mandera Lugh basin and Hiran trough in northeastern Kenya and southwestern Somalia, respectively (Fig. 4.4). However, deep drilling for oil exploration in the Ogaden basin of Ethiopia, along with confidential company reports, have confirmed the existence of Karroo sediments up to Hilala and Calub areas, and beyond. These areas are located several hundreds of kilometers further to northeast of the Mandera Lugh basin. These areas provide evidence for the existence of Paleozoic sediments in the region. Discoveries of Hilala and Calub gas and gas condensates from the region provide additional evidence. This suggests that understanding of the structure and evolution of the Ogaden basin is still at its infancy.

Previous research (Coffin and Rabinowitz, 1987) has shown us that passive continental margins can persist for a very long time, building accretionary wedges that can extend hundreds of kilometers out to sea (Fig. 4.5). As the sediment wedge thickens the thickest portion can eventually rise above sea level, burying the original continental shelves and becoming 'new' dry land. This explanation holds true when seen with previous seismic results and the general sedimentary stratification in the regions as established elsewhere (Coffin and Rabinowitz, 1987).

However, it should be noted that sedimentary deposition rate and subsidence rate, as well as the age of the continental margin all influence the type of landforms created.

The sedimentary basins of the East African continental margin are shown in Fig. 4.6. Several of these basins have multiple, active and proven petroleum systems (Alconsult, 1996, BEICIP Franlab, 1998). The East African continental margin clearly has good potential for oil and gas exploration as has been proved by exploratory wells with oil and gas shows and gas discoveries in Ethiopia, Tanzania and Mozambique. However, compared to other sedimentary basins in the region, the Ogaden basin has the least number of wells drilled with the smallest seismic data coverage for the largest area.

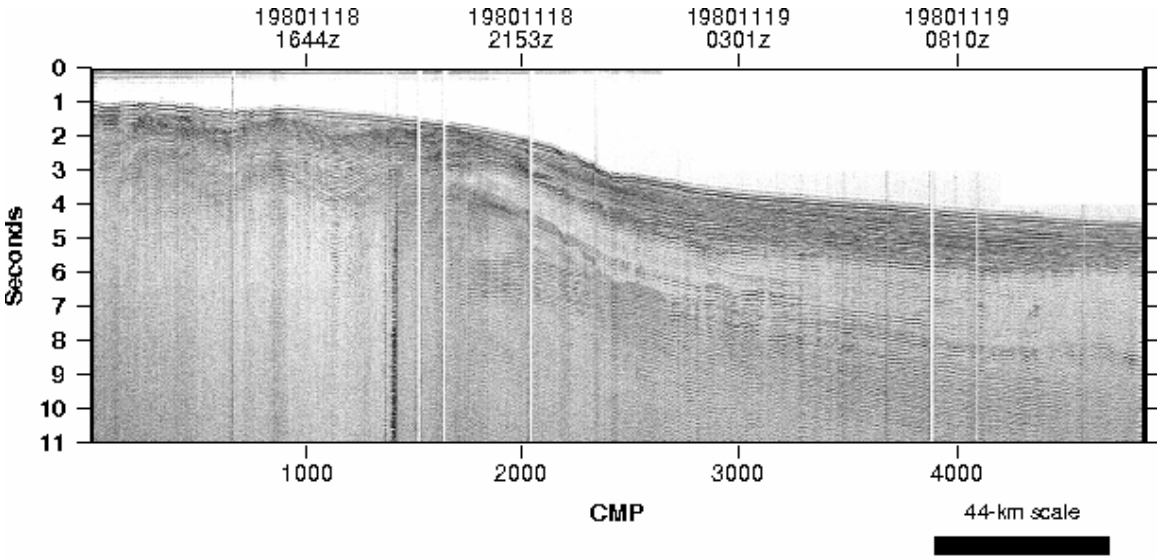

Figure 4.5: Seismic section showing accretionary sedimentary wedge across the passive margin of costal Somalia. The sedimentary package thickens towards the ocean and thins towards the land (after Coffin and Rabinowitz, 1987).

4.3 Sedimentary basins of Ethiopia

In the past, the Afar and the Main Ethiopian Rift (MER), along with their volcanic products, have been the focus of many scientific studies, but there has been little emphasis on petroleum exploration. However, more than 30% of Ethiopia is covered with sedimentary rocks. The sedimentary basins of Ethiopia with known and possible hydrocarbon potential are shown in

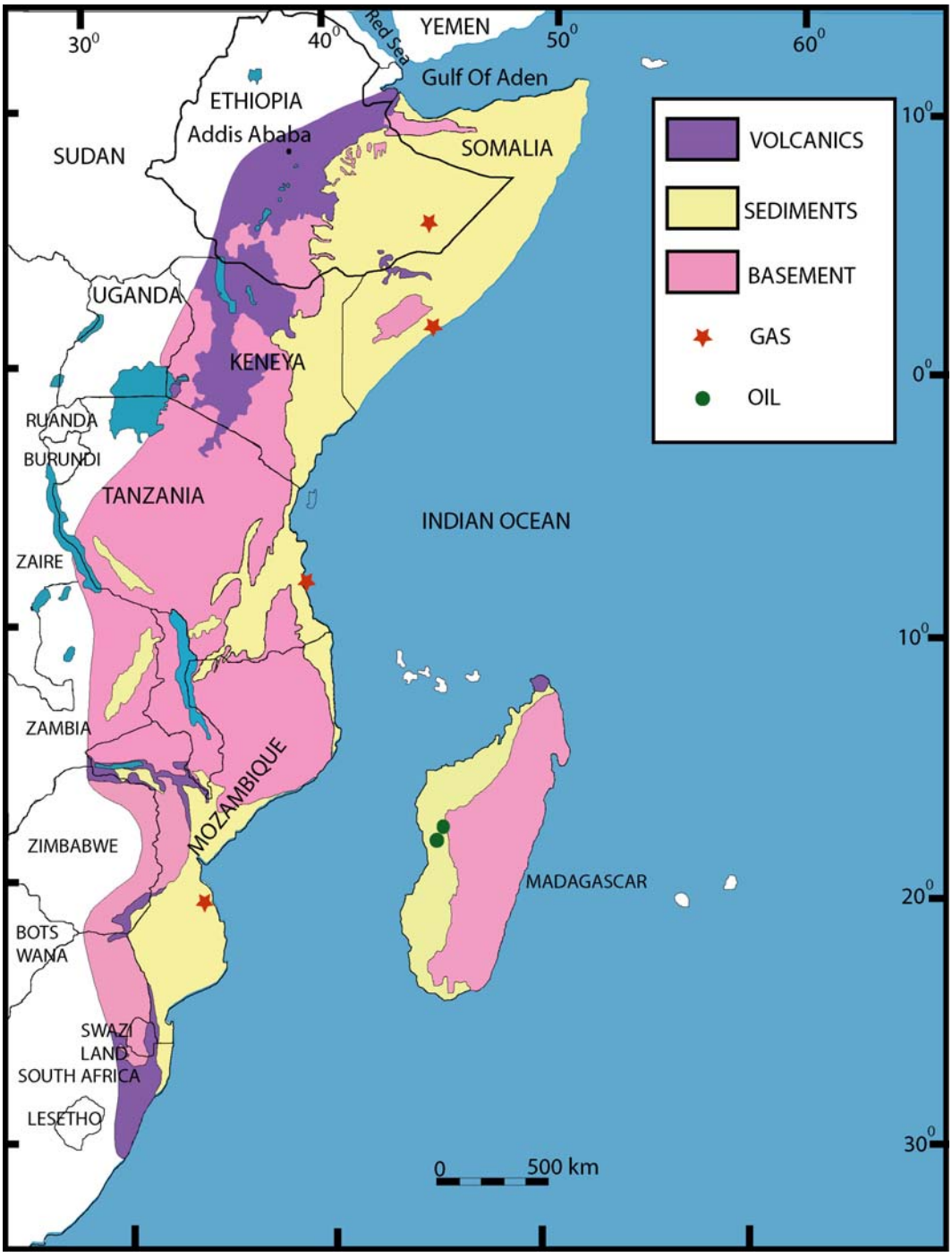

Figure 4.6: Sedimentary basins of the costal margin of East and Southern Africa as well as Madagascar, showing the distribution of sediments, oil and gas discoveries in the region (modified after Alconsult, 1996).

Figure 4.7. Most of these basins appear to be the result of extensional processes, however there is still much to be learned about them. In some of these basins, the structural framework and prospectivity are not yet established.

Prospecting for oil and gas has been going on in Ethiopia since the 1950s. As a result of past exploration efforts, gas and gas condensate have been discovered in two areas within the Ogaden basin in southeastern Ethiopia (Fig. 4.7). In addition oil inflows and shows have been reported to exist in some of the exploratory wells in the Ogaden basin. Oil seeps exist in the Ogaden and Abbay basins. Oil shale and coal deposits have been discovered north of the Southern Ethiopian Rift basins (Omo-Chew Bahir or Turkana area). Clastic and marine sediments, which are possible source, reservoir and seal rocks have been known to exist in abundance. Although little is known about the sedimentary basins of Ethiopia, it is appropriate to analyze the prospectivity of each basin through research such as this study.

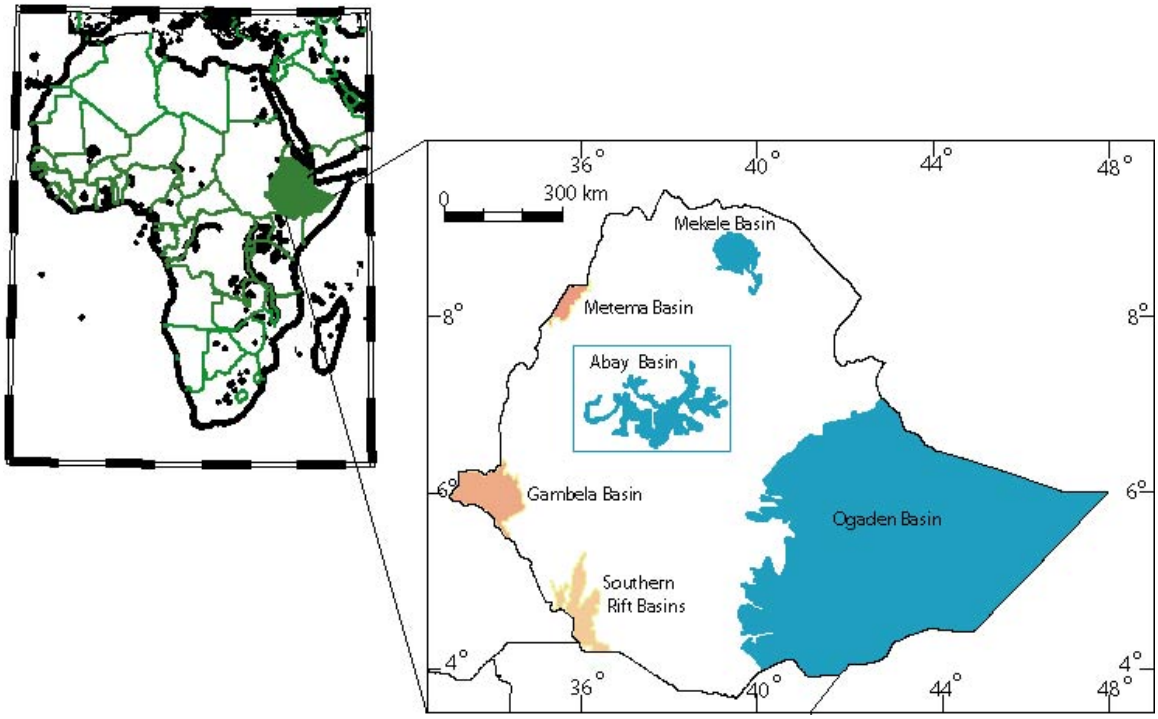

Figure 4.7: Index map of the six sedimentary basins of Ethiopia

4.4 The Ogaden Basin

The Ogaden basin has an area of about 350000 km^2 and its tectonic evolution (Fig. 4.7) includes a complex overprint of two Permo-Triassic to early Jurassic rift basins that do not outcrop because they are overstepped by a passive margin sag basin of late Jurassic age. The rifting phase (Permian, Triassic and lower Jurassic) can be explained as the process during which predominantly continental sediments were deposited at relatively high sedimentation rates in rift basins.

The drifting phase is assumed to have occurred between the Middle Jurassic – Cretaceous/Neogene. During this phase, oceanic crust formed between the physically separated parts of the supercontinent. Sedimentation rates were somewhat slower than during the preceding rift phase and were predominantly of marine origin. Continental margins formed during this phase are commonly termed passive margins, because they are at the trailing edges of drifting continental plates (Alconsult, 1996).

Of all the sedimentary basins in Ethiopia, the Ogaden basin has been the most studied. However, there remains a scarcity of data and lack of detailed analysis. Review and re-analysis of existing data, as well as adding new data sets based on modern acquisition and processing techniques are needed. It is assumed that some of the gaps in our understanding of this basin's evolution and structural framework can be overcome by an integrated analysis that includes the new data that are available for this study.

4.4.1 Geology of the Ogaden Basin

Various evidences about Ethiopian geology and its potential for petroleum prospects are available (Mohr, 1962; Jelenc, 1966; Kazmin, 1972; Geological Survey of Ethiopia, 1976). A geological map of the Ogaden basin (BECIEP, 1984) is an amalgamation of geological maps made by Tenneco, Whitestone, and the Soviet Petroleum Exploration Expedition (SPEE). This map serves as a working document for the Ogden basin. Tefera et al. (1996) have prepared the

most recent geologic map of Ethiopia, which also updated the Ogaden basin. Prior to this, Maxus Energy Corporation, Hunt Oil Company, and SPEE each prepared their own geological maps for their contract areas while working in different parts of the Ogaden basin. Figure 4.8 shows a simplified geological map of the Ogaden basin and adjacent areas.

The structural framework of the Ogaden basin is related to the breakup of Gondwanaland and is believed to be a classical type of continental passive margin related to the plate tectonic development of the Indian Ocean (Smith and Hallman, 1970; Emery, 1980; Fairbridge, 1982). Others have suggested continental boundaries that have nothing to do with plate tectonics (Kent, 1974; Tarling and Kent, 1976). More recent studies (Coffin and Rabinowitz, 1987; Bosellini, 1988) have supported the plate tectonic idea of structural development of the region. The sedimentary history of most of the East African continental margin is related to two phases of rifting and seafloor spreading (Alconsult, 1996; BECIEP Franlab, 1998; and Worku, 1988). The first phase of rifting is assumed to have occurred in Late Carboniferous to Early Jurassic (i.e. Karroo). The rift system was developed across Gondwanaland with north-south, northeast-southwest and northwest-southeast trends, starting from present day South Africa to Ethiopia (Fig. 4.9) and is commonly termed the Karroo rift system. This structural framework has been explained in detail for the Ogaden basin by Purcell (1979), where he emphasized that the Marda fault zone is one of the principal structural controls for the evolution of the Ogaden basin (Fig. 4.10).

The Karroo rift system formed the main structural control for the deposition of syn- and post- rift sedimentation in the region. To date, continental sediments are known to be in the range of 1 to 10 km thick in different parts of the EACM, including the Ogaden basin. Successive uplift and subsidence occurred in the region after the onset of rifting (Arkell, 1956; Kent, 1974). This resulted in alternating marine transgressions and regressions producing widespread marine

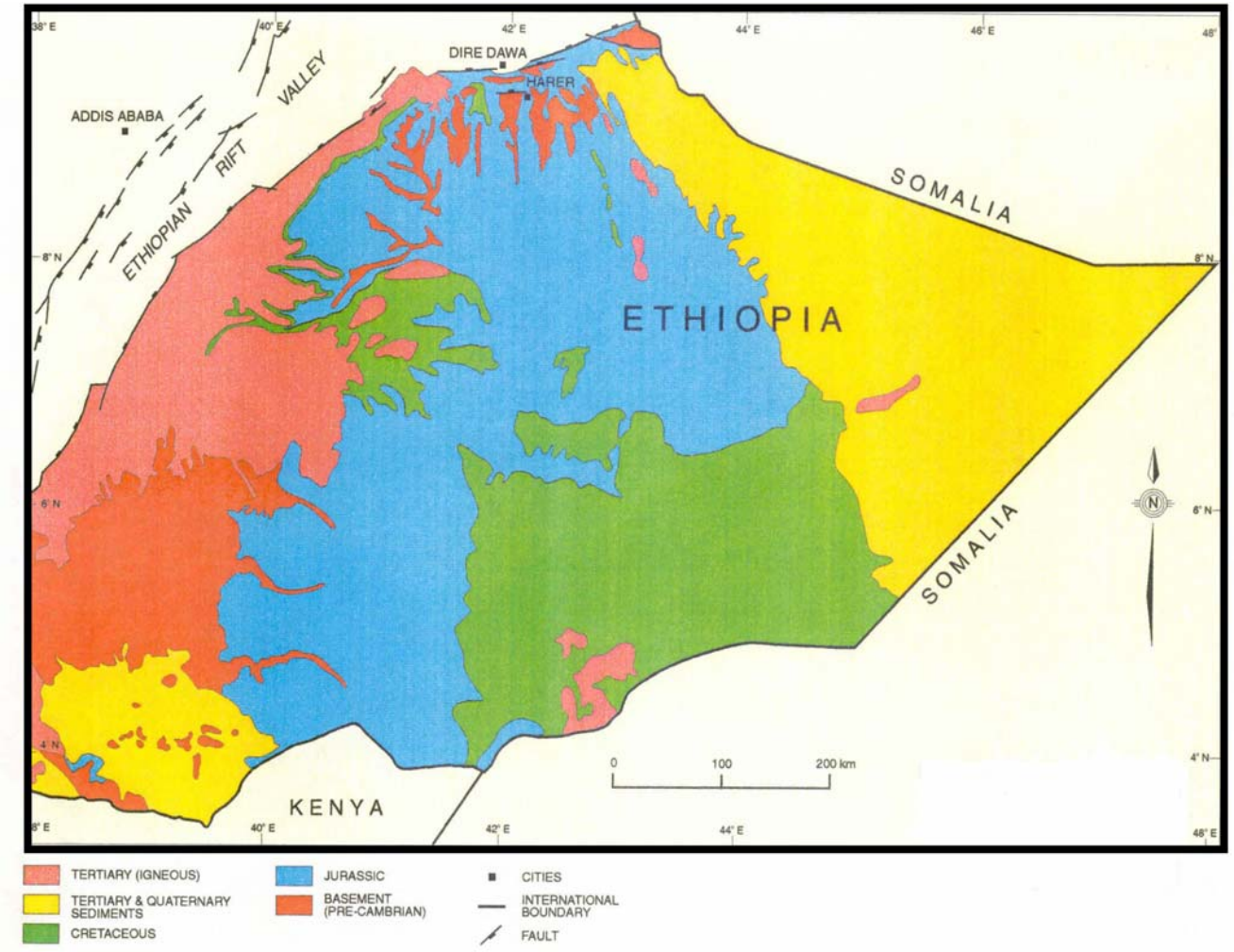

Figure 4.8: Simplified geological map of the Ogaden basin, showing the distribution of Jurassic, Cretaceous, and Quaternary sediments along with basement outcrops.

sediments of Jurassic age. Ethiopian geologists have discussed the possible existence of landward projections of the Karroo rifts. Thus in this study, the results of the EAGLE seismic experiment, and industry seismic reflection data, were integrated with gravity and magnetic data to investigate the possible existence of northwest trending Karroo rifts that extend landward from the continental margin.

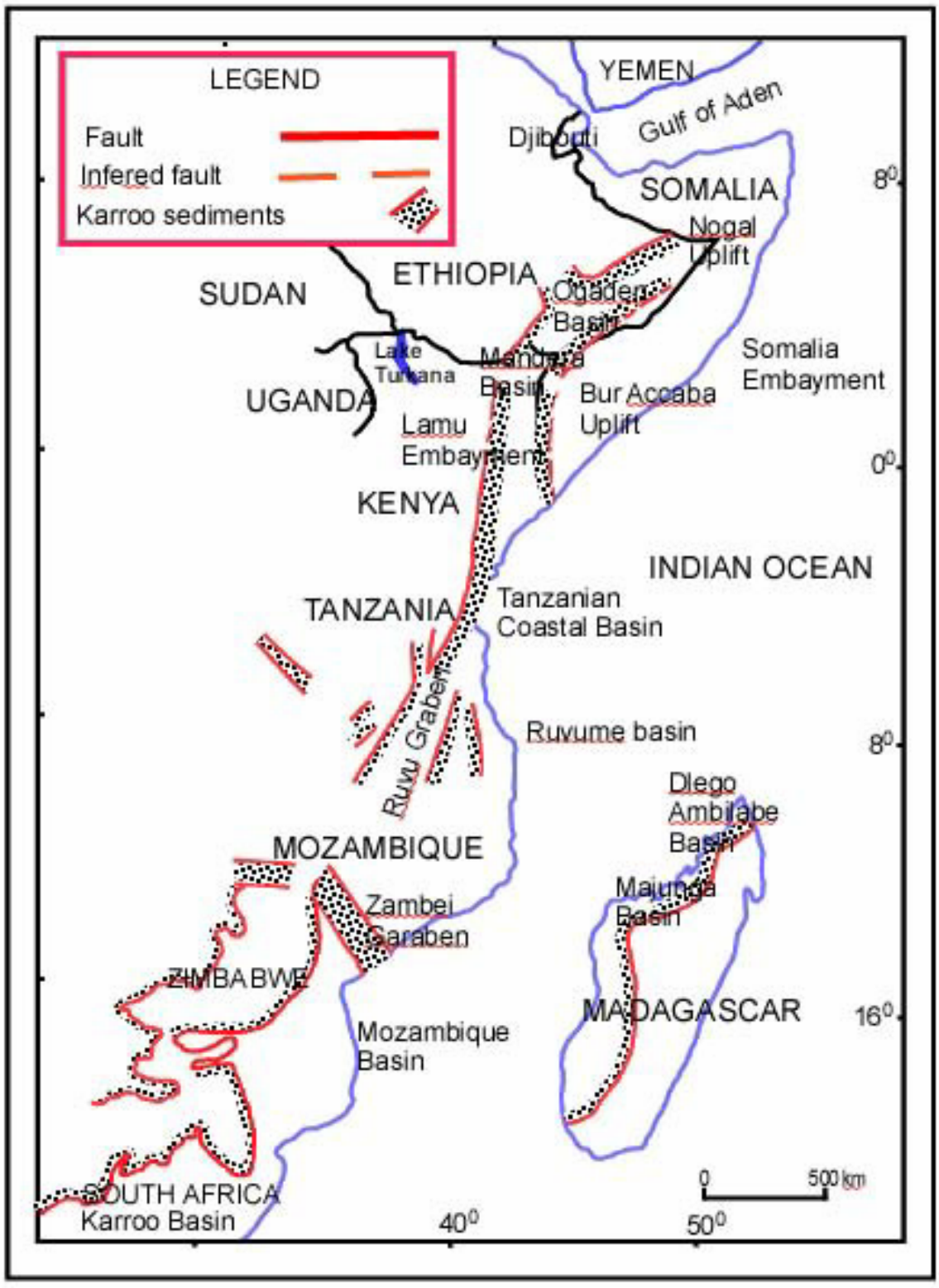

Figure 4.9. Regional structure map of the Karroo rift system along the coastal margins of East Africa (modified after Flores, 1973)

The second phase of rifting is a Cenozoic event associated to the East African Rift system that stretches from Mozambique in the south to Syria in the Middle East, and contains many recent rift basins throughout its length.

The Ogaden basin is filled with of Phanerozoic sediments (Fig. 4.10). Paleozoic sediments generally classified as Karroo sediments in the region are divided into the Calub Sandstone, Bokh Shale and Gumburo Sandstone. However, Worku (1988) included the Adigrat Sandstone as part of the Karroo group within the Ogaden basin. The given names are associated with the locality names where the type sections were first found. The Karroo formations do not outcrop on the surface in the Ogaden basin, but they are known to exist in the subsurface by deep drilling results from exploration and development wells in Calub and Hilala areas. The Adigrat Sandstone is widespread in Ethiopia and Somalia.

Mesozoic sediments consist of Jurassic Carbonates, associated shale deposits and sandstone formations younging upwards. These as well as the Lower, Middle, and Upper Hamanlei, and the Urandab Shale and Gebredare Limestone formations, Gorahei Evaporites, Ferfer Limestone, Belet Uen Limestone, and Jessoma Sandstone are more recent formations such as the Faf and Auradu Limestones (Fig. 4.11).

Various oil companies have reported that the Hamanlei Formation shows numerous oil inflows as well as shows. This formation has been major exploration target, and encompasses most of the exploratory wells drilled since the 1970s. The stratigraphic column of the Ogaden basin together with lithology and depositional environments is given in Figure 4.11.

Arkell (1956) suggested that the largest sea transgression to have occurred in Ethiopia and Somalia was during Bathonian time (Jurassic). This is supported by the existence of thick Jurassic sediments both in Ethiopia and Somalia. Jurassic seas appear to invade the horn of Africa from the south and reach their greatest extent during Collovian time (Jurassic) (Beltrandi

and Pyre, 1973). It appears that Jurassic sea invasions came from both the south and north in East Africa (Barnes, 1976).

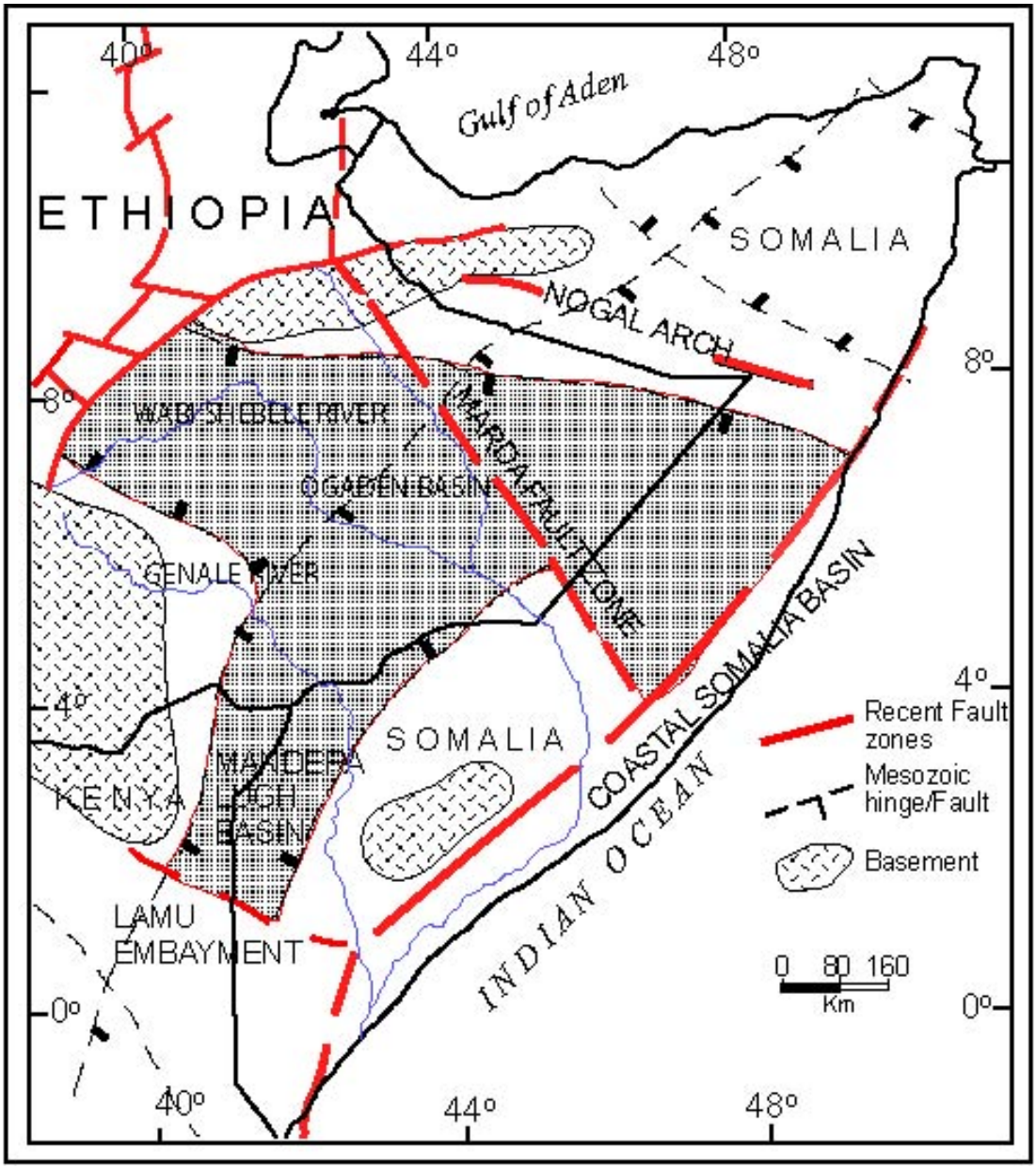

Figure 4.10: Structure map of the Ogaden basin showing the main sediment depocenter of the Ogaden basin, the Mandera Lugh Basin and the Marda fault zone, Nogal arch and related basement uplifts. (modified after Purcell, 1976).

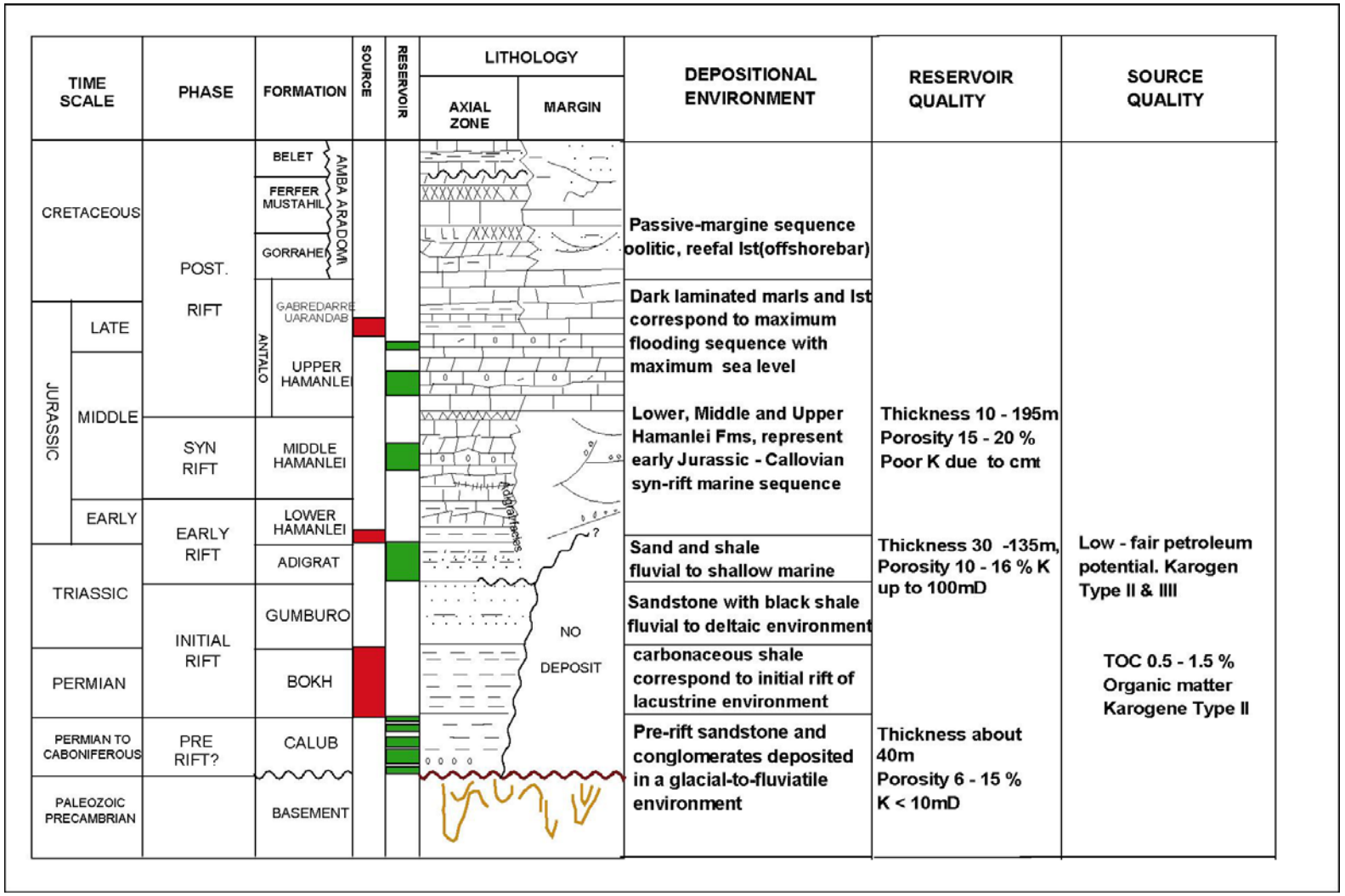

Figure 4.11: Stratigraphy of the Ogaden basin showing lithology, and depositional environment.

4.4.2 Geophysics of the Ogaden Basin

Geophysical investigations based on seismic, gravity, and magnetic methods have been carried out in different parts of the Ogaden basin. Oil companies have acquired gravity and magnetic data in the basin since the 1960s. Only a small amount of magnetic data has been acquired in conjunction with the gravity data and data collection has been in separate locations. Thus, these data sets lack a general connection to one another, since they were acquired in different blocks. Some gravity data were acquired by various oil companies prior to the 1970s. These data were at the disposal of every company who took a concession in the country but are not yet fully crafted into a modern database. Data acquired as of the late 1980s have been archived in appropriate formats and are available for immediate use and promotional activity as well as some for sale in some instances.

Seismic data have been acquired in the Ogaden basin in an on-off manner since the 1950s. The seismic data from the Ogaden basin ranges from low fold (as low as 6 fold) to a high-resolution data (as high as 80 fold), the latter being most recently acquired in the early 1990s.

Most of the geophysical results were presented in the form of isochron, isopach maps and structural contours based on seismic interpretations and targeting of structural traps in the Ogaden basin. This is due to an earlier conception that prospectivity was mainly supported by structures alone, and companies like Sinclair, Elwareth, Tenneco and SPEE were all focused on structures. Drilling results of some of the structures identified in places such as El Kuran, Abred, Galadi, Magan, and Hilala were oil shows and oil inflows that appeared mainly in the Upper and Middle Hamanlei Formations.

The usefulness of gravity and magnetic data in various exploration and research activities is well established. In addition, the availability of software for analyzing these data has made potential field methods more important and complementary to techniques such as seismic

reflection. One of the applications of potential field techniques is defining regional extent and geometry of sedimentary basins. The Ogaden basin in the southeastern part of Ethiopia has been known for a long time due to its hydrocarbon potential. Fairly good coverage of gravity data is available for integrated data analysis and interpretation. However, the basin is still being studied and additional data may help for more detailed analysis and to fill the remaining data gaps.

In the Ogaden basin of Ethiopia (Figs. 4.7 and 4.12) two types of sediments cover the basement. This gross classification includes the Permo-Triassic clastic sediments and the Jurassic marine sediments. The thick sedimentary cover in the Ogaden basin does not allow for the resolution of structural displacements especially those associated with the basement structures.

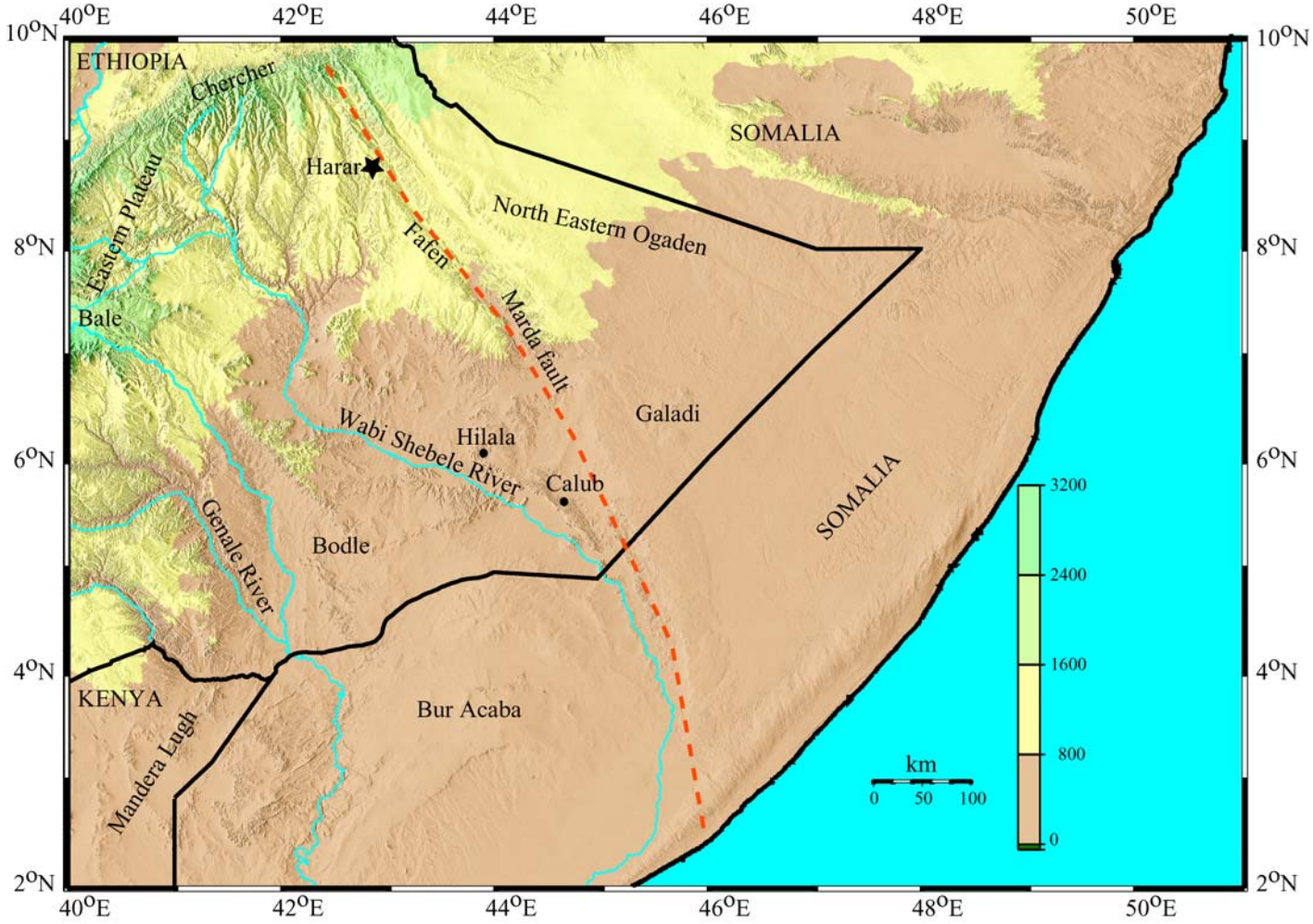

Figure 4.12: Topographic map of the Ogaden basin constructed from 90 meter digital elevation showing the lowland of the Ogaden basin which is similar to the costal regions of Somalia.

The subtlety of structural elements necessitates detailed data processing and use of a wide range of enhancement techniques and display parameters. Thus in this study, applying different filtering techniques using potential field data have allowed unraveling these subtle structures. Gravity and magnetic data were acquired in the region by various oil companies such as SPEE, Maxus Energy, and the Hunt Oil Company. Yet the results of these studies are inconclusive and a sound oil discovery has not been made.

In addition, some of the basins that were interpreted to be deep were found to be shallow based on drilling results. In some parts of the basin, the drilling results did not encounter the basement rocks. Knowing this backdrop, a gravity database for the whole Ogaden basin region was compiled, edited and processed as part of this study.

4.5 Analysis of Gravity data

The Ogaden basin is the largest basin in Ethiopia and fairly good gravity data coverage exists (Figs. 4.7 and 4.13). A wide range of gravity data were obtained from the Petroleum Operations Department (POD) of the Ethiopian Ministry of Mines and Energy (MME). These data cover the region with variable density and spacing. In the northeastern part of the Ogaden basin, data were acquired along profiles with 2 and 4 km station intervals by Maxus Energy (Fig. 4.13). Confidential reports (e.g., Maxus Energy Ltd., 1993; Alconsult, 1996; BECIP Franlab, 1998) explain that care was taken to insure that reliable base station ties were maintained for the surveys. These base stations were tied to the nearest IGSN71 stations in the area. For much of the central Ogaden basin data acquired by SPEE were evenly distributed and, in most cases, follow the existing seismic lines. The other data were acquired by the Hunt Oil Company. All data from the three companies were acquired in late 1980s to early 1990s. For most of these data, GPS instruments and/or barometric altimeters were employed for elevation determinations. The available reports claim a maximum error of ±1 meter exists in the elevation values (Hunt Oil

Company, 1994). The data acquired by Maxus and Hunt employed Lacoste and Romberg gravity meters. In general, data quality for the Ogaden basin was rated as good.

The International gravity formula of 1976 was employed in the gravity reduction.

$$g_{th} = 978031.85(1 + 0.005278895\sin^2(\phi) + 0.000023462\sin^4(\phi) \qquad (4.1)$$

where g_{th} is the theoretical gravity and ϕ is the latitude

A density value of 2.67 gm cm^{-3} was used for the calculation of the Bouguer correction (e.g., Hinze, 2003).

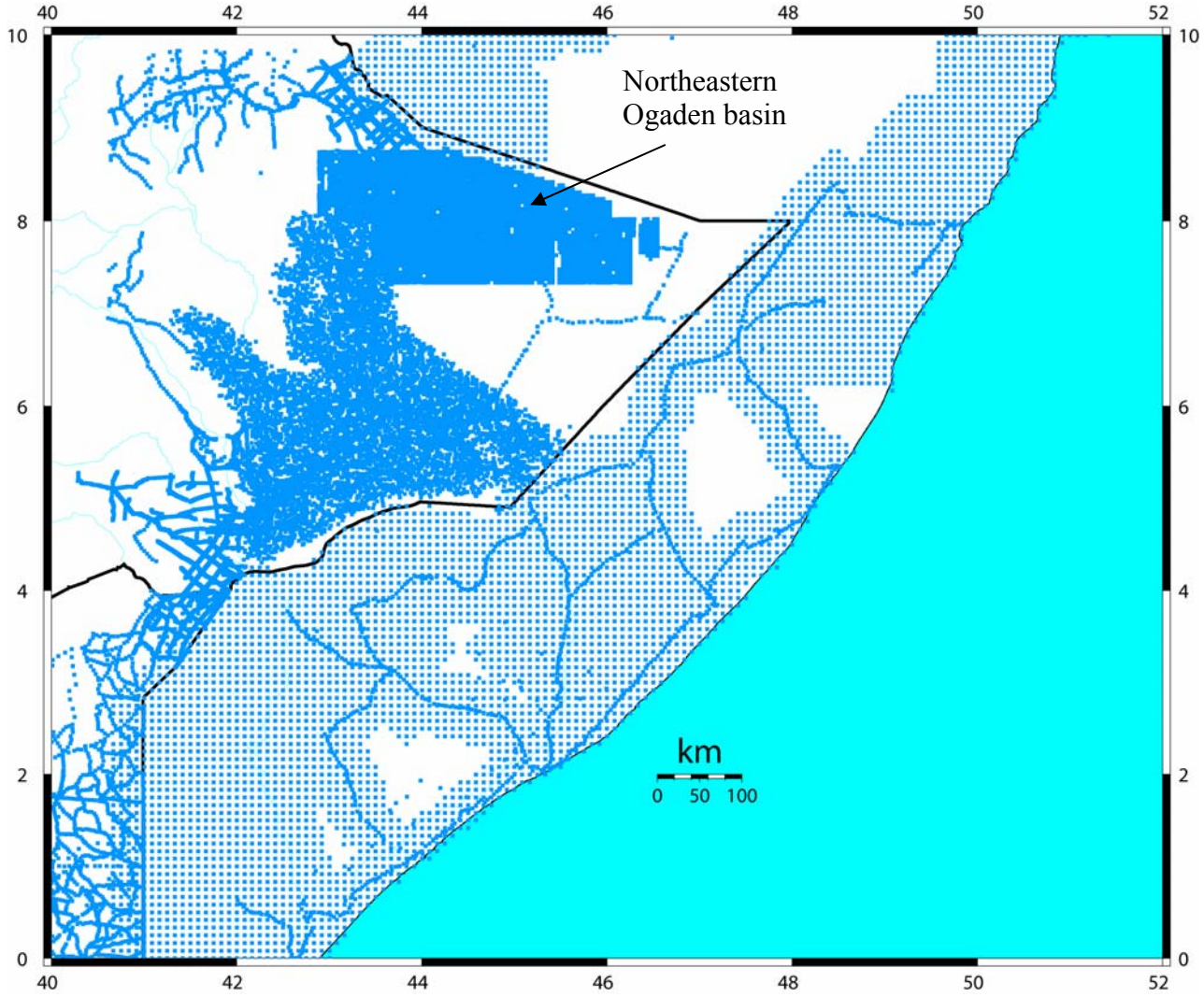

Figure 4.13: Gravity station distribution in the Ogaden basin and adjacent areas such as Somalia and part of the eastern Ethiopian plateau. Blue dots are gravity stations.

4.5.1 Terrain correction

Assuming that the area is flat in most cases, terrain corrections were not employed for data acquired by Maxus and Hunt oil companies. In this study, we calculated terrain corrections for the uncorrected surveys using Shuttle radar topography (SRTM) 90 meter Digital Elevation Model (DEM) data. A physiographic map of the Ogaden basin and adjacent areas was generated from the same DEM data (Fig. 4.12). We employed the Hammer zone approach to calculate the terrain corrections (Hammer, 1939). The calculation was for the outer zones up to zone M, which has a radius of about 22km. A density of 2.4 gm cm^{-3} was used in all the surveys for the terrain correction.

4.5.2 Bouguer gravity Anomaly map of the Ogaden basin and adjacent areas

A Bouguer gravity anomaly map of the Ogaden basin and adjacent areas was constructed to analyze basin geometries, determine the basement depth, and resolve structural trends in the basin (Fig. 14). More than 38,000 gravity points from the Ogaden region and gridded data from adjacent areas were used to produce this map (Fig 4. 14). The gravity anomaly values range from -180 to 30 mGals (Fig. 4.14). The minimum gravity anomalies are associated with the uplifted region of the eastern Ethiopian plateau which borders the Ogaden basin on the northwest.

The Bouguer anomaly map shows several major structural trends, and the Ogaden basin is bordered by the large negative gravity anomaly (A) caused by the thick crust of the eastern Ethiopian plateau (Mackenzie et al., 2006). However, thinning under the crust of the basin due to extension has produced a relative gravity high that causes the strong NW-SE increase in gravity anomaly values. The highest anomaly values lie along the coast of Somalia and are due the thinning crust along the continental margin that is a result of the break up of Gondwanaland during Permo-Triassic time.

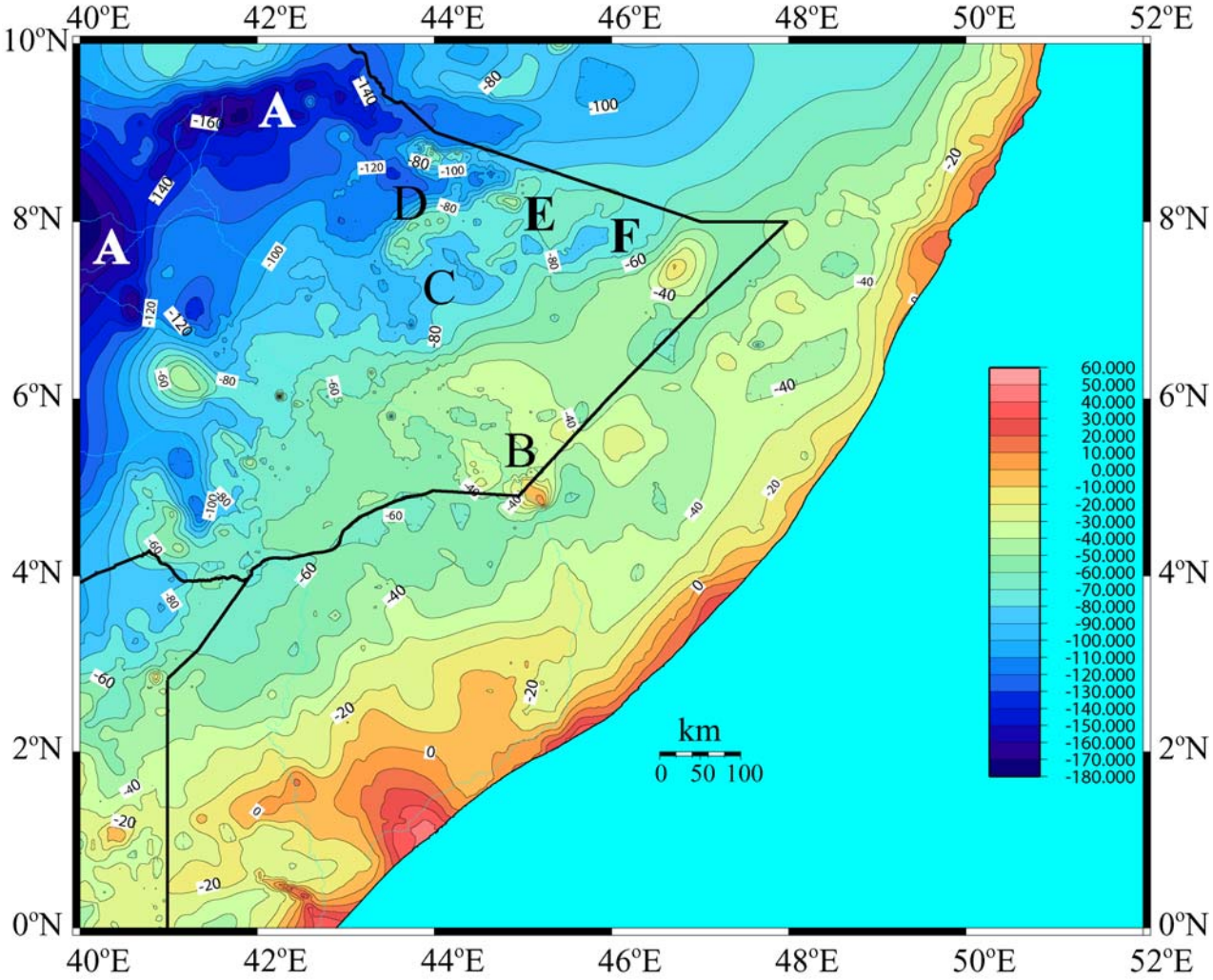

Figure 4.14: Bouguer gravity anomaly map of the Ogaden basin region, anomalies A, B, C, D, E and F are anomalies of interest.

There is a distinct trough like anomaly marked by the -110 mGal contour line. Parallel to this is the -100 mGal contour line (Fig. 4.14). This may suggest a structural trend in the direction of the uplifted part of the eastern plateau. Other noticeable anomalies are more localized and are positive and negative in their respective areas (Fig. 4.14). A relative low associated with the orientation of the Marda fault zone, which starts at the southern Ethiopian-Somalia border is delineated in a north-south Such as (anomaly B) that appears to continue to the north area of anomaly C. These two anomalies have the same north-south trend, but with different values, where the minimum gravity anomaly values are associated with the higher elevation region. This north-south alignment could be attributed due to the Marda fault zone (Fig. 4.12). This fault zone may be a large fault zone associated with one of the gas discoveries (e.g., Calub) in the Ogaden basin. The other distinct anomalies seen of this Bouguer gravity anomaly map are those of the northeastern Ogaden area. Like the south-central Ogaden, there is good data coverage in the northeastern region (Fig. 4.13) and anomalies depicted are reliable, since the very high precision data are available in this region. These anomalies D, E and F. have a NE SW trends and occupy small regions compared to the whole basin. These relative high amplitude, short wavelength anomalies could be due to localized basins or graben like structures. The difference in the trend of anomalies between the central Ogaden and northeastern Ogaden may be due to differences in the development of structural grains in each region. In general, the Bouguer gravity anomaly map shows a broad structural grain in the northwest direction, which it may be associated with older fabrics related to the evolution of the Ogaden basin. The Marda fault zone is a prominent structural feature in the region (e. g., Purcell, 1976; Boccaletti et al., 1998) and is characterized by a disconnected fault system as well as by another structural grain.

4.5.3 Residual gravity anomaly map of the Ogaden basin

Anomalies of interest in gravity surveys can be concealed by regional effects such as gravity responses of deeper geologic features. In this case, a crucial first step in the interpretation of anomalies is to separate the regional from the residual, where the regional is considered to be due to deeper effects with the residual due to local or shallow geologic features effects. There are a number of regional residual anomaly separation techniques available (e.g., Nabighian, et al., 2005). In this study, we selected the technique using the Bouguer gravity anomaly and the upward continuation computation method to produce a residual anomaly map.

The mathematical process of using observations on the land or sea surface to simulate observations made at a higher elevation is called upward continuation (Nabighian et al., 2005). Upward continuation attenuates short wavelength anomalies (Kellogg, 1953).

The basic frequency domain equation for upward computation is:

$$L(r) = e^{-hr} \qquad (4.\ 2)$$

Where h - is the distance in ground units to continue up relative to the plane of observation

r - wave number (radians/ground unit) where $r = 2\pi k$ is cycles/ground unit

Since it produces no side effects, upward continuation is considered to be a clean filter. It is believed that it can be used to remove or minimize the effects of shallow sources and noise in grids.

Therefore, we upward continued the gravity anomaly to an equivalent elevation to the base of the crust at a depth of 30 km. The resulting map is shown in Figure 4.15. The upward continued map shows smooth, gradually varying, positive gravity values from the coastal margin

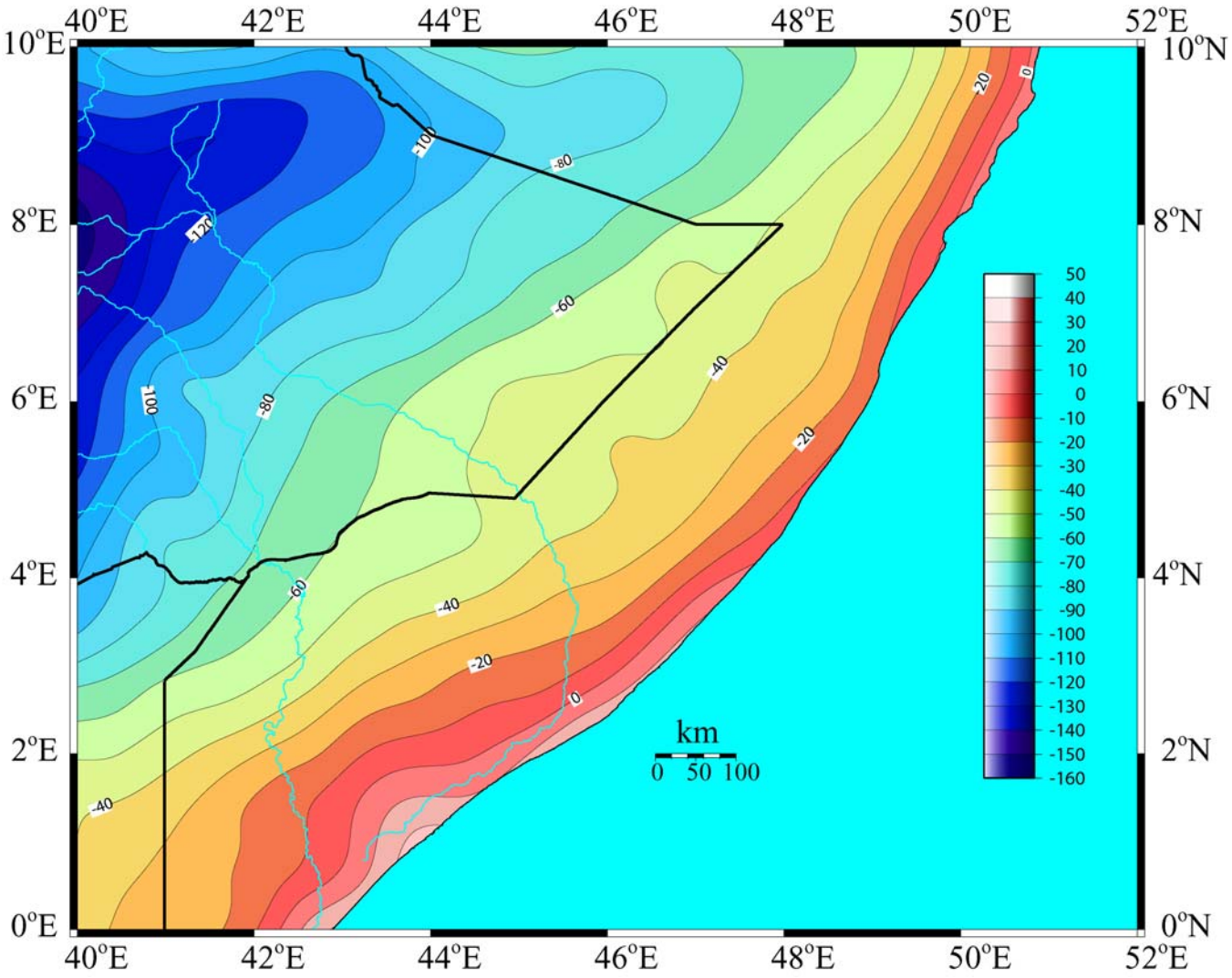

Figure 15: Map of upward continued gravity anomaly values in the Ogaden basin and adjacent areas, showing a regional low associated with the Plateau region and a region maximum along the costal region.

and decreases to a minimum in the plateau region where thick crust and low density material are present. The residual anomaly is produced by subtracting the upward continued values (Fig. 4.15) from the original Bouguer anomaly (Fig. 4.14). Figure 4.16 show the residual gravity anomalies for the Ogaden basin and adjacent areas.

One of the important features depicted in this map is the local positive anomaly in the central Ogaden with an almost E-W orientation (C). This relative positive anomaly may be associated with a graben-like structure possibly filled with relatively denser sediments such as limestones, which are prevalent in the region. Interesting features that are depicted in the eastern Ogaden basin are NE-SW trending anomalies which are relative negative anomalies of localized features (E and F). These anomalies are also shown in the Bouguer gravity anomaly map. In general, the residual map shows a broad feature trending towards the northwest narrowing in the direction of the northwest (D) and broadening to the south. In addition, several shorter wavelength features have this trend. These features may be related to the original basin rift structures formed during the break up of Gondwanaland in the Permo-Triassic.

4.5.4 Filtering and Anomaly Enhancement

Prior to interpretation, gravity data should be enhanced based on filtering techniques. Filtering and image enhancement involves digital processing based on Fourier analysis (e. g., Blakely, 1996; Nabighian, et al., 2005). The goal of filtering depends on the choice of the filtering techniques. Qualitative or quantitative filtering can be applied on the basis of anomalies wavelength or trends (Blakely, 1996). Others suggest filtering on the basis of geologic origin of anomalies such as the isostatic residual anomaly (e. g., Simpson et al., 1986). Gravity data can be filtered in order to compare with the results of other techniques, and to enhance gravity anomalies of interest. It is also possible to make a preliminary assessment, such as location of a source or the density contrast of causative bodies.

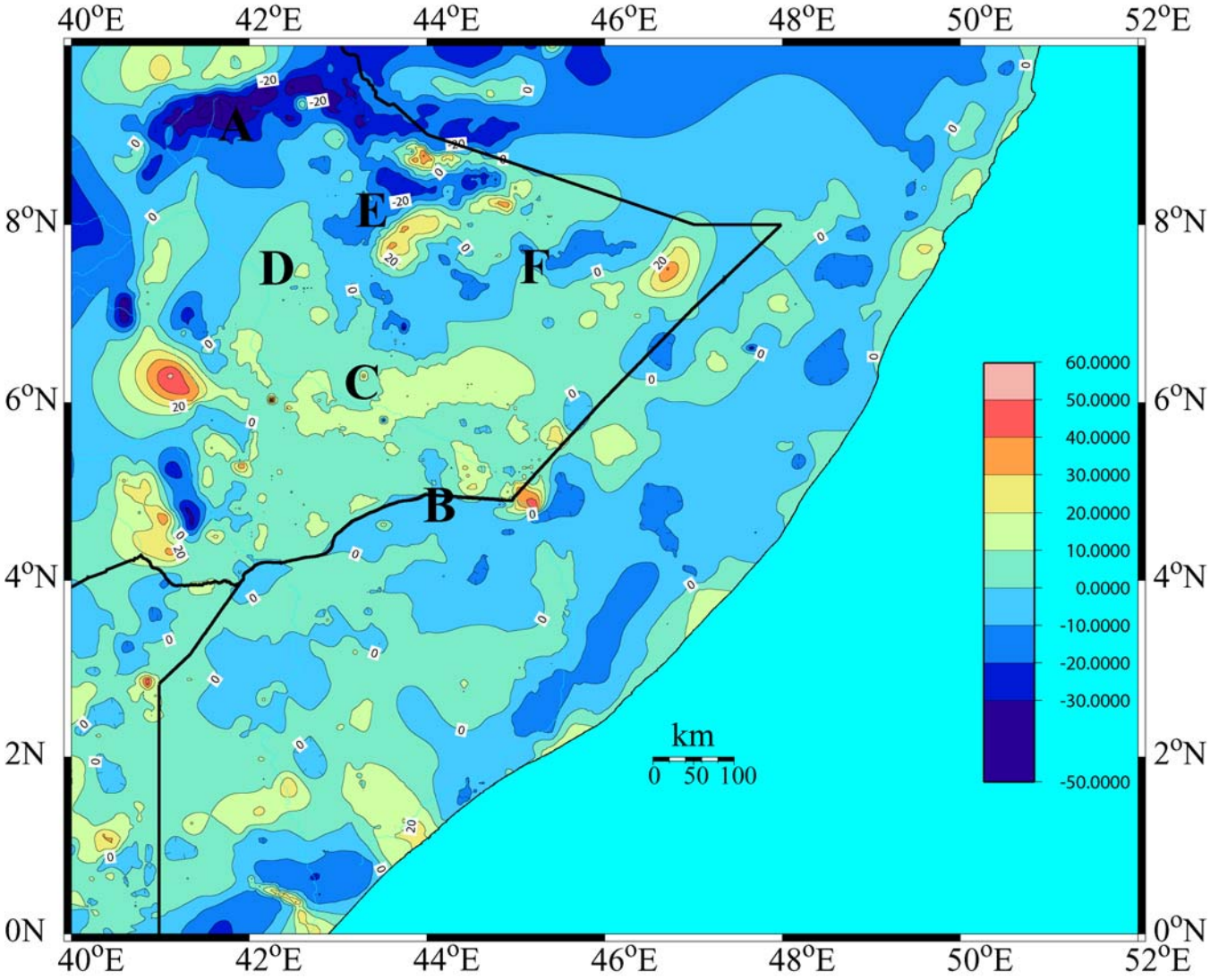

Figure 4.16: Residual gravity anomaly map of the Ogaden region showing localized anomalies depicted as relative highs and lows. A, B, C, D, E and F indicate anomalies of interest

In this study, we selected areas of good data coverage and applied various filtering techniques (Fig. 4.17). The Bouguer gravity anomaly of the selected area is from central part of the Ogaden basin (Fig. 4.17). In this map it is possible to see a positive gravity anomaly that trends in a northeast southwest direction and branches out to the northwest. The relative negative in the northwestern part of this selected area is associated with the high elevation of the region, which probably is caused by the asthenospheric upwelling that forms the Ethiopian rift and the Ethiopian plateaus. This grid (Fig. 4.17) is used for most of the filtering techniques applied in this study. For a better visualization purposes a 3D view of the same gravity anomaly map in the same area was produced (Fig. 4.18). In this map, it is apparent that a tri-radial structural grain exists. This is in agreement of the suggestion that the evolution of the Ogaden basin could be a tri-radial rift system in the central part of the basin (e.g., Hunegnaw et al., 1999).

In our analysis we removed the regional trend based on the second order polynomial fitting to prepare the grid for application of the Fast Fourier Transform (FFT). The assumption in this procedure is that the effect of deeper geologic features can be removed and effect of the local anomalies or short wavelengths can be easily considered. The area we selected is from a large grid to avoid edge effects in our analysis and ensure the best data distribution exists in the selected area. Unwanted wavelengths can be removed with the residual or desired filtering, such as the small positive anomalies shown in the southwest section of the selected area. The data are then transformed forward. The desired filtering technique is then selected. Finally, after the desired filter is applied the data is transformed back to the space domain and the desired interpretation can be made. Accordingly, a number of filtering techniques were applied and only selected results are presented here.

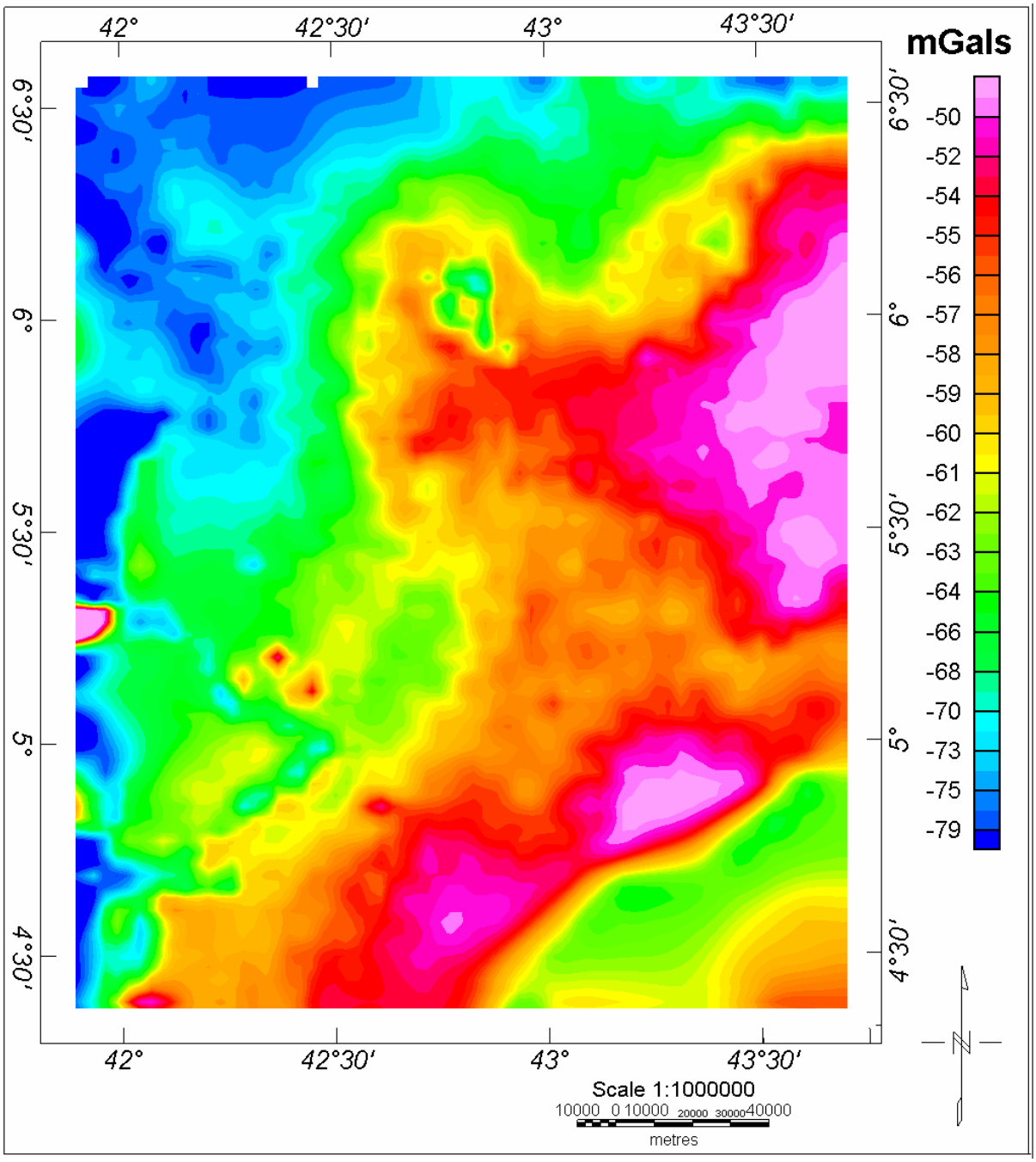

Figure 4.17: Bouguer gravity anomaly of a selected area within the Ogaden basin for detailed analyses.

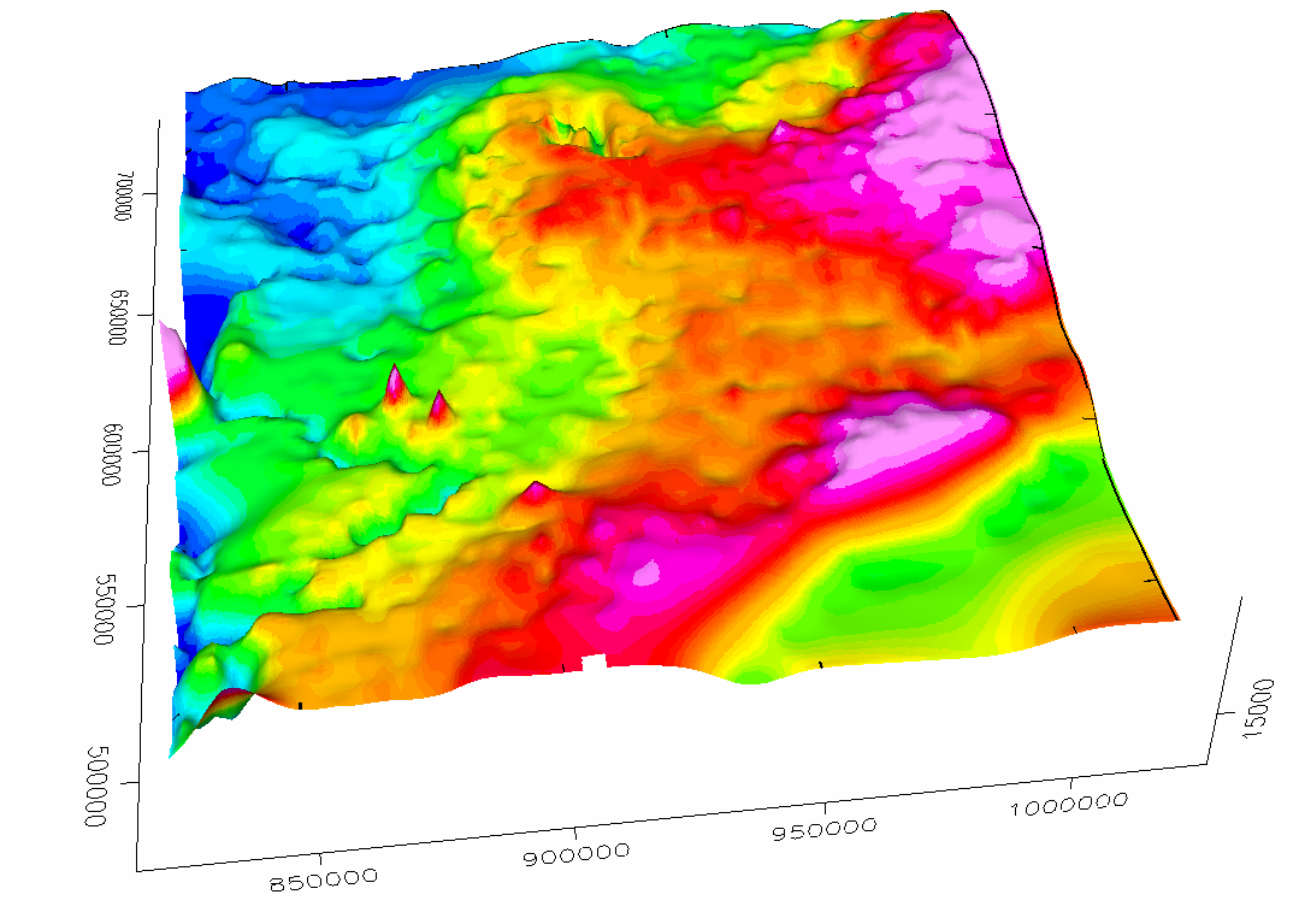

Figure 4.18: 3D view of the Bouguer gravity anomaly map of the central Ogaden region

4.5.5 Directional Filtering

Directional filtering is a technique used to select gravity and magnetic anomalies based on their trend. The goal of directional filter in gravity data processing is to remove or accept the effects of linear trends with a particular azimuth. These linear features may be related to older fabrics and usually obscure anomalies of younger feature. After preparing the grid for the FFT, and performing the FFT, the azimuth of the center of the strike of the feature is identified and used for passing or rejecting of the directional features. The directional cosine filter equations are given as follows:

$$L(\theta) = \left|\cos^{n}(\alpha - \theta + \frac{\alpha}{2})\right| \text{ to reject direction } \alpha \qquad (4.\ 3)$$

$$L(\theta) = 1 - \left|\cos^n(\alpha - \theta + \frac{\alpha}{2})\right| \text{ to pass direction } \alpha \qquad (4.\ 4)$$

where α is direction of the filter in degrees azimuth from North and is the azimuth of the cosine function.

Accordingly, the filter with an azimuth of 270^o and a cosine squared function was applied to pass first northeast trends (Fig. 19) and then northwest trends (Fig. 20) for the central Ogaden region. In Figure 4.19, we can see the linearity of features in the NE-SW direction. There remains a relative high anomaly extending towards the NW. This may be because of an older regional tectonic feature that may be developed in the form of rift that created accommodation space for the deposition recent formations such as the clastic and marine sediments dominating the region. In Figure 20, northwest trends were allowed to pass and the anomaly patterns indicate an older structural fabric that may be related to the development of tri-radial rift system in the central Ogaden basin. Thus, we assert the existence of a rift system in the northwest direction as part of the tri-radial Karroo rift system.

4.5.6 Horizontal Gradient

By calculating horizontal gradients in the gravity anomaly values, abrupt geologic changes that exhibit a relative density contrast can be imaged. Such features can be faults, facies changes or depositional environment changes. Simple difference equations are usually employed to calculate the gradients along rows and columns of the grid. A linear maximum in the gradient is interpreted as a discontinuity such as a fault. The method is robust in delineating both shallow and deep sources in comparison with the vertical gradient method, which usually is suitable for identifying only shallow features. The amplitude of the horizontal gradient is given as follows

$$dg_h = \sqrt{(\frac{dg}{dx})^2 + (\frac{dg}{dy})^2} \qquad (4.\ 5)$$

where $\frac{dg}{dx}$ is the horizontal derivative of the gravity field in the x direction and $\frac{dg}{dy}$ is the horizontal derivative of the gravity field in the y direction.

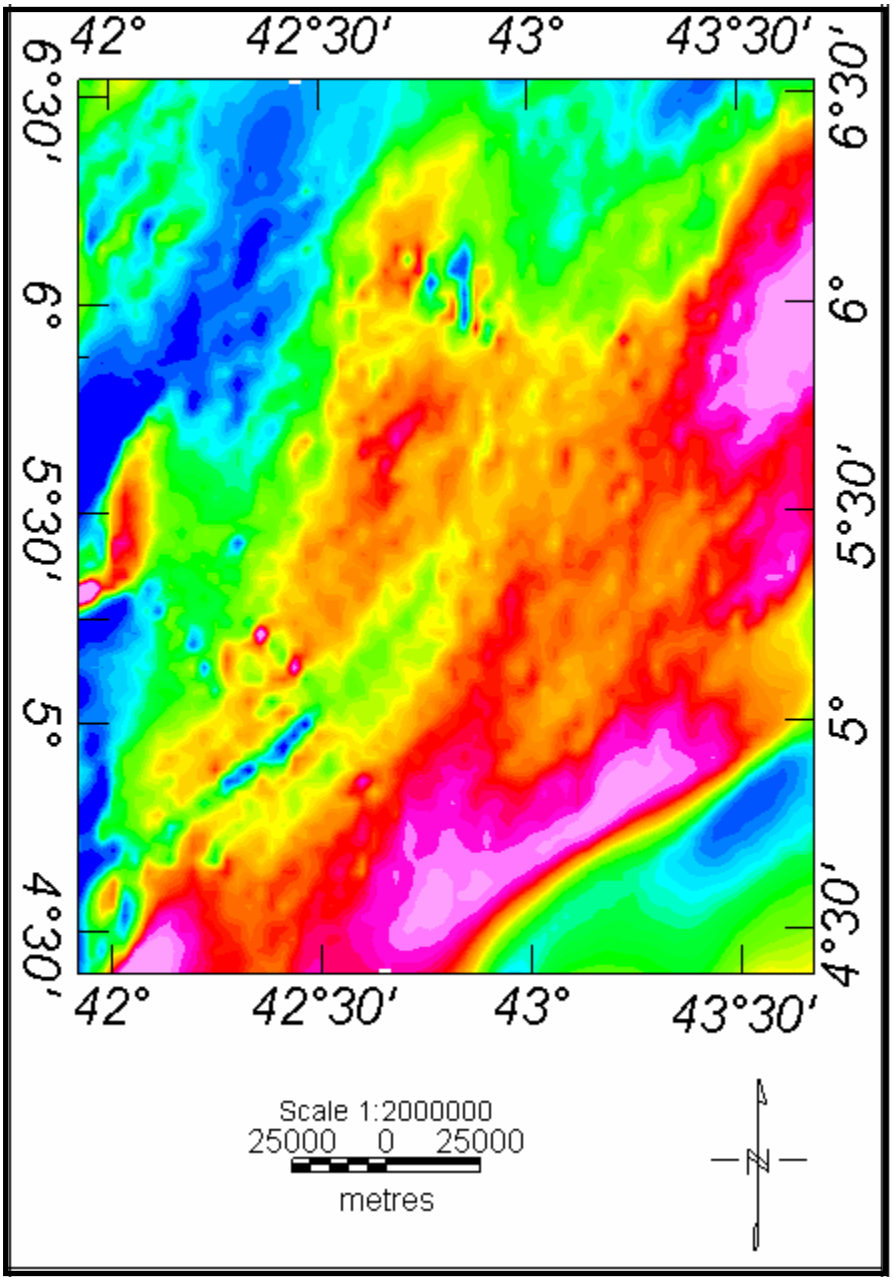

Figure 4.19: Result of direction filter to detect the existence of older fabrics in the region. The figure shows rejection of the features trending at 120o azimuth, allowing the passing of the anomaly that strike to the northeast**.**

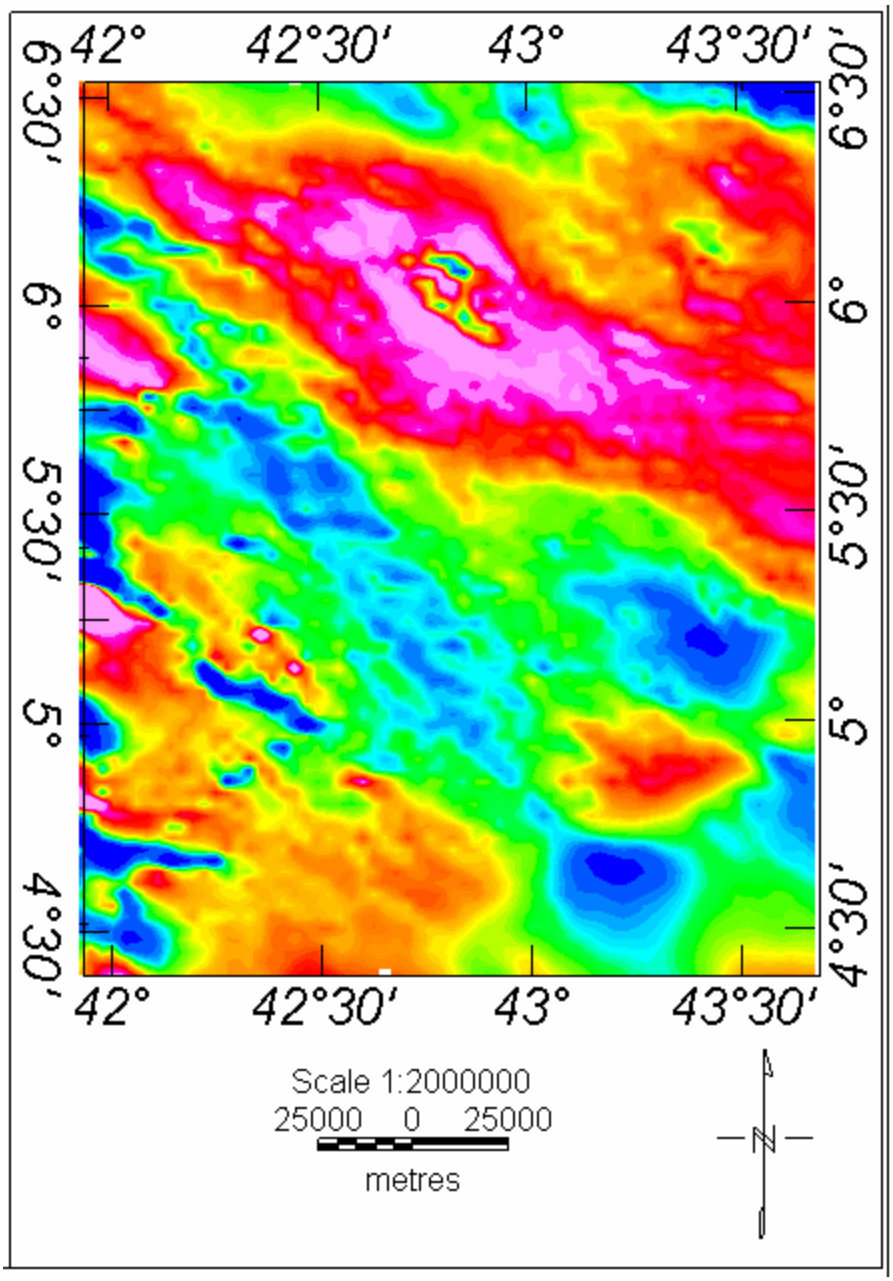

Figure 4.20: Direction filter applied on the Bouguer gravity anomaly allowing anomalies caused by older structural features trending 120o to be passed.

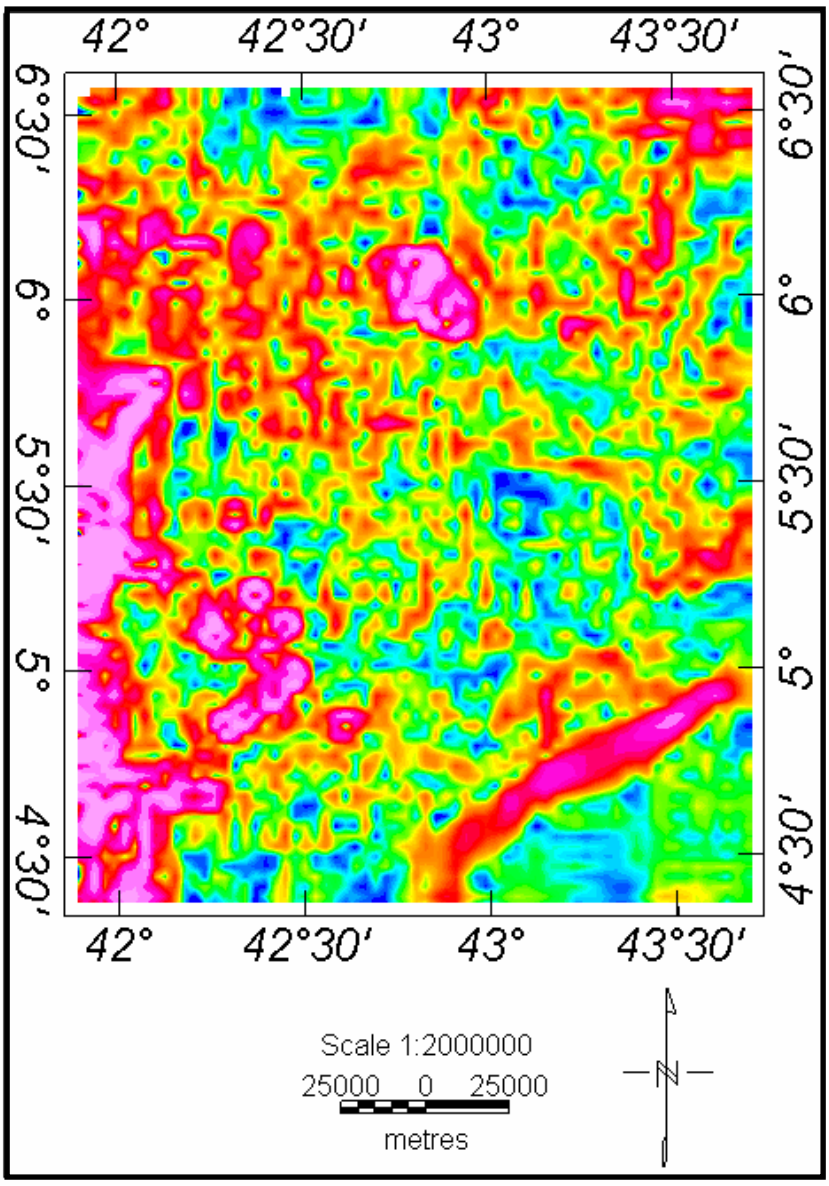

Figure 4.21: Total horizontal derivative solution for the central Ogaden region showing the deepest part of the basin causing relatively low gradients due to the thick sedimentary sequence.

According to Eq. 4.5, the square root of the sum of the two derivatives gives the gravity gradient, which is presented in Fig. 4.21. For comparison purpose the various components of the different directional derivatives are given in Appendix I. In Figure 4.21 we can observe a relative low gradient trending in a northeast direction from Mandera Lugh at about 42º 30' E into the Ogaden basin. Although the amplitudes appear subdued, the relative gravity low widens in a northwest direction. The subdued nature of the anomaly may be due to two factors: 1) gravity data is limited for such process (e.g. Grauch and Cordell, 1987) and 2) the edges of structural features may not be vertical and could be deep. In general, the indicated region depicted as a relative low is associated with the deepest part of the basin. Seismic and drilling information from the Ogaden basin also indicate this region is the deepest part of the basin, where thick sediments exist, such as the Bodle deep (e.g. Hunegnaw et al. 1998).

4.5.7 Gravity Models

Gravity profiles were extracted from the residual gravity anomaly grid of the Ogaden basin. Two profiles are constructed in the general dip direction (NW-SE) of the basin. One long profile lies along the strike direction (SW-NE) of the Ogaden basin (Fig. 4.22). The modeling was carried out using Gravity and Magnetics Modeling System (GMSYS) 2 1/2D industry software. Geologic cross sections and geological maps and seismic sections of the region were assessed to construct the subsurface model parameters. Four gross subsurface sedimentary units were used throughout the basin. These are: the basement, Karroo sediments, the Hamanlei Formation carbonates and more recent sediments. The density values assigned to these formations are 2200 kg m^{-3} for alluvium, 2450 kg m^{-3} recent sediments, 2610 kg m^{-3} for Hamanlei Formation carbonates, 2660 kg m^{-3} for Karroo sediments and 2670 kg m^{-3} for the basement. Interactive adjustments of model parameters and interfaces were made using until a

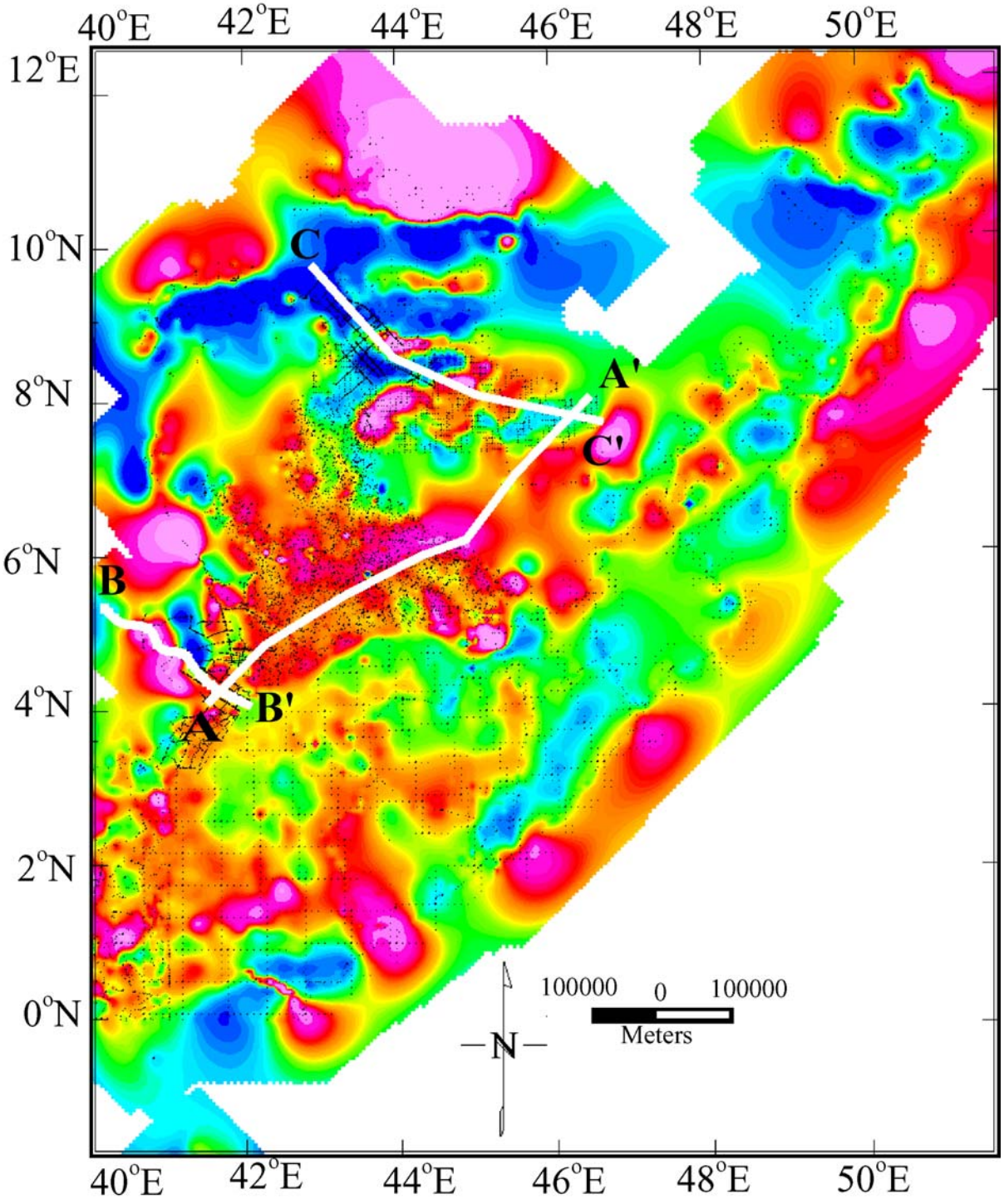

Figure 4.22: Index map of gravity profiles extracted for modeling from the residual gravity anomaly map of the Ogaden basin.

satisfactory fit between observed and calculated values were obtained. A maximum depth of 15 km was chosen for the modeling.

Profile A-A'

This profile trends from the SW to the NE of the basin and is 710 km long. The gravity model that best fits the residual gravity anomaly along this profile shows about 8.5 km of sedimentary strata in the SW part of the Ogaden basin [Bodle deep (Bo)]with relatively less thick sediment around Ghumburo (Gh) and Galadi and thicker on the NE end in the NE Ogaden region (Fig. 4.23). On the northeastern side of the profile, lithologic units dipping to the NE are used to fit the gravity model. This is in agreement with the evolution of the basin in this area, which is believed to be developed at a later stage with restricted transgression and regression of the sea to the NE Ogaden and NE Somalia. NE Ogaden section of the basin could be separated from the SW section by the Marda fault zone.

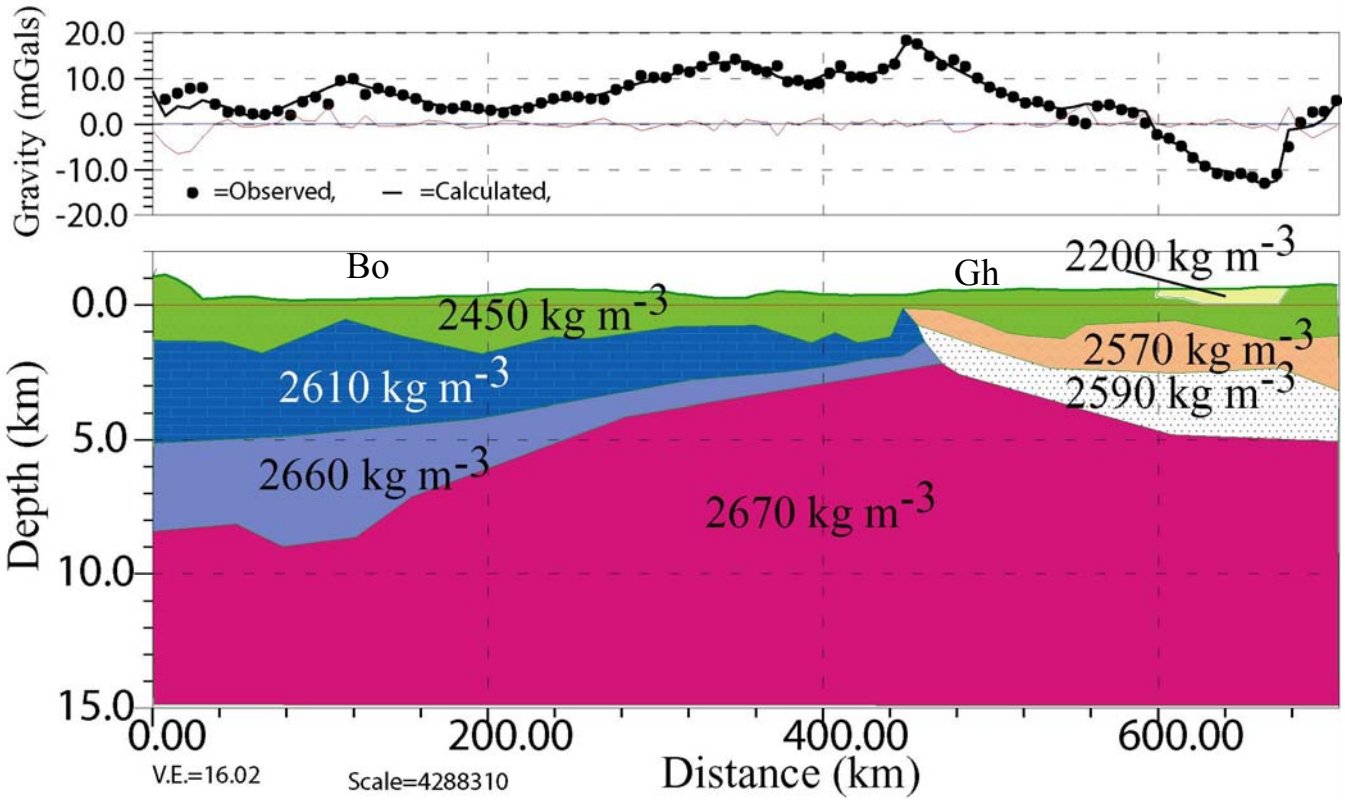

Figure 4.23: Gravity profile along the strike direction of the Ogaden basin with SW–NE orientation (AA'). Bo indicates Bodle deep area and Gh is Ghumburo and Galadi areas.

.

Profile B-B'

The NW SE oriented profile B-B' (Fig. 4.23) is from the southwestern section of the Ogaden basin and crosses the strike profile at the SE section in the main sedimentary depocenter. It is designed to be aligned with one of the regional seismic lines and is about 232 km long. Similar to the seismic section, there is a thick sedimentary wedge in the southeastern section of the profile with a thickness of about 8.5 km. The sedimentary package shallows upward to the northwest. There is a low gravity anomaly at the center of this profile which could be associated with low density alluvial fill/material. The seismic section does not show this anomaly because it may have been recorded oblique to the structure.

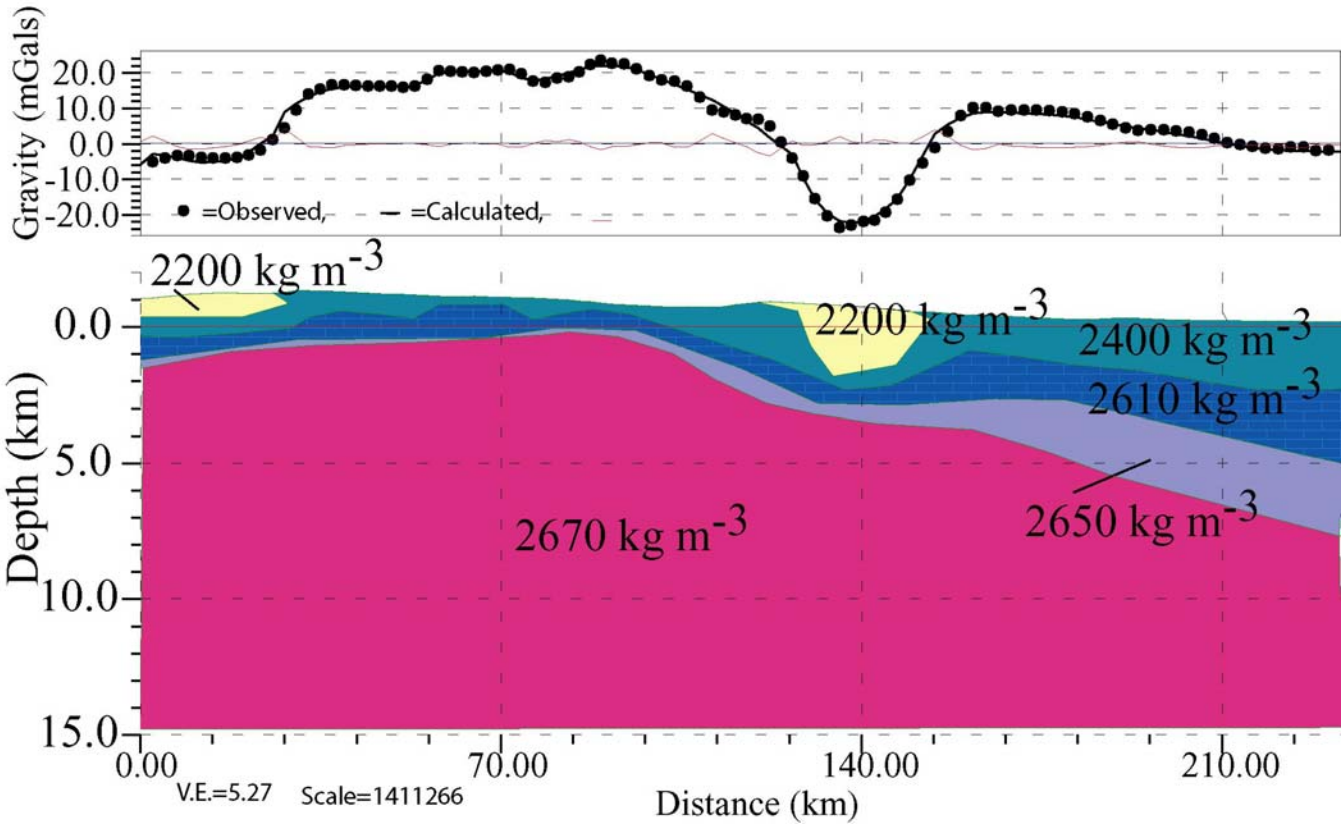

Figure 4. 24: Gravity profile along BB' (Line 01 seismic profile) from the Ogaden basin.

Profile C-C'

Profile CC' (Fig. 4.25) shows series of horst and graben-like structures in a NW SE direction along the northeastern Ogaden basin. Possible volcanic sills or plugs may exist at shallower depth in places as indicated by high density intrusives in the model (Fig. 4.25). However in between these structures there are grabens filled with sediments. The maximum thicknesses of sediments are mainly associated with grabens and attain a maximum thickness of 5 km.

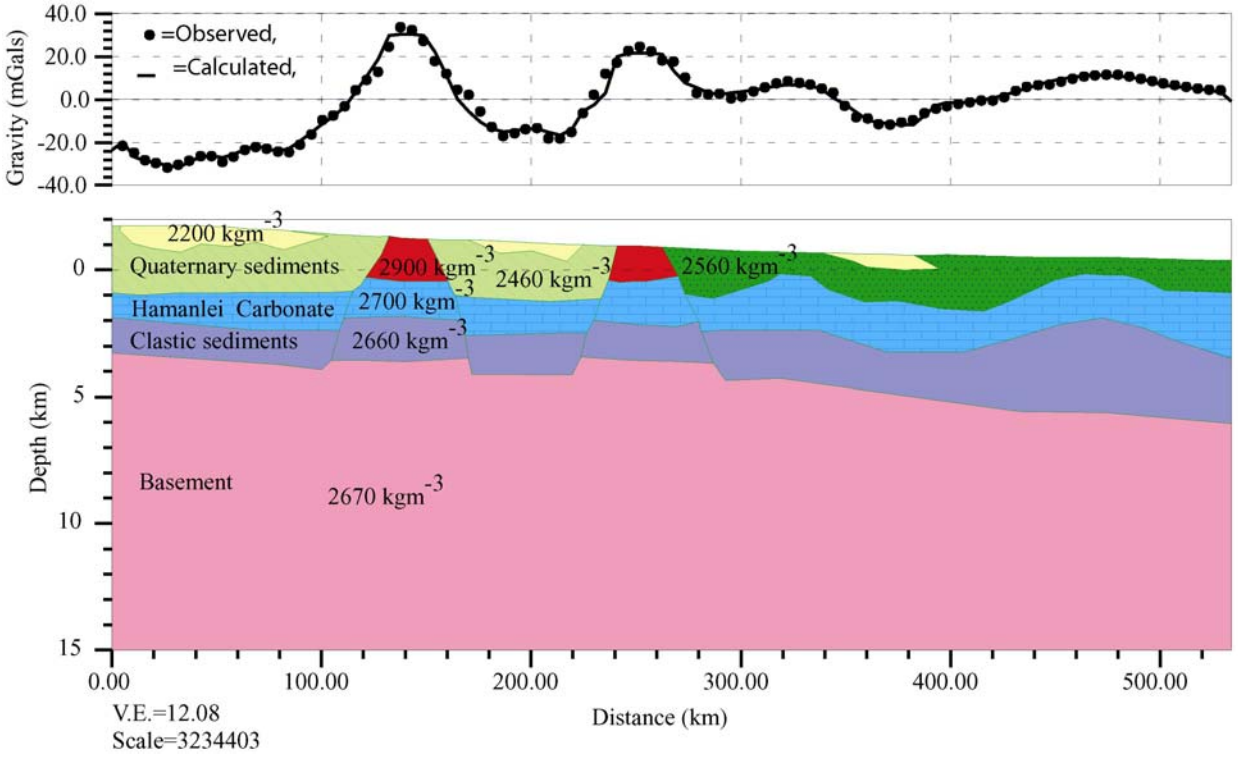

Figure 4.25: Gravity profile along C-C' the NE Ogaden in NW SE orientation

4.5.8 The northeastern Ogaden basin

Special analysis was carried out for the northeast Ogaden basin area where good data density is available with regular data point intervals (Fig. 4.13). A number of filtering techniques were applied as discussed in the previous sections. The Bouguer gravity anomaly shows some localized relative negative and positive anomalies and as shown on the model for profile C-C', these anomalies could be as a result of grabens filled with sediments and horsts. However, this phenomenon is not visible on the surface (Fig. 4.12). We focused on Euler deconvolution analysis of this area in order to determine the depth of the structural units in the region and detect some structural contacts.

One useful advancement in potential field data processing and interpretation is the application of Euler deconvolution. Applying Euler's homogeneity equation and assuming a simple magnetic source type, the lateral and vertical gradients of the measured magnetic or gravity field can be unambiguously related to the horizontal and vertical positions of the source (Thompson, 1982; Reid et al., 1990). Euler deconvolution is specifically good at delineating contacts and rapid depth estimation. The choice of proper structural index determines the quality of the depth estimation. The structural index is a function of the geometry of the causative bodies. The implementation of Euler deconvolution involves passing a moving window through the gravity anomaly grid. The window should be large enough to cover the desired anomaly. Equations relating the gravity field and gradient values to a hypothetical source location and type are constructed for each grid point in the window. Finally this forms a system of equations. After applying a least-squares inversion, estimate of source locations as well as uncertainties were determined. In the moving window operation the window is moved until the total grid area is covered with the analysis. Solutions were plotted and their consistency was examined. Good clusters of solutions indicate that a source location is well determined, but poor clustering of

solutions indicate poor resolution (Reid et al., 1990). For good results the choice of structural index is significant, because it yields the best cluster of solutions for horizontal location and depth used to characterize the source geometry. Table 4.1 shows structural index related to different geologic models.

Table 4.1: Different structural index values for different geometric bodies used in gravity processing

Source	Gravity Structural Index
Sphere	2
Horizontal cylinder	1
Fault	0

The original Euler deconvolution is of the following form and it takes the same form for gravity.

$$(x-x_o)\frac{\partial T}{\partial x}+(y-y_o)\frac{\partial T}{\partial y}+(z-z_o)\frac{\partial T}{\partial z}=-nT+\alpha, \qquad (4.6)$$

$$(x-x_o)\frac{\partial H_x}{\partial x}+(y-y_o)\frac{\partial H_x}{\partial y}+(z-z_o)\frac{\partial H_x}{\partial z}=-nH_x+\alpha, \qquad (4.7)$$

$$(x-x_o)\frac{\partial H_y}{\partial x}+(y-y_o)\frac{\partial H_y}{\partial y}+(z-z_o)\frac{\partial H_y}{\partial z}=-nH_y+\alpha, \qquad (4.8)$$

Where (x_o, y_o, z_o) represent the unknown source location, (x, y, z) the measurement location, T the measured field, H_x and H_y the calculated Hilbert transform components, n the

structural index, and α is related to the regional effect, which can be solved and removed during computation.

The resulting solutions are shown in Figs. 4.26, 4.27 and 4.28. The depth solutions as structural contacts were obtained for specific locations in the area and are given as grid maps instead of clusters. These can show the areal and depth extent of structural features in the region. There is gradational variation in depth solution as high and low elevations. This suggests there may be structures in the form of grabens and horsts trending in a NE-SW trend. The minimum depth obtained is about 3 km. Depending on the window size the depth solution also varies.

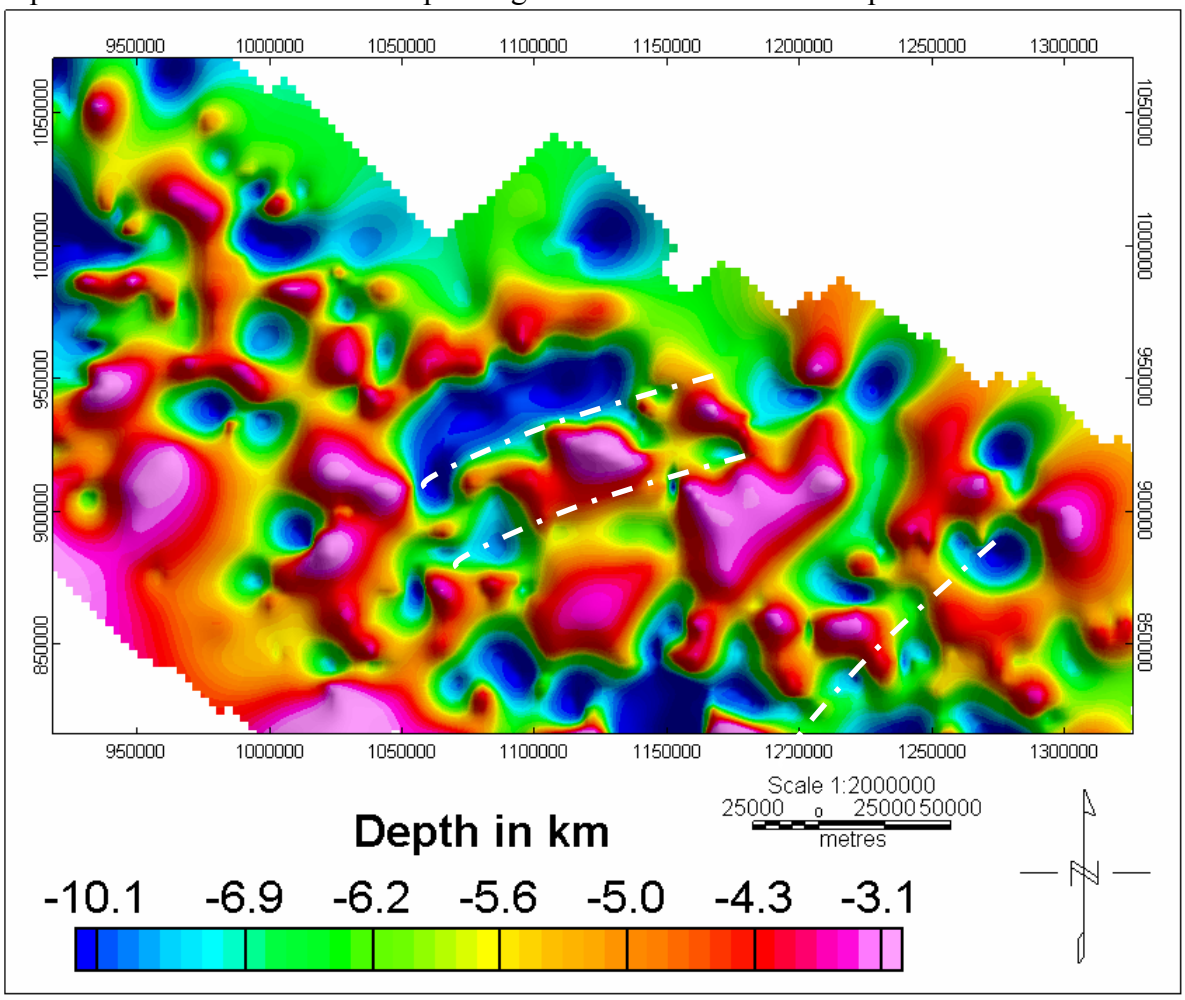

Figure 4.26: Euler deconvolution result with structural index 0 window size 3 km and depth 15km.

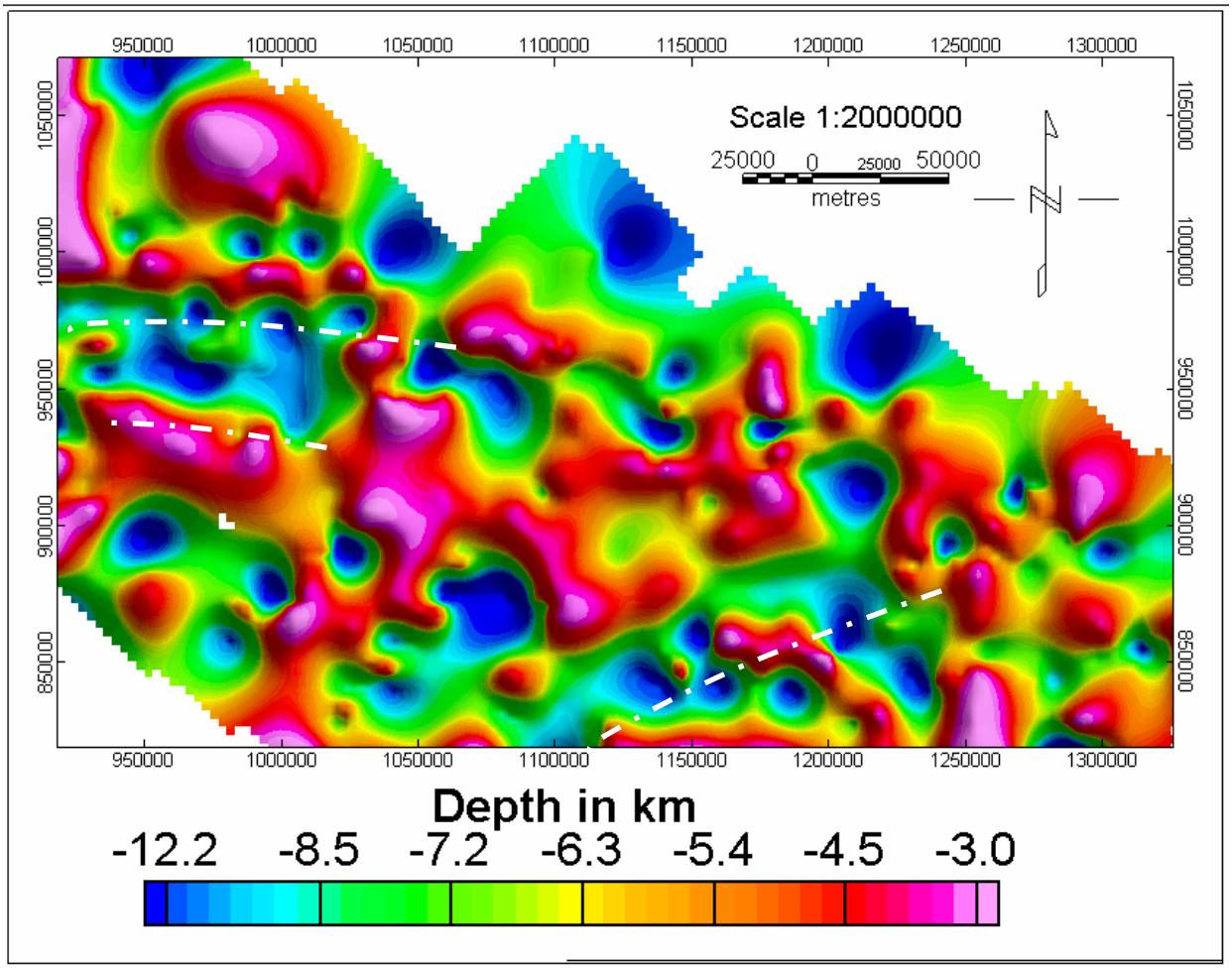

Figure 4.27: Euler deconvolution solution SI=0, W=5 and D=25 km

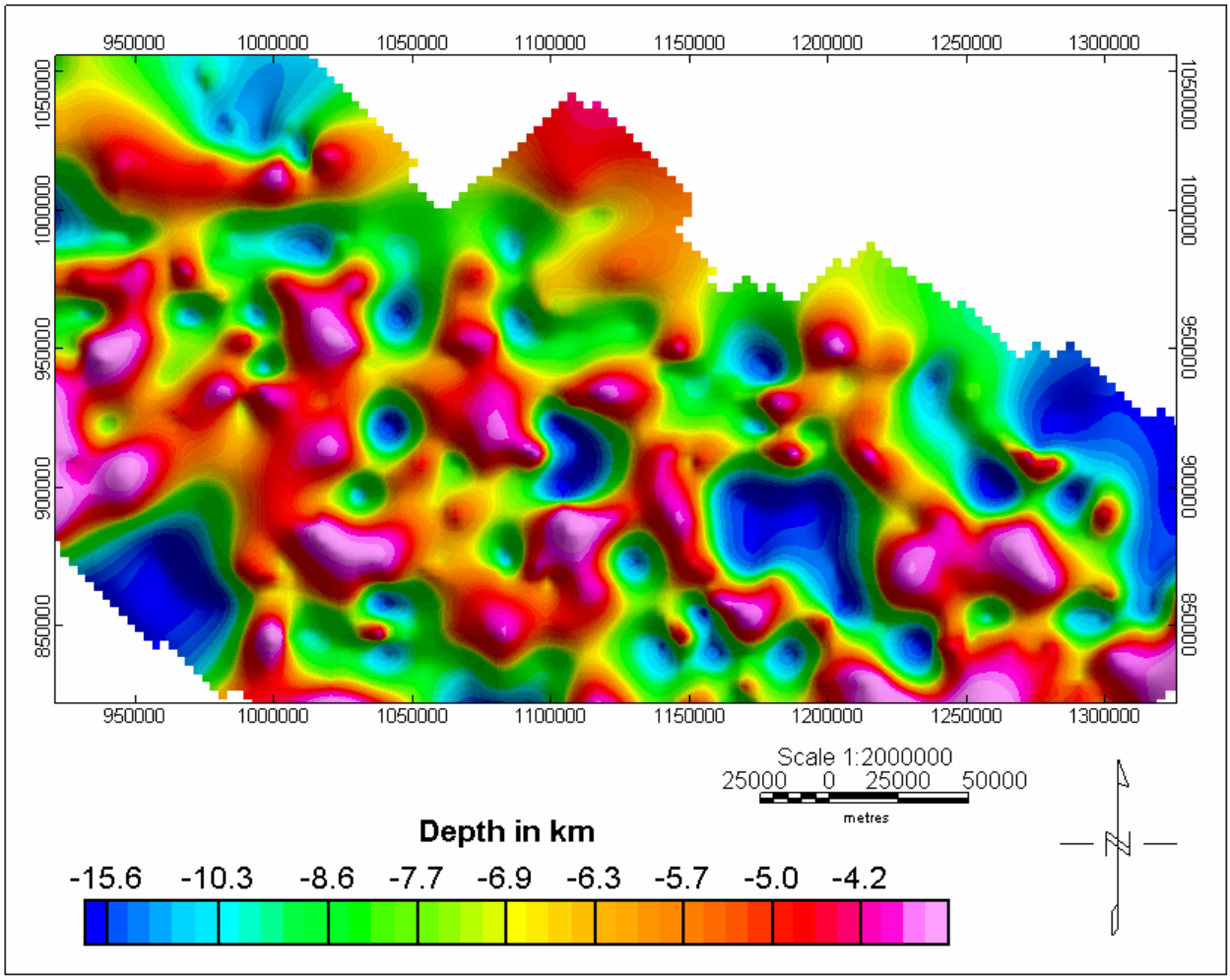

Figure 4. 28: Euler deconvolution solution SI=0, W=7 and D=35 km

Linearly clustered solutions coincide along the boundaries of the gravity anomalies. This may suggest faulted structures forming grabens and horsts in the area.

4.6 Magnetic anomalies of the Ogaden basin region

The magnetic method is another potential field technique commonly used for delineating sedimentary basins. In the Ogaden basin and the adjacent areas, aeromagnetic surveys were carried out by different companies (Figs. 4.29). Similar to the Bouguer gravity anomaly (Fig. 4.17) there is a relatively high magnetic anomaly of the central Ogaden region (A). This could be associated with one arm of the tri-radial rift system developed during the Permian time. Other features with relatively low susceptibility trending in a NWSE direction (B and C) and can be associated with local features such as narrow graben. The SE part of the NE Ogaden region shows NE-SW trending anomalies similar to the gravity anomalies discussed in section 4.5.4. These may be associated with grabens and horst structures anticipated in the region. For regional assessment purposes data were obtained from GTECH for the Somalian region (Fig. 4.30). The magnetic anomaly map shows structural features trending in the direction of some anomalies in Ethiopia and appears to merge (C). This indicates that most of the structures are regional extending further to the southeast and also to the northeast into Somalia. However, the big gap in between the different aeromagnetic surveys in the Ogaden basin did not allow me to make a basin wide interpretation. The existing surveys and the results obtained indicate a potential interpretation can be made if additional aeromagnetic data are available and effective depth to basement detection can be made.

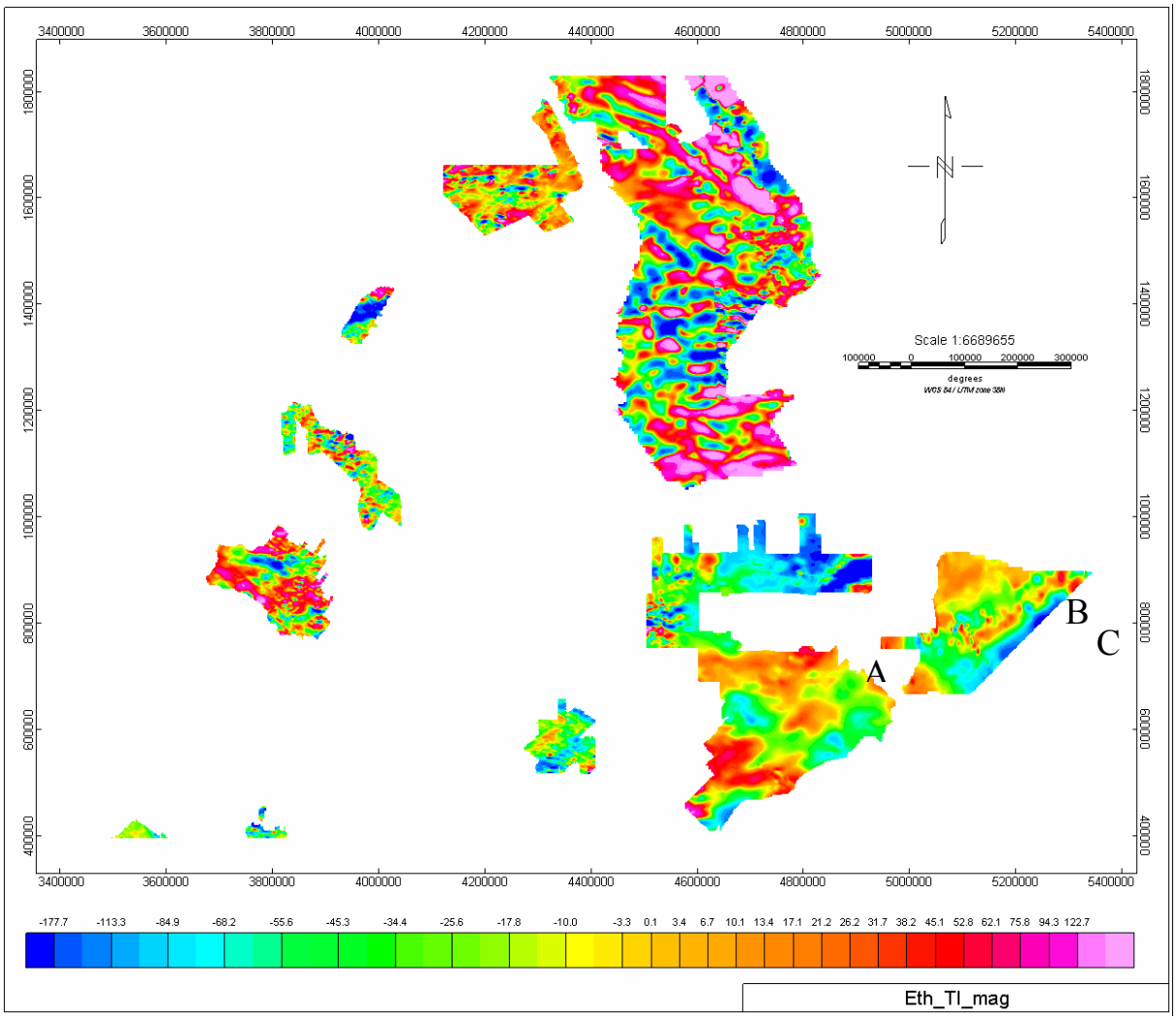

Figure 4.29: Magnetic anomaly map of the Ogaden region and other regions in Ethiopia. The Ogaden region shows structural anomalies trending in both NW-SE and NE-SW directions.

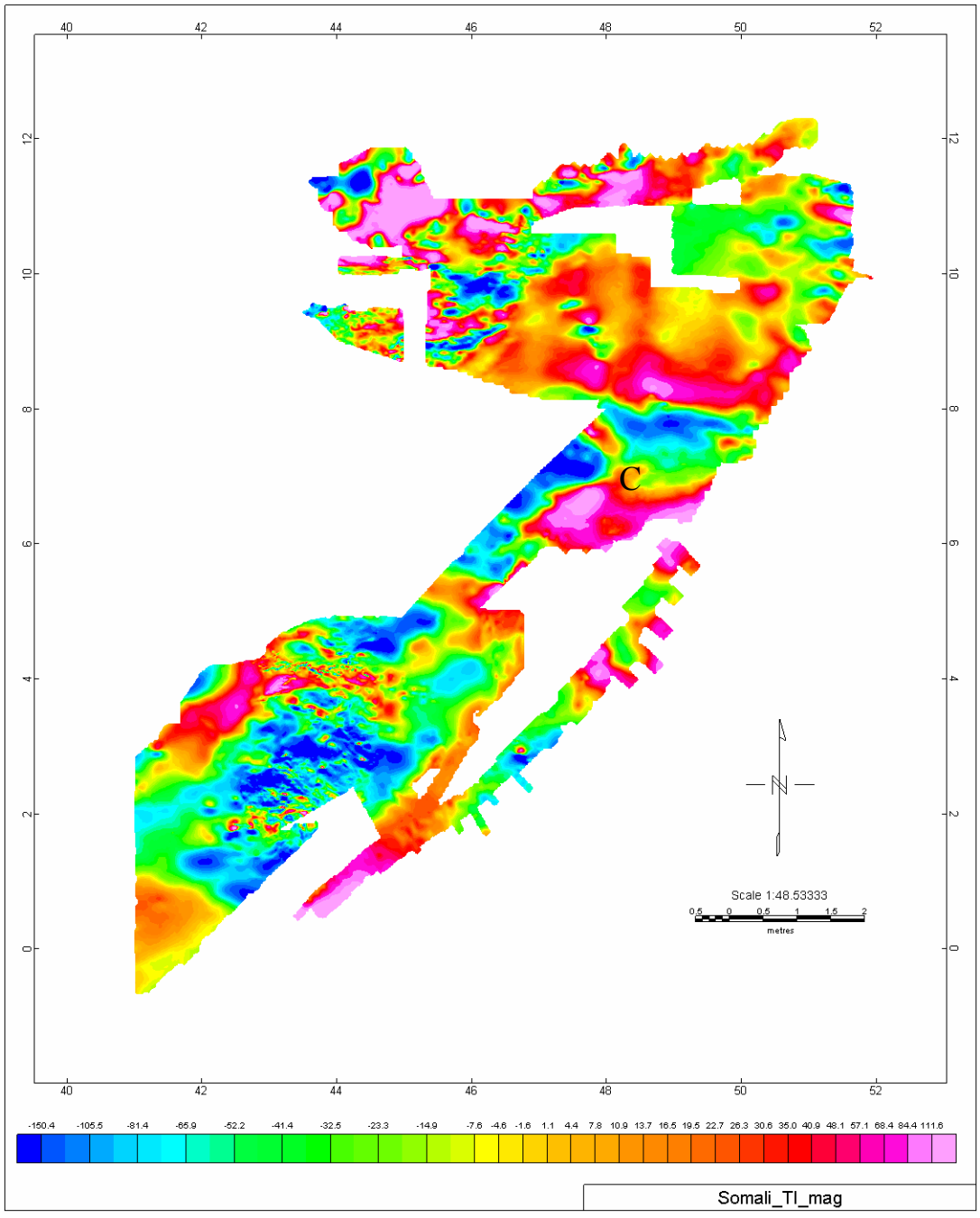

Figure 4.30: Magnetic anomaly map of the Somalian region showing structural features trending and merging into the structural anomalies in the Ogaden basin of Ethiopia.

4.7 Seismic reflection data processing and analysis

In order to conduct a detailed basin evolution analysis it is necessary to interpret the changing geometries of reflection packages from seismic data. In this study high resolution seismic reflection data allowed delineation of different horizons associated with different depositional characteristics from the Ogaden basin of southeastern Ethiopia. Some 17 relatively high resolution 2D seismic reflection profile data were obtained for interpretation and reprocessing from Hunt Oil Company by the permission of the Ministry of Mines and Energy (MME) of Ethiopia. Most of the long lines were acquired in the dip direction (10 out of the 17 lines). The remaining 7 lines were acquired along the strike direction (Fig. 4.31). The total length of the seismic lines was more than 1000 km. The dip lines are oriented in the northwest-southeast and east-west directions, where towards the southeast it is the main depot center of the Ogaden basin (Fig. 4.31). The data obtained and analyzed in this study are from the southwestern part of the Ogaden basin (Figs. 4.7 and 4.12) and cover a small portion of this large basin.

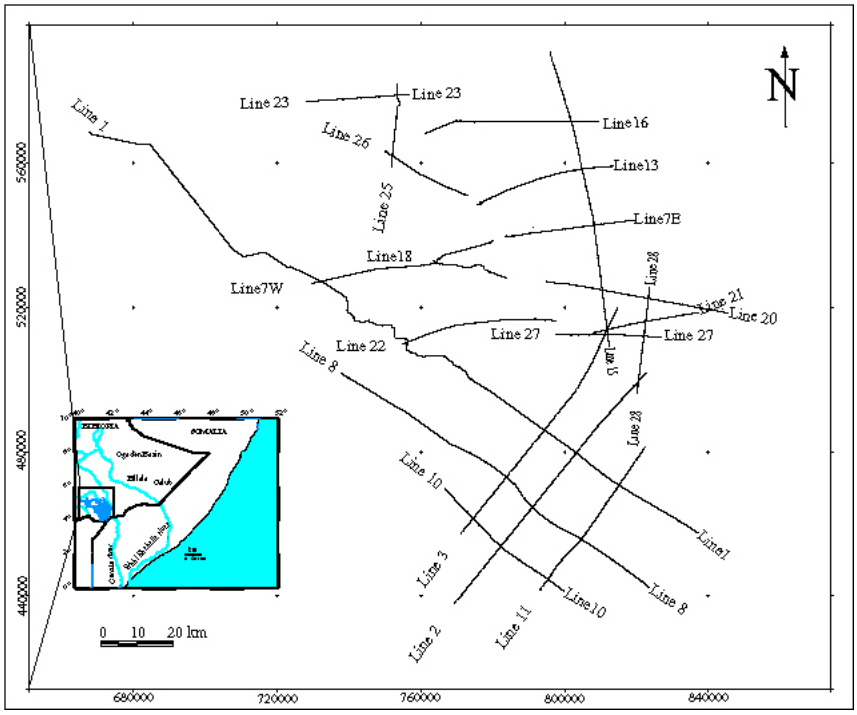

Figure 4.31: Location map of the seismic lines used in this study. Inset indicates the location of the seismic lines in blue dots.

Due to obstacles and ground conditions some of the lines are crooked. The elevations of the profiles in general are not too complicated, thus data processing could be assumed to be fairly straightforward. The common midpoints fold for stacking the data is about 80 in most cases. Assessment of spectral analysis reveals the useable frequency band to be about 12 to 67 Hz (Fig. 4.32).

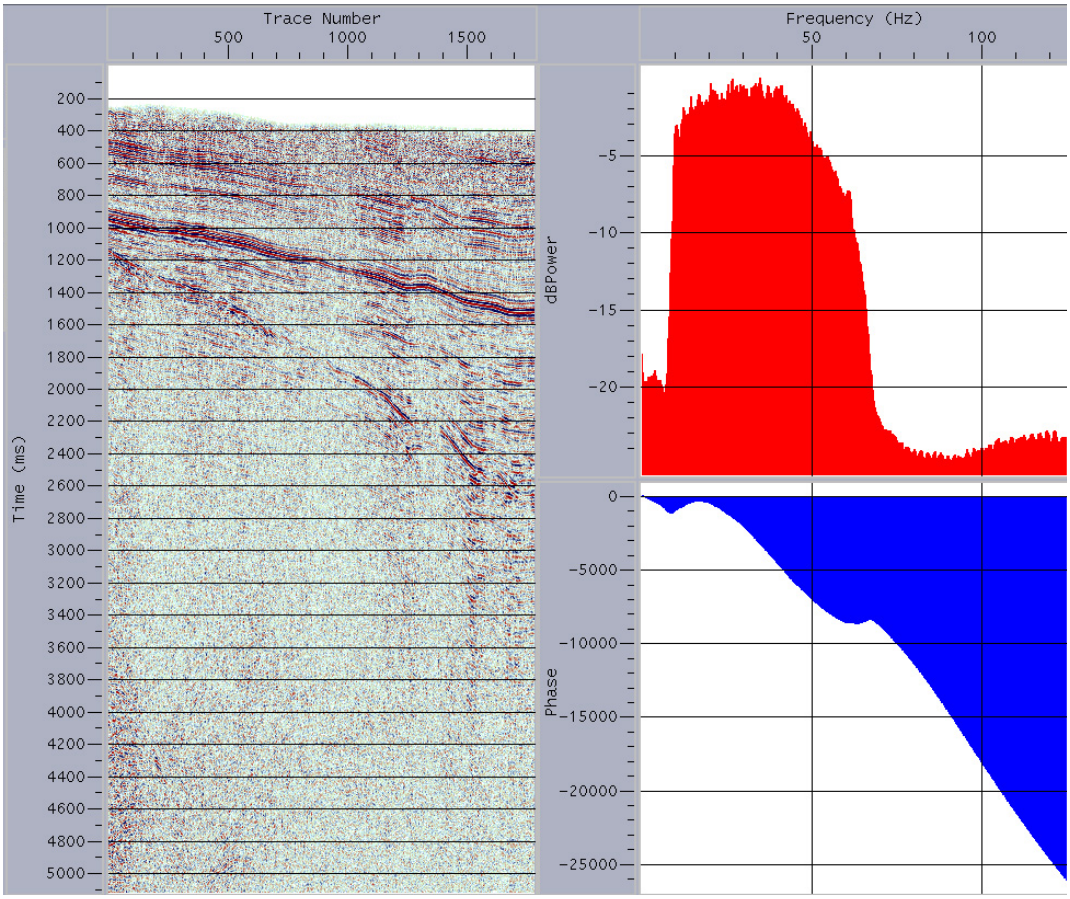

Figure 4.32: Spectral analysis of post stack data from the Ogaden region to determine the frequency content of the data. The left panel shows the seismic data, the red is the frequency spectrum and the blue is the phase spectrum.

Asymmetric split spread geometries were employed in the data acquisition which may have provided the added benefits of enhanced continuity and increased velocity and dip control in comparison to strictly end-on or symmetric split-spread configurations. The basic architecture

processing sequences followed to produce the final stacked sections were similar to conventional petroleum industry flows (Yilmaz, 1987; 2001).

4.7.1 Data Quality

The data quality along each line was been examined and much of the data were of high quality. Reflection events the northwest on the dip lines get poorer as the major reflection horizons become shallower. The data were recorded in 1993 in the Genale River area of the Ogaden basin (Fig. 4.31). The coverage is very regional and line spacing is in general large, usually ranging from 15 to 20 km. All the lines were acquired by the same company (by Western Geophysical for Hunt Oil Company) and with the same recording parameters were used. This helped to some extent to facilitate interpretation and data loading on the computer system. As the interpretation proceeded lines that did not tie were made to tie with minor time shifts.

The lines were surveyed with GPS instruments. Vibroseis was the energy source used with a sweep frequency of 8-12 Hz, a 8s upsweep, and a vibration point interval of 50 meters. The data were recorded on 160 channels at 50 m group intervals. The sample rate of the data was 2 ms with 5120 ms. record length. The nominal fold of the data is 80. The long offset is 6025 m and the short offset 2025 m with a near offset of 75 m. The data were acquired in an asymmetric split spread array. The data were correlated in the field by Western Geophysical Crew 720 during acquisition.

Color display is an essential element to help seismic interpretation and to see geological details along horizons and over all in a seismic section. In Landmark software (Seisworks) there are a number of color options for seismic data display and interpretation purposes. The most commonly used color scheme for seismic data interpretation is blue-white-red. In this interpretation the seismic sections are displayed in blue-white-red and some times in wiggle trace

mode. Throughout the interpretation blue employed for positive amplitudes and red for negative amplitudes.

Faults are interpreted based on reflection offsets and diffraction patterns diagnostic of bed terminations. In general individual faults have very small displacements (10-15~milliseconds) but across large displacement zones displacements exceed 20-25 milliseconds.

It is well known that prior to any seismic interpretation all the available information especially well log data must be tied together to the seismic data. Unfortunately, there is no well data released for this study area. Since the main target of the current interpretation is not extracting stratigraphic reservoir or fluid information, it is possible to make and correlate an interpretation. Since most of the seismic lines are interlocked. It is possible to trace misties and uncorrelated horizons and apply corrections to them. The interpretation was carried out line by line and some of the lines and is discussed below.

4.7.2 Reprocessing of Seismic Reflection Data

The geology of the Ogaden basin is known to consist of Precambrian rocks overlain by sedimentary strata ranging from Permian to Cenozoic in age. These sedimentary rocks cover a large area. As a result seismic reflection data coverage is sparse and wells are present in only a few places. However, it is necessary to come up with integrated interpretation for further exploitation of the resources in the basin. With the aims of exploring the possibility of improved seismic data processing and learning the state-of-the art seismic data processing, Profile 07E was chosen for reprocessing and is a dip line with a northwest-southeast trend. About 20 km of seismic reflection data were processed using the ProMax2003 seismic data processing software. Both basic and advanced techniques were applied to the data using the processing flow shown in Fig. 4.33 in order to increase the signal/noise ratio and define reflection events in the subsurface.

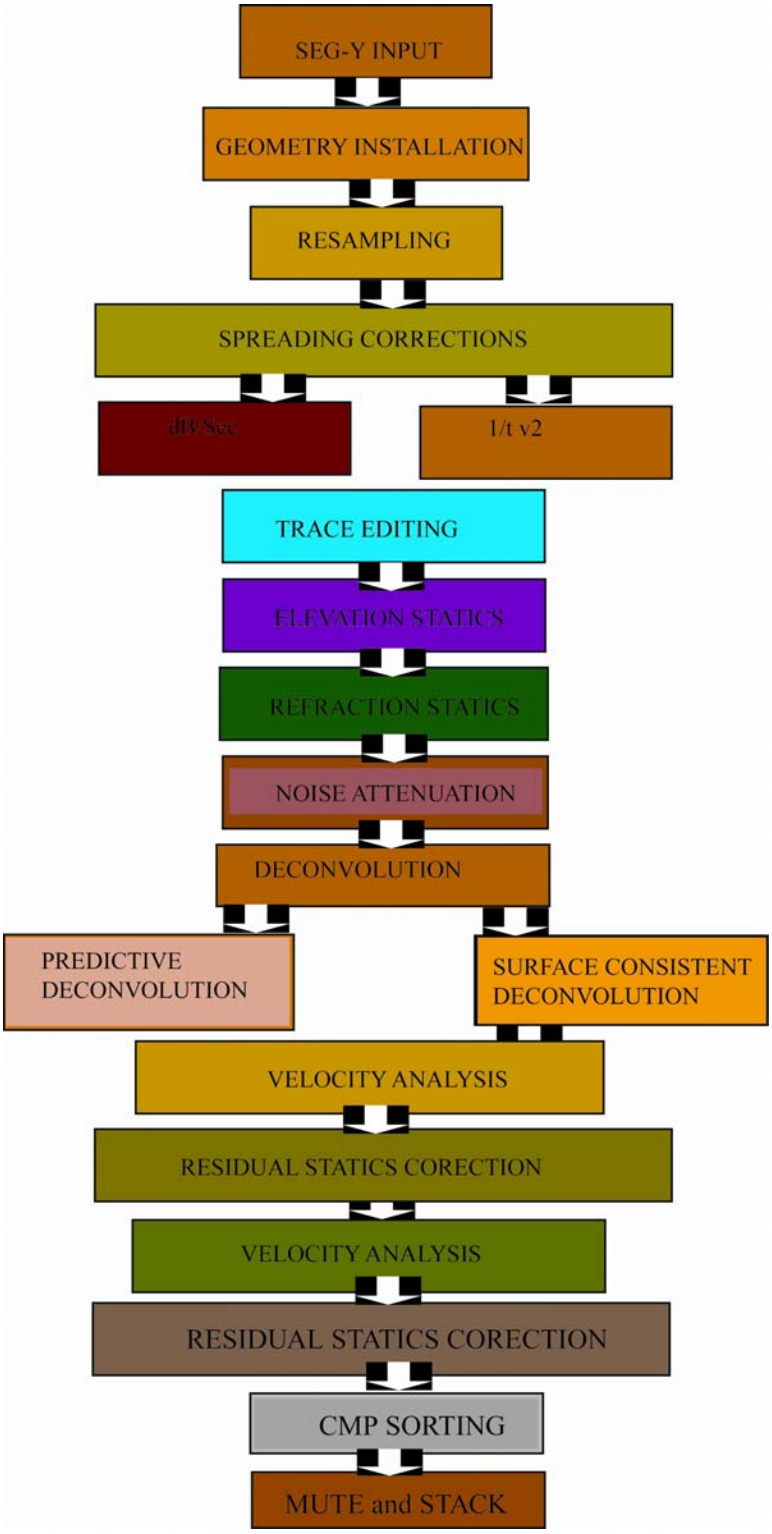

Figure 4.33: Processing flow designed for reprocessing the seismic reflection data.

Common midpoints (CMP) sorting was based on a straight-line geometry using the 2D land geometry installation module in ProMAX. A final datum of 400 meters and replacement velocity of 3500 m/sec was used. A top mute was applied to avoid the NMO stretch part of the direct arrivals. After stacking, the signal amplitudes were restored using an automatic gain control (AGC) with a 500 ms operator length based on comparison of the results of using several operator lengths. The noise level in the shot gathers differ slightly from shot to shot, however, the ground roll was prominent. This noise was attenuated by applying a fan filter that rejected apparent velocities between $\pm 500 ms^{-1}$ and $\pm 2500 ms^{-1}$ and frequencies between 5 – 12 Hz. In order to attain temporal resolution and reduce noise, as well as remove multiples, deconvolution was applied to the shot gathers. Deconvolution test parameters were used and viewed by comparing the autocorrelation lag times varying from 24 to 80 ms, prediction length was varied from 120 to 240 ms. Among the various tests performed, and the prediction length of 240 and a lag of 60 ms gave a better result in surface consistent deconvolution. We chose optimal pre-whitening of 0.1%, which ensured numerical stability (Yilmaz, 1987; 2001).

For determining the correct stacking velocity for normal moveout correction (NMO) velocity analysis was done. Repeated velocity analysis was carried out after applying refraction and residual statics at smaller CDP intervals each time. The different outputs of the processing stages are shown in Appendix III. Fig. 4.34 shows the final stack for the section of the line to compare and investigate the improvement of the new processing. The industry processing result is shown in Fig. 4.35 for comparison purposes. Note that the reprocessed section appears to have less reflection horizons compared to the industry processing. This may suggest that the deconvolution parameters applied in the reprocessing could have effectively removed the reverberations. This suggests that seismic data processing can always be improved since software facilities and techniques are improving from time to time.

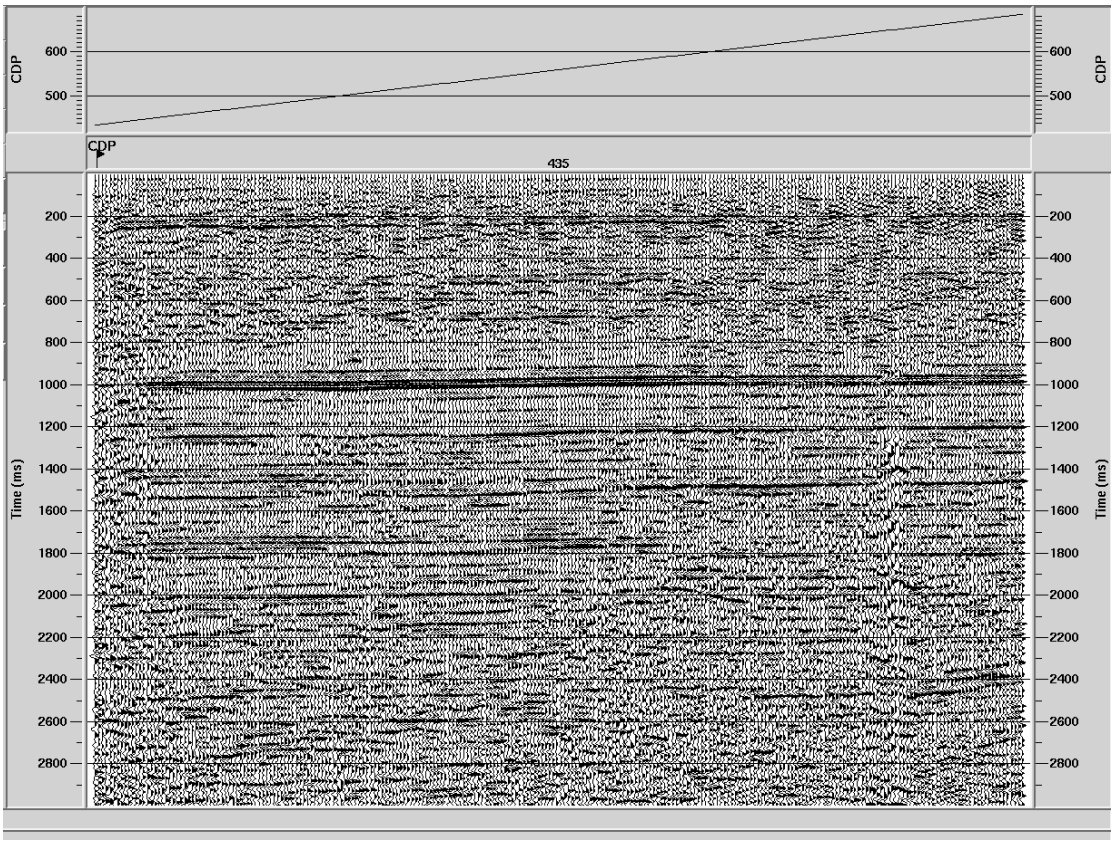

Figure 4.34: Final stack after reprocessing, showing enhanced signals from reflecting horizons. Thus the deconvolution parameters applied in this process have removed reverberations effectively.

4.7.3 Seismic Data Interpretation

In this study three megasequences are interpreted and related to the possible corresponding lithostratigraphic units in the region. Since the region is known for its extensional development, prerift, synrift, post rift depositional environments are believed to dominate the region. This interpretation is carried out based on coherent reflection continuity through out the seismic line, reflection characteristics and internal deposition pattern.

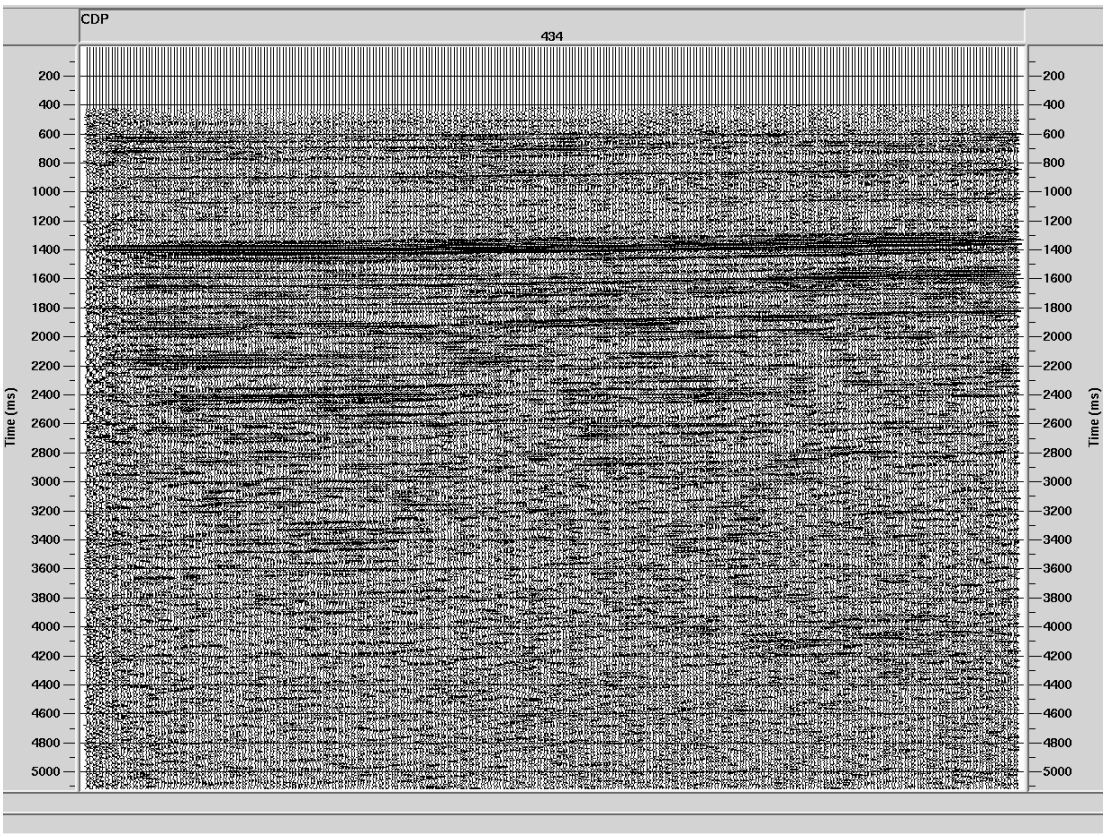

Figure 4.35: Part of the seismic section processed by industry originally showing continuity of the horizons and for comparison with Fig. 4. 34.

4.7.3.1 Line 10

Megasequences may be defined as units deposited during one distinct phase of basin evolution and can be characterized by changes in reflection strength and shape. Based on these criteria, megasequences were interpreted and notations are made starting from the deepest to the shallowest. Line 10 is one of the interesting profiles among the dip lines selected for interpretation. It has a total length of 44 km and oriented in a NW SE direction (Fig. 4. 31).

Line 10 is one of the interesting profiles among the dip lines and was selected for interpretation. It has a total length of 44 km and is oriented in a NW-SE direction (Fig. 4.31). The deepest horizon interpreted on this line starts at shot point 180 at about 2950 ms depth on the

southeast of the profile (Fig. 4.36). This horizon rises to the northwest with a gentle slope until it reaches shot point 400, where it forms a 2.5 km trough. Further to the northwest this horizon continues to rise with a relatively steep dip and ends at shot point 970. The second horizon interpreted, on this line starts at 1450 ms at shot point 180 and rises to the northwest with a gentle dip. It flattens towards the end of the line and reaches 800 ms beneath shot point 970. The third horizon of interest has a similar geometry to the second, and forms the upper boundary of megasequence 3 giving it nearly constant thickness.

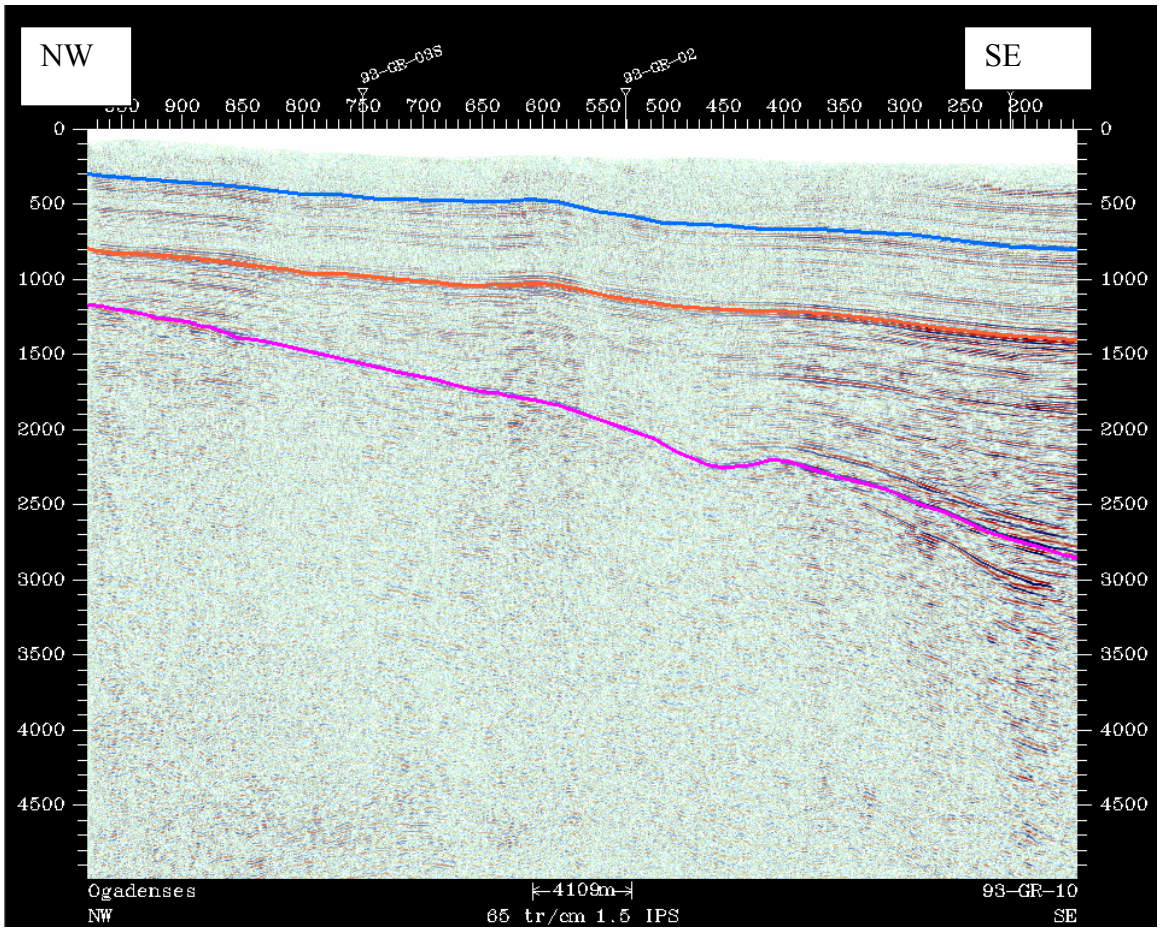

Figure 4.36: Megasequence interpretation along line 10 showing a thick sedimentary wedge to the southeast and a channel-like structure at the top of megasequence 1.

4.7.3.2 Line 08

Line 08 is parallel to line 10 and is about 15 km to the northeast of it (Fig. 4.37). The total length of line 08 is about 105 km. The sedimentary package strongly thickens towards the southeast (Fig. 4.37). The deepest interpretable reflection horizon (top of megasequence 1) starts at about 3800 ms from the southeast at shot point 170. It rises shallower to the northwest towards the Eastern Ethiopian plateau. The shallowest depth is at about 710 ms at shot point 2220. The top of the second megasequence (M2) is a strong reflection horizon clearly visible almost in almost all of the seismic sections in the basin. After shot point 1750, it almost merges with the deepest megasequence (M1).

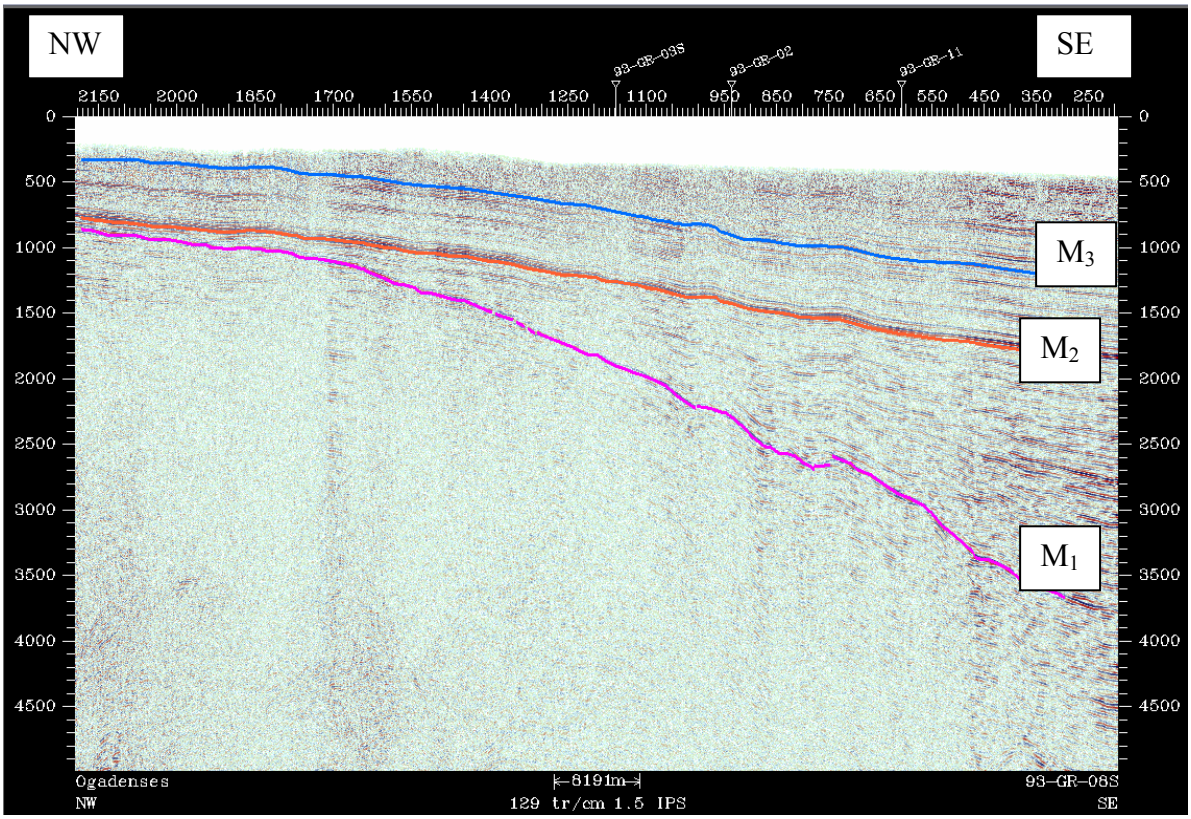

Figure 4.37: Megasequence interpretation along Line 08 showing that Megasequence 2 forms a thick wedge to SE, whereas megasequence 3 forms nearly a uniformly thick sedimentary package.

The other major horizon interpreted as the top of a shallower megasequence (M3) starts at about 1100 ms at the southeast end of the profile. It has a fairly gentle slope and rises towards the northwest. Megasequence 3 has a fairly uniform thickness across the profile and becomes very shallow to the northwest at about shot point 2100.

4.7.3.3 Line 16

Line 16 is one of the lines to further the northeast in the study area. It is also one of the shortest lines interpreted. It is oriented almost in an east-west direction, so is not exactly parallel to the other dip lines (Fig. 4.31). However, its orientation approximately follows the dip direction. In this section of the basin, the deepest horizon (M1) is relatively shallower and starts at about 1550 ms beneath shot point 0 on the southeast (Fig. 4.38). With a gentle slope M1 rises to the northwest and reaches 1000 ms after shot point 900. The red horizon is the second horizon (M2) and is a strong reflection interpreted on the other lines the top of the second megasequence M2 appears to pinch out further to the northwest after shot point 900 and reaches at 900 ms. In this area the two horizons (M1 and M2) are separated by about 100 ms. The blue horizon that is also interpreted as the third horizon (M3) in the other lines is marked by its gentle slope and uniformly thick sedimentary package. It starts at about 750 ms and the top of this megasequence appears to pinch out around station 880.

4.7.3.4 Line 20

Line 20 is about 52 km long, and is oriented in a northwest-southeast direction, but it is not exactly parallel to the other long dip lines (Fig. 4.31 and 4.39). Similar to the other dip lines, the deepest horizon (M1) is beneath shot point 280 at the southeast end of the line. It forms a gentle trough horizon near shot point 350 and rises to the northwest with a slope that gradually decreases. The second horizon (M2), which is clearly distinguished by its strong reflection, starts at about 1550 ms. Its shape is similar to M1 with the slope more gentle slope, which causes

megasequence 2to thin to the northwest. The uppermost horizon (M3), which is marked in blue (Fig. 4.38) is parallel to M3. Thus, the megasequence 3 is uniform across the line.

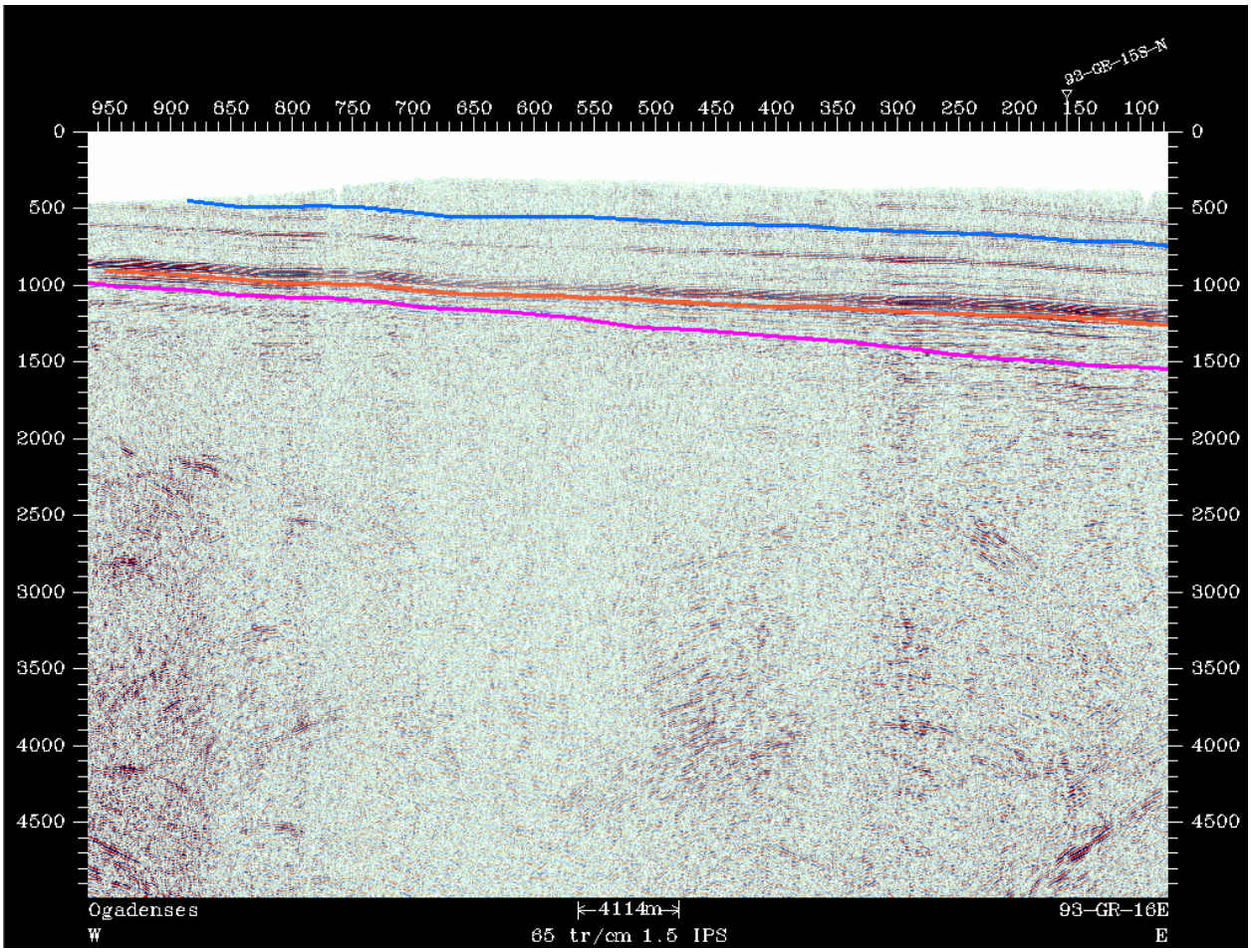

Figure 4.38: Megasequence Horizon interpretation along profile 16, which is oriented in an east-west direction in the dip direction.

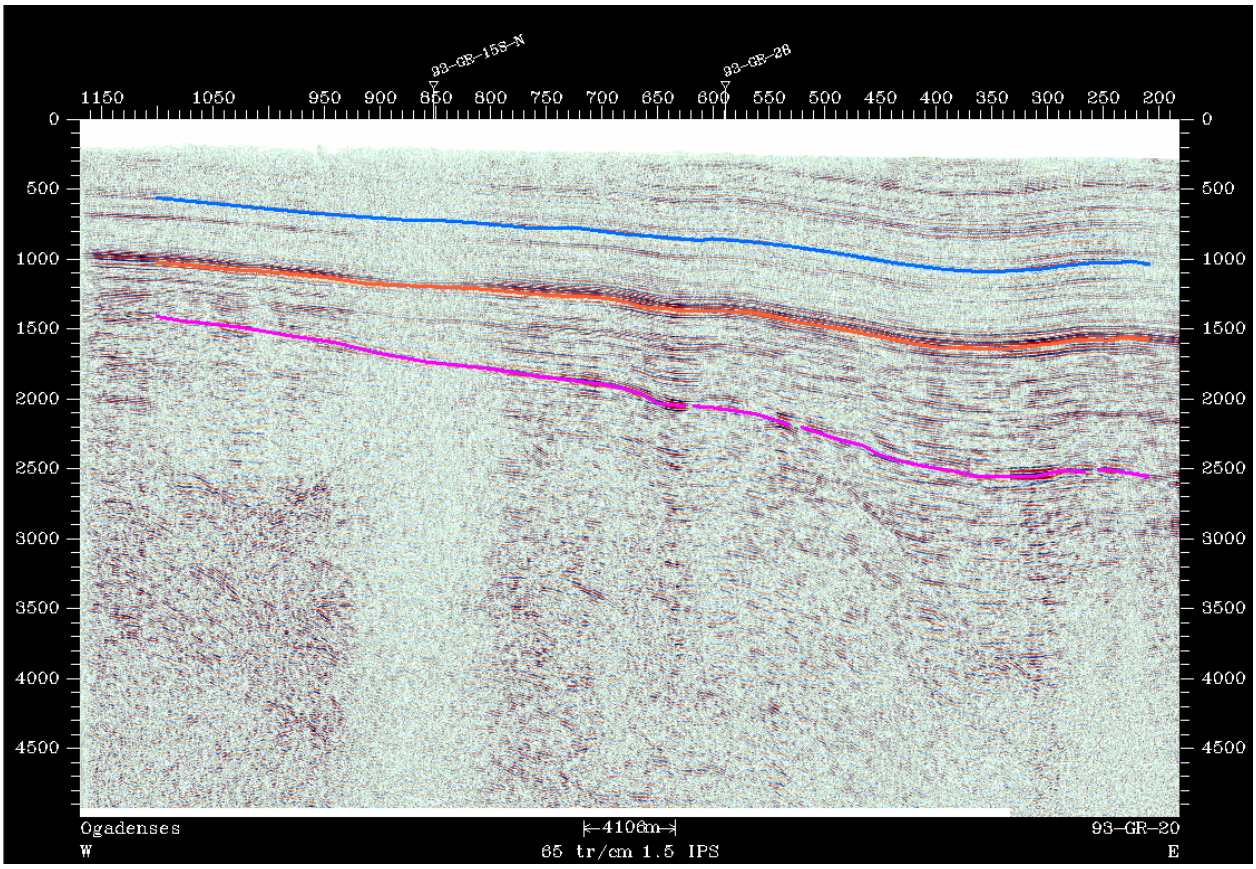

Figure 4.39: Megasequence interpretation along line 20 showing three megasequences shallowing up to the NW.

4.7.3.5 Line 02

Line 02 is one of the strike lines (Fig. 31) and has a length of 83 km (Fig. 40). It trends from northeast to southwest and crosses four dip lines (line 10, 08S, 01S-N-A and 28). The deepest horizon (M1) shown in purple is characterized by discontinuous reflections (Fig. 4.40). This may be associated with faulting as a result of the initial rift development and extension processes. However, the fault throws appear to be small. The other horizon interpreted in red is the second horizon (M2) along this line. The blue line marks the top of the last megasequence (M3) interpreted in the region. Similar to most of the lines in the previous interpretation the megasequence bounded by the blue and red horizons extends with similar thickness. All the horizons deepen towards the north east.

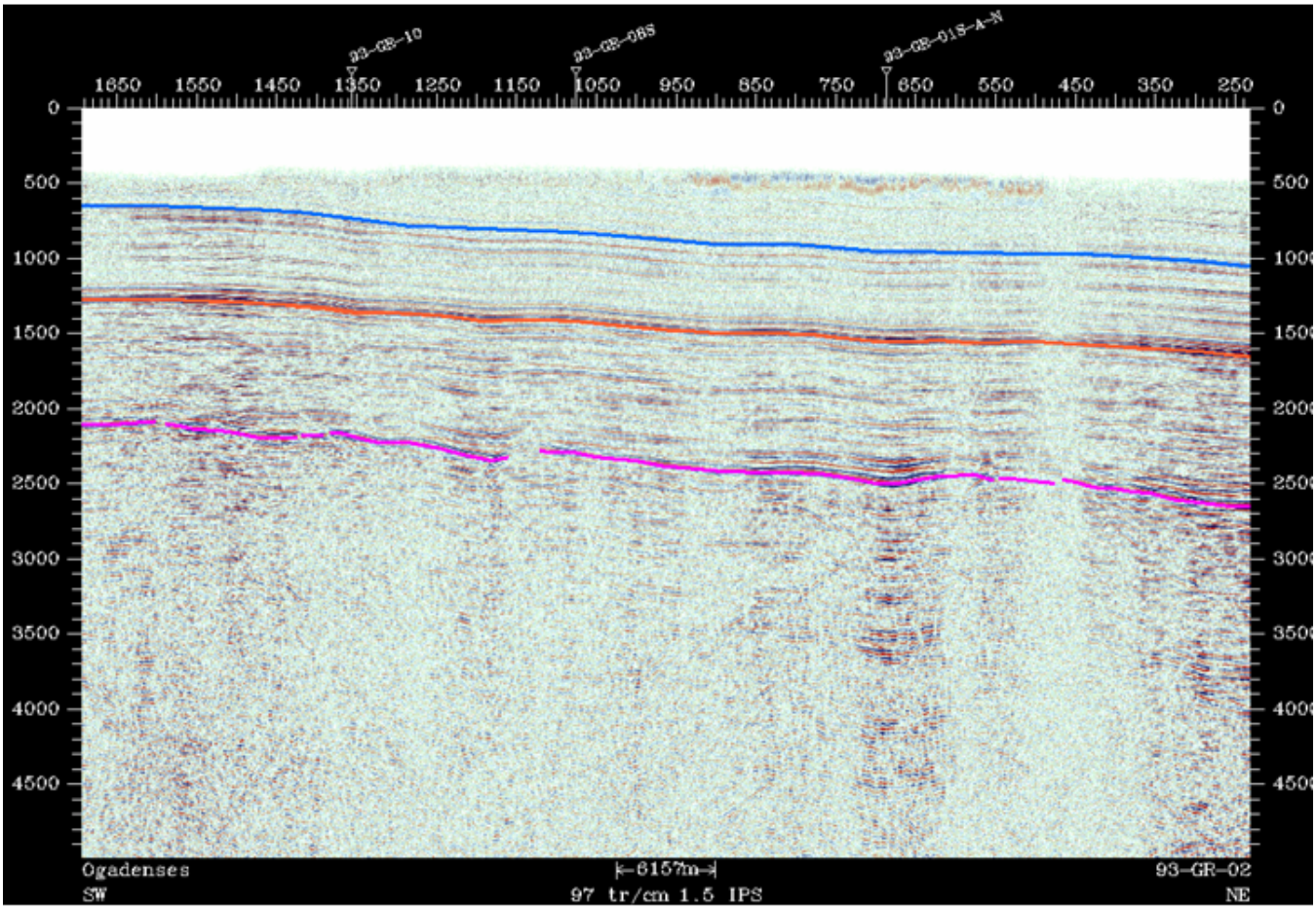

Figure 4.40: Megasequence interpretation along line 02 that is oriented in a southwest-northeast direction.

4.7.3.6 Line 03

Line 03 is oriented in a southwest-northeast direction and crosses four dip lines (Fig. 4.31 and 4.41). These are line 10, 08S, 01S-N-A and 27. The line is acquired in the up-dip section of the basin compared to the other strike line oriented southeast of this line (Fig. 4.31). The top two megasequences (M2 and M3) above the deepest megasequence are almost parallel to each other striking northeast-southwest. The megasequence whose top is interpreted in red (M2) is thicker than the megasequence (M3) above it. The megasequences are shallowing slightly towards the

SW and deeper to the NE. However, compared to the other lines, in this line the formations are shallowing up.

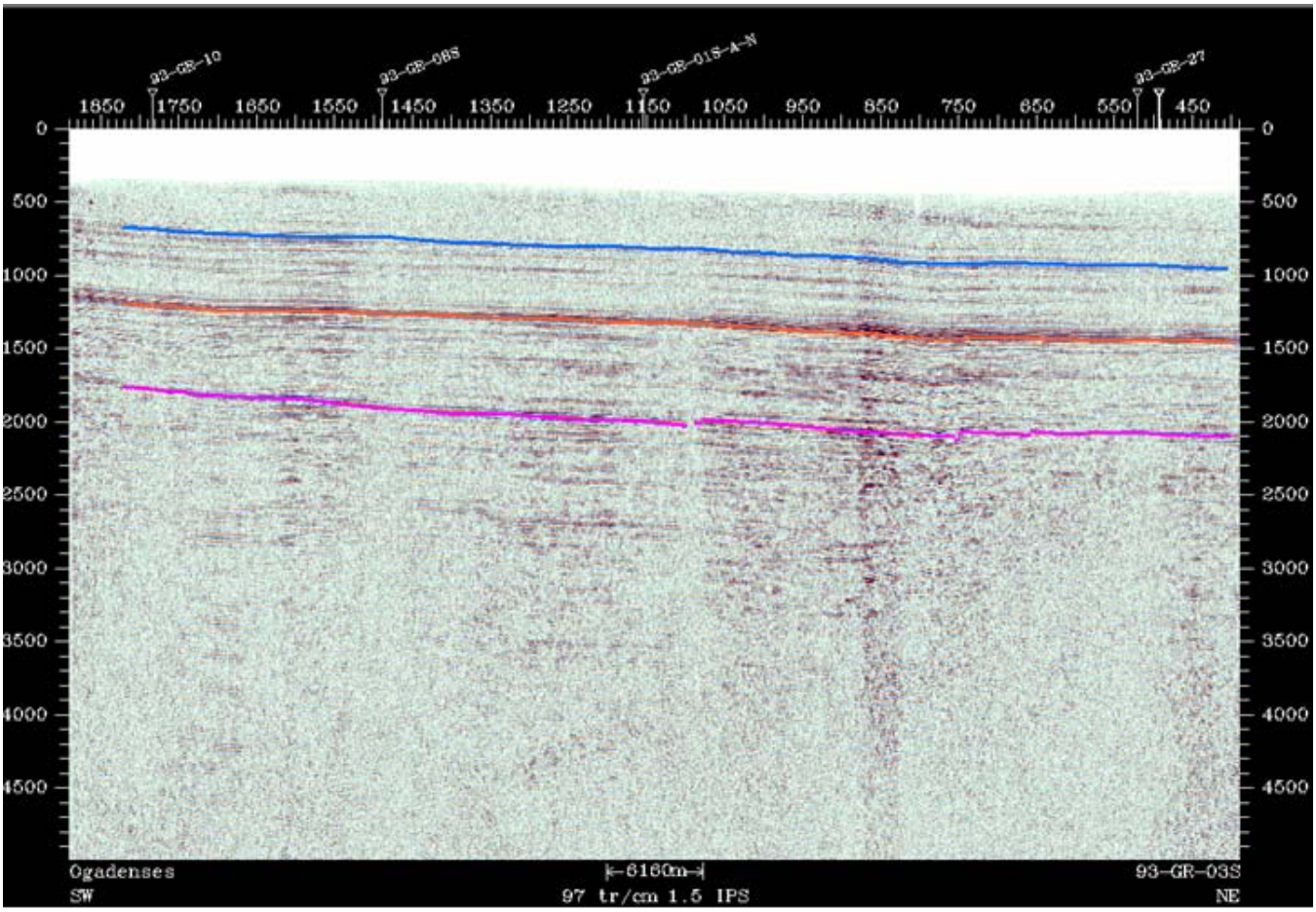

Figure 4.41: Megasequence interpretation along line 03, which is a strike line

4.7.3.7 Line 15

This line is oriented north-northeast further to the north east of the study area (Fig. 4.31 and 4.42). The line crosses about 5 dip lines. Similar to the other horizon interpretations the megsequences are marked by purple for the deepest horizon (M1), red for the middle horizon (M2) and blue for the top horizon (M3). The middle megasequence thickens to the south-southwest and thins to the NNE. In general the formation dips gently. The top megasequence

(M3) as in the other lines gently deeps with similar thickness to the south-southwest. The depth of this formation gets shallower to the north-northeast and deeper to the south-southwest.

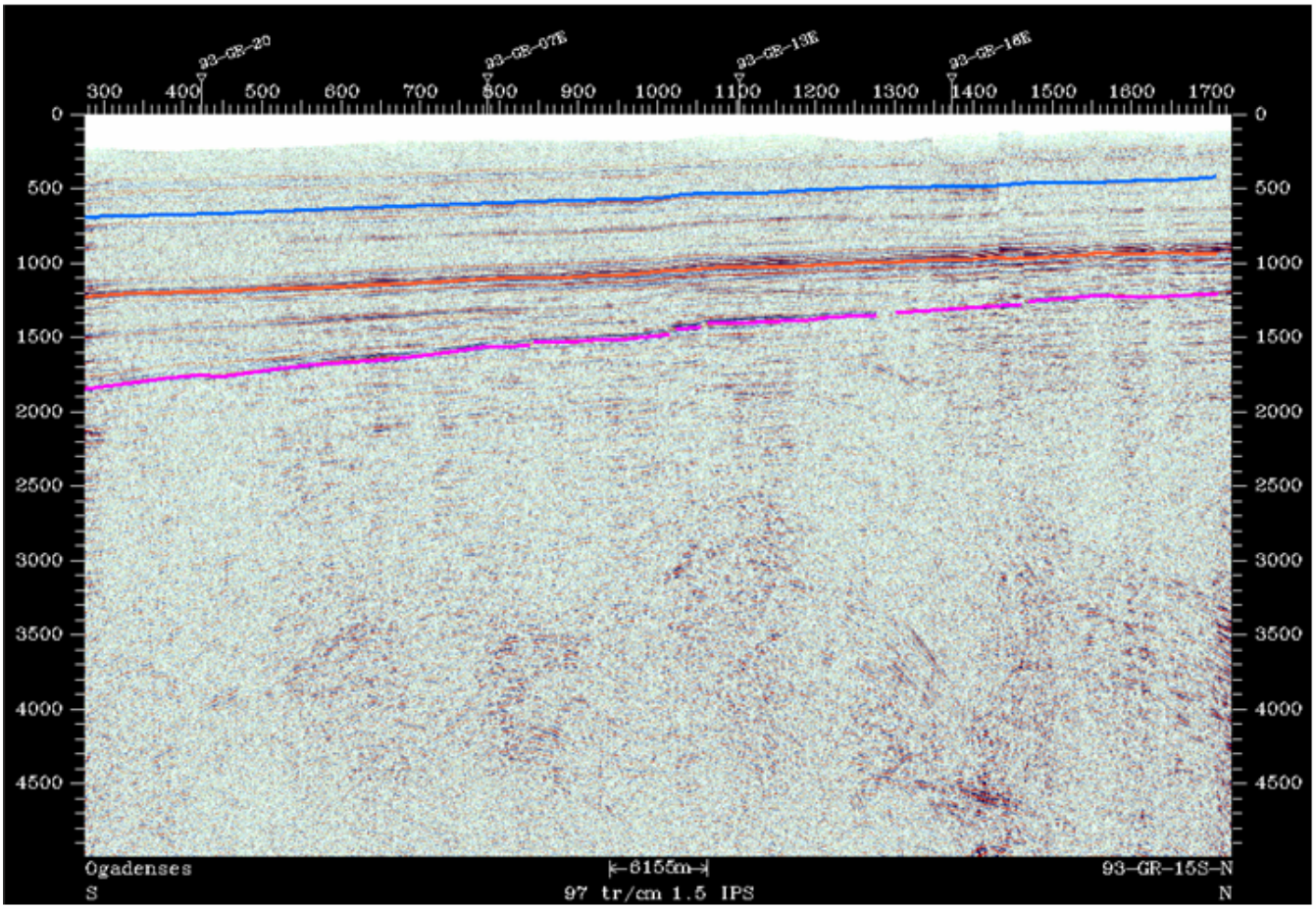

Figure 4.42: Megasequence interpretation along one of the strike line (15), which is to the northeast of the study area.

4.7.3.8 Line 11

This line is located to the southeast of strike line 02 and 03 (Fig. 4.31). It crosses three dip lines and appears almost parallel to the other two strike lines (Figs. 02, 03 and 11). The megasequences in this line appear almost parallel (Fig. 4.31). The formation tops are deeper in this lines compared to other strike lines. This line may correspond to the deepest part of the basin

in this region. The lower megasequence top starts at about 2700 ms and with minor undulation, it ends at about 2750 ms at shot point 200.

The top of M2 starts at depth of 1400ms in the south-southwest, and ends at 1500ms in north-northeast. It is nearly parallel with a slight dip to the north-northeast. Similarly the top of the megasequence marked in blue (M3) dips to the north-northeast starting at 750 ms at about shot point 1050 and dips to 850 ms at about shot point 200 (Fig. 4.43).

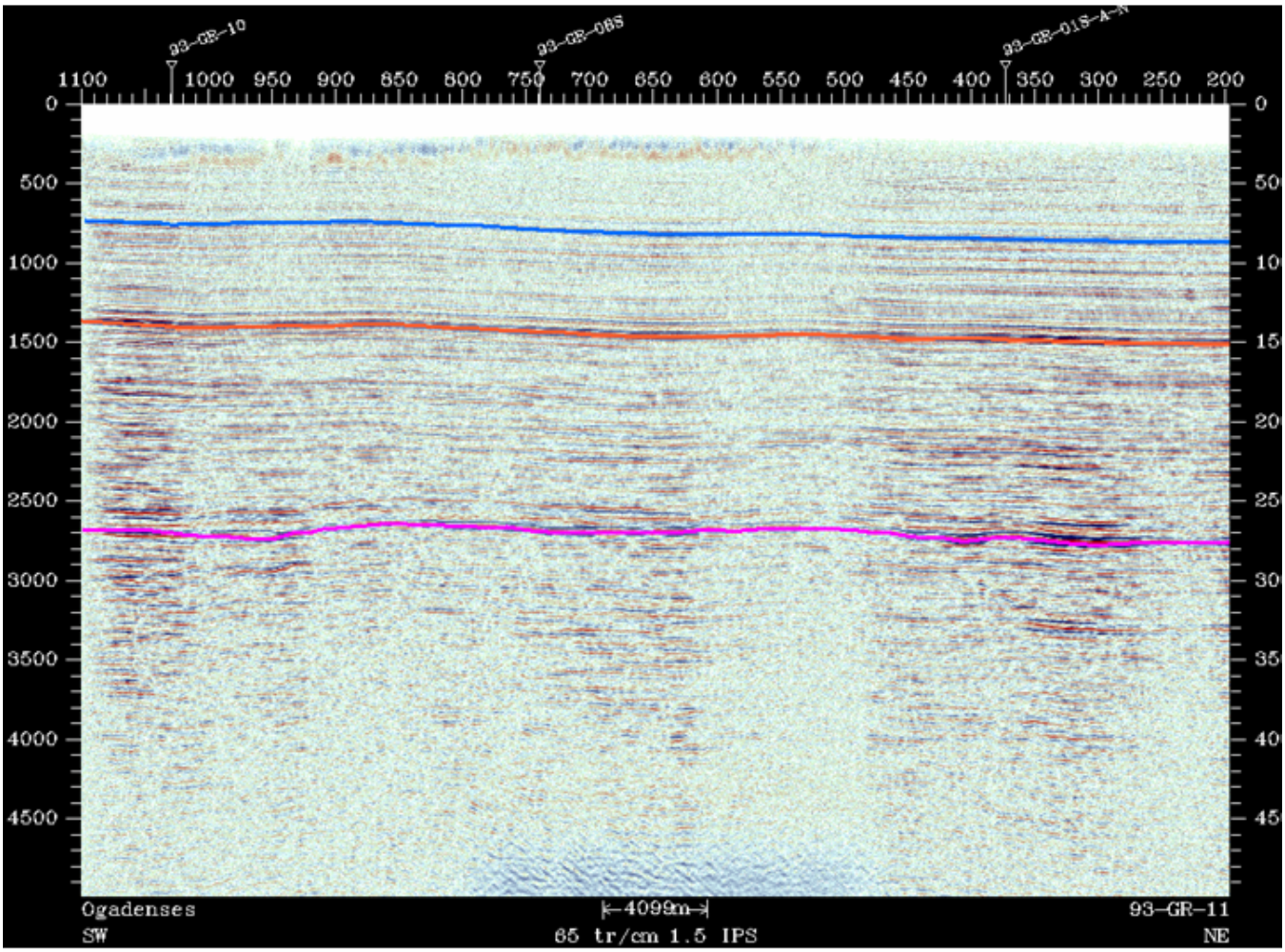

Figure 4.43: Megasequence interpretation along line 11 in the strike direction of the basin.

4.8 Sequence stratigraphy

Models for sequence stratigraphic interpretation have been developed by various researchers. This includes carbonate rocks (e.g. Loucks and Sag, 1993), nonmarine sediments, and shelf margins (e.g. Van Wagoner et. al., 1995, van Wagoner et al., 1990). Conceptual models of these works were used for the sequence stratigraphic interpretation considered in this study. An attempt has been made to exploit possible interpretations that the seismic data allowed us and traces are examined in detail.

Most of the seismic sections used in this study from the Ogaden basin are fairly suitable for sequence stratigraphic interpretation (e.g. Figs. 4.36, 4.37, 4.38, 4.39 and 4.40). This is based on the observation of the seismic reflections suggesting sequences onlapping the underlying sequences identified using seismic images. Slope fan deposits are onlapping against the basement. The clinoforms have a shoaling nature towards the NW. The down lapping section is not clearly visible. There is a sequence boundary on the top of the sequences that are pinching or onlapping against the megasequence 1 or the basement surface. This sequence boundary is recognized based on the reflection terminations seen below and above it. Nearly similar reflectors are onlapping on the sequence boundary [SB-10-red (Fig. 4.44)]. The onlapping reflectors are clearly interpretable for much of the SE section of the profile. The most important feature that has a bowl shape is located between shot points 400 to 500. This may be an incised valley along or close to the fault zone developing into a large incision. This feature is observed on similar seismic section along the dip direction. The units below and above the identified boundary sequence appear to be lowstand prograding wedges. These sedimentary packages are dominated by slope deposits. The channel-like structures may be important features and further detailed study may be needed to focus on such types of features.

Similar sequences are observed on the subsequent dip lines such as 08S and 01. To generalize the sequence stratigraphy, the sequence boundary may be related to the top of Calub

Sandstone Formation which is a proven reservoir in the Calub and Hilala gas discoveries some 200 km northeast of this study area. The fact that the thickness of the sequence is thicker to the southwest portion of the study area may also suggest Calub Sandstone is thicker. As shown in most of the seismic sections, the Calub Sandstone pinches out more quickly than the rest of the formations above it.

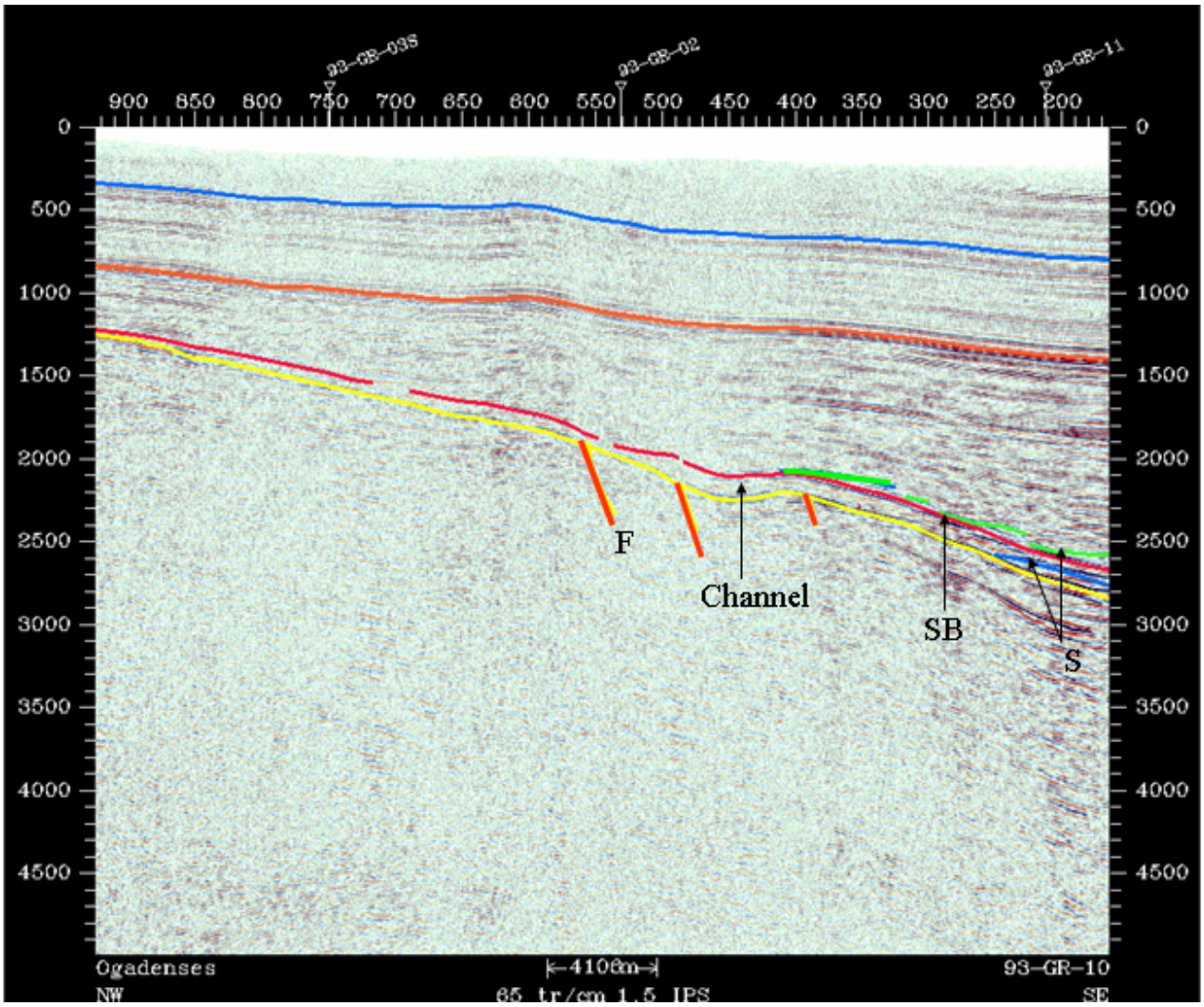

Figure 4.44: Sequence stratigraphic interpretation along line 10 showing onlapping sequences (s) against the basement and a sequence boundary (SB) as well as possible channel. F indicates possible faults.

Most of the reflectors above megasequence 1 are prograding to the up dip direction with gentle slope. Sequences within megasequence 2 are almost parallel to each other and have minor dip. This suggests that the sequences were developed under a large body of water and quiet depositional environment. Reflectors of a similar nature are observed along lines 08S, 01 and 10, which are dip lines.

4.9 Seismic attribute analysis

The main aim of seismic exploration in the oil industry is to map targets associated with petroleum deposition, generation and entrapment. In this regard, it is essential to characterize the seismic data in various forms and interpret the result in terms of structures, stratigraphy and fluid properties. These characteristics can be quantitative measures of seismic characteristics called seismic attributes. A seismic attribute either is directly sensitive to the desired geologic feature or reservoir property of interest or should allow us to define the structure or property of interest. In general, the definition of seismic attributes consists of all quantities derived from seismic attributes from seismic data; thus it is essential to consider interval velocity, inversion for acoustic impedance, pore pressure prediction, reflector terminations, as well as complex trace attributes and amplitude variation with offset (AVO), depositional environment and thereby to infer some feature or properties of interest (Chopra and Marfurt, 2005).

A number of authors have suggested classification of attributes in many forms and divisions (e.g., Tanner et al. 1994; Chen and Sidney, 1997; Brown, 1996b, 2004, Liner et al., 2004; and Barnes 1997). The two general categories of seismic attributes are geometrical and physical. The geometrical classification includes structures such as azimuth, continuity, etc mainly visibility. The physical is related to lithology. Tanner (2001) suggests attributes can be classified into pre-stack and post-stack attributes that can be computed after or before migration.

Pre-stack attributes such as directional and offset related information can be related to fluid properties and fracture orientations.

Post-stack attributes based on their computational characteristics are classified as instantaneous attributes, wavelet attributes, physical attributes and geometrical attributes, reflectivity attributes and transmissive attributes. In this study we have employed post stack processing to extract different attributes for interpreting possible lithologic information.

4.9.1 Instantaneous Frequency

The instantaneous frequency is the time derivative of phase (Cohen. 1995, Barnes, 1991, 1992). It is a physical attribute because its instantaneous frequency responds to both wave propagation effects and depositional characteristics; hence it is a physical attribute and can be used as an effective discriminator of lithology.

It is also:

a. Hydrocarbon indicator by low frequency anomaly. This effect is sometimes accentuated by unconsolidated sands due to the oil content of the pores
b. Fracture zone indicator since fractures may appear as lower frequency zones
c. Bed thickness indicator. Higher frequencies indicate sharp interfaces such as exhibited by thinly laminated shales; lower frequencies are indicative of more massive bedding geometries e.g., sand-prone lithologies.

Selected lines from the study area were analyzed in Seisworks project in order to obtain the most out of the 2D seismic data. Instantaneous envelope or reflection strength is sensitive to changes in acoustic impedance and thus to lithology, porosity, hydrocarbons, and thin bed tuning (Chopra and Marfurt, 2005).

Instantaneous frequency is useful in identifying abnormal attenuation and thin-bed tuning. The instantaneous frequency analysis of Line 10 is shown in Fig. 4.45. The prominent low frequency anomaly associated with M1, which is interpreted as the basement structure can clearly be seen. The other horizons show very similar frequency content. The low frequency anomaly associated with the dipping horizon which is interpreted as a Calub Sandstone formation, may be due to some hydrocarbon effects associated with it or the effect of pore spaces filled with fluid as it is a known reservoir rock in the region (Fig. 4.11).

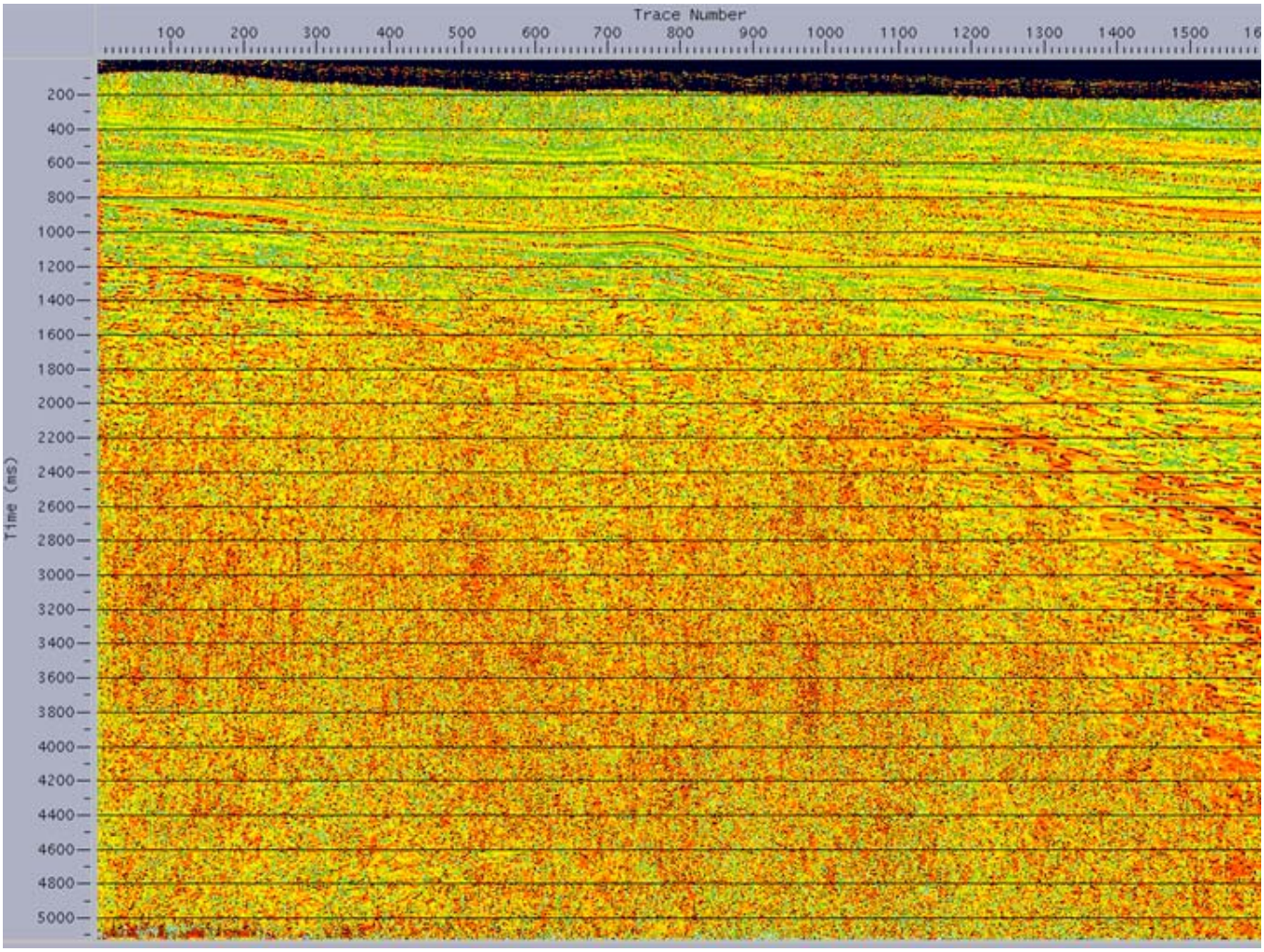

Figure 4.45: Instantaneous frequency display for line 10

4.9.2 Reflection Strength

The three mega sequences which begin at about 900 ms, 1450 ms 3000 ms in the southwestern part of line 10 are strong reflection horizons interpreted in the reflection strength analysis. M1 (megasequence 1) shows continuous strong envelopes from the beginning of the line around shot point 100 to shot point 380. In between shot points 400 and 500 there is a trough along the same reflection horizon. This area is anomalous compared to all the horizons interpreted in the region. This could be either a large channel or reflection sag that may be caused due to hydrocarbon effect in that region. By analogy from the central part of the Ogaden basin, the horizon just above the basement is the Calub Sandstone of Karroo group. This lithologic unit is the deepest reservoir rock in the Ogaden where the Calub and Hilala gas discoveries were made.

With minor interruption of the reflection strength, the megasequence shallows up rapidly to about 1200 ms. The prominent strong reflector just above megasequence 1 shows a continuous reflection from about 2800 ms at about shot point 100 and continues with a similar dip like the M1 reflector until shot point 380. It is hard to trace the continuity of this reflector beyond shot point 380 except for a shadow-like feature with the trough to the northwest (Fig. 4.46).

M2 (the top of megasequence 2) is continuous throughout the profile. This suggests the existence of a strong reflection or impedance contrast between the top and lower formation along this horizon. In addition, there are thin reflectors seen above and below this strong reflector. In between megasequences 1 and 2 we can see a wedge shaped sedimentary package about 1800 ms thick in the SE that thins to about 200 ms in the NW. This may be the sedimentary package identified as Karroo sediments from drilling results in the other part of the Ogaden basin, about 200 km NE of this study area (e.g., Worku, 1988, Habtezgi, 1989, Alconsult, 1996, Hunegnaw et al., 1998). The Karroo sediments are known as Calub Sandstone, Bokh Shale and Gumburo Sandstone. The sediments also include the Adigrat Sandstone as part of the Karroo Group, although others do not include this formation as Karroo Group (Purcell, 1979, Hunegnaw et al.,

1999). The strong reflection horizon just above M1 could be the Calub Sandstone, which is a proven reservoir in the Calub area from drilling results.

The other recognizable reflector is M3, which starts at 800 ms in SE and reaches 300 ms in the NW. It shows a constant, uniform thickness. Stratigraphic records and drilling results in the Ogaden basin shows that above the Adigrat horizon is the Hamanlei Formation divided into the: Upper, Middle and Lower Hamanlei Limestone. The top of the Hamanlei Formation shows strong reflection in the SE and NW part in the middle of the profile.

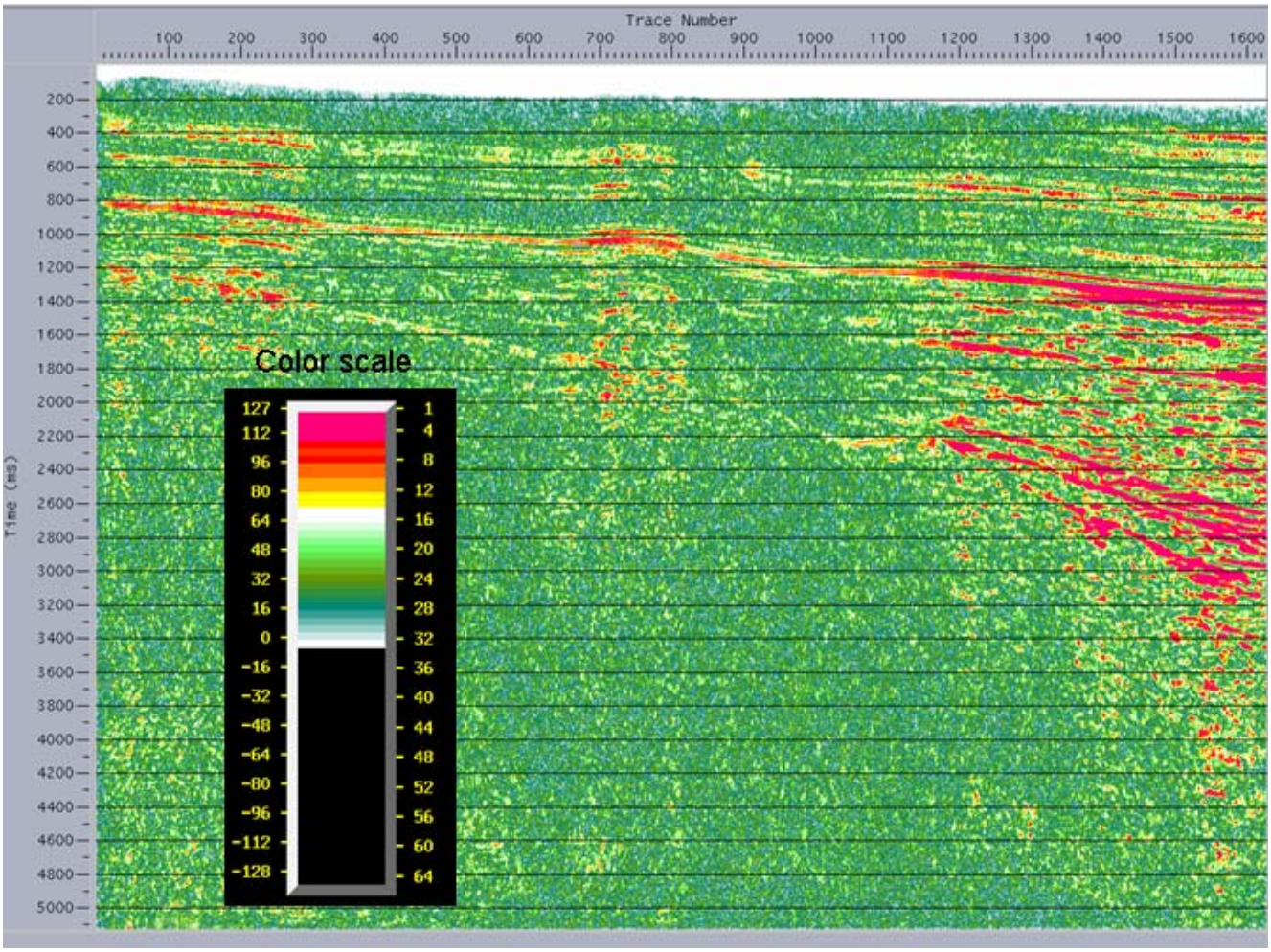

Figure 4.46: Reflection strength showing most of the sequences to the SE of the basin are strong reflectors. The three megasequences are fairly clearly seen, indicating a strong impedance contrast.

4.9.3 Instantaneous Phase

Wave fronts are defined as lines of constant phase. This phase attribute is also a physical attribute and can be effectively used as a discriminator for geometrical; shape classifications. Instantaneous phase is a:

a. Good indicator of lateral discontinuity
b. Relates to the phase component of wave propagation
c. Used to compute the phase velocity
d. Devoid of amplitude information, hence all events are represented
e. Detailed visualization of stratigraphic elements

Instantaneous phase is an important attribute for tracing the continuity of a reflector and therefore for detecting an unconformity or unconformities, faults and lateral changes in stratigraphy. Fig. 4.47 shows the instantaneous phase analysis for Line 10. Since phase is a good indicator of lateral continuity, it is possible to see M1 or the basement reflector clearly. It is visible throughout the line with minor interruption at about shot point 500 to 550. In this section, even the diffuse reflection which is detected as anomalous trough shows a continuous reflection when displayed using phase attribute. The other horizons identified as M2 and M3 are also continuous in the phase attribute and can be clearly traced and followed throughout the line. M3 shows a minor interruption in the continuity of the reflector but in most cases it is continuous along the line. In this case the horizon can be traced and followed in the attribute display more easily than the conventional seismic trace display.

A more elaborate display of the section to the southeast shows clear continuity of formation in between M1 and M2. The small formations which are pinching out against the basement and the top of the Calub Formation can clearly be seen (Fig. 4.47). This suggests that the thickest part of the basin is towards the SE. It also indicates much thick source rock with a possible pinch out in the NW direction. The other important conclusion that can be drawn from

this display is a possible stratigraphic trapping mechanism with pinchouts against the basement and the Calub Sandstone. Towards shallower time, most of the layers, especially between M2 and M3, are nearly uniform and parallel with constant dip angle inclination.

Another attribute analyzed is quality factor (Q). Fig. 4.48 shows the quality factor display of line 10. It is possible to distinguished M2 and M1 to some extent. It is obvious that M2 is the strong reflector seen in all the sections through out the study area.

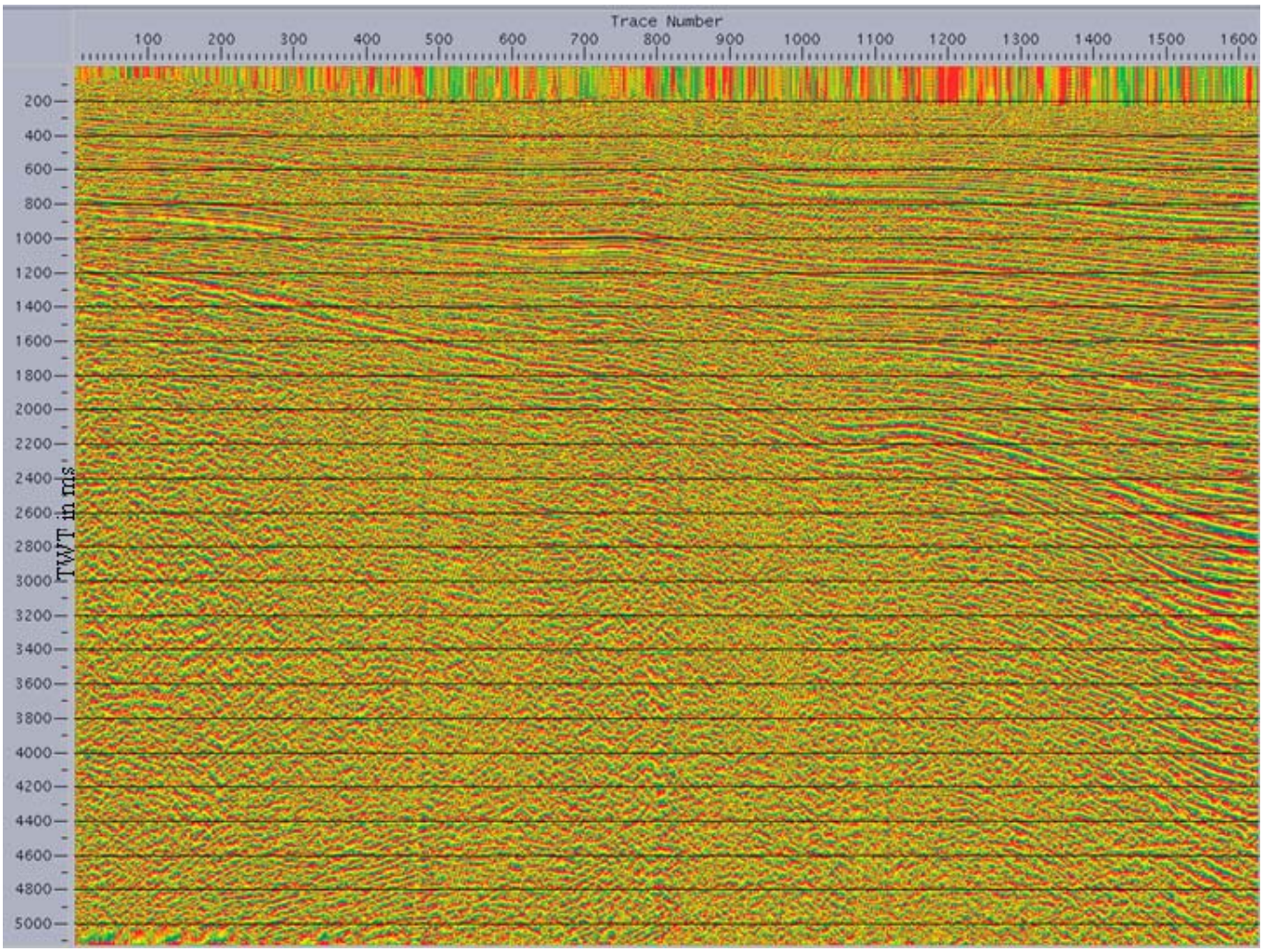

Figure 4.47: Instantaneous phase display of the dip line 10 showing continuity of reflection horizons.

Few studies of Q (e.g., Klimentos, 1995) are relevant to hydrocarbon exploration. Klimentos (1995) reports, based on sonic waveform analysis, that Q falls between 5 and 10 in gas sandstones of about 12% porosity (Q -1 between 0.1 and 0.2) while it may easily exceed 100 (Q-1<0.01) in oil- and water-saturated intervals. Attenuation is large in rock with partial gas saturation and small in liquid-filled rock. Accordingly we can see a distinct anomaly along the sequence above M_1 which could be related to the Calub Sandstone. Accordingly, strong low quality factor is seen along M_2, which is interpreted as Adigrat Sandstone.

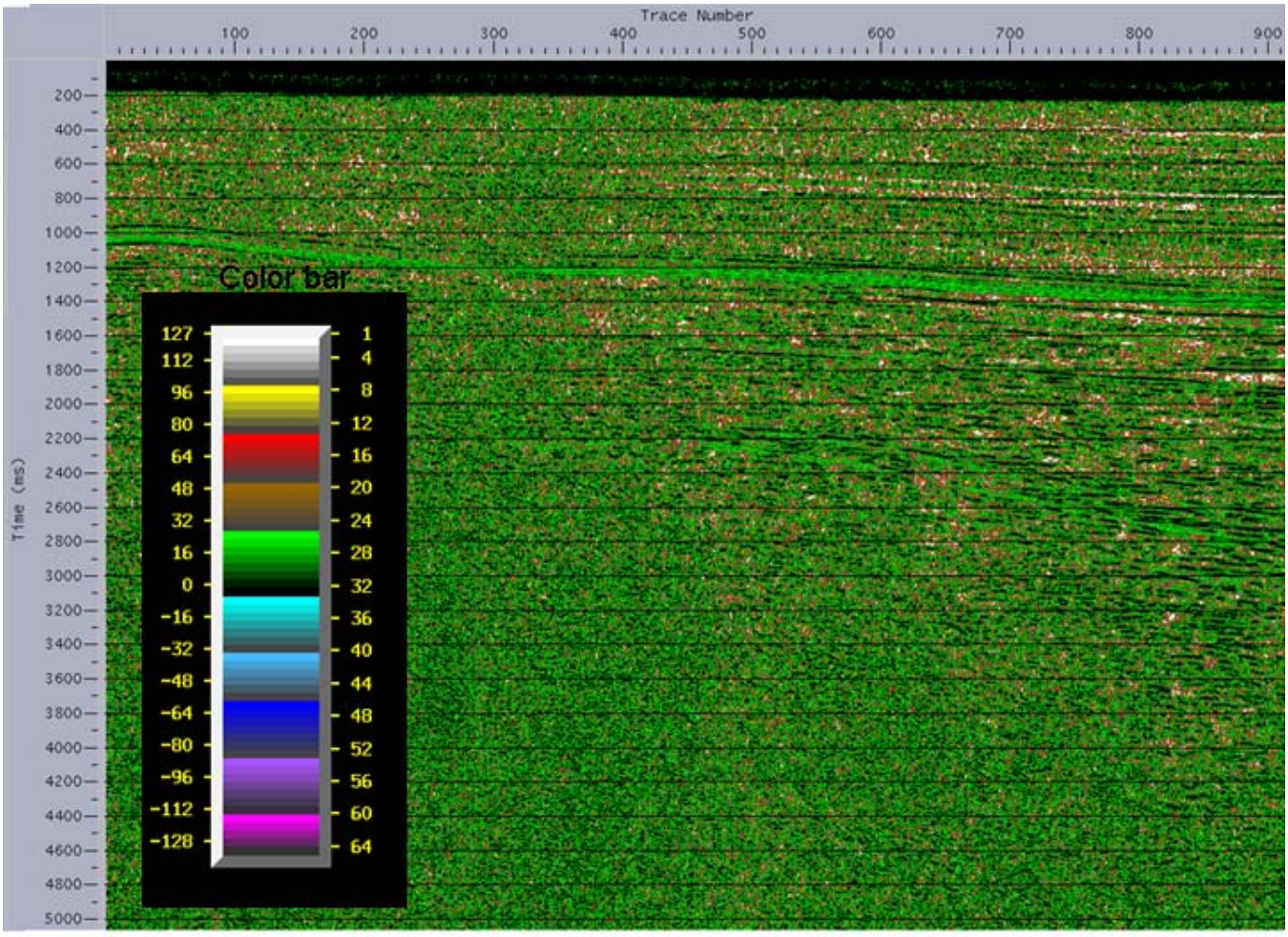

Figure 4.48: Quality factor display of the seismic section along line 10.

4.10 Structure Maps

Based on the megasequences interpretation, three time structure maps were produced (Figs. 4.31, 4.49, 4.50 and 4.51) using the Seisworks mapping facilities. **The megasequences interpreted here are correlated to lithologic units based on similar reflectors interpreted in regions where wells and well logs are available such as Hilala and Calub regions. Megasequence 3, which can be correlated to the top of Hammanlei Formation, appears to be restricted to the Ogaden region (Fig. 4.49). In general we can see parallel contour lines shallow.

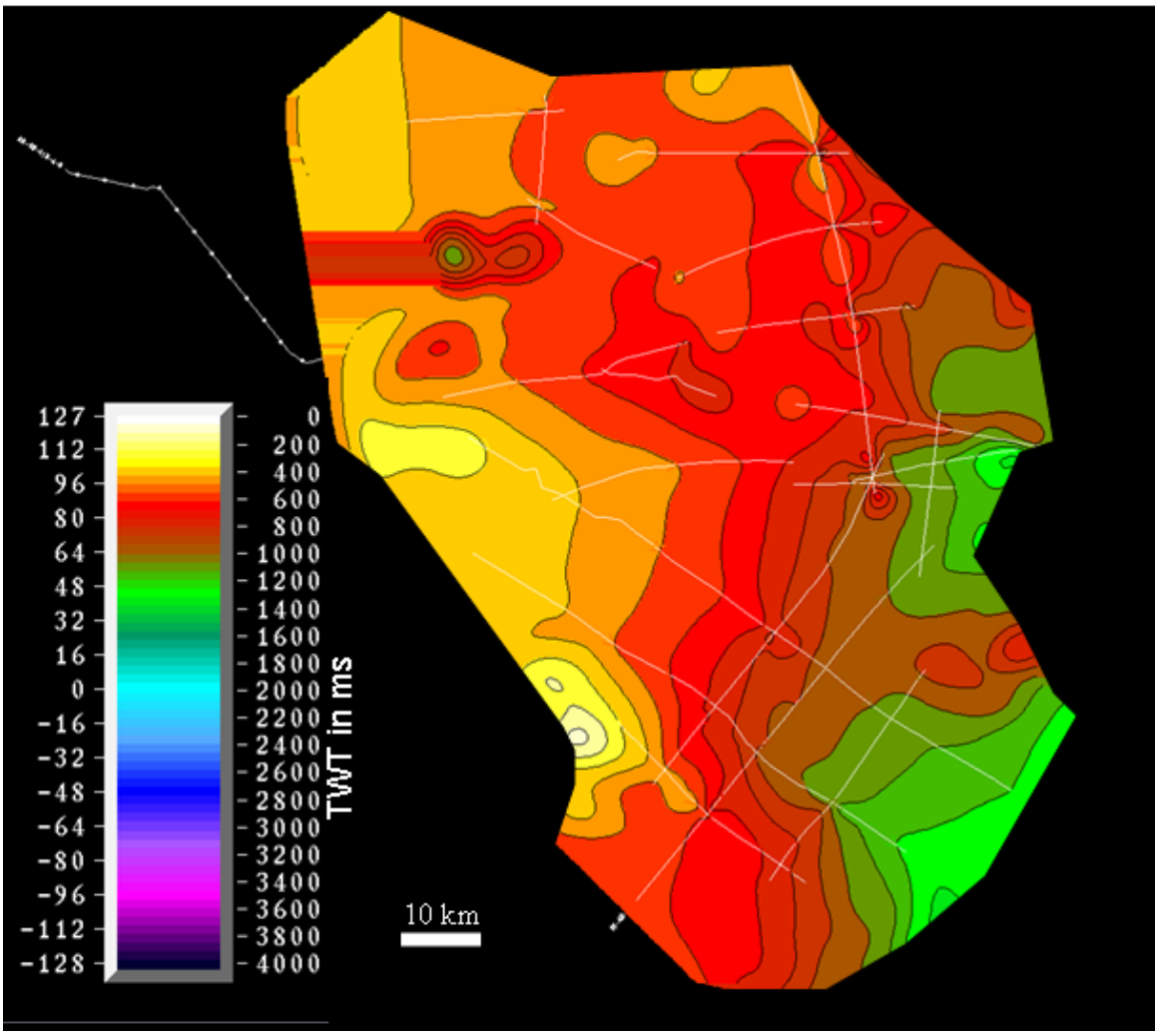

Figure 4.49: Time structure map of the top of megasequence 3

shallowing toward the northwestern side of the basin. This is an indication of the pinching out of the top of the Upper Hammanlei formation towards the northwest.

The top of megasequence 2 is the strong reflections that can be traced without any difficulty in the basin. This can be interpreted as the top of a known regional marker the Adigrat Sandstone. The Adigrat Sandstone shows a shallowing up contours towards the northwestern part of the basin. There is no faulted structure seen along this horizon as also indicated in the map (Fig. 4.50). A fairly variable structural configuration is observed along horizon or megasequence 1 (the basement). The structural map of this horizon shows fewer faults and incised channels (Fig. 4.3). The basement is deep in the southeast section of the study area and rapidly shallows up further to the northwest.

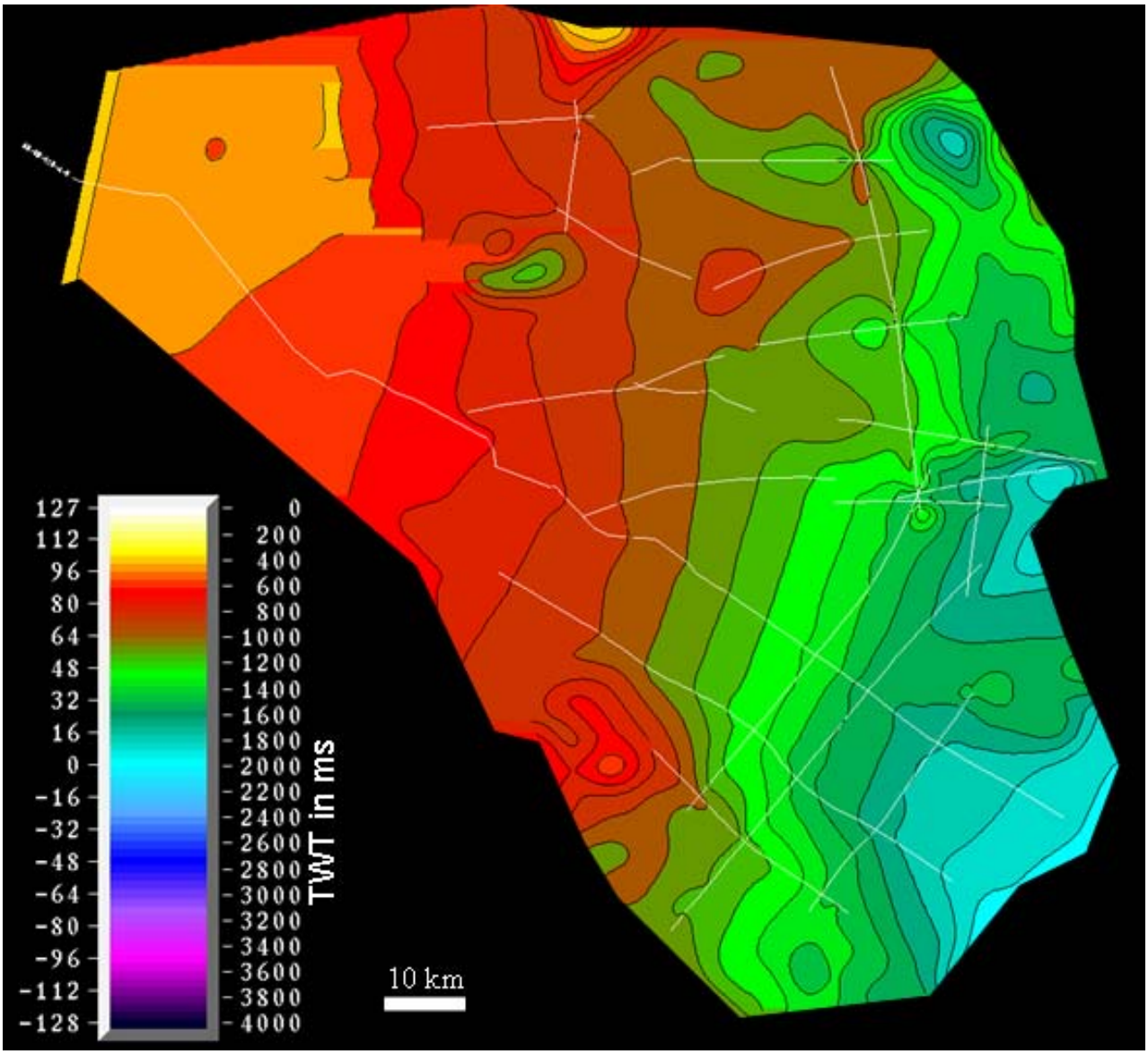

Figure 4.50: Time structure map of megasequence 2

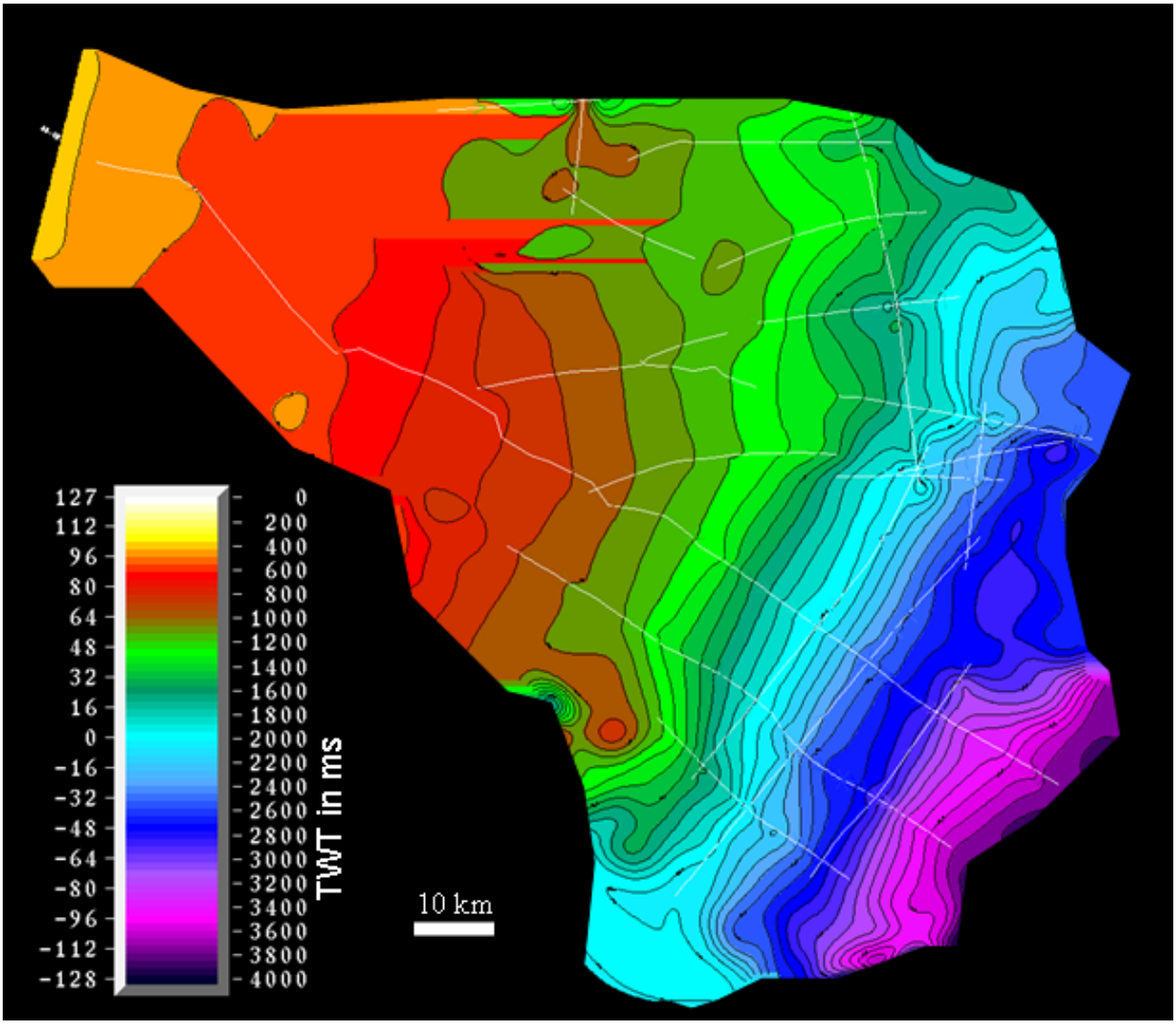

Figure 4.51: Time structure map of megasequence 1

4.11 Discussions and Conclusions

An integrated geophysical and geological data processing interpretation from the Ogaden basin reveals important information. First, the sedimentary package thickness is more than 8 km in the SW Ogaden basin in the area of Genale river. This assertion is based on the 2.5-D gravity profile modeling and the seismic reflection data interpreted in this study. The thickest part of the

sediment is attributed by Karroo sediments. Faulted structures are associated with the basement and are recognized based on the seismic data. The faulting system suggests that the evolution of the Ogaden basin is associated with extensional phenomena. The Calub Sandstone appears to pinchout against the basement earlier than the rest of the Karroo group sediments. Also structures associated with faults and channels are important features for hydrocarbon habitat and are identified in our interpretation. Attribute analysis reveals properties of the different lithologic units and affirms the continuity of horizons which were subtle in the conventional seismic trace display. Also some lithologic units such as the Calub Sandstone and Adigrat Sandstone exhibit unique properties in quality factor analysis and amplitude strength analysis, suggesting that they may be associated with hydrocarbon potential or contamination such as oil or gas. This is supported by existing discoveries and shows in the Ogaden basin such as Calub and Hilala gas fields and other oil shows in the area. Reprocessing of seismic reflection data has eliminated reverberations and has improved the continuity of reflection horizons. This suggests with improved analyses and modern software packages it is possible to make desired improvements in the seismic analysis. New depth analysis based on Euler deconvolution of the gravity data of the NE Ogaden reveals graben and horst-like structure, which could be an important hydrocarbon habitat. The negative residual gravity anomalies of the NE Ogaden basin can be attributed to Cretaceous sediments in graben-like structures and range up to 5 km in thickness. Residual gravity anomaly modeling results reveal variable sedimentary thicknesses in the Ogaden basin, that are attributed to variable structural and stratigraphic features in the basin.

Chapter 5: Relationship of the Ogaden and Abbay Basins

5.1 Introduction

Most geological and geophysical studies in Ethiopia have focused on the modern Ethiopian rift, the Afar triple junction and the flood basalts on the Eastern and Western plateaus. However, there are regional geological features and structures that are important in terms of understanding the geodynamics, tectonics, geologic hazards, and natural resources of the region. This chapter focuses on understanding the tectonics from the point of exploration for natural resources, specifically sedimentary basins and their hydrocarbon potential. The main emphasis is the relationship of the Ogaden basin to the Abbay or Blue Nile basin (Fig. 5.1), which is a subject of considerable interest in Ethiopia. The Ogaden basin is located in the southeastern part of Ethiopia and is the largest sedimentary basin in the country (Fig. 5.1). It is believed to contain 8-10 km of sediments in its deepest area. The Abbay basin is covered by the volcanics of the Western Plateau and is exposed only in the river valleys that have been cut through this cover.

There has been speculation that the Abbay basin is a continuation of the Ogaden basin as it developed during Permo-Triassic time when the Karroo rift system was formed (Fig. 5.2a). However, there has been no substantial geophysical study conducted in the regional to test this speculation. Thus, the purpose of this study is to provide the needed geophysical analysis. In our analysis, we have analyzed the regional gravity database that was complied as part of this study. We also included satellite gravity data from Gravity Recovery and Climate Experiment (GRACE) in our analysis in order to evaluate areas with sparse land data and to delineate regional structural trends.

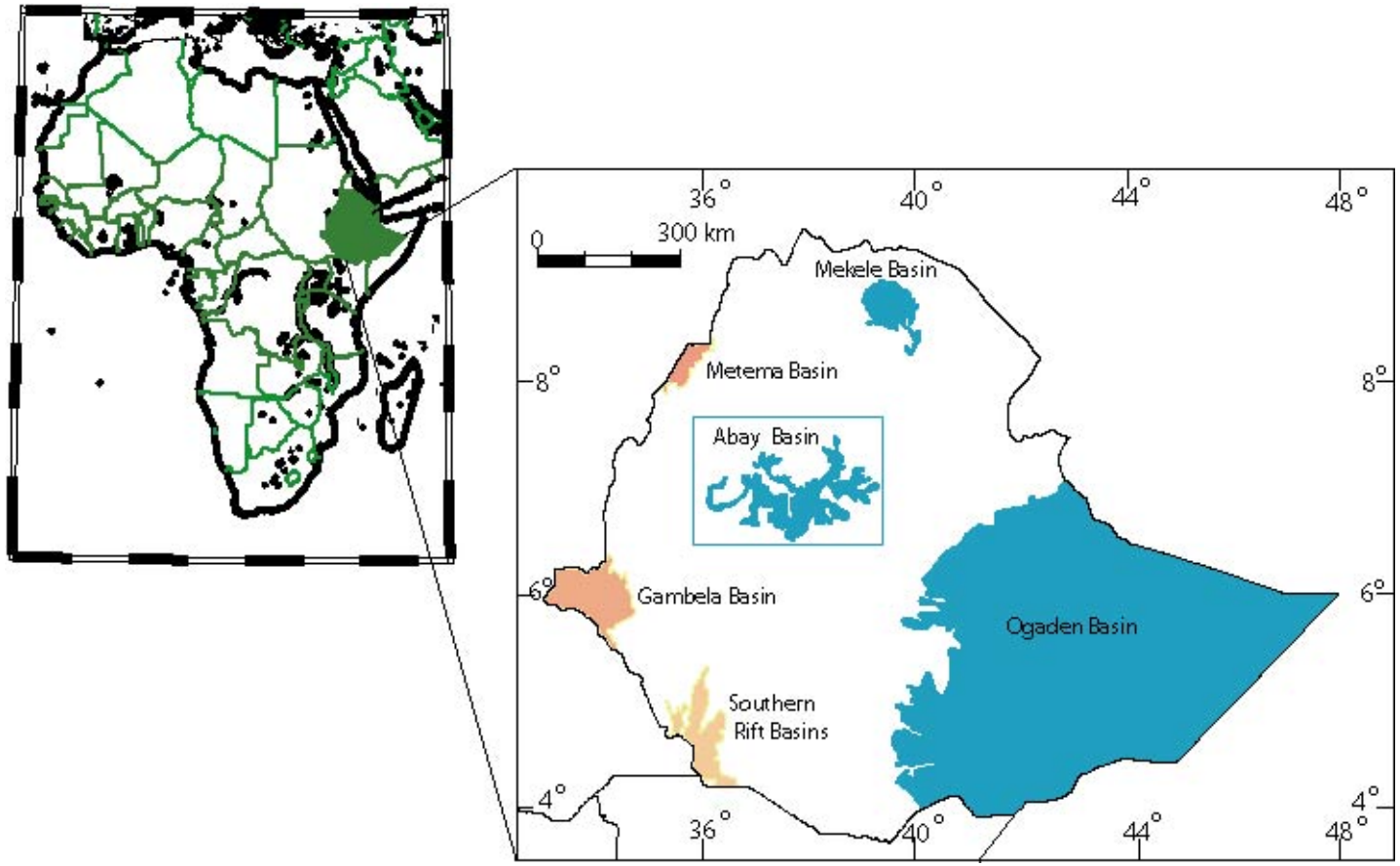

Figure 5.1: Location map of the Abbay and Ogaden basins in Ethiopia. The Ogaden basin is in the southeast part of Ethiopia and covers a vast area with similar lithologic units that extend into Somalia towards the passive margin. The inset is a map of Africa in which Ethiopia is highlighted in green.

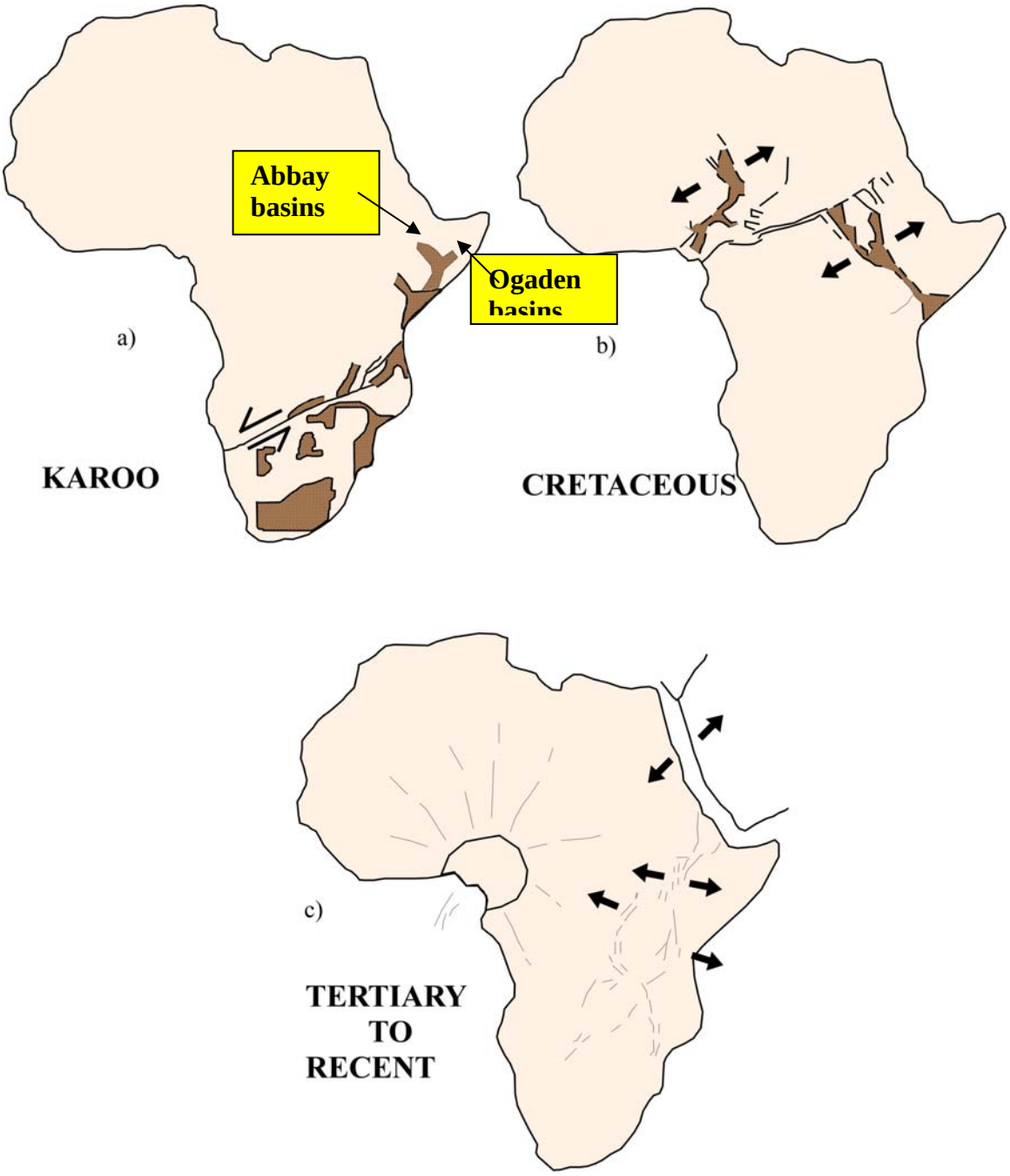

Figure 5.2: Diagrams illustrating the different tectonic regimes that the African continent has experienced since the Permian. In each case, rifts were developed and filled with sediments. Arrows indicate direction of motion. Shaded polygons are rift basins filled with sediments. Modified from Fairhead and Green (1989).

5.2 Stratigraphy and Paleogeography of the Ogaden and Abbay basins

The stratigraphy of the Abbay basin and the Ogaden basin has previously been discussed in Chapters 3 and 4, respectively, and Figure 5.3 provides a comparison of the stratigraphy of the Ogaden and Abbay basins. The extent of Karroo Group sedimentary rocks is a key consideration, and both basins contain pre-Adigrat Sandstone (Triassic) units lying above the basement. In the Ogaden basin, these basal sedimentary rocks are assigned to the Karroo Group and exist deep in the subsurface based on deep drilling results for oil and gas exploration (e.g. BEICIP, 1998; Alconsult, 1996; Worku, 1988). In the Abbay basin, these sediments are mainly a sandstone unit that has also been assigned to the Karroo Group (Mohr, 1963; Davidson and McGregor, 1976; Wolela, 1997). Different Karroo units have been classified as having source and reservoir potential in the Ogaden basin. Proven gas discoveries in the Calub and Hilala regions of the Ogaden basin are sourced from the Bokh Shale and accumulated in the Calub Sandstone. Both of these units are part of the Karroo Group (Worku, 1988; Worku and Austin, 1989).

Above the Adigrat Sandstone, Jurassic carbonates dominate the thickest portion of the section in both basins. However, these units are much thicker in the Ogaden basin. Jurassic strata are composed of shallow marine carbonates and evaporites and basinal shales (Habtezgi, 1989). In the Ogaden basin, the Jurassic carbonates are known as the Hamanlei Formation. In between the Adigrat Sandstone and Lower Hamanlei Formation a transitional zone with shale and clastic mixed facies is found. The Adigrat Sandstone is widespread from the Ogaden basin up to the Abbay basin (e.g., Habtezgi, 1989; Wolela, 1997) (Fig. 5. 4).

However, the Hamanlei Formation overlies the basement in some places such as the Danakil Alps (in Afar), parts of Western Ogaden, the Harar area of Ethiopia and Nogal uplift in Somalia (Barnes, 1976). Some authors suggest that the Lower Hamanlei Formation is restricted to the Ogaden basin (e.g., Habtezgi, 1989), while others correlate the fine grained clastics of the Abbay basin with the Lower Hamanlei Formation of the Ogaden basin (Wolela, 1997).

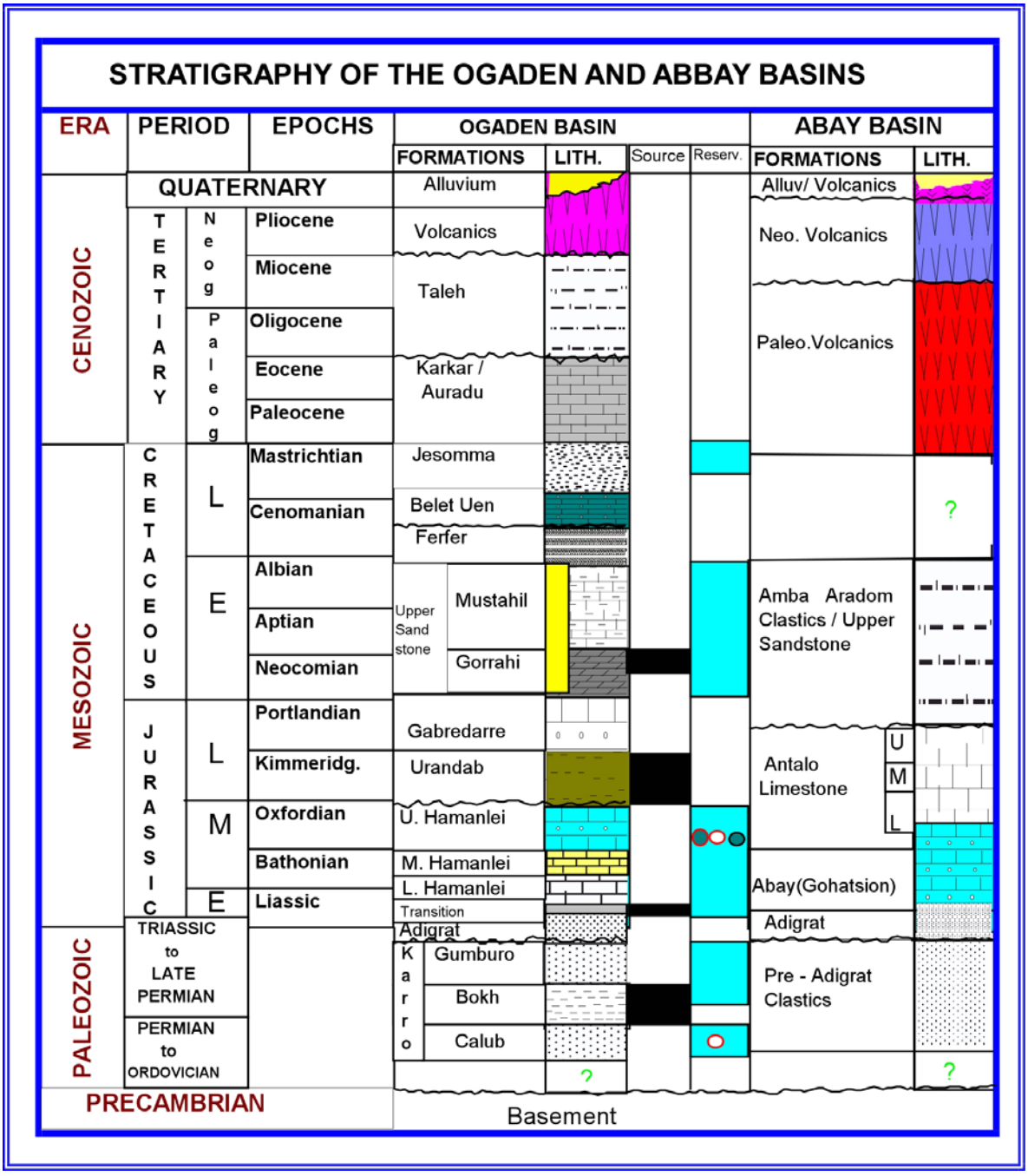

Figure 5.3: Stratigraphic correlation chart for the Ogaden and Abbay basins illustrating the similarities between the two basins. The clastic sediments of the Abbay basin on top of the basement are classified as pre-Adigrat in age by most authors and are generally thought to be part of the Karroo Group.

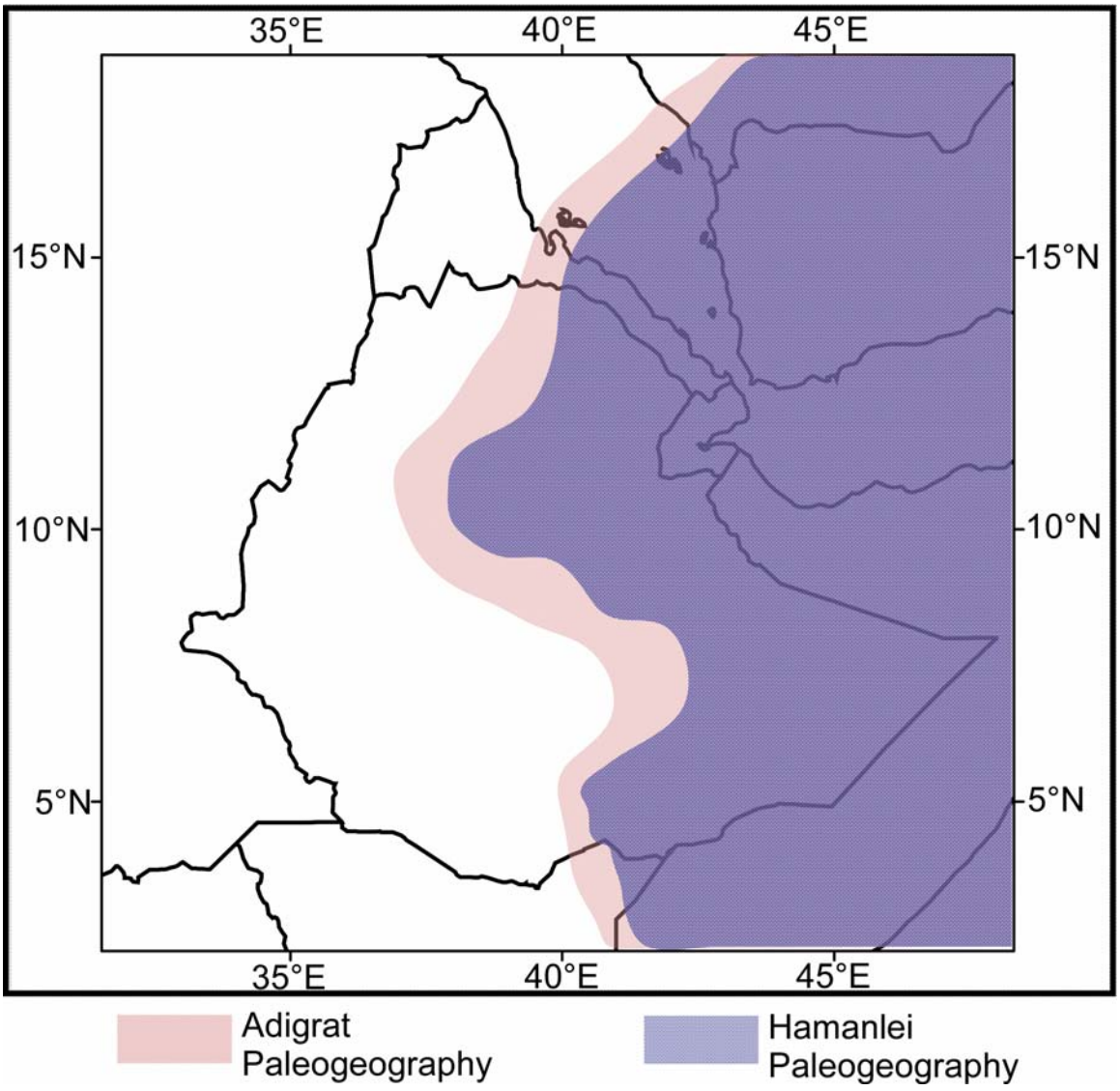

Figure 5. 4: The Bathonian –Upper Kimiridgian Adigrat Sandstone is overlain by the Hammanlei Limestone that covers a large portion of the Ogaden basin and northeastern Ethiopia and the Arabian Peninsula.

5.3 Physiography

Topography is an overprint of the geologic and geodynamic phenomena affecting a region. Ethiopia, sometimes called the roof of Africa, possesses varied topography ranging from as low as -110

m below sea level in the Dallol depression (D) in Afar to the high peak of 4620m above sea level at Ras Dashen (RD) Mountain on the Western plateau (Fig. 5.5).

The Abbay basin lies beneath the Western Ethiopian plateau basalts and is characterized by a highly dissected morphology due to the Abbay River and its tributaries (Fig. 5.5). It contains in excess of 3 km of sedimentary fill. Extensive fracturing together with widespread volcanism accompanied by out pouring of basic lava and pyroclastics initially formed the landscape of the plateau (Mohr, 1962). Extensive mountain ranges and shield volcanoes are accompanied by structurally controlled stream channels. The streams are characterized by sub-parallel drainage patterns. The highest elevations are associated with some of the shield volcanoes in the region such as Ras Dashen, Guguftu, Choke, and Guna (Fig. 5.5).

The Ogaden basin is part of the southeastern section of the lowlands of the Horn of Africa (Fig. 5.5) and includes the Somalian region and part of northeastern Kenyan (Mandera basin). In general, it is characterized by gentle rolling relief decreasing towards the south and southeast. Elevations in the Ogaden basin range typically from 500 m to 1500 m. but in some places, its elevation drops to 100 m in deeply incised valleys. The Ogaden basin is drained by two major rivers the Genale (G) and Wabi Shebelle (W), and the Fafen (F) River is seasonal.

5.4 Regional Tectonic Setting

The African continent has experienced a long and complex history of rifting. Beginning with the breakup of Gondwanaland, the rift systems that have developed in the interior of Africa were summarized by Fairhead and Green (1989). The three phases of rifting they identified are: 1) Late Paleozoic – Early Mesozoic Karroo rifting associated with the separation of Madagascar and Antarctica from east and southeast Africa (Fig. 5.2a); 2) Cretaceous rifting associated with the break-up and separation of South America from west and southwest Africa (Fig. 5.2b); and 3) Tertiary to recent rifting associated with the separation of Arabia from Africa and propagation of the East African rift (EAR) (Fig. 5.2c). The Red Sea rift, the Gulf of Aden rift and the East African rift system (EARS) meet at Lake

Abe in Afar to form the Afar triple junction. The Ethiopian rift is a major element of the EARS that is believed to modify the older NW-SE trending Karroo rift system in Ethiopia. The tectonic history of pre-Cenozoic structures in northeast Africa will be analyzed here in order to assess the relationship of the Ogaden basin to the Abbay basin based on geological and geophysical evidence.

It is important to understand older tectonic features because of the role they play in the development of relatively young features, such as the basin targeted in this study. Gondwanaland was assembled during the Neoproterozoic from two fragments, East and West Gondwanaland (McWilliams, 1981). Subsequently, the Neoproterozoic also included a protracted period of tectonism referred to as the "Pan-African" orogenic cycle (Stern, 1994 and references therein). This activity produced a complex orogen belt that Stern (1994) named the East African orogen (EAO). This orogen spans the region of the Abbay and Ogaden basins and provides a complex basement structure for the region. The rock record of events in the period between the development of the EAO and the Permian is almost completely absent so we know little about events during this time period.

The rifting that led to the break-up of Pangaea began during the Permian, and the principal effect of this tectonism was creation of significant relief between the subsiding basins along the new continental margin and adjacent sediment source areas. Sedimentation took place in subsiding prisms, and was accompanied locally by volcanism.

Rifting that extended completely across Africa (Figs.5.2b and 5.6) PRODUCED several uplift and subsidence events between the Late Cretaceous and Lower Miocene (Fig. 5.6). As a result, grabens and half grabens in southern Ethiopia and northern Kenya were created in the region in which Tertiary sedimentation took place.

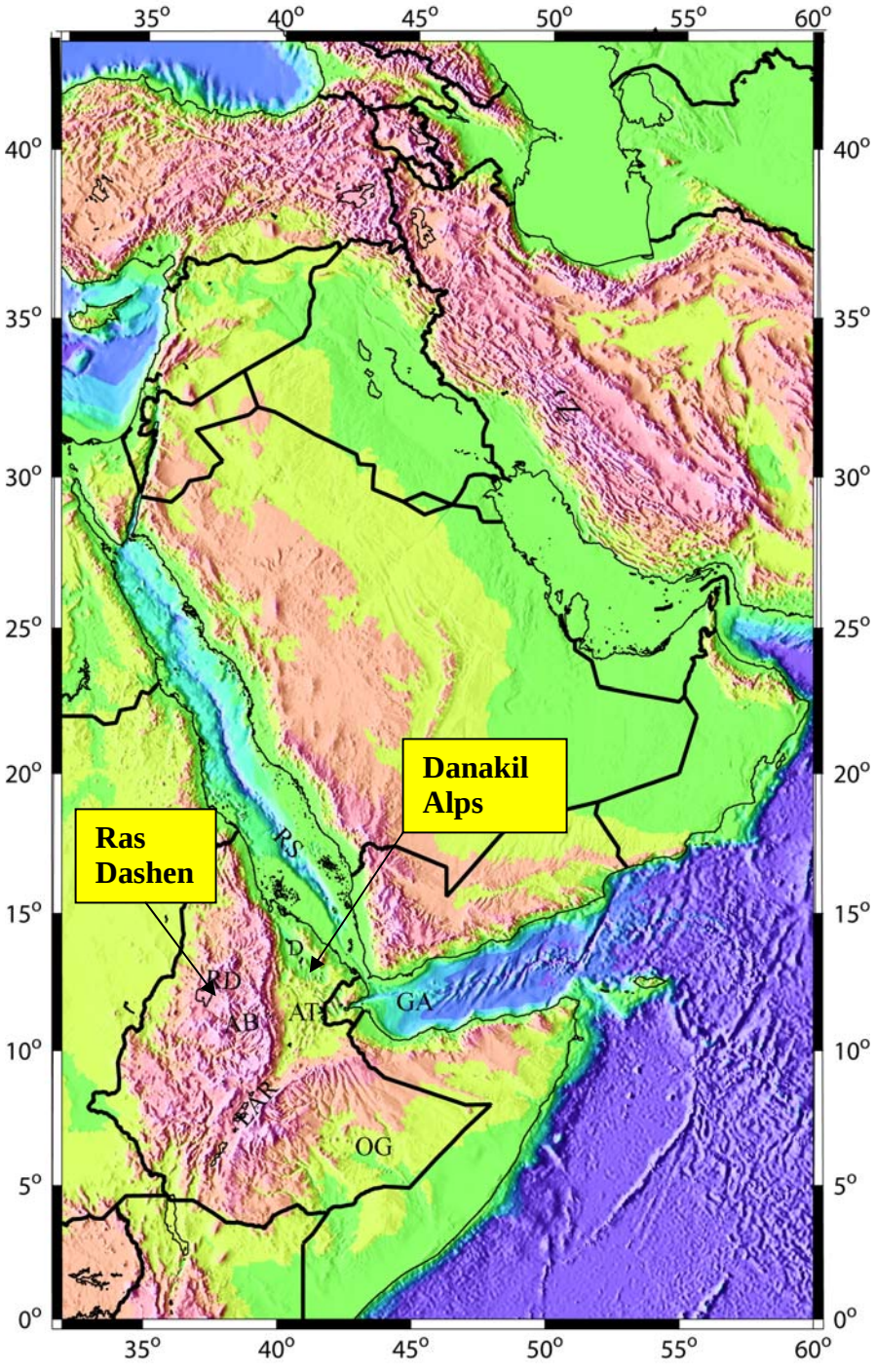

Figure 5.5: Physiography the East Africa-Middle east region. The Red Sea (RS), Gulf of Aden (GA), and the East African Rift (EAR) form the Afar triangle (AT) as the Arabian plate moves northward and subducts under the Zagros (Z) Mountains. The EAR splits the Ethiopian plateau, separating the Ogaden Basin (OG) to the southeast, the Abbay Basin (AB) to the northwest and Ras Dashen Mountain (RD).

It is generally accepted that the northern portion of the East African rift system and the Red Sea rift were activated by the impingement of plume material prior to 30 Ma. In the Abbay basin region volcanism produced flood basalts that covered all earlier sedimentary units. This plume activity then formed the tri-radial rift system of the Red Sea rift, Gulf of Aden and the Ethiopian rift. The younger rifts were developed along prior zones of weakness or structural trends that were established as a result of Precambrian and Paleozoic events (e.g. Mohr, 1967; Baker et. al, 1972; Rosendahl, 1987). The peak of rifting in eastern Africa was a Cenozoic phenomenon, and while some rifts continued extending into Late Tertiary or Recent times, many did not (Bosworth, 1987, 1989, 2005).

In summary, the different stages of rift development and sedimentation in the Abbay and Ogaden basin region are summarized as follows:

1) Peneplain stage: This stage represents the situation before the break-up of Gondwanaland. During the early and middle Paleozoic, the Pan African basement was eroded to a surface of low relief on which the Karroo Formation was sediments were deposited.
2) Intra-continental rift stage: the break up of Gondwanaland produced continental rifts along the eastern border of African continent as a result of northwest-southeast tensional stresses presumably with corresponding thinning of the continental crust.
3) Post-rift stage: This stage is known for the deposition of a basal sandstone following the rifting throughout East Africa.
4) Flooding of the craton: Following the rifting stage and syn-rift sediment deposition in the rift basins, subsidence of the continental margin was believed to occur as sea level rose. Flooding occurred in the Early Liassic time (Getaneh, 1980; Wolela, 1997)
5) Drowning of the craton: This stage is related to a major Collovain –Early Oxfordian transgression caused by Gondwanaland break up and by formation of the African continental margin. The deposition of the muddy sandstone and Upper Sandstone (Amba Aradom Clastics) units is a result of this event.

6) Regression stage: In the late Jurassic to early Cretaceous, the sea withdrew from northern and central Ethiopia, probably as a result of an intraplate effect related to the separation of Africa and South America (Bosellini, 1989).

Late stage marine transgression: As a consequence of the late stage marine transgression in the eastern Ogaden basin, late Mesozoic and Cenozoic formations such as the Urandab (shale), Gebredare (limestone), Gorrahie (evaporites), Mustahil (shale and limestone), Ferfer (anhydrite) and Belet Uen (limestone) were deposited. These younger formations are totally absent in the Abbay basin (Habtezgi, 1989; Wolela, 1997).

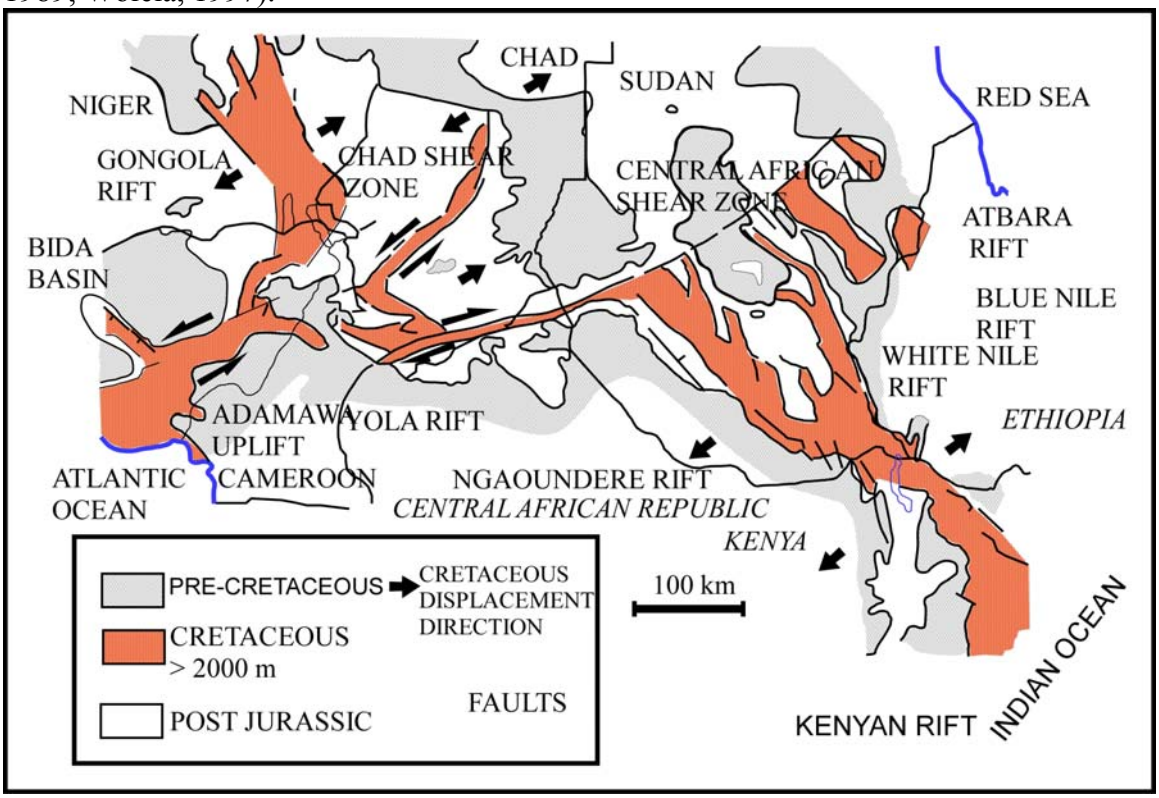

Figure 5.6: Tectonic configuration of the West and Central African rift system during Cretaceous (Modified from Fairhead and Green, 1989) development of several rift basins. Cretaceous sediments are confined within the basins. Solid arrows show direction of motion during extension

5.5 Regional Gravity Data Analysis

The gravity method was the first to be used in oil and gas exploration (Nabighian et al., 2005) and has continued to have an important place in exploration efforts, especially in salt tectonic and volcanic provinces. Thus it is one of the approaches used to assess the large region of the Ogaden and Abbay basins and the area in between them using an integrated approach based on gravity data. The area of the Abbay basin and the Ethiopian rift region is covered by volcanic products; however, there are sub-basalt sediments present that require a detailed investigation based on the available gravity data throughout the region (Fig. 5.7).

Gravity data in the study area more collected from land as well as from the seas and the Indian Ocean to aid in better understanding the regional structural features. Bouguer gravity data gridded at a cell size of 5 km have been generated for the whole East Africa (Fig.5.8). Many regional and local tectonic features are represented on this map. In this map major structures such as the Western plateau and the Eastern Plateau (A and B) are separated by the Afar triangle and Ethiopian rift (C and D). The plateaus are characterized by broad wavelength negative gravity anomalies whereas the rift which divides the two plateaus is a relative positive with the maximum positive Bouguer gravity anomaly in the Afar triple junction/triangle area.

The Ogaden basin has (E) contains gravity anomalies that represents both regional and local causative bodies. Chapter 4 contains a detailed analysis of the Ogaden basin. It is worth noting the anomaly F could be associated with a regional structure. This anomaly trends in a NW–SE direction crossing the Eastern Plateau and joins the rift in the direction of the Abbay basin. NW-SE trending anomalies on the Western Plateau are also depicted. These anomalies trend towards the Ogaden basin to the SE until they are obstructed by the Ethiopian rift and some shield volcanoes in the Western Plateau. These anomalies on both the Eastern Plateau and the Western Plateau may suggest an older fabric associated with an older rift system, which could be the original Karroo rift system.

5.5.1 Gravity Recovery and Climate Experiment (GRACE) Data

The Earth's gravity field is currently being measured by twin satellites launched in March 2002 (http://www.csr.utexas.edu/grace). The new understanding of the Earth's gravity field provided by the GRACE data may lead to natural resource evaluation and discoveries in the subsurface. The GRACE data are prepared in various forms and made available for public access on their website (http://podaac.jpl.nasa.gov/grace). We used the gravity field data that was averaged from several months of measurements and called Level-2. The gravity anomaly is computed as the difference between the observed gravity based on geoid heights and the normal gravity on the ellipsoid.

The gravity field is a simple derivative computation because the geoid is its integral. Improved GRACE data and processing methods were used to obtain more accurate data. Grace Gravity Model 02 (GGM02) is being provided as higher order (360) spherical harmonic coefficients and as gridded surfaces. As a result, the GGM2 models are more accurate than the previous models at all wavelengths.

Data from the GRACE web site were downloaded and analyzed. The main objective of this data analysis was to obtain a uniform data set based with wide regional coverage. The gravity data were gridded using a 5x5 km cell size and a gravity anomaly map of Eastern Africa and part of the Arabian Peninsula was produced (Fig. 5.8). The focus of our study is the Ogaden and Abbay basin. However, since the evolution of the Ogaden and Abbay basins, is influenced by the regional tectonics we integrated available geological and geophysical data in our analysis for this region. As a result we can clearly see features associated with major structural trends in both basins. As expected, the major structural discontinuity between the two is the Ethiopian rift.

In regard to our interest in the Ogaden basin, the most interesting aspect of this map are the NW-SE trending anomalies that are obstructed by the Ethiopian rift but appear again

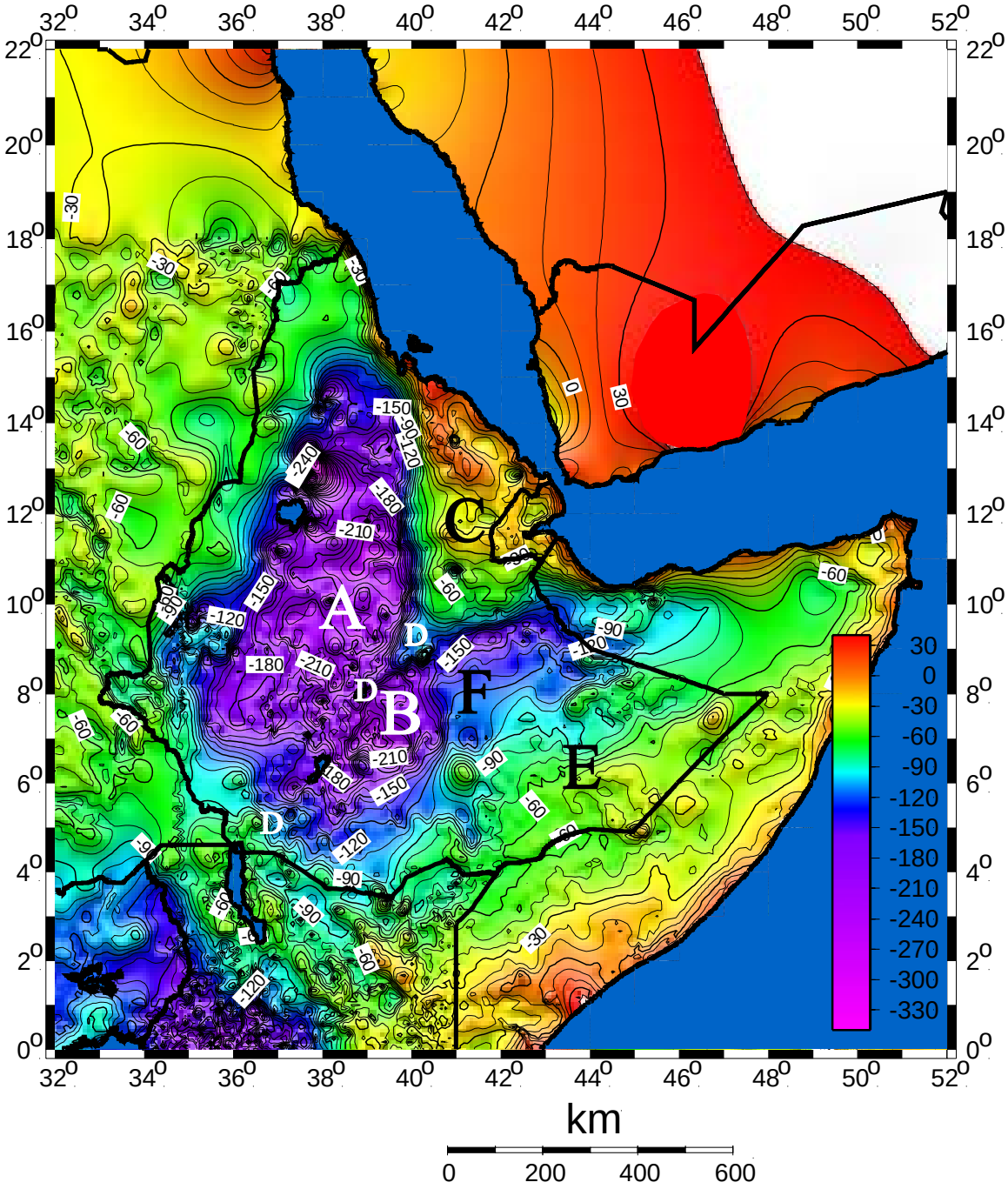

Figure 5.7: Bouguer gravity anomaly map of the Horn of Africa, showing long wavelength negative gravity anomalies on the plateaus (A and B) and relatively broad positive anomalies over the basin areas (E and F) such as the Ogaden (in Ethiopia) and the Somalia to the SE. The Sudan region to the NW also shows broad relative positive gravity anomalies are superimposed on relative negative short wavelength anomalies. Positive anomalies are seen in Afar (C) and the Ethiopian rift (D).

under the Western Plateau (Fig. 5.8). These anomalies could be due to subsurface density variations associated with rift structure that may be related to the older Karroo rift system assumed to exist in the region.

The anomalies on the Western Plateau features are spatially associated with the sedimentary outcrops of the Abbay basin (Fig. 5.8). This indicates that these features may also be associated with the older structures.

In order to take the effects of topography better, we produced a Bouguer gravity anomaly map of the region derived from GRACE data (Fig. 5.9). We used a DEM to compute the Bouguer slab correction for each GRACE grid point and used the same spacing with the same coordinate system. Fairly smooth anomalies that are similar to the data observed on the surface resulted (Fig. 5.8). The rift and plateaus (Western and Eastern) are shown as broad relative positive and negative respectively. The regions containing the Ogaden and Abbay basins contain clear shorter wavelength features trending in a NW SE Major features associated with Cretaceous rift basins such as the Anza graben, Gambela basin (western Ethiopia) and other basins in the Sudan area are clearly shown. Some of the features depicted in Sudan appear to extend southeastward into Ethiopia. The Sudan region is dominated by Cretaceous rift basins that developed orthogonal to the CASZ (Fig. 5.6). These basins are currently producing oil and exploitation is underway

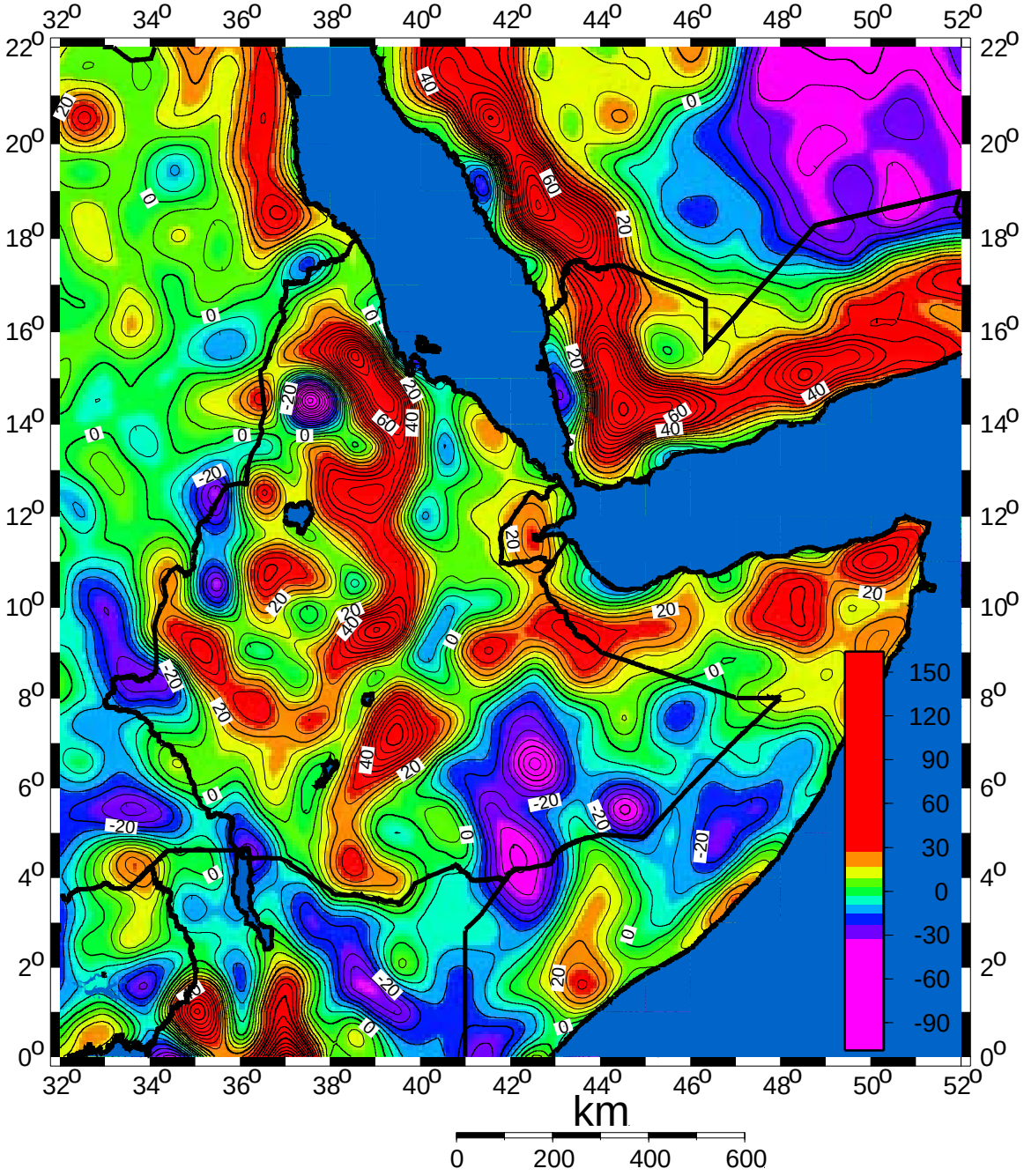

Figure 5.8: GRACE gravity data extracted from the GRACE web site. A number of structural features are depicted on this map including, the Ethiopian rift, the Eastern and Western plateaus. In the Ogaden basin, series of NS trending features are present but the main trend of the anomalies in NW.

5.5.2 Regional Isostatic Analysis

The long wavelengths components of the Bouguer gravity field correlate inversely with the long wavelengths of topography. According to the theory of isostacy, the topographic roots at the base of the crust supporting the topography cause these anomalies. These anomalies are prominent mostly in the mountainous regions and obscure anomalies caused by upper crustal structures. Regional residual separation using various techniques such as wavelength filtering can remove induced regional effects due to topography and other regional effects. However, most of these techniques eliminate features beyond the desired threshold and can not effectively separate local and regional anomalies when local features are broad like the Ogaden basin.

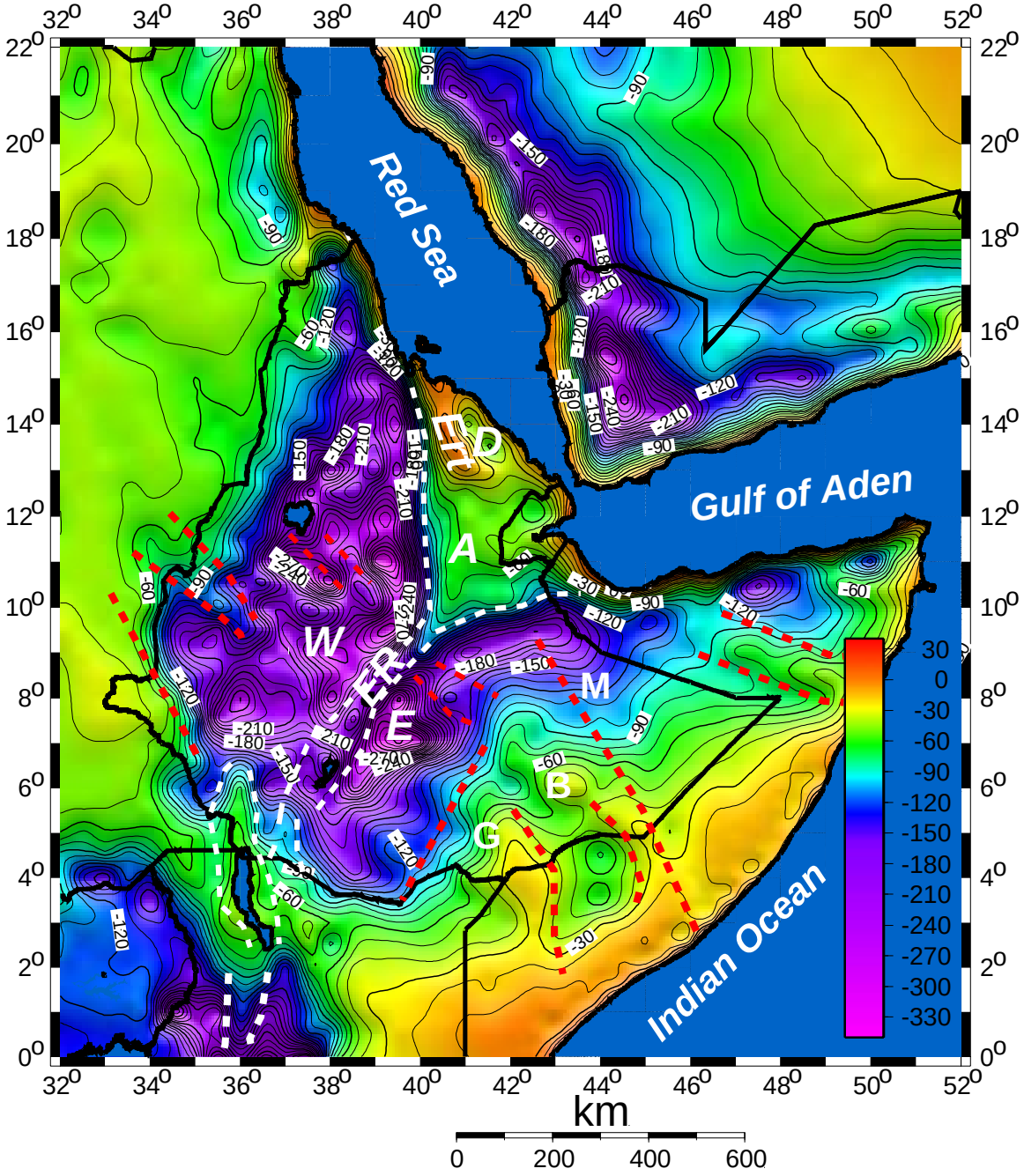

Figure 5.9: Bouguer gravity anomaly map of the Horn of Africa and Arabian peninsula derived from GRACE data. Like the land data, the Bouguer gravity data derived from the satellite data show nearly similar anomalies with smooth trends. Broad low gravity anomalies (W and E) are clearly divided by the Ethiopian rift (ER). The Maximum positive is depicted over Erte Ale region (Ert) in Afar. The broad relative positive anomalies coincide with Ogaden basin and Somalia region to the SE and the Sudan to the NW and along the Anza graben in between the Ethiopian and Kenyan domes. M is the Marda fault.

In many cases, an isostatic residual anomaly (Simpson et al. 1986) is preferable for geologic interpretation because the isostatic regional accounts for the topographic root, thereby removing the observed correlation between the Bouguer values and topography. An isostatic residual anomaly, usually better the true signature of subsurface densities related to the upper crustal structures, and it is geological and physics-based rather than mathematical. We selected the GRACE Bouguer gravity anomaly grid and produced regional and isostatic residual grids for the whole of East Africa and part of Arabian Peninsula for comparison and interpretative purposes (Figs. 5.8 and 5.9).

Our goal was to better define the nature and extent of existing structures, particularly the older rifts. Use of an isostatic correction requires a large area with a high gravity station density or satellite gravity anomalies computed with a high spherical harmonic order as well as good elevation control. We used the SRTM 900m DEM to compute the regional isostatic effect based on the formula given in section 5.5.3.

We have also incorporated a large data set from the seas and ocean for wider regional analysis to validate the isostatic computation for longer wavelengths. Since our objective in this study is to examine the relationships between the Ogaden and Abbay basins, we presented anomalies related to terrestrial regions only.

5.5.3 Isostatic residual map

The idea of isostacy is that excess mass represented by topographic loads at the surface are compensated by mass deficiencies at depth, which are commonly known as roots. An isostatic correction attempts to remove the gravity effect of isostatic roots. The depth of the roots can be estimated based on the Airy–Heiskanen model (Simpson et al., 1986). For land areas the depth of the root can be calculated based on the following formula

$$D = d_s + e(\frac{\rho_t}{\Delta\rho}) \qquad (5\text{-}1)$$

Where D = depth to the bottom of the root

d_s = the depth of the compensation for sea level compensation (35 km)

e = elevation

ρ_t = density of the topography (2670 kg m^{-3})

$\Delta\rho$ = density contrast between the root and the underlying mantle material (3300-2670 kg m^{-3})

Depth of the root over oceanic areas is defined as follows:

$$D_w = d_s - d_w(\frac{\rho_t - \rho_w}{\Delta\rho}) \qquad (5.2)$$

Where

D_w = depth of water and ρ_w = density of the water (1030 kgm^{-3})

The computation of the grid of root depths was carried out using gridded topographic and bathymetric data.

This regional isostatic anomaly (Fig. 5.10) was then subtracted from the regional Bouguer gravity (Fig. 5.9) anomaly, which was computed from the GRACE data to obtain the residual isostatic anomaly map (Fig. 5.11). The regional isostatic anomaly map shows a high amplitude long wavelength negative anomaly in central Ethiopia. Similar anomalies are associated with the Yemen volcanic massif and Kenyan dome.

The isostatic residual anomaly map (Fig. 5.11) shows shorter wavelength features as intended. For the purposes of this study, the clear NW-SE trending features that extend from Sudan across the Western Plateau and Abbay basin region and appears to connect across the Eastern Plateau into the Ogaden basin area. This observation suggests possible a structural relationship between the two basins (Abbay and Ogaden) via a NW SE trending rift system of Karroo age that may include Cretaceous effects to the northwest. The most reliable features shown as local minima in the southwest Ogaden basin indicate the presence of thick sedimentary strata in the region. This has been confirmed in Chapter 4 and is known to be the deepest section of the Karroo rift system in the Ogaden basin. This region is known to contain more than 8 km of thick sediments based on seismic reflection data.

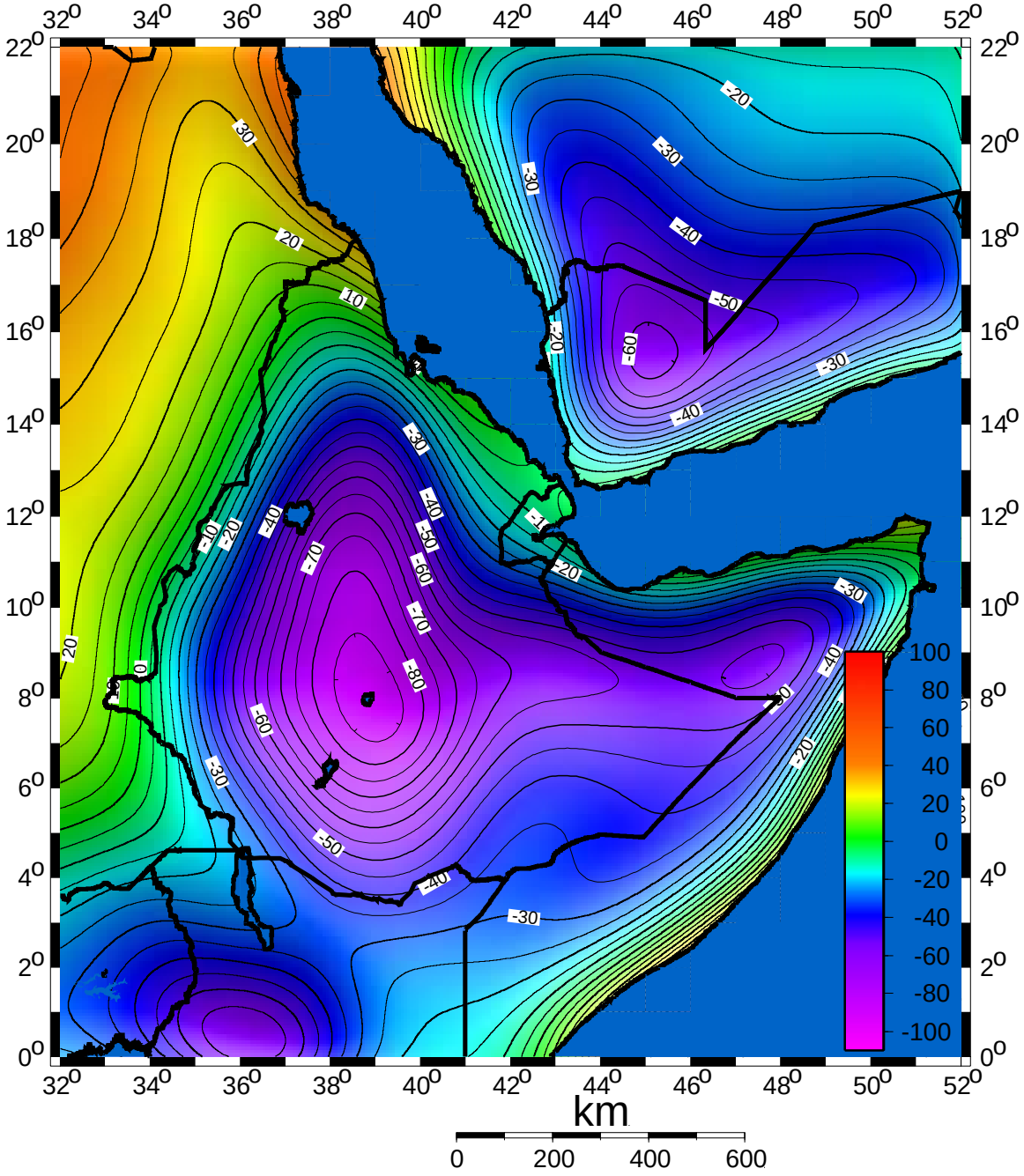

Figure 5.10: The calculated regional isostatic effect due to compensation for the topographic load map of the Horn of Africa, showing a minimum over Ethiopian plateau. The apex coincides on the MER. It also show the Kenyan dome separated by the Anza trough by a NW SE trending anomaly.

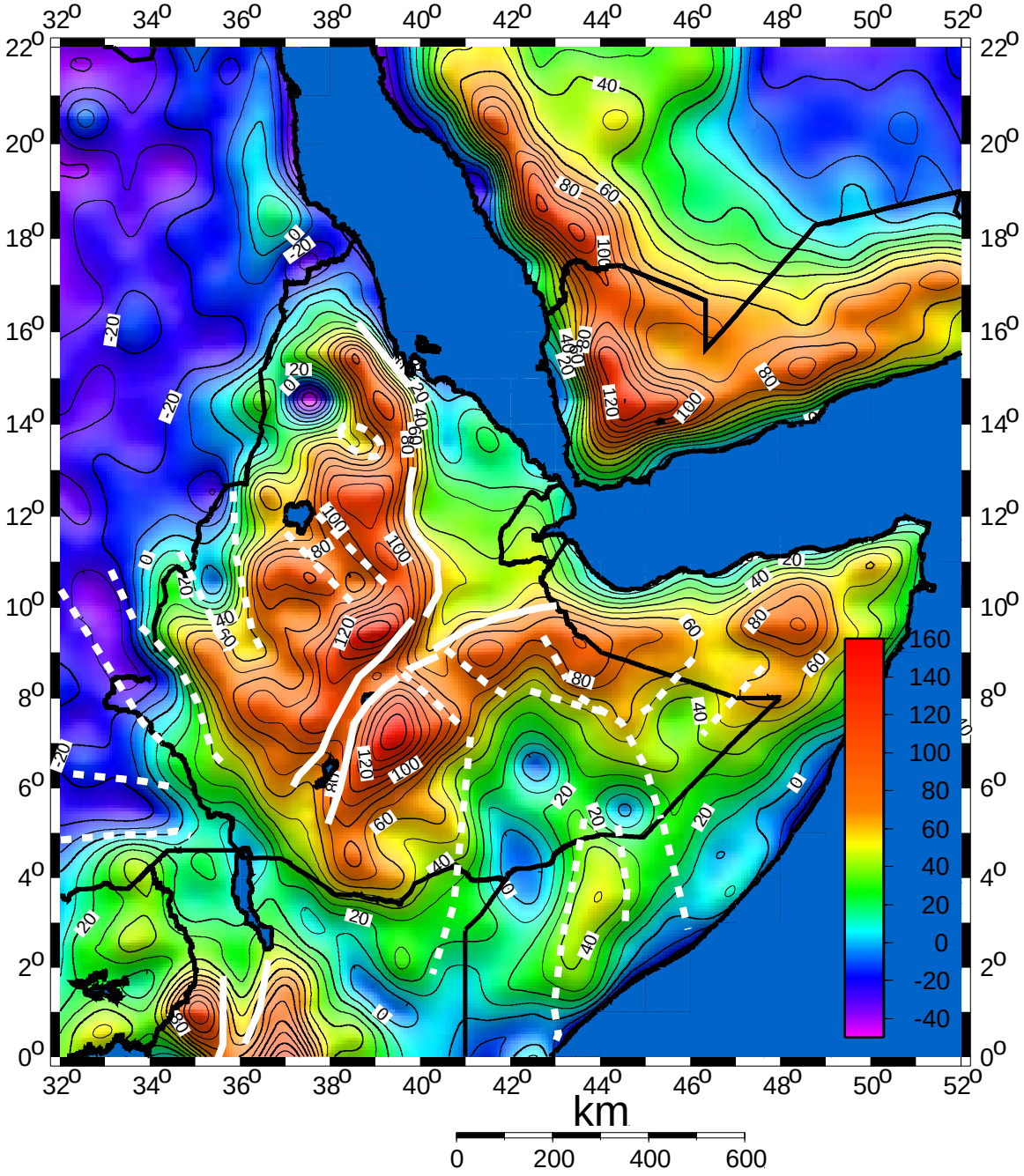

Figure 5.11: Isostatic residual anomaly map of the Horn of Africa derived from the GRACE satellite data. The northwest trending features are primary interest in this study.

5.6 Discussions and Conclusions

Various regional structural analyses based primarily on gravity data have been made a comprehensive interpretation of the Ogaden basin and its relationship with the Abbay basin. After applying various corrections for the observed ground gravity and/or satellite gravity data the best regional map for interpreting short-wavelength anomalies due to upper crustal features is the isostatic residual anomaly map (Fig. 5.11). The isostatic residual anomalies were computed by removing from a 5x5 km Bouguer anomaly grid computed for the GRACE gravity data, a regional isostatic anomaly computed for compensating masses of surface topography. However, all of the gravity anomaly maps produced from different sources show a prominent NW-SE structural trend, which is the reflection of lateral density changes in the upper portion of the crust. This could be due to a failed rift arm that extends northwestward from the Ogaden basin towards the Abbay basin. Karroo sediments would have been deposited in this aulacogen type rift basin. These structural trends are in the direction of a rift that was suggested by some researchers and consulting firms (e.g. Wolela, 1997; BEICIP, Franlab, 1998) based on sparse control. Our map makes a strong case for the presence of structures that are otherwise obscured by the Cenozoic Main Ethiopian rift and the flood basalts that covered the Western Plateau and the Eastern Plateau. This MER thinned the crust and modified earlier structures via volcanic segmentation along its axis (e.g., Basset, Kone volcanic segments). Also shield volcanoes on the Western Plateau produce local high amplitude short wavelength positive anomalies that obscure older features. The EAGLE controlled source experiment results delineated an underplated lower crustal layer beneath the Western Plateau (McKenzie et al., 2005). This may also have impacted the older rift system close to the western Ethiopian rift flank. In general, it is possible to see a relationship between the Abbay and Ogaden basin in relation to the geological correlation from stratigraphic comparisons. Our gravity analysis has shown that there is a structural relationship and attests to the usefulness of potential field data in delineating regional structures, in the absence of regional seismic refraction or reflection data. The various gravity maps we produced showed a fairly broad zone of northwest trending anomalies. However, the rift system may be narrower, and restricted to the NNW part of the Ogaden

basin, and joining the Abbay basin from there. However, further detailed analysis and more data can improve this deduction and provide a better economic resource evaluation. Therefore, we suggest that the rift system was continuous up to the Abbay basin as shown in an enlarged version of the residual isostatic gravity anomaly map (Fig. 5.12).

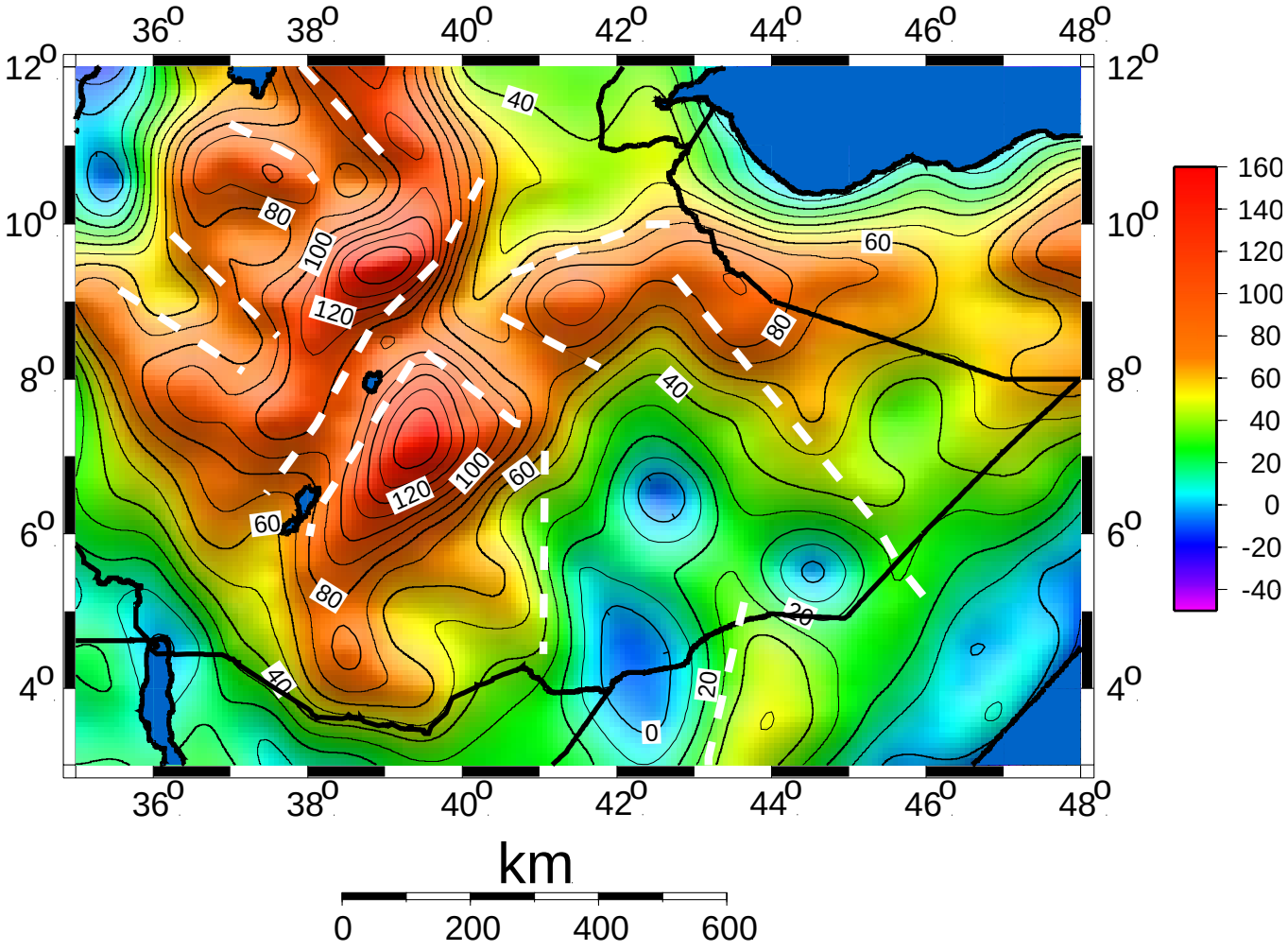

Figure 5.12: Enlarged in part of the Eastern African isostatic residual anomaly map derived from GRACE gravity data, showing structural relationship of the Abbay basin, Ogaden basin and the Ethiopian rift as well as other rift basins.

Chapter 6: Conclusions

Integrated geophysical data processing and interpretation from the Ethiopian rift and adjacent areas is presented in this dissertation. Gravity, remote sensing, digital elevation mapping (DEM), and refraction data were integrated and processed in order to investigate the crustal structure variation of the Ethiopian rift and adjacent areas. Regional and residual Bouguer gravity anomaly maps, as well as various filtered maps, segregate the plateaus and the rift areas. Localized volcanic segments, volcanic complexes and calderas are associated with relative gravity highs. Most of these features are depicted as short wavelength, high amplitude anomalies

New evidence for crustal structure variations along the axial direction of the northern sector of the EARS was obtained by integrated modeling of gravity profiles employing a 2.5 D approach. The axial variations were constrained by and tied to a series of profiles crossing the rift. The axial model was constrained by previously processed seismic data from Kenyan rift (KRISP project) and the new EAGLE project results from Ethiopia. The crust thickness is about 26 km in the Afar triple junction. It gradually thickens to 35-40 km in MER, and southward, the crust thins and attains a minimum thickness of about 22 km in the Turkana area. Again the crust thickens gradually towards the central part of the Kenyan rift via underplating. Here it attains a thickness of 35 km. The broad crustal thinning in Afar could be due to mantle plume uplift and magma assisted extensional processes, while in Turkana it could be due to multiple episodes of rifting and extension.

The cross profiles across the Ethiopian rift and the Eastern and Western Plateaus reveal relatively narrow zone of crustal thinning beneath the rift while broad region of thinned crust exists along the southern Afar profile. This is mostly due to a mantle plume uplift causing extensive melting, volcanism and broad extension in the region. The MER shows narrowly thinned crust and relatively thicker crustal formation. This may be due to minimum crustal modification and minimal extension in the MER. The western plateau shows thicker crust that may be due to underplating causing elevated regions by heating and expansion in volume.

Geological and geophysical data including remote sensing images, gravity anomalies and DEM were used to assess the thickness of Mesozoic sedimentary strata beneath the volcanic cover and geometry of the Abbay basin. The integration of all these data indicate sedimentary strata extend further east than previous thought and gravity modeling indicates that these strata attain a maximum thickness of 3 km. Previously subtle geological lithologic units that outcrop in the canyons are distinguished clearly based on the classification analysis of satellite imagery and support the geophysical interpretation that these geologic units extend further to the east beneath the basalt cover.

The break up of Gondwanaland in Permo-Triassic to Late Jurassic-Cretaceous time led to the opening of the Indian Ocean and initiated the formation of sedimentary basins along the newly formed margins of eastern Africa. The rift basins that generally trended N-S was filled with sediments of the Karroo Group. The Karroo rift system in Ethiopia has been speculated to form a tri-radial rift... However, Karroo strata are not exposed on the surface but are confirmed to present by deep drilling results in the Ogaden basin. In this study, the presence of a NW-SE trending Karroo rift system in Ethiopia strongly supported based on geophysical evidence. This rift system appears to connect the Ogaden and Abbay basins suggesting the two basins similar geologic histories.

Integrated geophysical and geological data processing interpretations from the Ogaden basin provided several new types of information. Gravity profile modeling and seismic reflection data interpreted in this study indicate that the total sedimentary package thickness is more than 8 km in the southwest Ogaden basin in the area of Genale River. The thickest part of the sediment is attributed to Karroo strata. Faulted structures are associated with the basement and are recognized based on seismic data. The faulting system suggests that the evolution of the Ogaden basin is associated with extensional phenomena. Sequence stratigraphic analysis indicates ideal target for the development of traps in the Karroo Group. The Calub Sandstone Formation appears to pinch out against the basement earlier than the rest of the Karroo group sediments. Also structures associated with faults and channels are important features for hydrocarbon habitat and are identified in our interpretation.

New depth analysis based on 3D Euler deconvolution applied the detailed gravity data in the northeastern Ogaden reveals graben and horst like structures, which could be important hydrocarbon habitats. Attribute analysis reveals physical properties of the different lithologic unit and affirms the continuity of horizons that were subtle in the conventional seismic trace display. Also some lithologic units such as the Calub Sandstone and Adigrat Sandstone exhibit unique properties in quality factor analysis and amplitude strength analysis, suggesting that they may be associated with hydrocarbons such as oil or gas. In addition to these factors, they may also have the good porosity for fluids. This optimistic assessment is supported by existing discoveries and shows in the Ogaden basin such as the Calub and Hilala gas fields and oil shows in other areas. In these areas the Adigrat and Calub Sandstones are quality reservoirs known as the upper and lower reservoirs, respectively. Another positive result from the standpoint of petroleum exploration was that of reprocessing seismic reflection data has eliminated reverberations and has improved the continuity of reflection horizons. This result suggests that reprocessing of exiting seismic reflection data with modern software packages can make useful improvements to the data. The negative residual gravity anomalies of the NE Ogaden basin can be attributed to Cretaceous sediments in graben-like structures and ranges up to 5 km thickness. Modeling results based on profiles extracted from residual gravity anomalies reveal variable sedimentary thicknesses and dip orientation of formations in the Ogaden basins, which is attributed to the variable structural and stratigraphic setup of the basin.

Satellite gravity data were used to evaluate regional features in Ethiopia and adjacent areas has been compared with the available land data results. Comparable results were found to be in agreement, delineating sedimentary basins as gravity lows. Most of these anomalies depicted the known sedimentary basins such as the Ogaden basin, Mekele basin, Abbay, Metema and Gambela basins fairly well. Major structures such as the Ethiopian rift and the Afar triple junction are well resolved in various satellite anomaly maps and boundaries of tectonic features and their trends are demarcated. Possible Cretaceous rift systems from the Sudan boarder appear to extend into Ethiopia and may indicate areas

with hydrocarbon potential regions. Other possible Cretaceous graben and horst structures are delineated within the northeastern Ogaden basins and their thickness may be up to 5 km from $2.5D$ modeling results. The Abbay and Ogaden basin relationship is assessed. Based on results of a residual isostatic gravity anomaly map of Ethiopia and adjacent areas, a northwest trending structural grain is present. This could be a failed arm of a rift that connected the Ogaden and Abbay basins during Permian time.

References

Acocella V. and T. Korme, 2002. Holocene extension direction along the Main Ethiopian Rift, East Africa. Terra Nova, Vol. 14, 191-199.

Alconsult, In. Ltd., 1996. The Hydrocarbon Potential of the Ogaden Basin, Ethiopia. Petroleum Operations Department, Ministry of Mines and Energy, Addis Ababa, Ethiopia.

Alemu, A., 1992. The gravity field and crustal structure of the Main Ethiopian rift. PhD Thesis, Royal Institute of Technology, Sweden, 126 pp.

Allen, A. Tadesse G. 2003. Geological setting and tectonic subdivision of the Neoproterozoic orogenic belt of Tuludimtu, western Ethiopia, Journal of African Earth Sciences, *3*6, 329-343(15)

Arkell, W. T., 1956. Jurassic Geology of the World. Henry Publishing Company Inc, New York, 806 pp.

Asrat A, Barbey P, Gleizes G., 2001. The Precambrian geology of Ethiopia: a review. Africa Geoscience Rev. v.8: 271–288

Aubry, A., 1886. Observations geologiques sur le royaume de Choa et les pays Gallas. Comp. Rend. Acad. Sci. France.

Ayalew D., Yirgu. G., 2003. Crustal contribution to the genesis of Ethiopian plateau rhyolitic ignimbrites: basalt and rhyolite geochemical provinciality. J Geol Soc Lond 160:47–56Baker, 1996,

Baker , B. H., Wohlenberg, G. J., 1971. Structure and evolution of the Kenyan rift valley. Nature, 229, 583-542.

Baker, B.H., Mohr, P. A., and Williams, L.A.J., 1972. Geology of the eastern rift system of Africa. Geological Society of America, Special paper. 136, 67p.

Barberi, F., Varet, J. 1977. Volcanism of Afar: small-scale plate tectonics implications. Bull. Geol. Soc. Am. 88. 1251-1266.

Barnes, S. U., 1976, Geology and oil prospect of Somalia, East Africa: AAPG Bulletin, v.60, p.389 – 413.

Bastow, I.D., G.W. Stuart, J.-M. Kendall, and C.J. Ebinger, 2005. Upper mantle seismic structure in a region of incipient continental breakup: northern Ethiopian rift, *Geophys. J. Int.*, *162, 479-493*.

BEICIP Franlab, 1998. Petroleum potential of Ethiopia. Petroleum Operations Department, Ministry of Mines and Energy, Addis Ababa, Ethiopia.

Berkhemer, H., Baier, B., Bartlesen, H., Behle, A., Burkhardt, H., Gebrande, H., Makris, J., Menzel, H., Miller, H. and Vees, R. 1975. Deep seismic soundings in Afar region on the highlands of Ethiopia, in Afar Depression of Ethiopia., edited by A. Pilger and A. Rosler, 89-107, E. Schweizerbart, Stutgart. West Germany.

Beyth, M., 1972. Paleozoic sedimentary basin of Mekele Outlier, North Ethiopia. American Association of Petroleum geologists, Bull., 12: 2426-2639

Blakely, R. J., 1996. Potential theory in gravity and magnetic applications Cambridge University Press, Cambridge.

Blanford, W. T., 1869. On the geology of a portion of Abyssinia. *Quart. J. Geol. Soc. London*, **25:** 401-406.

Boccaletti, M., Getaneh, A., and Tortorici, L., The Main Ethiopian Rift: an example of oblique rifting. Annales Tectonicae, VI, n.1, 20-25, 1992.

Boccaletti, M., Bonini, M., Mazzuoli, R., Abebe, B., Piccardi, L., Tortorici, L., 1998. Quaternary oblique extensional tectonics in the Ethiopian Rift (Horn of Africa). Tectonophysics 287, 97-116.

Bonini, M., Corti, G., Innocenti, F., Manetti, P., Mazzarini, F., Abebe, T. and Pecskay, Z., 2005, Evolution of the Main Ethiopian Rift in the frame of Afar and Kenya rifts propagation, Tectonics 24, TC1007 doi:10.1029/2004TC001680

Bosellini, A. (1986): East Africa continental margins: Geology, 14, 76-78.

Bosellini, A. (1987): The continental margins of Somalia: their structural evolution and sequence stratigraphy - GEOSOM 87, Int. Meeting. Geology of Somalia and surrounding regions, abstracts, 38-39; Mogadishu, (Somali Nat. Univ).

Bosellini, A. (1989): The continental margins of Somalia: Their structural evolution and sequence stratigraphy.- Mem. sc. Geol., XLI, 373-458, Padova.

Bosellini, A. (1992): The continental margins of Somalia.- In: WATKINS, J.S., ZHIQIANG, F. & MC MILLEN, K.J. (eds.): Geology and Geophysics of Continental Margins.- Am. Assoc. Petrol. Geol. Mem., 53, 185-205, Tulsa, Oklahoma.

Bossellini, A., Russo, A., and Assefa, G., 2001. The Mesozoic succession of Dire Dawa, Harar province, Ethiopia. Journal of African Earth Sciences. 32, 403-417.

Bosworth, W., and C. K. Morley, 1994. Structural and stratigraphic evolution of the Anza Rift, Kenya: Tectonophysics, 236, 93-115.

Bosworth, W., P. Huchon and K. McClays, 2005. The Red Sea and Gulf of Aden Basins. Journal of African Earth Sciences, 43, 334-378.

Briggs, I. C. 1974. Machine contouring using minimum curvature. Geophysics, 39, 39-48.

Brown, A.R. (1991). Interpretation of three-dimensional seismic data. AAPG. Mem. 42. 1-341.

Browne, S. E., Fairhead, J. D., and Mohamed, I, I., 1985, Gravity study of the White Nile Rift, Sudan, and its regional tectonic setting: Tectonophysics.

Cady, W. J., 1980. Calculation of gravity and magnetic anomalies of finite –length right polygons prism. Geophysics, 45, 1507-1512.

Chernet, T., Hart, W. K., Aronson, J. L. and Walter, R.C. 1998. New age constraints on the timing of volcanism and tectonism in the northern Main Ethiopian Rift-southern Afar transition zone (Ethiopia). Journal of Volcanological and Geothermal Research, 80, 267-280.

Coffin, M. F., and P.D. Rabinowitz, 1983, East African Continental Margin transect , in A. W. Bally, ed., Seismic expression of structural styles: A picture and world atlas AAPG Studies in Geology, V.2, p.2.3,22-23.3.29.

Coffin, M. F., and P.D. Rabinowitz, 1987, Reconstruction of Madagascar and Africa: Evidence from the Davie fracture zone and western Somali basin: Journal of Geophysical Research, v.92, p. 9385-9406.

Coffin, M.F., and Rabinowitz, P.D., 1988. Evolution of the East African continental margin and the Western Somali basin, Geological Society of America Special Paper 226: 78 pp.

Chorowicz, J., Collet, B., Bonavia, F., Korme, T., 1994. NW to NNW Extension direction in the Ethiopian rift deduced from the orientation of extension structures and fault-slip analysis: Geol. Soc. Am. Bull. 105, 1560-1570.

Courtillot. V., J., Achache F., Landre, N. Bonhommet, R. Montigny and G. Feraud , 1984. Episodic spreading and rift propagation. New paleomagnetic and geochrnologic data from the Afar nascent passive margin. J. Geophys. Res. 89, 3315-3333.

Courtillot. V., J., Juupart, C., Manighetti, I., Tapponier, P. and Besse, J. 1999. On causal links between flood basalts and continental break-up. Earth and Planetary Science Letters. 166, 177-195.

Dainelli, G. 1943. Geolgia dell' Africa Orientale. Accad. Italia, Centro Studi. AOI. Vol. 4.

Davidson, A.1983. The Omo river project, reconnaissance geology and geochemistry of parts of Illubabor, Kefa, Gemu Gofa and Sidamo. Ministry of Mines and Energy. Ethiopian Institute of Geological Surveys, Bulletin 2, 1-89.

Davidson, A. and D. C. McGregor, 1976. Palynomorphs indicating Permian rocks in Ethiopia. Nature, Vol. 262, 371-373.

Di Pola, G. M., 1972, Ethiopian Rift Valley (between 7^{o} and 8^{o} $40^{'}$ lat. North): Bulletin Volcanologique, v.36, p.517-560.

Dugda, M., Nyblade, A., Julia, J, Langston. C., Ammon, C., and Simiyu. S. 2005. Crustal Structure in Ethiopia and Kenya from Receiver Function Analysis: Implications for the development in Eastern Africa. Journal of Geophysial Research. 110B101303.

Ebinger, C. J., Ibrahim, A., 1994. Multiple episodes of rifting in Central and East Africa: A re-evaluation of gravity data. Geologische Rundschau 83, 689-702.

Ebinger , C.J. and Casey, M. 2001. Continental Breakup in magmatic provinces: An Ethiopian example. Geology, 29, 527-530.

Ebinger, C. J. and Ibrahim, A. 1994. Multiple episodes of rifting in Central and East Africa: a re-evaluation of gravity data. Geologische Rundschau, 83, 689-702.

Ebinger, C. J., T. Yemane, S. Tesfaye, S. Kelley, D. J. Harding, and D.C. Rex, 2000. Rift Deflection, migration, and production: Linkage of the Ethiopian and Eastern Rifts, Africa. Geological Society of America Bulletin: Vol. 112. No.2.pp.163-176.

Ebinger, C. J., Bechtel, T.D., Forsyth, D. W. and Bowin, C. O., 1989. Effective elastic thickness beneath the East African and Afar plateaus and dynamic compensation of the uplifts. J. Geophys. Res., 94, 2883-2901.

Fairbridge, R. W., 182. The Fracturing of Gondwanaland. In: R. A Scrutton and M. Talwani (eds.) The Ocean Floor. New York, John Wiley, 297-315 pp.

Fairhead, J. D. & Okereke, C. S. (1987). A regional study of the West African Rift system in Nigeria and Cameroon and its tectonic interpretation. *Tectonophysics* 143, 141–159

Fairhead, J.D., 1992. The West and Central African Rift systems: Foreword: Tectonophysics, v. 213, p. 139–140.

Fairhead J. D. and Green C. M. (1989). Controls on rifting in Africa and the regional tectonic model for Nigeria and East Niger rift basins. J. Afr. Earth Sci. 8. 231-249.

Fairhead J. D., Green, C. M., and Dickson, W. G., 2001a. Oil exploration from space: fewer places to hide. First Break, 19. 9, 514-519.

Fernandes R. M. S., R.A.C. Ambrosius, R. Noomen, L. Bastos, L. Combrinck, J. M. Miranda, W. Spakman, 2004. Angular velocities of Nubian and Somalia from continuous GPS data: implications on present-day relative kinematics. Earth and Planetary Science Letters 222, 197-208.

Ferris, C., (1972). Use of gravity meters in search for traps. Mem. Am. Ass. Pet. Geol. 16. 252-270.

Flores, G., 1973. The Cretaceous and Tertiary Sedimentary basins of Mozambique and Zulu land. In: G. Blant (ed.), Sedimentary basins of the African coasts. Pt.2. South and east coast: Paris, assoc. African Geol. Surveys 81 -111 pp.

Floyd F. Sabins, 2000, Remote Sensing Principles and Interpretations, Third Edition, W. H. FREEMAN AND COMPANY, New York.

Floyd F. Sabins, 1998, Remote sensing for petroleum exploration, Part 1, The Leading Edge.

Floyd F. Sabins, 1998, Remote sensing for petroleum exploration, Part 2, The Leading Edge.

Gebreyohannes Habtezgi, 1989. Facies, Depositional Environments, Diagenesis and Hydrocarbon Potential of the Jurassic Hammanlei Formation (Carbonate –Evaporite Rocks) in Ogaden Basin, Southeast Ethiopia. M.Phil. Thesis, University of Reading, United Kingdom.

Getaneh, A., 1979. Clay mineralogy of the Mesozoic sequence in the upper Abbay (Blue Nile) River Valley region, Ethiopia. *Sinet, Ethiop. J. Sci.,* **3:** 37-65.

Getaneh, A., 1980**.** Stratigraphy and sedimentation of the Gohatsion Formation (Lias-Malm), Abay River basin, Ethiopia. *Senet, Ethiop. J. Sci.* **3:** 87-110.

Getaneh, A**.,** 1981. Gohatsion Formation: A new Lias-Malm lithostratigraphic unit from the Abay River basin, Ethiopia. *Geosci. J.,* **2**: 63-88.

Getaneh, A., 1991. Lithostratigraphy and environment of deposition of Late Triassic to Early Cretaceous sequences of the central part of Northwestern Plateau, Ethiopia. *N. Jb. Geol. Palaont. Abb.* 182 (3): 255-284.

Geological Survey of Ethiopia, 1976, Oil and gas in Ethiopia, Geological Survey of Ethiopia Mineral Circular 4.

Girdler, R. W., 1992. The Afro-Arabian rift system: An overview. Tectonophysics 197, 139-153.

Hammer, S., 1939. Terrain corrections for gravity stations. Geophysics, 4, 184-194.

Hay, D. E., Wendlandt, R. F., Keller, G. R., 1995b. The Origin of Kenya rift plateau type flood phonlites: Integrated petrologic and geophysical constraints on the evolution of the crst and upper mantle beneath the Keyna Rift. J. Geophys. Rs. 100. 10549-10557.

Hayward, N. J., Ebinger, C. J., 1996. Variations in the along axis segmentation of Afar rift system, Tectonics 15, 244-257.

Hendrie, D. B., N. J. Kusznir, C. K. Morley, C. J. Ebinger, 1994. Cenozoic extension in northern Kenya: a quantitative model of rift basin development in Turkana region. Tectonophysics, 236, 409-438.

Hunegnaw, A., Sage, L. & Gonnard, R. (1998): Hydrocarbon potential of the intracratonic Ogaden Basin, SE Ethiopia.- J. Petrol. Geol., 21, 401-425,

Jepsen, D. H. and Athearn, M. J., 1961. Geological plan and section of the left bank of Blue Nile Canyon near crossing of Addia Ababa-Debre Markos road. U.S. Department of Interior, Ethiopia's Water Resources Department, Addia Ababa.

Jelenc, D.A., 1966, Mineral Occurrences of Ethiopia, Ministry of Mines, Addis Ababa, Ethiopia.

Jepsen, D. H. and Athearn, M. J., 1964**.** Land and water resources of the Blue Nile basin. Appendx II, 221p., Geology, U. S. Dept. Interior, Addis Ababa.

Kazmin, V., 1972. Geological Map of Ethiopia. Geological Survey Ethiopia, Addis Ababa.

Kazmin, V., 1975. Explanation of the Geological Map of Ethiopia. Ethiopian Geol. Surv. Bull., 1: 1-15.

Kazmin, V., Shiferaw A. and Balcha, T. 1978. The Ethiopian Basement and possible manner of evolution. Geologische Rundschau 67, 531-546.

Keller, G. R. Mechie., J Braile, L. Mooney. W. D., and Prodehl, C., 1994. Seismic structure of the upper most mantle beneath the Kenyan Rift. Tectonophysics, 236. 201-216.

Keller, G.R., Harder, S.H., O'Reilly, B.R., Mickus, K., Tadesse, K., Maguire, P.K.H., 2004. A preliminary analysis of crustal structure variations along the Ethiopian rift. EARS conference, June 20-24, Addis Ababa, Ethiopia.

Kendall J., -M., G. W. Stuart, C. J. Ebinger, L. D. Bastow and D. Keir, 2005. Magma –assisted rifting in Ethiopia. Nature, 433, 146-148.

Kent, P. E., 1974. Continental Margins of east Africa: A region of vertical movements. In A. Burk and C. L. Drake (eds), The Geology of Continental Margins. Springer – Verlang, New York, 313 -320 pp.

Ketsela Tadesse, 1996, Seismic data Processing and interpretation from the Ogaden Basin, Ethiopia. MPhil. Thesis. The University of Leeds, United Kingdom.

Kieffer, B., Arndt, N., Lapierre, H., Bastiern, F., Bosch, D., Pecher, A., Yirgu, G., Ayalew, D., Weis, D., Jerram, A. D., Keller, F., and Meugniot, C., 2004. Flood and Shield basalts from Ethiopia: magmas from the African Superswell. Journal of Petrology, 45, 793-834.

Klimentos T. 1995. Attenuation of P- and S-waves as a method of distinguishing gas and condensate from oil and water. *Geophysics* **60**, 447–458.

Mackenzie, G. D., Thybo, H. and Maguire, P. K. H. 2005. Crustal velocity structure across the Main Ethiopian rift: Results from 2-dimensional wide angle seismic modeling. Geophysical Journal International. 162. 994-1006.

Maguire, P. K. H, G.R. Keller, S.L. Klemperer, G.D. Mackenzie, K. Keranen, S. Harder, B. Oreilly, H. Thybo, L. Asfaw, M.A. Khan and M. Amha, 2006. Crustal structure of the northern Main Ethiopian Rift From the EAGLE controlled-source survey; a snap shot of incipient lithospheric

break-up. From: Yirgu, G. Ebinger, C. J. and Maguire P.K. H. (eds). The Afar Volcanic Province within the East African Rift System. Geological Society of London, Special Publication. 259. 269-291.

Mahatsente, R., Jentzsch, G., Jahr, T., 1999. Crustal structure of the Main Ethiopian Rift from gravity data: 3-dimensional modeling. Tectonophysics 313, 363-382.

Makris, J., Menzel, H., Zimmermann, J., Goiun, P., 1975. Gravity field and crustal structure of northern Ethiopia. In: Pilger, A., Rosler, A. (Editors), Afar Depression of Ethiopia. Schweizerbart. 135-144. Stuttgart.

Makris, J. and A. Ginzburg, 1987. The Afar Depression: Transition between continental rifting and sea floor spreading. Tectonophysics. 141, 199 – 214.

Mamo, T., 2004. Mapping the Crust-Mantle Boundary Beneath Afar Depression. Gondwana Research, V. 7, No. 3, PP. 855-861.

McConnel, R. B., 1972. The geologic development of the rift system of eastern Africa. Geol. Soc. Am., Bull. 2549-2572.

McKenzie G. D., H. Thybo and P. K. H. Maguire, 2005. Crustal velocity structure across the Main Ethiopian Rift: results from two-dimensional wide-angle seismic modeling. *Geophys. J. Int.* (2005) **162,** 994–1006

McWilliams, M. O., 1981. Palaeomagnetism and Precambrian tectonic evolution of Gondwana. In Precambrian Plate Tectonics, ed. A Kroner, pp.649-87. msterdam: Elsevier.

Mechie, J. and Prodehl, C., 1988. Crustal and uppermost mantle structure beneath the Afro-Arabian rift system. In: X. Le Pichon and J.R. Cochran (Editors), The Gulf of Suez and Red Sea Rifting. Tectonophysics, 153: 103-121.

Mechie, J., Keller, G.R., Prodehl, C., Gaciri, S., Braile, L. W., Mooney, W. D., Gajewski, D., Sandmeier, K. J., 1994. Crustal structure beneath the Kenya Rift from axial profile data. In:

Prodehl, C., Keller, G. R., Khan, M. A., (Eds.), Crustal and Upper Mantle Structure of the Kenya Rift. Tectonophysics, 236. 179-199.

Mechie.J., Keller, G.R., Prodehl. C., Khan. M. A. and Gaciri, S. J., 1997. A model for the structure, composition and evolution of the Kenya rift. In Fuchs. K., Alther. R., Muller, B., Prodehl. C. (eds.), Structure and Dynamic Processes in the Lithosphere of Afro-Arabian Rift System. Tectonophysics. 278, 95-119.

Mengesha Tefera, Tadiwos Chernet and Workneh Haro, 1996. Geological Map of Ethiopia. GSE, Addis Ababa, Ethiopia.

Mickus, K., Tadesse, K., Keller, G., and Oluma, B., 2007. Gravity analysis of the Main Ethiopian Rift. Journal of African Earth Sciences .
.

Mohr, P.A., 1962. The geology of Ethiopia. Addis Ababa University Press, 268p.

Mohr, P. A. 1962b. The Ethiopian rift system. Bull. Geophysical Obs. Addis Ababa 5, 33-62.

Mohr. P. A., Gouin, P. 1967. Gravity traverses in Ethiopia. Bulletin of Geophysical Observatory (Ethiopia) 10. 15-52.

Mohr, P. A., 1983. Ethiopian Flood basalt province. Nature. 303, 577-584.

Mohr, P. and Zanettin, B., 1998. the Ethiopian flood basalt province: in Macdougall, J. D., ed., Continental flood basalts: Dordecht. Kluwer Academic. P. 63-110.

Montelli, R., G., Nolet, F. Dhlen, G. Masters. E. Engdahl, and S. H. Hung, 2004. Finite frequency tomography reveals a variety of plumes in mantle. Science. 303, 338-343

Moore. J. M., and Davidson, A., 1978. Rift structure in Southern Ethiopia: Tectonophysics, v.46, p. 159-173.

Morelli, C., (ed.), 1974, The International Gravity Standardization Net 1971, International Association of Geodesy, Special Publication 4.

Morley, C. K., Ngenoh, and J. K. Ego, 1999. Introduction to the East African Rift System. In: C. K. Morley (Ed.)., Geoscience of Rift Sytem –Evolution of East Africa: AAPG Studues in Geology. No. 44, P. 1-18.

Morley, C. K., 1996. Interpretation of deep and shallow processes in the evolution of the crust beneath the Kenyan rift. In: Prdehl, C., Keller, G. R., Khan. M. A. (Eds.), Crustal and Upper Mantle Structure of the Kenya Rift. Tectonphysics 236, 391-408.

Nabighian M. N., M. E. Ander, V. J. S. Grauch, R. O. Honsen, T. R. LaFehr, Y. Li, W. C. Pearson, J. W. Peirce, J. D. Phillips, and M. E. Ruder, 2005; Historical development of the gravity method in exploration. Geophysics, 70, P.63ND-89ND.

Nafe, J. E. and Drake, C. L., 1957. Variation with depth in shallow and deep water marine sediments of porosity, density and the velocities of compressional and shear waves. Geophysics, 22, 523-552.

Neal, J., Risch, D., and Vail, P. (1993). Sequence Stratigraphy - A global theory for local success. Schlumberger Oilfield Rev.5 (1), 51-62.

Pacht, J. A., Bowen, B., Schaffer, B.L., and Pottorf, W.R.(1993). System tracts, seismic facies and attribute analysis within a sequence stratigraphic frame work –example from the offshore Gulf coast. In "Marine Clastic Reservoirs"(E. G. Rhodese and T. F. Moslow, eds.), pp.3-21 Springer-Verlag, Berlin.

Payton, C. E. (ed). (1977). Seismic Stratigraphy _ Application to hydrocarbon exploration. Me. –Am. Assoc. Pet. Geol. 26, 1- 56.

Peccerillo A. and Bekele, M., 1992. Petroleogical and geochemeical variations associated with the transition from Plateau Basalt to Central Volcanoes along the Muger_Termaber transect. Programs and abstracts of the second Ethiopian Geosciences and Mineral Engineering Congress. P. 10-13.

Pik, R., Marty, B., Carignan, J., and Lave, J. 2003. Stability of the Upper Nile drainage network (Ethiopia) deduced from (U-Th)/He thermochronometery: Implications for uplift and erosion of the Afar plume dome. Earth and Planetary Science Letters, 215, 73-88.

Prodehl, C., Keller, G.R., Khan, M. A., 1994a. Crustal and upper Mantle Structure of the Kenya Rift. Tectonophysics, 236, 483 pp.

Purcell, P. G. 1976. Petroleum Exploration in the Ogaden basin, Geological Survey of Ethiopia. Unpublished report.

Raaben, V. P., Komenyev, S. P., Lissin, V. N. and Kitachew W. T., 1979. Preliminary report on the evaluation of petroleum prospects of the Ogaden basin, Ethiopia. Ethiopian Inst. Geol. Surv., Note, 112.

Reid A.B., Allsop J.M., Granser H., Millett A.J. and Somerton I.W. 1990. Magnetic interpretation in three dimensions using Euler deconvolution. Geophysics 55, 80±91.

Ritsema, J., van Heijst, H. J. and Woodhouse, J. H., 1999. Complex shear wave velocity structure imaged beneath Africa and Iceland. Science 286, 1925-1928

Ritsema J. and H. Van Heijst, 2000. New seismic model of the upper mantle beneath Africa, Geology; V. 28; no. 1; p.63-66.

Ruegg, J. C. (1975), Main results about the crustal and upper mantle structure of the Djibouti region (T. F. A. I.), in Afar Depression of Ethiopia, edited by A. Pilger and A. Rosler, pp. 120–134, E. Schweizerbart, Stuttgart, Germany.

Russo, A., Getaneh, A. and Balemwal, A., 1992. Sedimentary evolution of the Blue Nile basin. Program and Abstracts of the Second Ethiopian Geoscience and Mineral Engineering Congress, 8-10.

Sabins, F. F. (1996). "Remote Sensing: Principles and Interpretation, " 3rd ed. Freeman, San Francisco.

Smith, A. and Hallam, A. 1970. The fit of the Southern continents,. Nature, 225: 139-144. pp.

Sandvol, E., Seber, D., Barazangi, M., Vernon, F., Mellors, R., and Al-Amri, A., 1998. Lithospheric seismic velocity discontinuities beneath the Arabian Shield. Geophysical Research Letters, 25, 2873-2876

Schandelmeier H., Reynolds, P.-O., 1997. Palaeogeographic–Palaeotectonic Atlas of Northeastern Africa, Arabia and Adjacent Areas. Rotterdam, Balkema

Searle, R., Gouin, P., 1972. A gravity survey of the central part of the Ethiopian rift valley. Tectonophysics. 15, 41- 42.

Shull, T. J., 1988, Rift Basins of interior Sudan: Petroleum exploration and discovery; AAPG Bulletin, 72, 1128-1142.

Simiyu, S. M. and G. R. Keller, 1997. An integrated analysis of lithosphere structure across the East African plateau based on gravity anomalies and recent seismic studies. Tectonophysics 278, 291-313.

Simiyu, S., and G. R. Keller, 2001, An integrated geophysical analysis of the upper crust of the southern Kenya rift: Geophysical Journal International, v. 147, p. 543-561.

Simpson, R. W., Jachens, R. C., Blakely, R. J., and Saltus, R. W. 1986. A New isostatic Residual Gravity Map of the Conterminous United States with a Discussion on significance of Isotatic Residual Anomalies. Journal of Geophysical Research. V. 91, No. 138, p. 8348-8372.

Steel, R. J., Felt, V. L.,m Johannsen, E. P., and Mathieu, C., eds. (1995). " Sequence stratigraphy on the Northwestern European Margin," NPF Spec. Publ. No.5 Elsevier, Amsterdam.

Stern, R. J., 1994. Arc assembly and continental collision in the Neoproterozoic East African Orogen: Implications for consolidation of Gondwanaland: Annual Rev Planet. Sci. 22. 319-351.

Swain, C. J., Maguire, P. K. M., Khan, M.A., 1994. Geophysical experiments and models of the Kenya rift before 1989. Tectonophysics, 236, 23-33.

Tadesse, K., and G. R. Keller, 2006. Crustal structure of the Ethiopian rift and adjacent plateaus. New results of integrated interpretation. AGU, EOS, 1263.

Tadesse, K. Workneh Tadele, Getachew Gebreyesus and Daniel Ayana , 1986. Bouguer Gravity Anomaly Map of the main Central Ethiopian rift and Adjacent areas. Techincal Report, Ethiopian Geological Surveys.

Talwani, M, Worzel, JL, and Landisman, M, 1959, Rapid Gravity Computations for Two-Dimensional Bodies with Application to the Mendocino Submarine Fracture Zone, Journal of Geophysical Research, 64:49-61.

Tarling , D. H. and Kent, P. E., 1976. The Madagascar controversy still lives: Nature, 261: 304 – 305 pp.

Tiberi, C., Ebinger, C., Ballu, V., Stuart, G., and Oluma, B., (2005). Inverse model of gravity data from the Red Sea-Aden-East Africa rift triple junction zone. *Geophysical Journal International. 63. 775-787.*

Teklay, M., A. Kroner, K. Mezer and R. Oberhansli, 1998. Geochemistry, Pb-Pb- single zircon ages and Nd-Sr isotope composition of Precambrian rocks from southern and eastern Ethiopia: implications for crustal evolution in East Africa. Journal of African Earth Sciences, Vol. 26, No. 2, pp207-727.

Teklewold, A. and Moore, J. M., 1989. Final report of the Gore-Gambella geotraverse, western Ethiopia. A report to the international development research center on cooperative project between Addis Ababa University, the Ethiopian Institute of Geological Surveys and the Ottawa-Carleton Geoscience Center, Canada.

Tessema, A., Antoine, L.A.G., 2003. Variations in effective elastic plate thickness of the East Africa lithosphere. Journal of Geophysical Research 108 (B5), 2224,

Thompson D.T. 1982. EULDPH: a new technique for making computer-assisted depth estimates from magnetic data. Geophysics 47, 31±37.

Ukstins , I., Renne, P., Wolfenden , E., Baker, J., Ayalew, D., and Menzies, M., 2002. Matching conjugate volcanic rifted margins: 40Ar/39Ar chronostratigraphy of pre-and syn rift bimodal flood volcanism in Ethiopia and Yemen. Earth and Planetary Science Letter, 198, 289-308.

Vail , P., Audemard, F., Bowman, S. A., Eisner, P. N., and Perez-Cruz., C. (1991), The stratigraphic signatures of tectonics, eustacy and sedimentology – an overview. In "Cycle and Event Stratigraphy" (G. Einsele, et al., eds), pp. 617-659. Springer-Verlag, Berlin.

Van Wagoner, J. C. Posamontier, H. W., Mitchum, R. M., Vail, P.R., Sarg, J. F., Loutit, T.S., and Hardenbol, J.(1988). An Overview of the fundamentals of sequence stratigraphy and key definitions. Spec. Publ;. – Soc. Econ. Paleontol. Mineral. 42, 39-46.

Weimer, R. J. (1992). Developments in sequence stratigraphy: Foreland and Cratonic basins. AAPG Bull 74, 837-856.

Williams, LA J, 1970. The volcanics of the Gregory rift valley, East Africa. Bull. Volc., 34, 439-465 .

Wohlenberg, J. 1971. Structure and evolution of. the Rift Valley. Nature, 229:538–542

WoldeGabriel, G., Aronson, J. L., Walter, R. C. 1990. Geology, geochronology and rift basin development in the central sector of the main Ethiopian Rift. Geological Society of American Bulletin 102. 439-458.

Woldetinsae, G., 2005. The Lithosphere of the East African Rift and Plateau (Afar-Ethiopia-Turkana): Insights from Integrated 3-D Density Modelling. PhD. Dissertation, University of Kiel, Kiel, Germany. 126pp.

Wolela, A**.,** 1997. Sedimentology, diagenesis and hydrocarbon potential sandstones in hydrocarbon prospective Mesozoic rift basins (Ethiopia, UK, USA). PhD Thesis, The Queen's University of Belfast, UK

Wolfenden, E., Ebinger, C., Yirgu, G., Deino, A. Ayalew, D., (2004). Evolution of the Northern Main Ethiopian Rift: birth of a triple junction. Earth and Planetary Science Letters. 224. 213-228.

Worku, T., 1988**.** Sedimentology, Diagenesis and hydrocarbon potential of the Karoo sediments (late Palaeozoic to Early Jurassic), Ogadan Basin, Ethiopia. M. Phil Thesis, University of Reading, 222p.

Worku, T. Astin, T. R., 1992. The Karroo sediments (Late Palaeozoic to Early Jurassic) of Ogadan Basin, Ethiopia. *Sedimentary Geology,* 76**:** 7-21.

Yilmaz, O., 1987. Seismic Data processing: Society of Exploration Geophysicists, Tulsa, Oklahoma, 526 pp.

Yilmaz , O., 2001. Seismic data Analysis: Processing, Inversion and Interpretation of Seismic Data (Vols. 1 & 2): Society of Exploration Geophysicists, Tulsa Oklahoma. 2027 pp.

Zanettin, B., Gregnannin, A., Justin-Visentin, E., Mezzacosa, G., and Piccerillo, E. M**.,** 1974. Petrochemistry of the volcanic series of the central Eastern Plateau and relationships between tectonic and magamatolgy. Consigli Nazionale delle Recerche Centro Di Studio Per La Geologia Delle Formazion Crystalline, Padova.Glossary

Appendix I

Different directional derivative maps for the central Ogaden region used for analytical solution computation

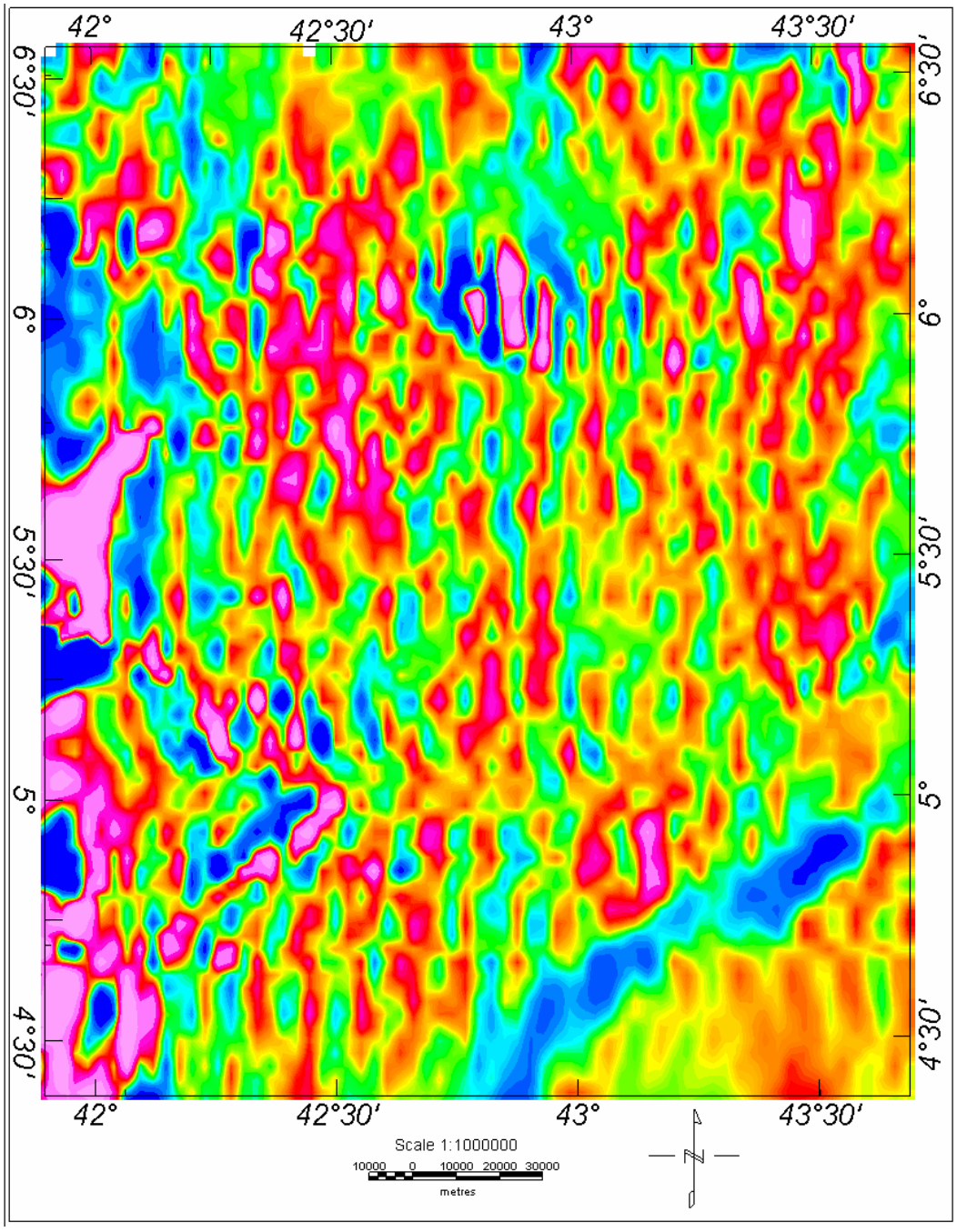

Figure A1.1: Horizontal derivative gravity map of the central Ogaden region in the x-direction

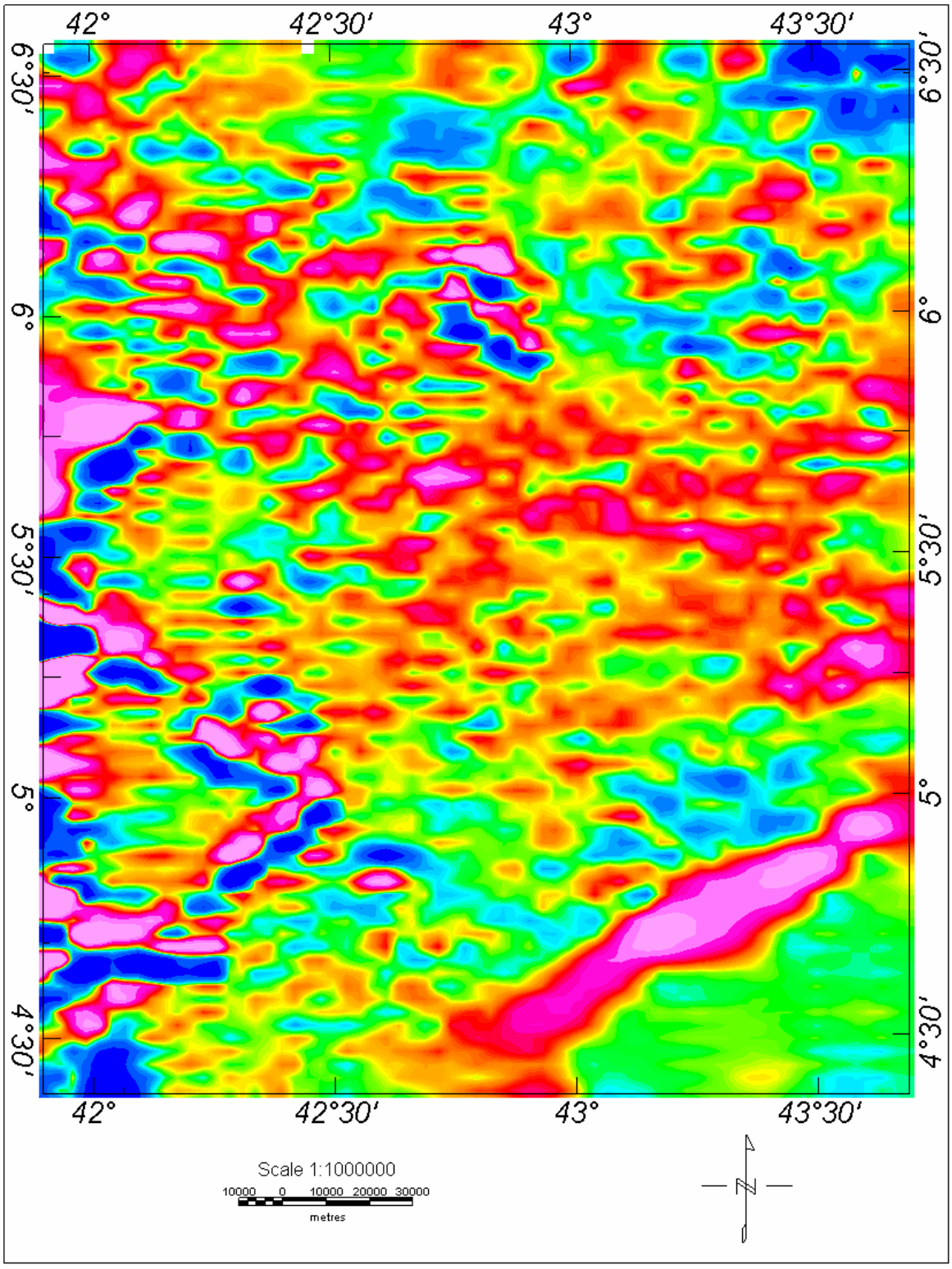

Figure A1.2: Horizontal derivative of gravity map of the central Ogaden region in the y-direction

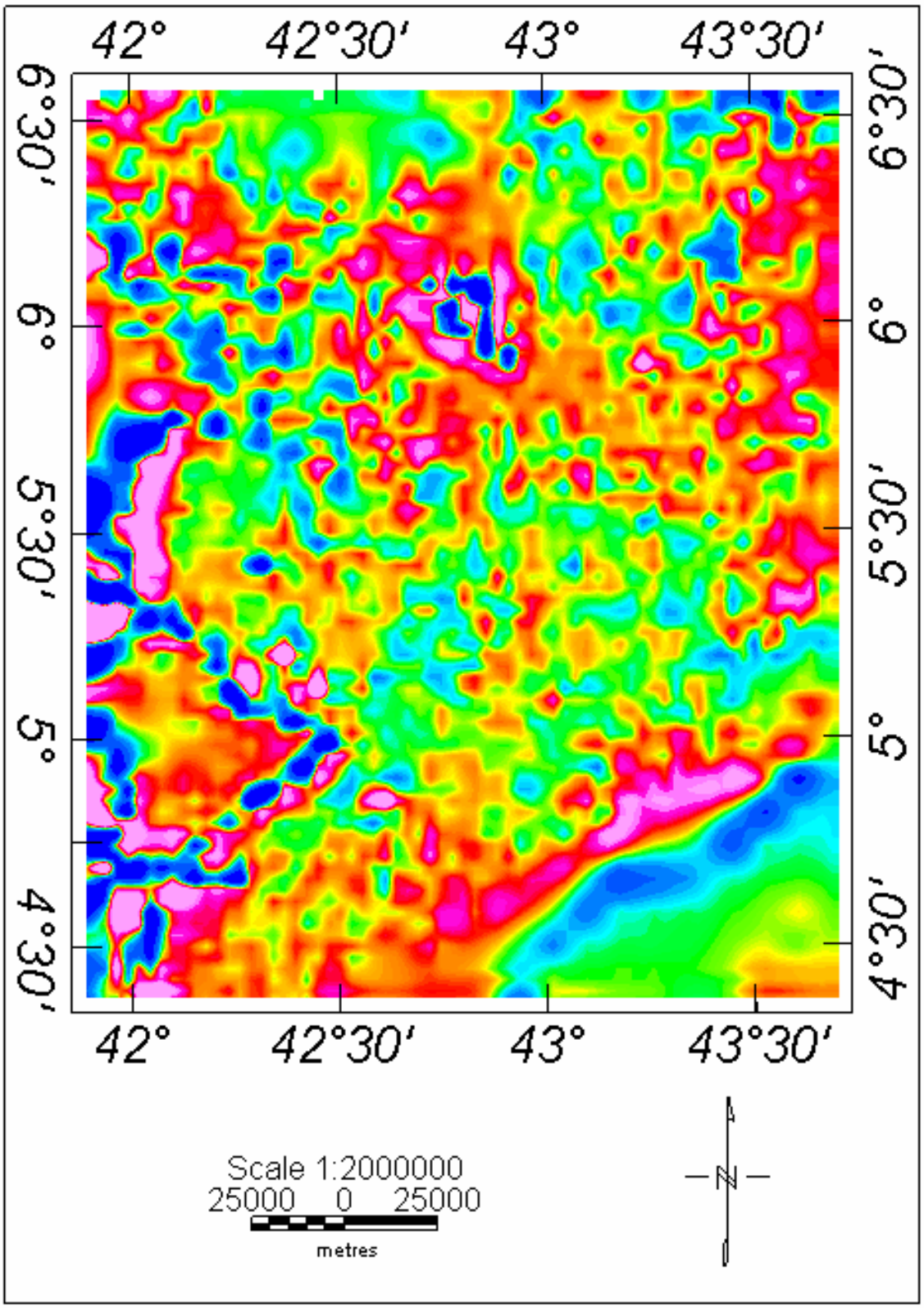

Figure A1.3: Verical dervative gravity map for the central ogaden region in the z-direction.

Appendix II

Different filtering analysis and derivative maps for computing the Euler 3D deconvolution for the northeastern Ogaden basin.

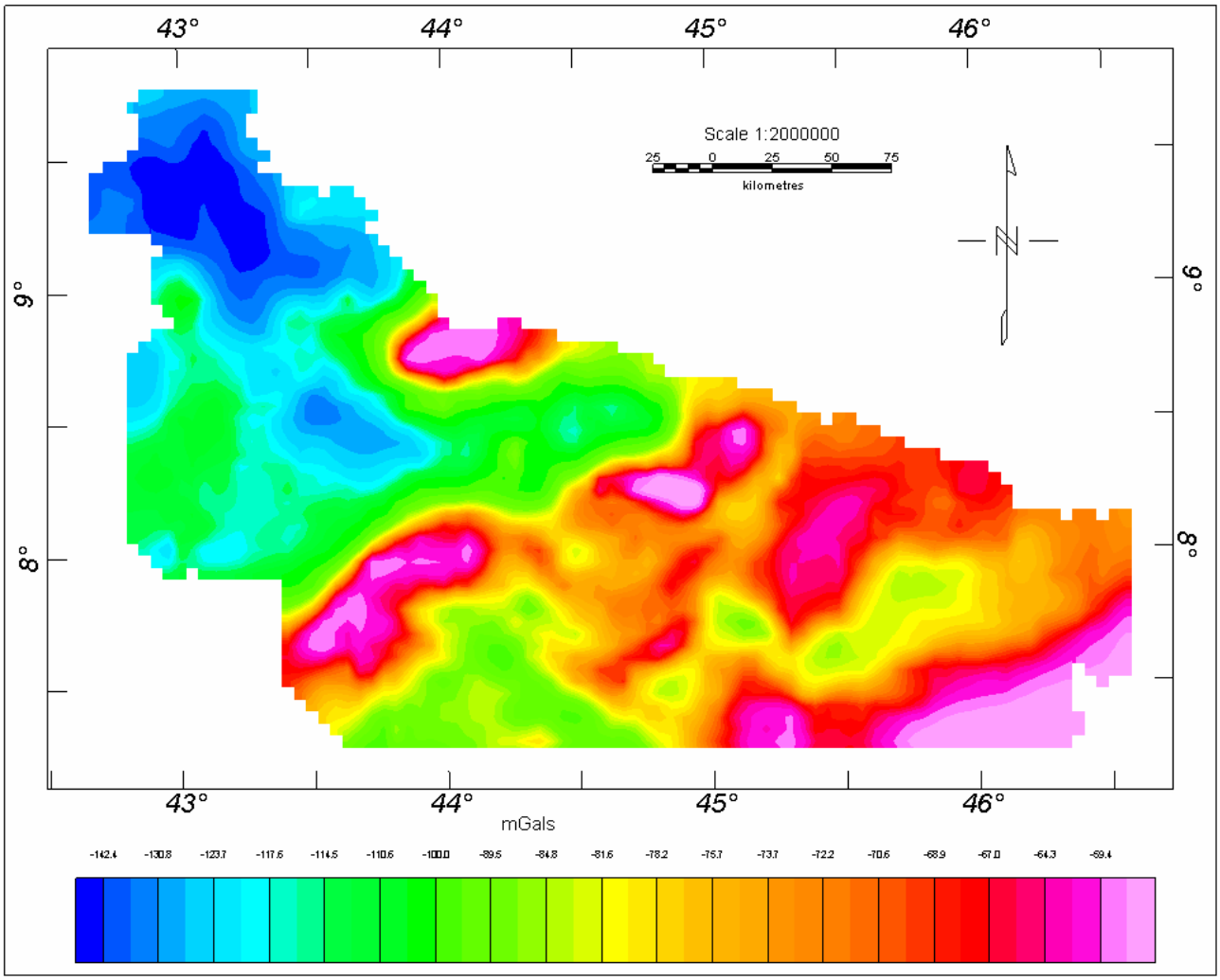

Figure A2.1: Bouguer gravity anomaly map of northeast Ogaden basin, showing relative positive and negative anomalies related to possible horst and graben structures respectively.

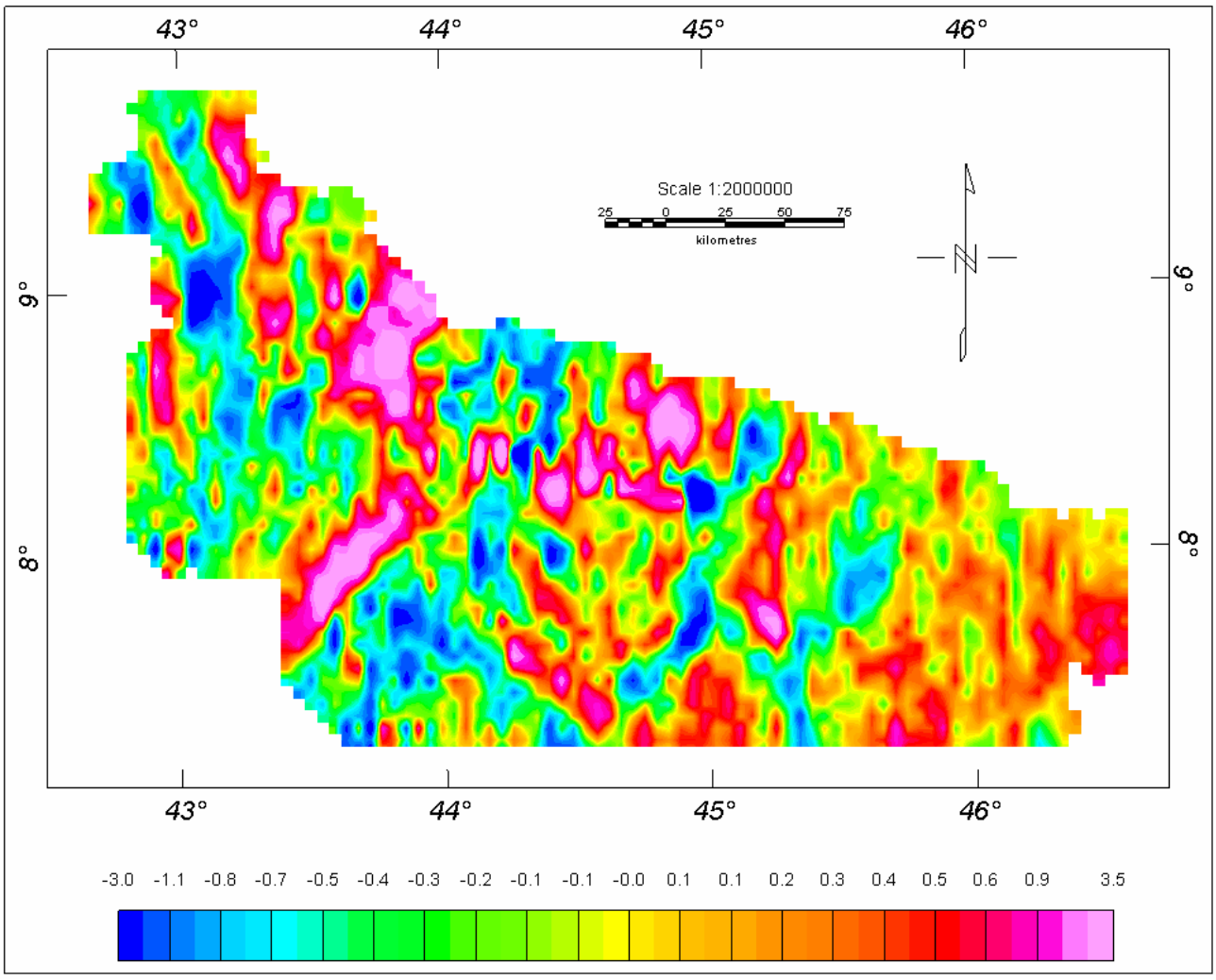

Figure A2.2: x-directional derivative map of northeastern Ogaden basin

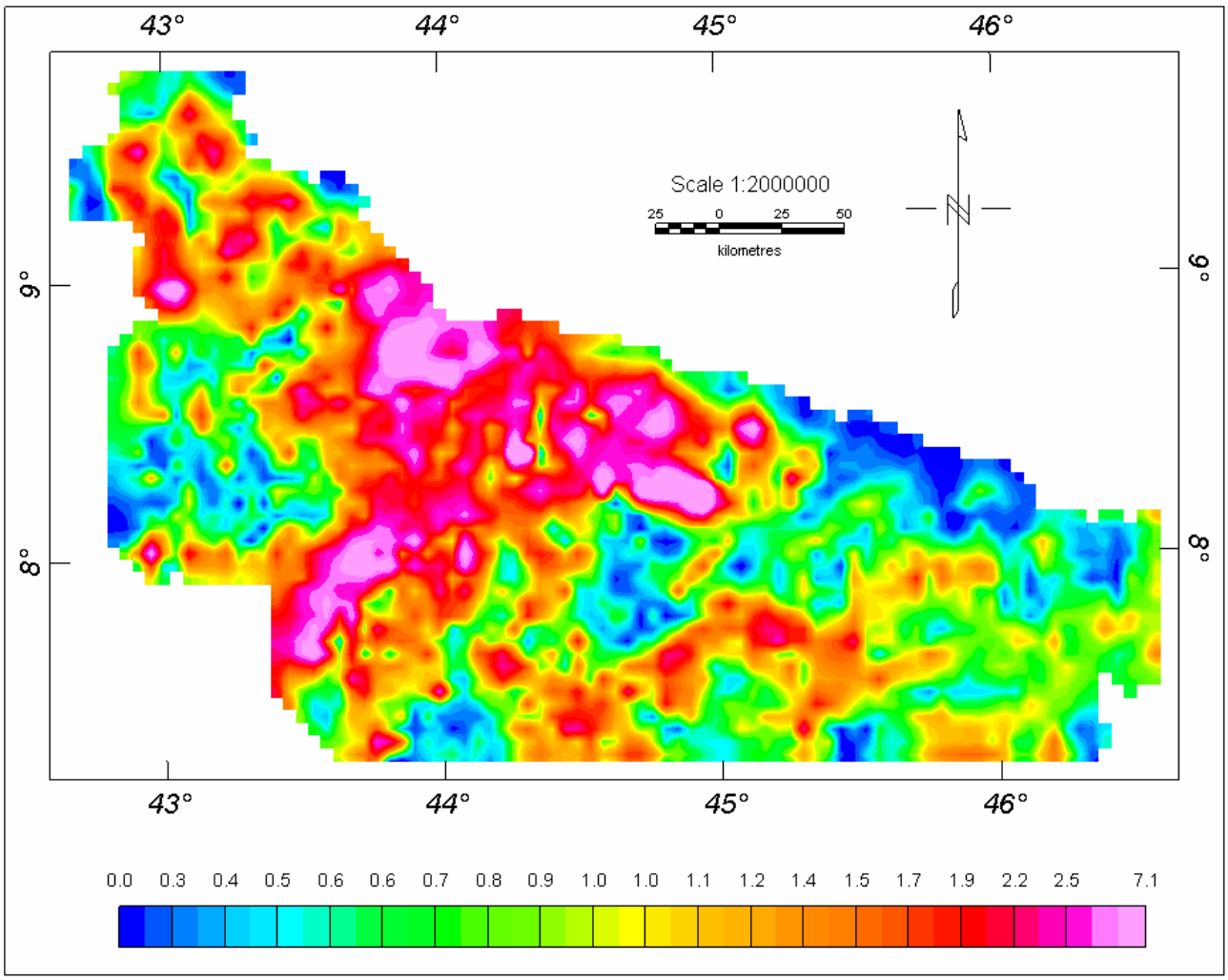

Figure A2.3: Analytical solution for the northeast Ogaden basin indicating possible structural contacts forming NE-SW trending grabens and horst.

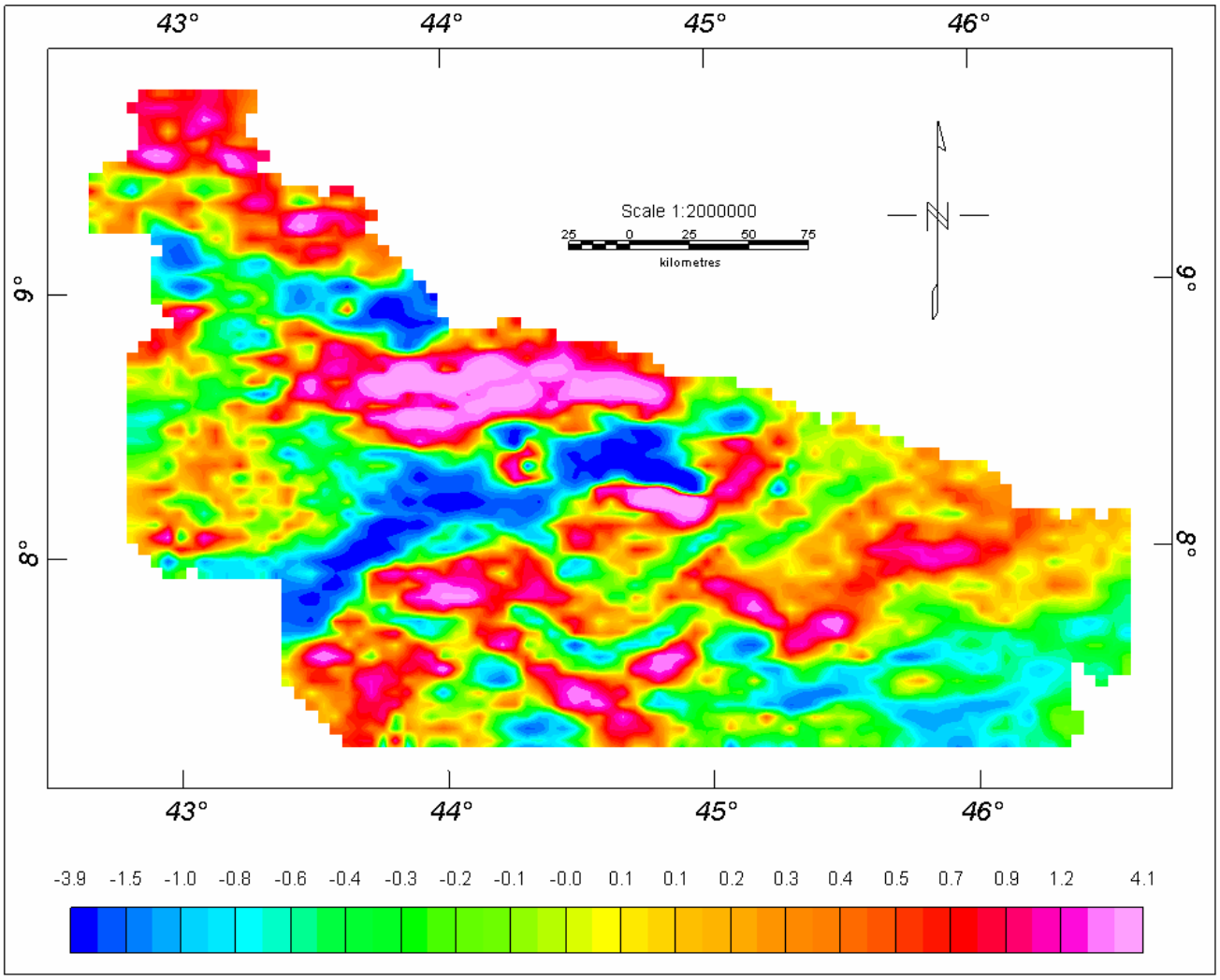

Figure A2.4: Y-direction derivative map showing gravity gradient with relative negative and positive, possibly associated to the nearest grabens and horsts respectively.

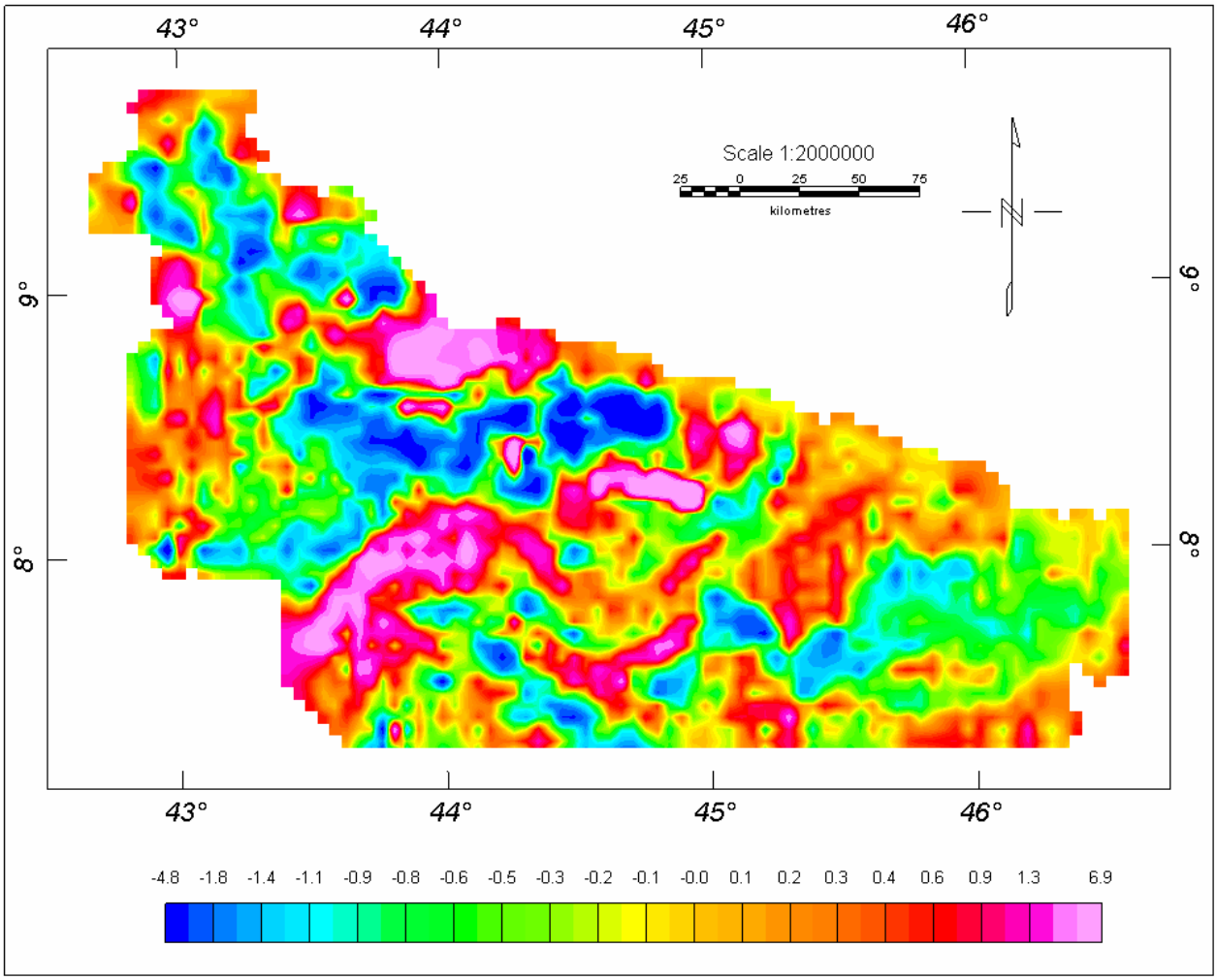

Figure A2.5: z-direction derivative map of the northeastern Ogaden basin

Appendix III

Some example of the reflection seismic data reprocessed and related results for comparison purposes.

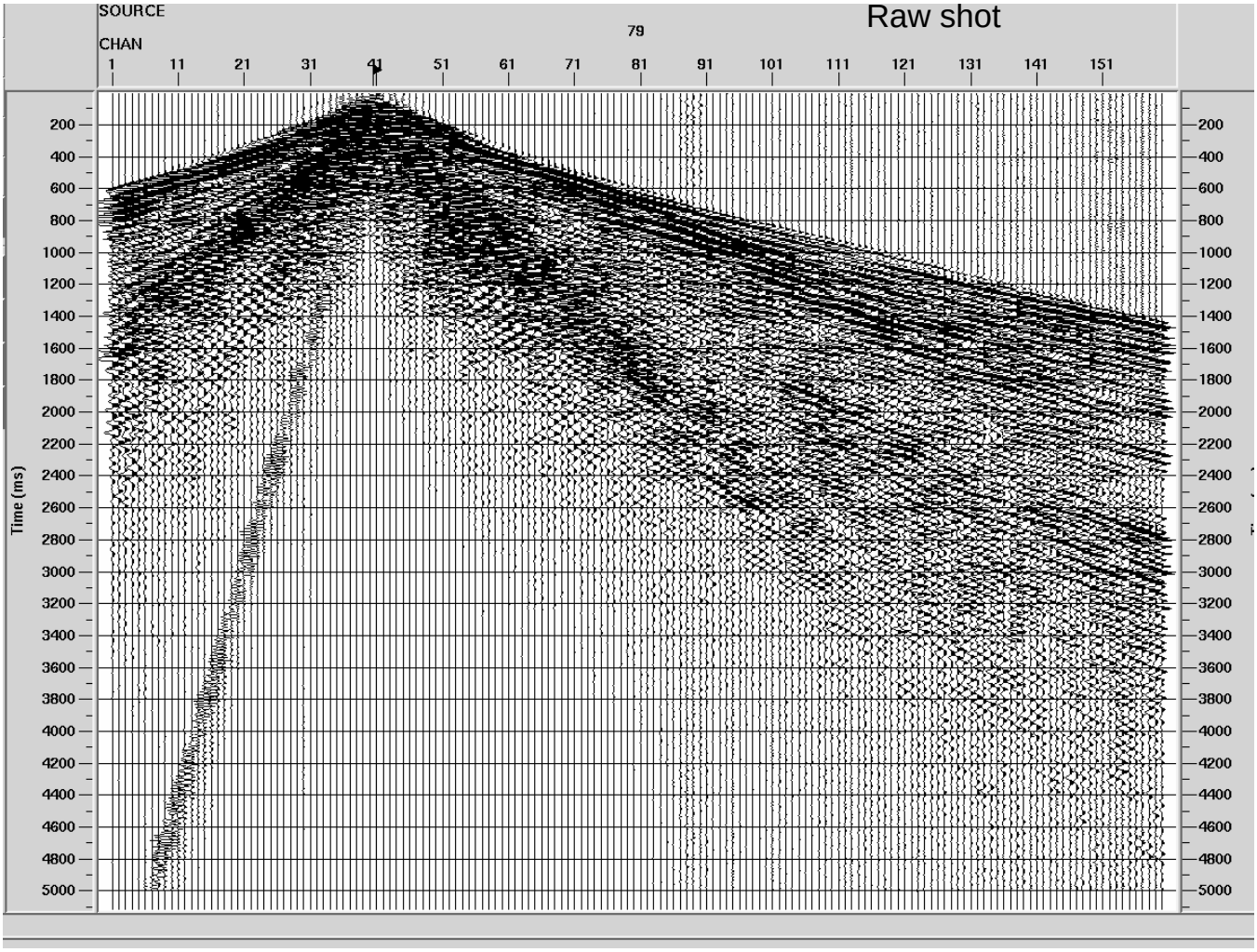

Figure A3.1: Raw shot gather acquired using asymmetric split spread array, the short offset is 2025 meters and the long offset is 6025 m.

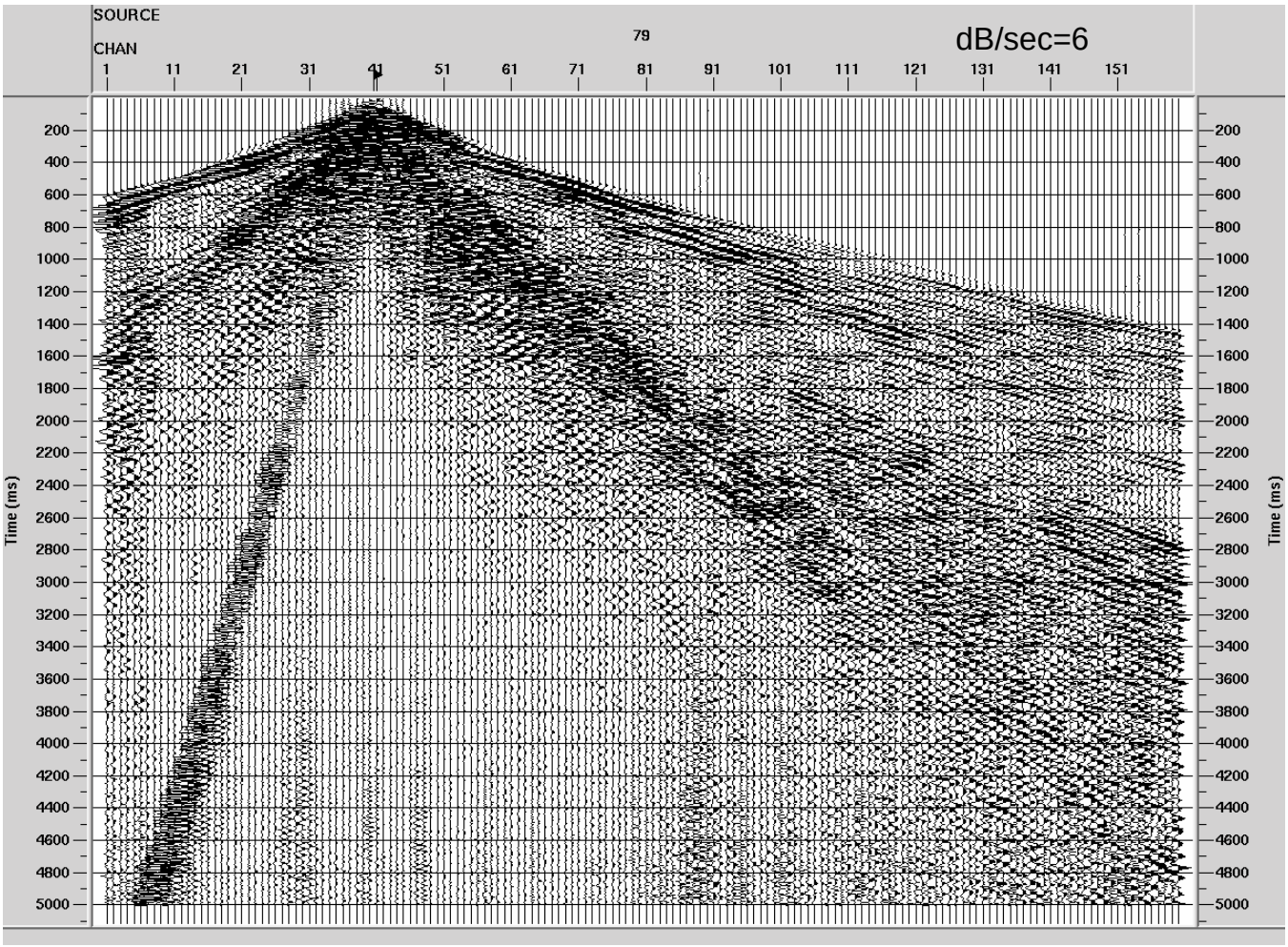

Figure A3.2: True amplitude recovery using dB/second method, showing amplitude recovery used for comparison with other methods.

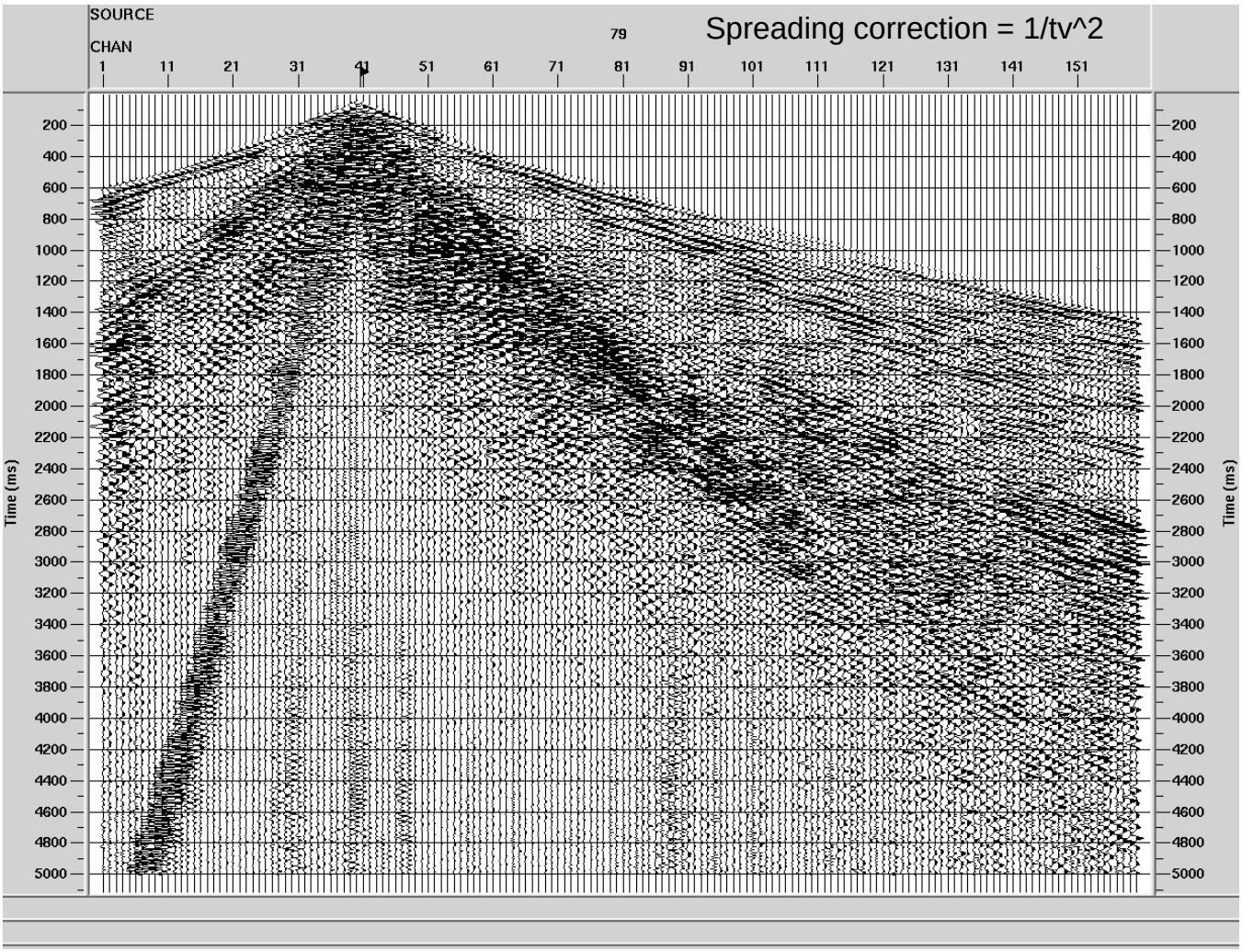

Figure A3.3 True amplitude correction based on the method $1/tv^2$, where v is the smooth velocity function taken for the study area.

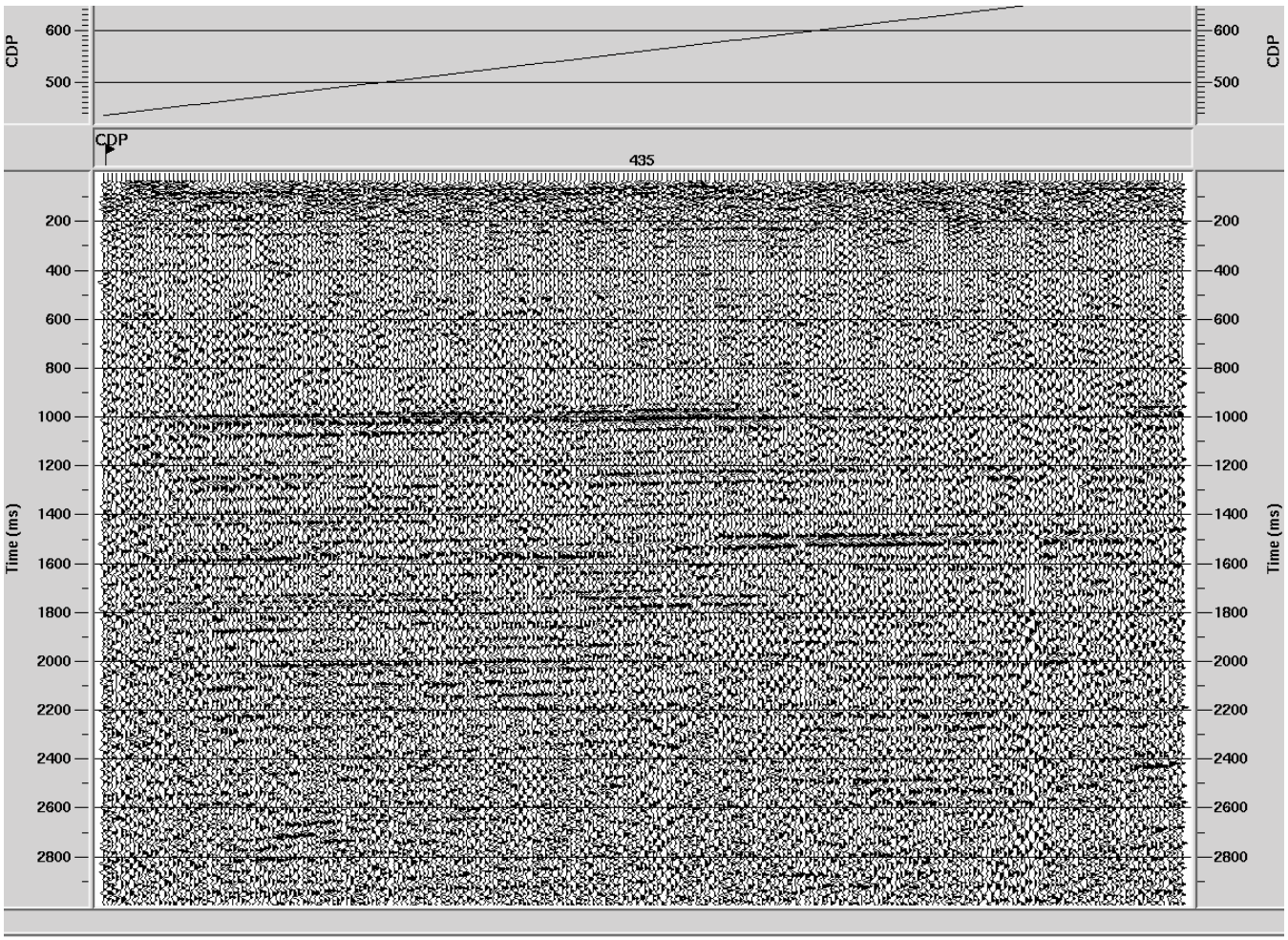

Figure A3.4: An example brute stack section from the reprocessed data after the geometry installation and true amplitude recovery applied.

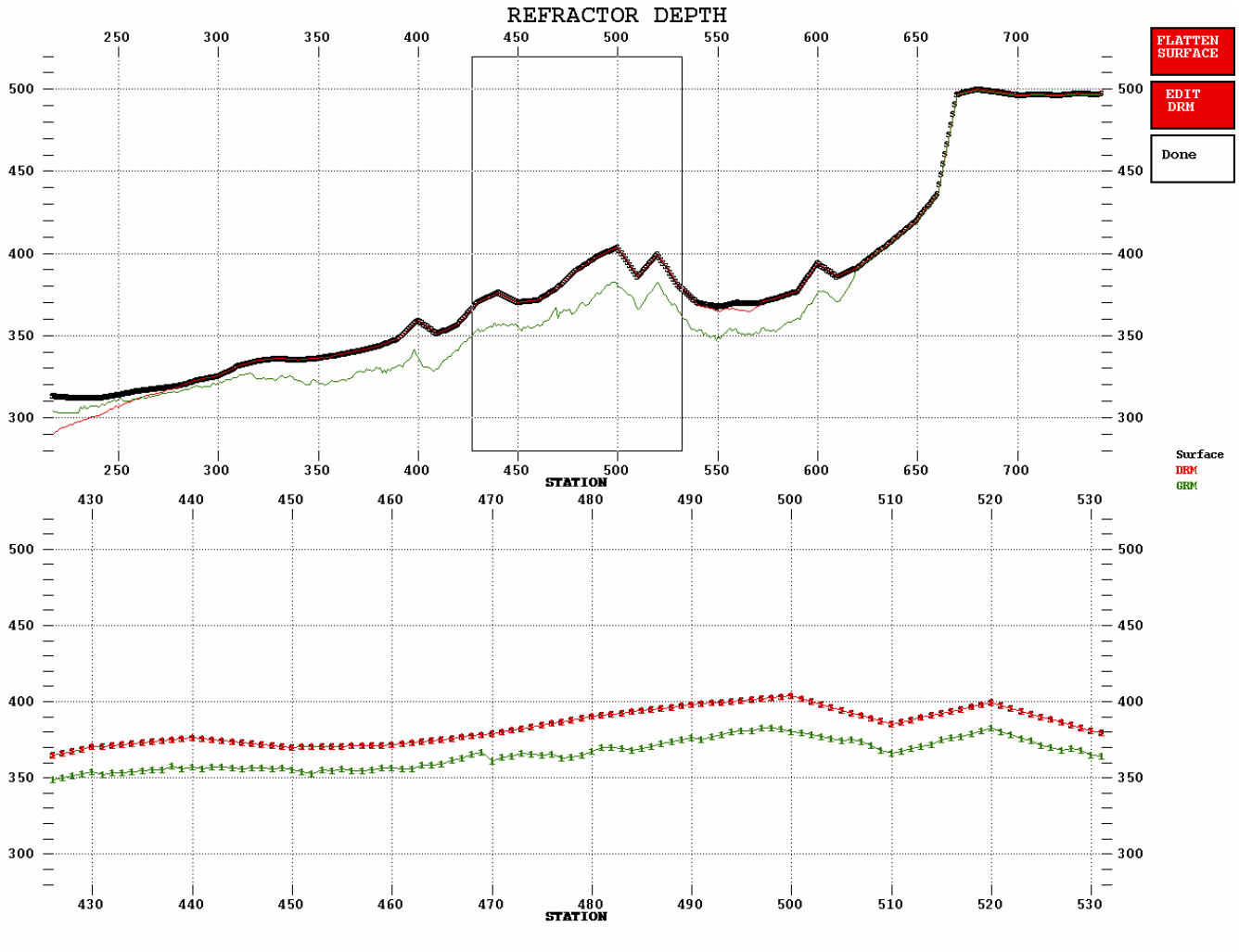

Figure A3.5: A result of refractor depth after refraction statics analysis based on GRM/ genralized reciprocal refraction method (green) and DRM/diminishing residual matrices. The top figure shows the solution along the whole profile in green and red, elevation along the profile is shown by the black line. The lower figure is a zoomed solution indicated by the rectangle in the top figure.

Curriculum Vita

Ketsela Tadesse, the son of Tadesse Habtegebreal and Fetlework Beneberu was born in North Shoa. He obtained his Bachelor of Science Degree in Physics at Addis Ababa University, Addis Ababa, Ethiopia. After graduation he worked for the Institute of Geological Survey of Ethiopia in various sectors as a geophysicist. He again studied at the University of Leeds, Leeds, United Kingdom and received a Master of Philosophy (MPhil) degree in Exploration Geophysics. From 1997 to 2003 he worked as a team leader in the Petroleum Operations Department, under the Ministry of Mines and Energy of Ethiopia. In 2003, he entered the University of Texas at El Paso and received the Doctor of Philosophy degree in Geological Sciences in July of 2007.

Permanent address: P.O. Box 751
Addis Ababa, Ethiopia

This dissertation was typed by Ketsela Tadesse.